Towards a Fully Mechanistic Prediction of Oral Drug Absorption: Investigating Intestinal Transporter Abundance & Function Relationships

A thesis submitted to the University of Manchester for the degree of

Doctor of Philosophy

In the Faculty of Medical and Human Sciences

2015

Matthew Harwood

School of Medicine

Institute of Inflammation and Repair

Table of Contents

Table of Contents **2**
Table of Figures **6**
Table of Tables **9**
Abstract **11**
Declaration **12**
Copyright Statement **12**
Dedication **13**
Acknowledgements **14**
List of Contributed Publications **15**
Abbreviations **16**
Chapter 1 – General Introduction **20**
1.1 Introduction 21
1.2 Oral Drug Absorption 21
1.3 PBPK-IVIVE Modelling & Simulation Approaches 22
1.4 Oral Drug Absorption and the Role of Transporters 23
1.5 *In Vitro* Systems and Determining Transporter Kinetics 25
1.5.1 The Pitfalls of Determining Transporter Kinetics by Conventional Approaches 26
1.5.2 Determining Transporter Kinetics by Mechanistic Compartmental Models 27
1.6 IVIVE-PBPK Linked Models of Intestinal Transporters 28
1.7 Tissue and Relative Transporter Scaling Factors for IVIVE Oral Intestinal Absorption 30
1.7.1 Tissue-Based Scaling Factors – Membrane Protein Scalars 30
1.7.2 Relative Transporter Expression Scaling Approach 30
1.7.3 Relative Expression Factors (REFs) for Scaling 31
1.8 Transporter Abundance Determination by Mass Spectrometry 33
1.8.1 LC-MS/MS Proteomic Techniques to Determine Transporter Abundances 33
1.8.1.1 Selection and Labelling of Peptide Standards 34
1.8.1.2 Preparation of the Biological Sample 34
1.8.1.3 Reduction, Alkylation and Proteolytic Digestion 35
1.8.1.4 Reverse-Phase LC 36
1.8.1.5 Peptide Mass Analysis 36
1.8.1.6 Absolute Quantification (AQUA) Standards 37
1.8.1.7 Quantification Concatamer (QconCAT) Standards 38
1.8.1.8 Label-Free MS Approaches 38
1.9 Absolute Transporter Abundances in IVIVE-PBPK 39
1.9.1 Between Laboratory Considerations 39
1.9.2 Absolute Abundance Generated REF 39
1.9.3 Intestinal PBPK Models and Absolute Transporter Abundances 42
1.9.4 Function *versus* Abundance Scalars 42
1.10 Study Aims & Objectives 45
Chapter 2- Materials and Methods **46**
2.1 Materials 46
2.1.1 Cell Culture & Transport Experiments 46
2.1.2 Cell and Human-Based Membrane Extraction 46
2.1.3 Protein Digestion 47

2.1.4 Proteomic Analyses 47
2.1.5 Gene Expression Analysis 47
2.2 Methods 48
2.2.1 Cell Culture 48
2.2.2 Preparation of Membrane Fractions from Cultured Cells 48
2.2.2.1 Flask-Based Membrane Extraction 48
2.2.2.2 Filter-Based Membrane Extraction 48
2.2.2.3 Human Intestinal Tissue Harvest & Membrane Extraction 52
2.2.2.4 Enterocyte Chelation: 52
2.2.2.5 Mucosal Crushing: 53
2.2.3 Histological Assessment of Human Enterocyte Chelation 54
2.2.4 Assessment Membrane Purity 54
2.2.4.1 Alkaline Phosphatase Activity Assay 54
2.2.4.2 Cytochrome C Reductase Activity Assay 55
2.2.5 Immunoblot Analysis of P-gp Expression 55
2.2.6 Generating Standard Peptides for Protein Abundance Quantification 56
2.2.6.1 Generation of AQUA SIL peptides: 56
2.2.6.2 Generating the 'TransCAT' (QconCAT) construct: 56
2.2.7 Protein Digestion 58
2.2.7.1 Protein digestion (AQUA & QconCAT - University of Manchester) 58
2.2.7.2 Protein digestion (AQUA – Bertin Pharma (BPh)) 58
2.2.8 LC-MS/MS Analysis 59
2.2.8.1 Preparation of NNOP (Glu-Fib) Assay Mix for SRM Analysis 59
2.2.8.2 Sample Analysis by LC-MS/MS 59
2.2.8.3 Assay Quality Control - Establishing Linearity, Limits of Quantification & Precision 59
2.2.8.4 Calculation of Transporter Abundance Values 60
2.2.8.5 Gravimetric Determination of Peptide Quantity for Abundance Determinations 61
2.2.8.6 Bertin LC-MS/MS Conditions 61
2.2.9 Analysis of Transporter Gene Expression 64
2.2.9.1 RNA Isolation and cDNA Generation 64
2.2.9.2 Gene Expression Analysis by Real-Time PCR 64
2.2.10 Determining Transporter Function by Monolayer Transport Assays 66
2.2.10.1 Bi-Directional Monolayer Transport Assay: General Methods 66
2.2.11 Analysis of E-3-S Protein Binding 68
2.2.12 Estimation of Transporter Kinetic Parameters by Compartmental Modelling 68
Chapter 3 -Development and Validation of Membrane Extraction Techniques for Quantitative Targeted Absolute Proteomic Studies 72
3.1 Introduction 73
3.2 Methods 74
3.2.1 Preparation of Membrane Fractions from MDCK-II-WT and Caco-2 Cells 74
3.2.1.1 Method 1 74
3.2.1.2 Method 2 74
3.3 Results 75
3.3.1 Optimising Membrane Extractions in Flask-Grown MDCK-II-WT Cells 75
3.3.2 Optimising Membrane Extractions in Flask-Grown Caco-2 Cells 78
3.3.3 Characterising Membrane Extractions in Filter-Grown Caco-2 Cells 80

3.3.4 Harvesting and Characterising Membranes from Eluted Human Enterocytes 85
3.4 Discussion 89
3.5 Conclusion 96
Chapter 4 - Development of Digestion and LC-MS/MS Methods for Quantification of Human Intestinal Transporter Proteins' Absolute Abundance using a QconCAT Technique 97
4.1 Introduction 98
4.2 Materials & Methods 99
4.2.1 Materials 99
4.2.2 Methods 99
4.2.2.1 Nvoy Proteolytic Digestion Protocol 99
4.3 Results 100
4.3.1 Initial Development of Proteolytic Digestion and LC-MS/MS QTAP Assays 100
4.3.1.1 Preliminary Development of an In-Solution Proteolytic Digestion Strategy 100
4.3.1.2 Caco-2 Cell Plasma Membranes Digestion: The Initial Phase 100
4.3.1.3 A Strategy Adaptation for Obtaining Absolute Transporter Abundances 105
4.3.1.3.1 University of Manchester Strategic Plans 105
4.3.1.3.2 Contingency Plan – An External Source for Abundance Quantification 105
4.3.1.3.3 AQUA-Based Villin and Na/K-ATPase Absolute Abundance Quantification 106
4.3.2 Development of an LC-MS/MS Method for the Simultaneous Quantification of Transporter Proteins Absolute Abundance using a QconCAT Technique 107
4.3.2.1 Development of the LC-MS/MS Analysis 107
4.3.2.2 Method Validation – Linearity and Precision of the TransCAT Assay 110
4.3.2.3 Quantifying Absolute Transporter Protein Abundances in Human Intestine 114
4.4 Discussion 116
4.5 Conclusion 123
Chapter 5 - Breast Cancer Resistance Protein Abundance, but not mRNA Expression Correlates with Estrone-3-Sulfate Bi-directional Transport Activity 124
5.1 Introduction 125
5.2 Methods 128
5.2.1 Bi-directional Monolayer Transport Assay: E-3-S Transport 128
5.3 Results 130
5.3.1 Characteristics of Caco-2 Monolayers 130
5.3.2 Age-Dependent Transporter Gene Expression Analysis in Caco-2 Cells 131
5.3.3 Age-Dependent Transporter Protein Abundance Analysis in Caco-2 Cells 134
5.3.4 Assessing BCRP Abundance-Transport Relationships in Caco-2 Cells 141
5.3.4.1 Determining E-3-S Binding to BSA 141
5.3.4.2 E-3-S Transport in 10 and 29d Caco-2 Monolayers 142
5.4 Discussion 150
5.5 Conclusion 157
Chapter 6 - A Cross Laboratory Comparison of Human Intestinal and Caco-2 Drug Transporter Protein Abundances 158
6.1 Introduction 159
6.2 Methods 161
6.3 Results 163
6.3.1 Human Intestinal Transporter Abundance Quantification by Bertin Pharma 163
6.3.2 Method Comparison Across Groups Quantifying Transporter Protein Abundances 164
6.3.3 Cross Laboratory Comparison of Absolute Protein Abundances 167

6.3.4 An Appraisal of Selected P-gp and BCRP Peptides....172
6.3.5 A Comparison to Published Data: UoM *Versus*. The University of Greifswald Transporter Abundances....174
6.3.6 The Impact of Enterocyte Harvest Method on Transporter Abundances....174
6.4 Discussion....176
6.5 Conclusion....181
Chapter 7 - Efflux Ratio and Intrinsic Clearance of Vinblastine are Associated to P-gp Abundance in Caco-2 Cells....182
7.1 Introduction....183
7.2 Methods....186
7.2.1 Bi-directional Monolayer Transport Assay: VBL Transport....186
7.3 Results....188
7.3.1 Characteristics of Caco-2 Monolayers....188
7.3.2 Transporter Gene Expression Analysis in Caco-2 Cell Variants....189
7.3.3 Protein Abundance Analysis in Caco-2 Cell Variants....189
7.3.4 VBL Transport in Caco-2 Cell Variants....191
7.3.5 Permeability and Kinetic Estimates of VBL by Compartmental Modelling....196
7.4 Discussion....203
7.5 Conclusion....212
Chapter 8 - Lost in Centrifugation! Accounting for Transporter Losses in Quantitative Targeted Absolute Proteomics....213
8.1 Introduction....214
8.2 Theoretical Background....215
8.2.1 Protein Losses in Centrifugation: The Utility of Recovery Factors....215
8.2.2 Accounting for Protein losses in QTAP Abundance Analysis....216
8.2.3 Correcting for Protein Losses in Centrifugation....218
8.3 Methods....221
8.4 Results....222
8.4.1 The Expected & Actual Enrichment in Abundance....222
8.4.2 Generating & Applying Recovery Correction Factors to Correct for Protein Losses....223
8.5 Discussion....225
8.6 Conclusion....229
Chapter 9 - Final Conclusion & Future Work....230
Appendices....236
Appendix 1....236
Appendix 2....237
Appendix 3....239
Appendix 4....240
Appendix 5....246
Appendix 6....252
Appendix 7....255
Bibliography....258

Word Count: 71038

Table of Figures

Figure 1-1. Schematic representation of the ADAM model....**31**
Figure 1-2. An overview the three categories of transporter-IVIVE scalars....**32**
Figure 1-3. A representative illustration of the configuration of a triple quadrupole mass spectrometry instrument....**37**
Figure 2-1. Schematic describing the plasma membrane extraction protocol from cells grown on filters....**51**
Figure 2-2. Human tissue adaptor used for chelating and harvesting human enterocytes....**52**
Figure 2-3. The structure of the three compartment model to estimate the transporter kinetic parameters from bi-directional transport assays....**69**
Figure 3-1. Alkaline phoshatase activity in various MDCK-II-WT cell fractions derived from method 1 membrane extraction protocol....**76**
Figure 3-2. The enrichment in alkaline phosphatase activity in the starting TP and subsequent MDCK-II-WT cell fractions derived from membrane extraction method 2....**77**
Figure 3-3. The enrichment in cytochrome c reductase activity in the starting TP and subsequent MDCK-II-WT cell fractions derived from membrane extraction method 2....**77**
Figure 3-4. Protein content of various MDCK-II-WT cell fractions derived from membrane extraction method 2 as measured by the BCA assay....**78**
Figure 3-5. The enrichment in alkaline phosphatase activity in various Caco-2 cell fractions derived from membrane extraction method 2....**79**
Figure 3-6. The enrichment in cytochrome c reductase activity in various Caco-2 cell fractions derived from membrane extraction method 2....**79**
Figure 3-7. Protein content of various flask-grown Caco-2 cell fractions (n=3) derived from membrane extraction method 2 as measured by the BCA assay....**80**
Figure 3-8. Assessment of monolayer integrity by lucifer yellow apparent permeability (Papp) in different Caco-2 cell variants....**81**
Figure 3-9. The enrichment in alkaline phosphatase activity in various Caco-2 cell fractions grown on filters for 10, 16, 21 and 29 days....**82**
Figure 3-10. An assessment of the relationship between membrane protein content and alkaline phosphatase activity by correlation analysis....**83**
Figure 3-11. Protein content of various filter-grown Caco-2 cell fractions (n=3-6 experiments, triplicate filters per experiment) as measured by the BCA assay....**84**
Figure 3-12. Assessing the enrichment of P-glycoprotein (P-gp) throughout the membrane fractionation procedure in 10d filter-grown Caco-2 cells using immunoblotting....**84**
Figure 3-13. Histological assessment of enterocyte elution by the EDTA chelation method in haematoxylin and eosin stained human distal ileum....**86**
Figure 3-14. Human enterocyte protein content (µg/cm2) in homogenate and total membrane protein fractions after EDTA chelation....**87**
Figure 3-15. Human mucosal protein content (µg/mg mucosal tissue) in homogenate and total membrane protein fractions....**87**
Figure 3-16. Alkaline phosphatase activity enrichment in the total membrane fraction compared to the original starting total protein fraction....**88**
Figure 4-1. Data-Dependent Acquisition (DDA) following the submission of orbitrap fragmentation spectra from a Caco-2 PM digest to the MASCOT search engine....**102**
Figure 4-2. A co-elution profile for Na/K-ATPase (IVEIPFNSTNK) from a Caco-2 cell PM Nvoy-based digest....**102**
Figure 4-3. Ion intensity signals for the 3 selected transition of the peptide IVEIPFNSTNK selective for Na/K-ATPase from a Caco-2 cell PM digest....**103**
Figure 4-4. Assessment of peptide (SpikeTide) loss through the SCX peptide purification procedure by the BCA assay....**103**
Figure 4-5. A schematic describing the digestion workflow and decision making for Sections 4.3.1.1 and 4.3.1.2....**104**
Figure 4-6. Co-elution profiles for Villin (AAVPDTVVEPALK) and Na/K-ATPase (IVEIPFNSTNK) peptides in a 16d grown Caco-2 PM digest....**106**
Figure 4-7. Villin and Na/K-ATPase absolute protein abundances in filter-grown Caco-2 cell PM digests for 10 (n=3), 16 (n=1) and 29 days (n=1)....**107**
Figure 4-8. Total ion chromatogram demonstrating the developed LC-MS/MS SRM method for simultaneous quantification of the selected proteotypic peptides for the selected transporter proteins....**108**
Figure 4-9. Co-elution and individual transition profiles for Na/K-ATPase (IVEIPFNSTNK, parts A-C) and P-gp (AGAVAEEVLAAIR, parts D-F) human intestinal TM digests....**109**
Figure 4-10 (A). Linearity of QconCAT quantification using the developed SRM assay for the NNOP peptide (Glu-Fib)....**112**

Figure 4-11. Linearity of transporter protein (OST-β (A) and OATP2B1 (B)) concentrations quantified over a 14-fold range of pooled human intestinal TM protein quantities **113**
Figure 4-12. Absolute abundances of transporter proteins in human distal jejunum and ileum total membrane fractions **115**
Figure 5-1. The chemical structure of Estrone-3-Sulfate (ammonium salt) **126**
Figure 5-2. Postulated transport pathways for E-3-S at the apical (A) and basaloteral (B) membranes in Caco-2 cells.....**126**
Figure 5-3. Assessment of monolayer integrity and growth by TEER for all cultured Caco-2 cells monolayers N=32 plates **130**
Figure 5-4. mRNA gene expression of MDR1, MRP2 and BCRP in 10 to 29 day cultured Caco-2 cells normalised to the housekeeper protein PPIA **132**
Figure 5-5. mRNA gene expression of OATP2B1, OST-A and OST-B in 10 and 29 day cultured Caco-2 cells normalised to the housekeeper protein PPIA. **133**
Figure 5-6. Plots showing the change in gene expression over Caco-2 cell cultivation time for all transporters **133**
Figure 5-7. The absolute Na/K-ATPase protein abundance determined by BPh analysis in 10, 21 and 29d cultured Caco-2 cell monolayers.....**134**
Figure 5-8. The absolute Na/K-ATPase protein abundance determined by analysis at The University of Manchester in 10, 21 and 29d cultured Caco-2 cells.....**135**
Figure 5-9. The absolute P-gp protein abundance determined by Bertin Pharma (BPh) analysis in 10, 21 and 29d cultured Caco-2 cell monolayers.....**136**
Figure 5-10. Comparison of P-gp protein abundances between Caco-2 cell monolayers across laboratories.....**137**
Figure 5-11. The absolute BCRP protein abundance determined by Bertin Pharma (BPh) analysis in 10, 21 and 29d cultured Caco-2 cells.....**138**
Figure 5-12. The absolute BCRP protein abundance determined at the University of Manchester in 10, 21 and 29d cultured Caco-2 cells **138**
Figure 5-13. The absolute protein abundance of MRP2 (A), OATP2B1 (B), OST-α (C) & OST-β (D) determined at the University of Manchester in 10, 21 and 29d cultured Caco-2 cells **140**
Figure 5-14. The relative levels of transporter mRNA gene expression and protein abundance in 21 and 29 day Caco-2 cells.....**140**
Figure 5-15. Transport of E-3-S (0.01 µM) in A-to-B (white) and B-to-A (black) transport directions across 10d (A) and 29d (B) cultured Caco-2 cell monolayers in the presence and absence of Ko143 (2 µM) at pH 6.5/7.4.....**142**
Figure 5-16. Transport of E-3-S (0.01 µM) in A-to-B (white) and B-to-A (black) transport directions across 29d cultured Caco-2 cell monolayers in the presence and absence of montelukast (100 µM) **143**
Figure 5-17. E-3-S monolayer content in the presence and absence of montelukast at pH 6.5/7.4 .....**144**
Figure 5-18. Transport of E-3-S (0.01 µM) in A-to-B (white) and B-to-A (black) transport directions across 10d (A) and 29d (B) cultured Caco-2 cell monolayers in the presence and absence of Ko143.....**145**
Figure 5-19. Transport of E-3-S (0.01 µM) in A-to-B (white) and B-to-A (black) transport directions across 10d (A) and 29d (B) cultured Caco-2 cell monolayers. 29d monolayers were also incubated in the presence and absence of Ko143 (2 µM) at pH 6.5/6.5 .....**147**
Figure 6-1. The absolute protein abundance of Na/K-ATPase (A), P-gp (B) and BCRP (C) in intestinal samples (n=9) from various regions of the gastrointestinal tract.....**163**
Figure 6-2. Absolute protein abundances of Na/K-ATPase, P-gp and BCRP determined by Bertin Pharma (black) and the University of Manchester (white) in Caco-2 cell monolayers (n=7) and human intestinal TM fractions (n=4).....**170**
Figure 6-3. Correlation analysis (Spearman's Rank) of the absolute protein abundances of Na/K-ATPase (A), P-gp (B) and BCRP (C) between Bertin Pharma and the University of Manchester .171
Figure 6-4. The location and nomenclature of the selected peptides for quantifying P-gp (A) and BCRP (B) absolute protein abundances **173**
Figure 6-5. The absolute protein abundances of P-gp, BCRP and MRP2 in distal jejunum measured at the University of Greifswald (UoG), the UoM and BPh.....**175**
Figure 6-6. A comparison of Na/K-ATPase, P-gp and BCRP protein abundances in matched human distal jejunum TM protein samples after enterocyte chelation or mucosal crushing **175**
Figure 7-1. The chemical structure of Vinblastine sulphate 184
Figure 7-2. Assessment of monolayer integrity and growth by TEER for all variant Caco-2 cell monolayers N=29 plates **188**
Figure 7-3. mRNA gene expression of MDR1 (A), BCRP (B) and MRP2 (C) in 21d cultured Caco-2 cells variants normalised to the housekeeper protein PPIA **190**
Figure 7-4.The absolute Na/K-ATPase protein abundance determined by Bertin Pharma analysis in all 21d cultured Caco-2 cell monolayers variants **190**

Figure 7-5. The absolute P-gp protein abundance determined by Bertin Pharma analysis in all 21d cultured Caco-2 cell monolayers variants **191**
Figure 7-6. Transport of VBL (0.03 µM) in A-to-B (white) and B-to-A (black) transport directions across 21d cultured Caco-2 cell monolayers in the presence and absence of verapamil (100 µM) **192**
Figure 7-7. Transport of VBL (0.03 µM) in A-to-B (white) and B-to-A (black) transport directions across 21d cultured Caco-2 cell monolayers (all variants) in the presence and absence of verapamil (100 µM). A, low passage, B, high passage and C, VBL-selected Caco-2 cell monolayers **193**
Figure 7-8. Transport of VBL (0.03 µM) in A-to-B (white) and B-to-A (black) transport directions across 21d cultured Caco-2 cell monolayers in the presence and absence of verapamil (100 µM) and lansoprazole over 60 min **194**
Figure 7-9. The A-to-B (dashed lines) and B-to-A (solid lines) transport of VBL at increasing concentrations increasing concentrations in 21d filter-grown Caco-2 cell variants **195**
Figure 7-10. Bi-directional fitting of VBL in the receiver chamber of a Transwell Caco-2 cell (low passage) system using a three-compartment model **201**
Figure 7-11. Observed and model predicted VBL concentrations following simultaneous fitting of bi-directional transport in low passage Caco-2 cell monolayers **202**
Figure 8-1. A - The fold enrichment 'actual enrichment' in selected peptide abundances measured in the whole cell and PM fraction of matched samples of the blood brain barrier cell model (hCMEC/D3) **218**
Figure 8-2. A schematic describing the generation of recovery factors (RF's) to correct transporter abundances in membrane fractions for protein losses encountered during centrifugation **220**
Figure 8-3. The protein content and the yield of protein as a percentage of the TP lysate in Caco-2 cell monolayers **222**
Figure 8-4. The abundances of Na/K-ATPase (white) and Villin (black) in Caco-2 cell monolayer TP lysate and membrane fractions **223**
Figure 8-5. The corrected abundances for Na/K-ATPase (A) and villin (B) from Caco-2 cell monolayer total protein (whole cell lysate) and PM fractions **224**
Appendix Figure A-1. Images of eluted material sampled onto slides from a human jejunum sample after 5 mM EDTA incubation over 45 min **236**
Appendix Figure B-1. Caco-2 PM digest submitted for fragmentation by an Orbitrap mass spectrometer and data-dependent acquisition (DDA) **237**
Appendix Figure B-2. Selected transition of the native peptides of a 21d-Grown Caco-2 cell plasma membrane DOC-digest for Villin (A) and Na/K-ATPase (B) **238**
Appendix Figure C-1. The TransCAT construct sequence annotating the target transporter and supporting peptides to permit successful expression in the host E.Coli vector **239**
Appendix Figure D-1. A schematic of the workflow to measure human intestinal transporter protein absolute abundance using a QconCAT method **240**
Appendix Figure D-2. Co-elution profiles for HPT1 (A), MRP2 (B), BCRP (C), OST-α (D), OST-β (E), and OATP2B1 (F) **244**
Appendix Figure E-1. The stability of the housekeeper gene PPIA in Caco-2 cell monolayers cultured from 10 to 29 days on filters **246**
Appendix Figure F-1. E-3-S monolayer content in 10 and 29d Caco-2 cells after incubation with Ko143 and montelukast at pH 6.5/7.4 ..... **253**
Appendix Figure F-2. E-3-S monolayer content in 10 and 29d Caco-2 cells after incubation with Ko143 at pH 7.4/7.4 ..... **254**
Appendix Figure F-3. E-3-S monolayer content in 10 and 29d Caco-2 cells at pH 6.5/6.5 ..... **254**

Table of Tables

Table 1-1. A summary of the available literature transporter abundance data in human intestinal regions....**41**
Table 2-1. Overview of the transition schedules and the respective ions selected for the native and isotope labelled peptides used for transporter quantification....**62**
Table 2-2. Overview of the transition schedule and the respective ions selected for the native and isotope labelled peptides used for transporter quantification....**63**
Table 2-3. Primer sequence and complementary hydrolysis probes used for the 8 selected genes analysed for relative gene expression analysis by real-time PCR.....**65**
Table 4-1. Donor demographics of intestinal samples including recent drug history in which protein abundances were quantified. **111**
Table 4-2. Precision (CV%) analysis is provided for transporter proteins in human intestinal total membrane (TM) digests (n=5) over 3 sample runs, on 2 separate days....**114**
Table 5-1. Physico-Chemical Properties of E-3-S, Metabolism & Transport Specificities **127**
Table 5-2. Endpoint TEER and LY permeability in filter-grown Caco-2 cell monolayers **130**
Table 5-3. Determining the binding of [3H]-E-3-S to BSA in transport buffer....**141**
Table 5-4. The effect of pH on monolayer integrity after lucifer yellow permeability assessment .**145**
Table 5-5. Transport of E-3-S and secretory efflux ratio in 10 and 29d Caco-2 cell monolayers at pH 7.4/7.4 under control conditions **148**
Table 5-6. The relationship between BCRP mRNA, total membrane protein abundance and E-3-S efflux ratio in 10 and 29d Caco-2 cell monolayers....**149**
Table 6-1. An outline of the methods specific to each laboratory for the absolute quantification of Na/K-ATPase, P-gp and BCRP **162**
Table 6-2. A comparative analysis of methods used for quantification of transporter protein absolute abundances across research groups **165**
Table 6-3. Individual abundances of human intestinal and Caco-2 cell monolayer with jejunal REF scaling factors **169**
Table 7-1. Physico-Chemical Properties of VBL, Metabolism & Transport Specificities....**185**
Table 7-2. Endpoint TEER and LY permeability in filter-grown Caco-2 cell monolayers at 21 days **188**
Table 7-3. The relationship between VBL efflux ratio, P-gp total membrane protein abundance and mRNA expression in all Caco-2 cell variants. **194**
Table 7-4.Three-compartment model structural parameters and initial drug parameter estimates **197**
Table 7-5. Model estimates of $P_{Passive}$ after simultaneous fitting of bi-directional VBL data....**198**
Table 7-6. Kinetic parameter estimates from simultaneous fitting by a three-compartment model and their relationship to P-gp abundance. **200**
Table 8-1.Recovery correction factors (RCF's) generated for Na/K-ATPase and villin to correct for protein loss in membrane fractionation....**224**
Appendix Table A-1. Donor demographics of intestinal samples, including recent drug history, in which alkaline phosphatase activity was determined **236**
Appendix Table D-1. Individual transporter protein abundance data from human intestinal tissues quantified by the QconCAT (also see Figure 4-12). **245**
Appendix Table E-1. Individual PPIA normalised mRNA gene expression of P-gp, MRP2 and BCRP in low passage Caco-2 cells **246**
Appendix Table E-2. Individual PPIA normalised mRNA gene expression of OATP2B1, OST-α and OST-β in low passage Caco-2 cells.....**247**
Appendix Table E-3. Individual Na/K-ATPase abundances in 10 to 29d cultured Caco-2 cells (p25-35) quantified at Bertin Pharma **247**
Appendix Table E-4. Individual Na/K-ATPase abundances in 10 to 29d cultured Caco-2 cells (p25-35) quantified at the University of Manchester....**248**
Appendix Table E-5. Individual P-gp abundances in 10 to 29d cultured Caco-2 cells (p25-35) quantified at Bertin Pharma....**248**
Appendix Table E-6. Individual P-gp abundances in 10 to 29d cultured Caco-2 cells (p25-35) quantified at the University of Manchester....**249**
Appendix Table E-7. Individual BCRP abundances in 10 to 29d cultured Caco-2 cells (p25-35) quantified at Bertin Pharma....**249**
Appendix Table E-8. Individual BCRP abundances in 10 to 29d cultured Caco-2 cells (p 25-35) quantified at the University of Manchester....**250**
Appendix Table E-9. Batch differences for Na/K-ATPase, P-gp, and BCRP protein abundances in Caco-2 cell 21 and 29d harvested TM fractions sent to Bertin Pharma **250**
Appendix Table E-10. Individual MRP2, OATP2B1, OST-α and OST-β abundances in 10 to 29d cultured Caco-2 cells (p25-35) quantified at the University of Manchester. **251**

Appendix Table E-11. E-3-S and Ko143 permeability for individual Caco-2 monolayers at pH6.5/7.4. ..... **252**
Appendix Table E-12. E-3-S and Ko143 permeability for individual Caco-2 monolayers at pH7.4/7.4. ..... **252**
Appendix Table E-13. E-3-S and Ko143 permeability for individual Caco-2 monolayers at pH6.5/6.5. ..... **253**
Appendix Table G-1. Individual PPIA normalised mRNA gene expression of P-gp, MRP2 and BCRP in Caco-2 cell variants **255**
Appendix Table G-2. Individual Na/K-ATPase abundances in 21 day cultured Caco-2 cells variants quantified at Bertin Pharma **255**
Appendix Table G-3. Individual P-gp abundances in 21 day cultured Caco-2 cells variants quantified at Bertin Pharma **256**
Appendix Table G-4. Individual Caco-2 monolayer variant permeability's of vinblastine (0.03 μM) with and without verapamil **256**
Appendix Table G-5. Kinetic bi-directional permeability data (in triplicate filters) in Caco-2 variants for vinblastine **257**

Abstract

The University of Manchester
Matthew Harwood
Doctor of Philosophy

Towards a Fully Mechanistic Prediction of Oral Drug Absorption:
Investigating Intestinal Transporter Abundance & Function Relationships
2015

Background: Elucidating the role of intestinal drug transporter function in drug development is crucial, as transporter proteins can impact on drug absorption, efficacy and adverse events. In Vitro-In Vivo Extrapolation linked to Physiologically-Based Pharmacokinetic (IVIVE-PBPK) models aim to predict the *in vivo* impact of transporters from *in vitro* cell–based transport data and expression-based scaling factors. Currently, these models depend on relative measurements of transporter expression *i.e.,* mRNA or immunoblotting. There is a critical need for physiologically relevant measures of transporter protein abundance to populate these biological frameworks.
Objectives: The key objectives were to develop and validate a targeted proteomics workflow to quantify transporter protein abundances in human enterocytes and Caco-2 cells with a QconCAT technique. A cross-laboratory comparison on matched samples was also performed to assess between-laboratory bias in abundance determination. Together with abundance data from each laboratory, BCRP and P-gp transporter activities from Caco-2 cells were used to identify function-abundance relationships, to facilitate the potential development of abundance-function scaling factors.
Results: Development of a differential centrifugation technique to obtain plasma membranes was undertaken using MDCK-II and Caco-2 cells. The plasma membrane fraction showed little enrichment from the preceding total membrane fraction and was contaminated with endoplasmic reticulum, as assessed by marker enzyme activities. There were also no differences in Na/K-ATPase, BCRP and P-gp abundances between plasma and total membrane fractions in Caco-2 cells. This may be due to losses of protein from the target membrane fraction, thus, a theoretical framework combining protein assay (BCA) and transporter abundance determinations was proposed. Pilot data on the generation of recovery correction factors using Villin and Na/K-ATPase abundances, to account for protein losses is also presented.
The abundances of 6 transporters in jejunal enterocyte membranes (n=3), including the key efflux proteins BCRP (2.56±0.82 fmol/µg), P-gp (1.89±1.07 fmol/µg) and MRP2 (0.59±0.246 fmol/µg) were determined with precision. In addition, peptide losses during protein digestion stages were accounted for in abundance determinations.
A cross laboratory comparison of transporter abundances from intestinal (n=4) and Caco-2 cells (n=7) measured in our laboratory and Bertin Pharma (BPh), showed that P-gp abundances were highly correlated (rs=0.72), yet BPh abundances were systematically lower than determined in our laboratory (2.0±2.08 *versus*. 4.8±3.51 fmol/µg, respectively). No differences or correlations were found for Na/K-ATPase and BCRP abundances between laboratories. A jejunal-Caco-2 cell relative expression factor (REF) for each protein for both laboratories was generated. The P-gp REF was similar for BPh and our laboratory (0.37 vs. 0.4, respectively) however, for BCRP there was a distinct difference (1.11 *versus* 2.22, respectively). These findings provide the first evidence that employing expression factors generated from abundances quantified in different laboratories may produce altered IVIVE-PBPK outcomes.
Functional studies in Caco-2 cells using E-3-S and vinblastine as probes for BCRP and P-gp, respectively, show that protein abundance is more closely correlated to transporter activity than mRNA expression. In addition, it was only possible to verify that increasing P-gp abundances in Caco-2 cells were ranked alongside vinblastine intrinsic clearance, as there was little consistency when estimating Km between the different Caco-2 cell models expressing increasing P-gp abundances, which may be attributed to limited absorptive transport saturation. Thus, forming any conclusions with confidence on concentration dependent abundance-activity relationships was difficult. These data suggest the value of REF scaling factors based on protein abundances, but emphasises the need to generate these from both *in vitro* and *in vivo* samples, using the same proteomic workflow. Further work to verify abundance-function relationships is required.
Conclusion: A targeted proteomic workflow has been developed allowing quantification of protein abundances for key drug transporters in human gut tissues and cell models. The study has highlighted important areas including losses of targeted proteins, contamination of plasma membrane fractions and standardisation between laboratories that need to be addressed before implementation of transporter abundances into PBPK models is undertaken. Nevertheless, the evidence for a close relationship between transporter abundance and function indicate the potential value of this data for generation of robust REF scaling factors.

Declaration

No portion of this work referred to in this thesis has been submitted in support of an application for another degree or qualification of this or any other university of other institute of learning.

Copyright Statement

i. The author of this thesis (including any appendices and/or schedules to this thesis) owns certain copyright or related rights in it (the “Copyright”) and s/he has given The University of Manchester certain rights to use such Copyright, including for administrative purposes.

ii. Copies of this thesis, either in full or in extracts and whether in hard or electronic copy, may be made **only** in accordance with the Copyright, Designs and Patents Act 1988 (as amended) and regulations issued under it or, where appropriate, in accordance with licensing agreements which the University has from time to time. This page must form part of any such copies made.

iii. The ownership of certain Copyright, patents, designs, trade marks and other intellectual property (the “Intellectual Property”) and any reproductions of copyright works in the thesis, for example graphs and tables (“Reproductions”), which may be described in this thesis, may not be owned by the author and may be owned by third parties. Such Intellectual Property and Reproductions cannot and must not be made available for use without the prior written permission of the owner(s) of the relevant Intellectual Property and/or Reproductions.

iv. Further information on the conditions under which disclosure, publication and commercialisation of this thesis, the Copyright and any Intellectual Property and/or Reproductions described in it may take place is available in the University IP Policy (see http://documents.manchester.ac.uk/DocuInfo.aspx?DocID=487), in any relevant Thesis restriction declarations deposited in the University Library, The University Library’s regulations (see http://www.manchester.ac.uk/library/aboutus/regulations) and in The University’s policy on Presentation of Theses.

Dedication

To my wife Alice and son William,

I hope I can do you proud

Acknowledgements

Thank you to my primary supervisor, Dr Geoffrey Warhurst for his continued support of this project; I hope I have enlightened you as much as you have enlightened me over the course of this PhD project.

Professor Amin Rostami-Hodjegan, you provided me with the opportunity to pursue my ideas in this exciting research area by enabling me to write the grant to sponsor this work. Your energy, intellect and ideas are an inspiration.

Thank you to Professor Gordon Carlson, Dr Zeni Haveliwala, Dr Sotoyne Tolofari and Dr James Berry for providing the access to, and for consenting the participants, permitting the work with the intestinal samples presented in this thesis.

Pamela Davies, you provided so much support with culturing the cells and lent an ear in times of need, thank you.

To my proteomics colleagues, Dr Matthew Russell and Dr Brahim Achour, you showed me the ropes with great patience and taught me about a new and fascinating area, thank you.

Thank you to my Simcyp colleagues, particularly Dr Sibylle Neuhoff, your insightful ideas have moved this project forward and Dr Howard Burt, for providing support on the kinetic modelling.

Thank you to The Royal Commission for the Exhibition of 1851 and Simcyp Ltd for providing the funding to undertake this work.

To my wife Alice! We have been through plenty over the course of this PhD and our lives have changed dramatically. You have held the fort and been a terrific support especially in the toughest times, you have made this all the more enjoyable and I could not have done this without you.

List of Contributed Publications

1. **M.D. Harwood**, S. Neuhoff, G.L. Carlson, G.Warhurst, A. Rostami-Hodjegan. Absolute Abundance and Function of Intestinal Drug Transporters: A Prerequisite for Fully Mechanistic *In Vitro-In Vivo* Extrapolation of Oral Drug Absorption. Biopharm Drug Dispos, 34, (2013), 2-28.
2. M.R. Russell, B. Achour, E.A. Mckenzie, R. Lopez, **M.D. Harwood**, A. Rostami-Hodjegan, J. Barber, Alternative fusion protein strategies to express recalcitrant QconCAT proteins for quantitative proteomics of human drug metabolizing enzymes and transporters, J Proteome Res, 12 (2013) 5934-5942.
3. **Matthew D Harwood**, Matthew R Russell, Sibylle Neuhoff, Geoffrey Warhurst, Amin Rostami-Hodjegan. Lost in Centrifugation! Accounting for Transporter Protein Losses in Quantitative Targeted Absolute Proteomics (QTAP). DMD, 42, (2014b), 1766-1772.
4. E. Sjogren, B. Abrahamsson, P. Augustijns, D. Becker, M.B. Bolger, M. Brewster, J. Brouwers, T. Flanagan, **M. Harwood**, C. Heinen, R. Holm, H.P. Juretschke, M. Kubbinga, A. Lindahl, V. Lukacova, U. Munster, S. Neuhoff, M.A. Nguyen, A. Peer, C. Reppas, A.R. Hodjegan, C. Tannergren, W. Weitschies, C. Wilson, P. Zane, H. Lennernas, P. Langguth, In vivo methods for drug absorption - comparative physiologies, model selection, correlations with in vitro methods (IVIVC), and applications for formulation/API/excipient characterization including food effects, Eur J Pharm Sci, 57, (2014), 99-151.
5. **M.D. Harwood**, B. Achour, M.R. Russell, G.L. Carlson, G. Warhurst, A. Rostami-Hodjegan. Application of an LC-MS/MS Method for the Simultaneous Quantification of Human Intestinal Transporter Proteins Absolute Abundance using a QconCAT Technique. J Pharm Biomed Anal, J Pharm Biomed Anal, 110, (2015), 27-33.

Abbreviations

AALS	Anionic Acid Labile Surfactant
ABC	ATP-Binding Cassette Superfamily of Transporters
ABL	Apical Boundary Layer
ACAT	Advanced Compartmental Absorption and Transit
ADAM	Advanced Dissolution, Absorption and Metabolism
ADME-T	Absorption, Distribution, Metabolism, Excretion and Toxicity
ANOVA	Analysis of Variance
AP	Alkaline Phosphatase
AQUA	Absolute Quantification
ATCC	American Type Tissue Culture Collection
A-to-B	Apical to Basolateral Transport
ATP1A1	Protein family nomenclature for Na/K-ATPase
BCA	Bicinchoninc
BCRP	Breast Cancer Resistance Protein
BLQ	Below the Limit of Quantification
BPh	Bertin Pharma
B-to-A	Basolateral to Apical Transport
Caco	Colon Carcinoma
CE	Collision Energy
CLint	Intrinsic Clearance
CV	Coefficient of Variation
CCR	Cytochrome C Reductase
CYP	Cytochrome P450
DC	Differential Centrifugation
DDA	Data-Dependent Acquisition
DDI	Drug-Drug Interaction
DMSO	Dimethylsulfoxide
DOC	Sodium Deoxycholate
DTT	Dithiothreitol
DMEM	Dulbecco’s Modified Eagle’s Medium
E-3-S	Estrone-3-Sulfate
EnR	Endoplasmic Reticulum
ER	Efflux Ratio

fa	Fraction absorbed
EDTA	Ethylenediaminetetraacetic acid
EGTA	Ethyleneglycoltetraacetic acid
FASP	Filter Aided Sample Preparation
F_G	Fraction of drug escaping gut wall metabolism
F_H	Fraction of drug escaping hepatic metabolism
GAPDH	Glyceraldehyde 3-Phosphate Dehydrogenase
FR	Fraction Recovered
GI	Gastrointestinal
Glu-Fib	Glu-Fibrinopeptide B
GMFB	Geometric Mean Fold Bias
GMFE	Geometric Mean Fold Error
HBSS	Hanks Balanced Salt Solution
HEK	Human Embryonic Kidney
HEPES	4-(2-hydroxyethyl)-1-piperazineethanesulfonic acid
HP	High Passage
HPLC	High Performance Liquid Chromatography
HPT1	Human Peptide Transporter
IAA	Iodoacetamide
ISEF	Inter-System Extrapolation Factor
IVIVE	In Vitro-in Vivo Extrapolation
Jmax	Maximal flux capacity of the transport protein
K_{CAT}	Catalytic rate constant
KCl	Potassium Chloride
Km	Michaelis-Menten constant
LC-MS/MS	Liquid-Chromatography-Coupled to Tandem Mass Spectrometry
LLC-PK_1	Lilly Laboratories Cells - Porcine Kidney Nr. 1
LLOQ	Lower Limit of Quantification
LSC	Liquid Scintillation Cocktail
LY	Lucifer Yellow
LYS-C	Lysyl endopeptidase
MDCK-II	Madine Darby Canine Kidney
mDDI	Metabolic Drug-Drug Interaction
MDR1	gene product of the Multidrug Resistance Protein 1

MES	2-(N-morpholino)ethanesulfonic acid
MgCL	Magnesium Chloride
MPPGL	Microsomal Protein Per Gram of Liver
MPPI	Microsomal protein per whole intestine
MRM	Multiple Reaction Monitoring
MRP2	Multidrug Resistance-associated Protein 2
MSP	Microsomal Protein
PBPK	Physiological-Based Pharmacokinetic (model)
PPIA	Peptidyl Propyl Isomerase A (Cyclophilin A)
NaCl	Sodium Chloride
Na/K-ATPase	Sodium/Potassium-ATPase
NALS	Non-ionic Acid Labile Surfactant
NBD	Nucelotide Binding Domain
NNOP	Non-Naturally Occurring Peptide
NTCP	Sodium Taurocholate Co-transporting Polypeptide
OATP2B1	Organic Anion Transporting Polypeptide family member 2B1
OCT	Organic Cation Transporter
OST	Organic Solute Transporter
Papp	Apparent Permeability Co-efficient
PBS	Phosphate Buffered Saline
PBPK	Physiologically-Based Pharmacokinetic (Model)
PepT1	Peptide Transporter 1
P-gp	P-glycoprotein
PM	Plasma Membrane
PMPPGL	Plasma Membrane Protein per Gram of Liver
P-NP	P-Nitrophenyl
P-NPP	P-Nitrophenylphosphate
PCR	Polymerase Chain Reaction
$P_{Passive}$	Passive Permeability
QC	Quality Control
QconCAT	Quantification Concatamer
QTAP	Quantitative Targeted Absolute Proteomics
RCF	Recovery Correction Factor
RE	Relative Error

REF	Relative Expression Factor
RF	Recovery Factor
RMSE	Root Mean Square Error
RT	Reverse Transcription
SA	Surface Area
SCX	Strong Cation Exchange
SDS	Sodium Dodecyl Sulphate
SIL	Standard Isotope Labelled
SILAC	Stable Isotope labelling of Amino Acids in Culture
SILAM	Stable Isotope labelling of Amino Acids in Mammals
SLC	Solute Carrier Superfamily of Transporters
SNP	Single Nucleotide Polymorphism
SRM	Selected Reaction Monitoring
TBS-T	Tris Buffered Saline-Tween
TCEP	Tris(2-carboxyethyl)phosphine
tDDI	Transporter Drug-Drug Interaction
TEER	Trans Epithelial Electrical Resistance
TM	Total Membrane
TP	Total protein (akin to whole cell lysate or tissue homogenate)
TransCAT	QconCAT construct designed for transporter protein quantification
TSE(M)	Tris-Sucrose-EGTA-(Magnesium) Buffer
UBL	Unstirred Boundary Layer
UGT	Uridine 5’-diphospho glucuronosyltransferase
UoG	University of Greifswald
UoM	University of Manchester
VBL	Vinblastine

Chapter 1 – General Introduction

Declaration

In the interests of brevity, additional details relating to the topics covered in the general introduction to this thesis can be found in the comprehensive review article written by the PhD candidate:-

M.D. Harwood et al., (***2013)****, Biopharm Drug Dispos. 34, 2-28.*

Excerpts of text from this chapter are extracted from the aforementioned article.

1.1 Introduction

The use of whole body physiologically-based pharmacokinetic (PBPK) models, linked with *in vitro-in vivo* extrapolation (IVIVE) of kinetic parameters from laboratory experiments, is becoming more embedded into practices within many of the pharmaceutical industry, is used as part of regulatory submissions and is cited in drug labelling for newly approved drugs (Rostami-Hodjegan et al., 2012; Smith, 2012; Zhao et al., 2012). The IVIVE practices include the prediction of oral drug absorption, accounting for gut metabolism and the simultaneous assessment of the potential influence of drug transporter proteins, a subject with an increased awareness amongst the science community (Zamek-Gliszczynski et al., 2013). This thesis aims to progress knowledge within the transporter IVIVE field to; develop better tools to quantify transporter expression, to use these to understand the relationships between the amount of transporter and function and, to determine whether this facilitates development of better predictive models of oral PK. This project was, in part, voted for by the members the Simcyp consortium of pharmaceutical companies as part of the annual 'wish list', which guides the development of IVIVE-PBPK practices. The candidate wrote the grant which was subsequently approved and co-funded by a charitable body, 'The Royal Commission for the Exhibition of 1851' (Harwood et al., 2013).

1.2 Oral Drug Absorption

The majority of therapeutic agents today are orally administered, since oral administration is usually preferred by the patient and can encourage compliance. In addition, oral formulations normally cost less to produce, even when poor drug solubility or degradation by enzymes or acidic conditions in the gastrointestinal tract (GI) need to be addressed. Thus, predicting the rate and extent of oral drug absorption accurately is a prerequisite of modern drug development. However, this becomes a significant challenge when it requires a detailed understanding of the complex role of drug transporters in the gut wall and the interplay between the physicochemical properties of a drug and the physiological parameters. Many of the factors potentially influencing drug absorption, including metabolising enzymes and transporters, are subject to regional differences along the gut wall that defines the absorptive barrier (the gut mucosa) (Varum et al., 2010). A coordinated framework across multiple groups 'Oral Bioavailability Tools (OrBiTo)' is currently ongoing to enhance our ability to predict oral drug absorption, in which work within this project is incorporated (Sjogren et al., 2014).

The bioavailability (F) of a drug can be directly (or indirectly) influenced by transporters expressed on either the apical or basolateral membranes of the enterocytes/colonocytes, affecting both the fraction of drug absorbed across the apical membrane (f_a), the fraction of drug escaping gut wall metabolism (F_G) (Benet, 2009) and the fraction of drug escaping hepatic metabolism (F_H) occurring down-stream in the liver, the first pass effect (Equation 1-1).

$$F = f_a \times F_G \times F_H = f_a \times (1 - E_G) \times (1 - E_H)$$ Equation 1-1

The processes that govern bioavailability, including gut transporters, can be of benefit or hindrance to drug action, depending on the compound in question. If the drug concentration at the target site (*i.e.,* liver for statins) is too low due to an extensive first pass effect, then the pharmacological action of the drug may not be conferred. Alternatively, a restricted first pass effect allowing a higher drug concentration in systemic blood and, therefore, increased organ drug concentrations can lead to a greater potential for tissue toxicity (*i.e.,* rhabdomyolysis). Therefore, understanding the role of transporters during early drug discovery and development by means of *in vitro* studies is becoming more common, although the ability to interpret the results from these studies and to extrapolate them quantitatively to *in vivo* effects is fraught with many unresolved problems (Jones et al., 2012).

1.3 PBPK-IVIVE Modelling & Simulation Approaches

Traditionally, PBPK models contain the mass and volume of a number of compartments corresponding to different organs interconnected by blood flows, where differential equations govern the mass transfer of drug into and out of these organs to generate drug tissue concentration-time profiles. These compartments were historically treated as perfusion-limited. PBPK models have been extended to incorporate models for drug absorption which take into account various physiological elements of the GI tract (Yu and Amidon 1999; Agoram et al., 2001; Tam et al., 2003; Jones et al., 2006; Jamei et al., 2009; Sun et al., 2010; Gertz et al., 2013). Moreover, in order to account for permeation and membrane transporter effects, many recent PBPK models treat the organs as permeability-limited compartments in combination with suitable algorithms to predict drug distribution (Rodgers and Rowland, 2007; Neuhoff et al., 2013). In PBPK models it is important to define and implement the elements that can influence the processes governing the fate of the drug within the tissues. It is critical when using modelling and simulation that the ‘system parameters’ describing the anatomy, physiology and genetics, their associated

variability and covariates within a given population are separated from those of the 'drug parameters' (Harwood et al., 2013; Jones and Rowland-Yeo, 2013).

The complexity of the human gut means that it cannot be easily reproduced within a laboratory setting. However, a host of *in vitro* assays together with the use of pre-clinical species are utilized in drug development to mimic the relationship between the intrinsic properties of the drug and the biological systems it encounters in man. Obtaining reliable *in vitro* physico-chemical, metabolism, permeability and transport data early in drug development permits the use of mechanistic in silico modelling and simulation techniques to scale from the *in vitro* setting, to gauge the impact of drug paritioning, permeability, metabolism and transporter(s) on drug disposition within an *in vivo* 'virtual human' (Tam et al., 2003; Badhan et al., 2009; Bolger et al., 2009; Darwich et al., 2010; Abuasal et al., 2012; Jones et al., 2012; Neuhoff et al., 2013; Varma et al., 2013). Hence, IVIVE links *in vitro* systems to the appropriate human *in vivo* system using algorithms and physiologically relevant scaling factors to bridge the gap between the *in vitro* and *in vivo* systems in a PBPK model (Rostami and Tucker 2007; Neuhoff et al., 2013). In early drug development an IVIVE approach allows assessment of the drug candidates in silico, without resorting to costly human administration, to improve safety, efficacy, candidate selection, dose optimisation and reducing drug attrition.

1.4 Oral Drug Absorption and the Role of Transporters

Transporter proteins are classified into two super-families, the ATP-Binding Cassette (ABC) and Solute Carrier (SLC), which together comprise greater than 400 proteins (http://nutrigene.4t.com/humanabc.htm, http://www.bioparadigms.org/slc/intro.htm). The ABC transporters move molecules through the energy generated by binding and hydrolysing ATP, while for the SLCs, solute transfer across the membrane is either via passive equilibrative transport based on local concentration gradients, or facilitated by co-transport with another molecule, resulting in cellular uptake (Li and Shu, 2014). A range of drug transporter proteins (approx. 30) expressed in the gut, liver, kidney and brain can impact directly or indirectly upon the pharmacokinetic processes of absorption, distribution, metabolism, excretion and toxicity (ADME-T), in turn playing a key role in the disposition and efficacy of drugs. The bioavailability of an orally administered drug is dependent to a large extent on the gut mucosal barrier which is composed of the unstirred boundary layer (UBL) and a polarized layer of epithelial cells (enterocytes), linked by tight junctions that form the structural barrier limiting the absorption of potentially toxic substances, including drugs, into the portal circulation. The drug can, in this process, also be metabolised

(either in gut lumen or gut wall). The epithelium expresses a variety of transporter proteins for endogenous compounds and xenobiotics capable of secreting compounds back into the gut lumen, which provides an additional "functional" barrier to the efficient oral absorption of therapeutics. Absorptive transporters (apical uptake or basolateral efflux), principally involved in nutrient absorption, are also present in the gut mucosa and are targeted to enhance drug absorption (Varma et al., 2010).

A key consideration in drug development is the role transporters play in oral dose non-linearity. It was demonstrated that increasing the oral dose of talinolol is associated with more than proportionate systemic exposure in humans, due to the role P-glycoprotein (P-gp, or the gene product of the multidrug resistance protein 1, MDR1) located on the apical membrane of the enterocyte to secrete (efflux) talinolol from the enterocyte into the lumen (Wetterich et al., 1996). The expression of P-gp is thought to vary along the GI tract, increasing towards the distal small intestine (Harwood et al., 2013; Drozdzik et al., 2014). Therefore, the functional impact of P-gp on drug absorption may be site dependent.

Another key apical efflux transport with broad substrate specificity is Breast Cancer Resistance Protein (BCRP). BCRP is implicated in restricting oral drug absortion (Su et al., 2007) and is shown to be expressed along the GI tract (Drozdzik et al., 2014). Multidrug resistance-associated protein 2 (MRP2), fulfils a similar functional role to P-pg and BCRP in the intestine. However, this apically localised transporter effluxes organic amphiphilic anions, including gluronidated molecules, rather than lipophilic cations favoured by P-gp and BCRP (Jemnitz et al., 2010). The distribution of MRP2 along the GI tract is uncertain as a meta-analysis of the literature showed that MRP2 was expressed at high levels in the proximal small intestine with considerably lower levels in the colon (Harwood et al., 2013). Yet in a recent study, the levels of MRP2 were higher in the colon than in the small intestine (Drozdzik et al., 2014). It is clear further work is required on these apical efflux transporters to determine their expression along the GI tract.

Intentional saturation of intestinal influx transporters can also be used to enhance the absorption of a compound via pro-drug strategies, leading to an increased bioavailability. The pro-drug of acyclovir, valcyclovir, relies on oligonucleotide influx transport by peptide transporter 1 (PEPT1), to enhance its permeability across the apical membrane of the enterocyte. However, when the active influx process saturates upon administration of high oral valcyclovir doses, there is an unexpected non-proportional reduction in the C_{max} and AUC and a delayed T_{max} (Weller et al., 1993).

Some transporter-mediated drug-drug interactions (tDDIs), whether involving absorption or disposition, can lead to adverse drug reactions or loss of efficacy. These are becoming of increasing concern to the regulatory bodies and pharmaceutical industry (Agarwal et al., 2013; Prueksaritanont et al., 2013). However, it should be noted that tDDIs are often confounded by metabolism-based DDIs (mDDIs). This follows since in most cases transporters and metabolic enzymes, including those resident in enterocytes compete for the parent compound and its metabolite(s) (Varma et al., 2013).

The transporter related problems for oral absorption does not apply to all drugs and may be related to the balance between the drugs passive permeability ($P_{Passive}$) and active transport. Nonetheless, since many new drug candidates no longer belong to biopharmaceutical classification I (highly permeable and highly soluble), *in vitro* screening to understand the role of drug transporters in gut wall permeability, has become a valuable tool in estimating tDDIs. *In vitro* screening could be a cost effective means to reduce adverse events or loss of efficacy in clinical practice due to tDDIs. The approach is encouraged in the latest regulatory 'DDI guidance' (CHMP, 2012; CDER, February 2012), despite the on-going debate on quantitative methods which should be applied to obtain information from such *in vitro* measurement.

1.5 *In Vitro* Systems and Determining Transporter Kinetics

To devise an effective mechanistic IVIVE strategy, incorporation of separate elements for the passive permeability and transporter-mediated flux is necessary. Subsequently, drug parameters are defined for each process within appropriate *in vitro* experiments and are used in conjunction with the models system parameters to predict the behaviour of the drug *in vivo*. When integrating drug parameters into a model, the key processes including active kinetics, after correction for the unbound fraction at the transporter binding site and deconvolution of the passive permeability, are often described by Michaelis-Menten kinetics (Km, Jmax or CLint) (Equation 1-2). It should be noted that passive permeability refers to lipoidal bilayer (Kell and Oliver, 2014), bi-directional transport component that can neither, be inhibited induced or saturated.

$$CLint = \frac{Jmax \cdot [S]}{Km + [S]} \qquad \text{Equation 1-2}$$

where CLint is the intrinsic clearance due to active transport, Km is the Michaelis constant, Jmax (or sometimes termed Vmax) is the maximal flux capacity of the transport protein and S is unbound drug concentration (at the transporter binding site).

In vitro cell based systems are used routinely to elucidate passive and active transporter processes acting to influence drug permeability. Caco-2 cells grown to confluent monolayers in bicameral filter systems differentiate into enterocyte-like cells that endogenously express the majority of the relevant transporters that are also expressed in the human intestine *in vivo* (Hilgendorf et al., 2007; Hubatsch et al., 2007). Alternatively, sub cell lines of dog and pig cell lines, Madine Darby Canine Kidney (MDCK-II) and Lilly Laboratories Cells-Porcine Kidney-1 (LLC-PK_1), selected due to their low endogenous transporter expression of mdr1, bcrp and mrp2 are transfected with human transporter proteins (single, double and even triple transfected cells), (Hirouchi et al., 2009) and are used to determine the impact of transporter proteins on drug transport. To delineate the $P_{Passive}$ from Km, Jmax or CLint in Caco-2 or human-transporter transfected cells, compounds inhibiting a specific transporter isoform are applied to the system, with the flux remaining after inhibition assumed to be passive. Inhibition of active processes can be problematic due to the lack of specificity of transporter inhibitors for certain isoforms (Matsson et al., 2009), therefore inhibitor usage is not always an optimal method to determine $P_{Passive}$. Obtaining a passive flux/permeability coefficient that is due solely to the cell monolayer (transcellular permeability) and not system specific characteristics, the correction for paracellular permeability, the UBL and filter impedance is also employed (Artursson and Karlsson, 1991; Karlsson and Artursson, 1991).

1.5.1 The Pitfalls of Determining Transporter Kinetics by Conventional Approaches

Active transport processes are conventionally determined using a 1-site binding Michaelis-Menten model by monitoring bi-directional drug transport across multiple substrate concentrations in filter-grown monolayer systems. It is assumed that Km, a biochemical constant, is similar in both transport directions if the buffer conditions *i.e.,* pH, are similar on both sides (Troutman and Thakker, 2003b). Using this approach however has several limitations including; the use of nominal donor drug concentrations, disregard for time and concentration-dependent integration of passive and active processes to estimate kinetic parameters and a limited consideration for the experimental system (Harwood et al., 2013). This approach has given rise to considerable bias in the estimation of apparent-Km, *i.e.,* a 'Km shift' (Horie et al., 2003; Troutman and Thakker, 2003b; Balakrishnan et al., 2007; Korjamo et al., 2007; Shirasaka et al., 2008). For a comprehensive appraisal of the potential grounds for this event, see these commentaries (Harwood et al., 2013; Zamek-Gliszczynski et al., 2013).

Drug concentrations within the donor and acceptor compartments are dynamic, thus assuming a nominal drug concentration, a common practice using the conventional Michaelis-Menten approach

to describe drug transfer processes is likely to lead to kinetic inaccuracies. Theoretically, for efflux transporters where binding sites are thought to be located facing the cytoplasm or inner membrane leaflet (Aller et al., 2009), the critical concentration driving active efflux is the unbound intracellular or membrane concentration (Korzekwa et al., 2012), therefore nominal concentrations in the donor compartment do not necessarily reflect the membrane or intracellular concentrations driving efflux. If the intracellular drug concentrations are substantially higher than the Km, active efflux saturates, leading to increasing intracellular drug concentrations and a high outwardly directed concentration gradient, driving a greater passive transfer of drug from the cell to the apical compartment, until equilibration is reached (Korjamo et al., 2007). If the appropriate unbound concentrations in all compartments are not considered at regular time increments, the synergistic active and passive processes are not accurately considered for subsequent statistical evaluation to estimate kinetics. Determining unbound intracellular drug concentration is a considerable challenge at early time points and may be critical for uptake transport investigations where ascertaining initial drug transfers between compartments will govern subsequent concentration dependent processes (Soars et al., 2007). Ultimately, if biased data are incorporated into an IVIVE model, erroneous outcomes are likely.

1.5.2 Determining Transporter Kinetics by Mechanistic Compartmental Models

The International Transporter Consortium, advocate that using mathematical models to describe drug concentration time courses at transporter binding sites should be performed, in order to accurately determine the intrinsic kinetics of active processes (Zamek-Gliszczynski et al., 2013). Using a global kinetic approach to simulate the time course of drug concentrations in multiple compartments of filter-based systems has now been undertaken by numerous groups (Kalvass and Pollack, 2007; Proctor et al., 2008; Heikkinen et al., 2010; Tachibana et al., 2010; Rolsted et al., 2011; Sugano et al., 2011; Korzekwa et al., 2012). By integrating the experimental kinetic data generated from *in vitro* cell systems possessing varying levels of P-gp into compartmental models, intrinsic Km values that were independent of P-gp expression were obtained, consistent with the notion of Km as a biochemical constant (Shirasaka et al., 2008; Tachibana et al., 2010; Sugano et al., 2011; Korzekwa and Nagar, 2014).

Key components to model drug transport-permeability time courses using real examples *in vitro* involve: sampling at multiple time points and concentrations in the donor and receiver compartments; estimating or measuring the unbound fraction of drug in the extra and intracellular milieu and defining the structure of the experimental system. The unbound fraction in the cell (fu_{cell})

can be difficult to measure experimentally. Nonetheless, the monolayer could be lysed to release intracellular contents with subsequent addition of the drug to the lysed cellular components (Sun et al., 2008). Drug partitioning between lysed cell components and the supporting media is then assessed to estimate fu_{cell} or binding in subcellular compartments, *i.e.,* lysomes. However, it was found that binding can vary considerably between cell types, therefore caution is advised when translating from binding prediction models which differ from the system under study (Mateus et al., 2013). Intracellular binding has also been estimated using simultaneous fitting within a compartmental model framework (Menochet et al., 2012a; Menochet et al., 2012b). It was noted that a lower extent of binding existed when comparing an experimental approach *versus* a simultaneous fitting approach in hepatocytes (Mateus et al., 2013). Monolayer volumes could be measured by determining individual cell volumes by flow cytometry (Oehlke et al., 2011), isotope dilution (Reinoso et al., 2001), microscopy (Heikkinen et al., 2010) and protein content (Burnham and Fondacaro, 1989). Therefore, a combination of experimental and compartmental modelling approaches may be advantageous to predicting intrinsic transporter kinetic parameter estimates.

1.6 IVIVE-PBPK Linked Models of Intestinal Transporters

In line with the advancement of PBPK models, is the increasing need for high quality biological data, including that for transporter expression, to enhance the proximity of the model's system parameters to the *in vivo* milieu. In addition, the IVIVE approach requires scaling factors to bridge any mechanistic gap between the *in vitro* systems used to represent the *in vivo* system and organ-based scaling factors. For any biological data incorporated into a PBPK model to generate scaling factors and drive functionality, there must be assurance as to the suitability of the data, and that any confounding factors associated with sample/tissue quality and methodological bias are factored into analysis prior to implementation (Harwood et al., 2013).

To model the intestine mechanistically, it is necessary to account for the region-specific anatomical and physiological differences that the compound encounters as it transits distally upon oral administration. This is achieved by representing the regions of the gut as compartments. The small intestine in a mathematical model generally contains seven segments, including one duodenal, two jejunal and 4 ileal segments, with each compartment potentially distinct from one another based on defined system parameters. Two of the most sophisticated models currently available are the Advanced Dissolution, Absorption and Metabolism (ADAM) model (Jamei et al., 2009; Darwich et al., 2010) and the Advanced Compartmental Absorption and Transit model (ACAT) (Yu and Amidon 1999; Abuasal et al., 2012), both of which now incorporate region-specific transporter

expression data. Both models demonstrate the utility of IVIVE approach to effectively address simultaneous gastrointestinal transporter-metabolism interplay by simulation.

Models of intestinal absorption have traditionally been based on predicting the permeability of drugs across the apical enterocyte membrane. A simple approach is to use a first order absorption model, in which there is a disregard for the region-specific physiology and variability typically represented within these mechanistic models. However, a more mechanistic IVIVE approach that does account for region-specific physiology and variability, is to utilise correlations linking the effective permeability (Peff) derived from loci-gut intestinal perfusion systems (Lennernas et al., 1993) to the apparent permeability (Papp) of *in vitro* cell monolayer systems (Sun et al., 2002; Yang et al., 2007). The loc-i-gut method relies on a human subject swallowing a tube system via the mouth which is fed into the jejunal region of the small intestine. Two ballons are inflated towards the front tips of the tubing and occlude a 10 cm piece of jejunum. It is assumed that this segment is now effectively sealed from material entering from the proximal or distal region. A drug is perfused down an inlet tube into the occluded 10 cm segment at a flow rate, deemed to be physiological, whereby the perfusate containing the drug is allowed to dwell for a set period of time. The drug is aspirated back up the tube and its concentration is measured. It is assumed that the differences in drug levels of the perfusate before and after dwelling in the occluded jejunal segment are due to disappearance across the gut wall, enabling the Peff to be calculated (Lennernas, 2007; Dahlgren et al., 2014). Other studies have generated correlations between physicochemical descriptors such as polar surface area and hydrogen bond donor number (Winiwarter et al., 1998) and facilitated the development of correlations from LLC-PK_1 and MDCK-II cells to predict in situ permeability (Tchaparian et al., 2008). Recently, models incorporating the structural architecture of the crypt-villus system have been implemented into the ADAM model, termed the Mechanistic Predicted Peff model (‘Mech Peff’). The model accounts for regional differences in passive permeability arising from distinct morphological differences in each intestinal region. It is aligned for use within early drug discovery as compound-specific physico-chemical parameters, $logP_{ow}$ (log of the octanol-water partition co-efficient), $logP_{PAMPA}$, molecular weight, pKa and their acid-base type can be used. Both the Papp-loci-gut-regression and Mech Peff models can incorporate the impact of transporters on drug absorption by the kinetic parameters already discussed.

1.7 Tissue and Relative Transporter Scaling Factors for IVIVE Oral Intestinal Absorption

1.7.1 Tissue-Based Scaling Factors – Membrane Protein Scalars

The IVIVE approach to predict drug pharmacokinetics relies on scaling factors from cells and subcellular fractions to bridge mechanistic gaps between the *in vitro* and *in vivo* system using expression-based scaling factors. An area within IVIVE that has been heavily studied is that of the metabolic scaling factors required for scaling a CLint per mg protein within hepatic-based *in vitro* assays, using the microsomal protein per gram of liver (MPPGL), to obtain a whole organ CLint. A similar scalar for intestinal metabolism is used that accounts for the microsomal protein per whole intestine (MPPI). However, none of the microsomal scalars are specific for transporter protein scaling, which should rely on plasma membrane (PM) protein scalars (Harwood et al., 2014). Recent studies broach this field and provide a crude membrane protein scalar for the liver (35.8 (n=13) and 37 mg (n = 65) crude membrane protein per gram of liver) (Tucker et al., 2012; Prasad et al., 2014). These values are similar to the human MPPGL derived from meta-analysis (Barter et al., 2007). In addition, Tucker's study provides a crude membrane protein per cm^2 of duodenal mucosal surface area of 1344 $\mu g/cm^2$, (n=14) for transporter scaling (Tucker et al., 2012). However, a plasma/brush border membrane-specific protein scalar rather than a crude membrane scalar could be more appropriate due to functional transporter protein expression on the PM.

1.7.2 Relative Transporter Expression Scaling Approach

There are known regional differences in transporter expression along the human intestine. The expression profile of P-gp in the ADAM model is shown in Figure 1-1. Further information on regional expression of MRP2, BCRP and CYP3A4 can be found in Figure 2 and Table 1 of the review article (Harwood et al., 2013). These models incorporate expression derived from relative quantitative methods to describe ABC or SLC transporter expression from immunoblot densitometry or mRNA gene expression. If mRNA expression is used it is assumed to directly correlate to protein activity, however, this may not always be the case (Berggren et al., 2007; Nies et al., 2013). A common practice when using relative expression data is to normalise the expression of a transporter throughout the intestine to a given segment, as is undertaken for transporter expression in the ADAM model, where all transporter expression data is normalised to the first jejunal segment. A study by Bruyere and co-workers has highlighted the importance of obtaining regional intestinal transporter expression data for incorporation in PBPK models (Bruyere

et al., 2010). Levels of the apical efflux transporters P-gp and BCRP were measured by immunoblot in various intestinal sites and the data implemented into the model was expressed relative to the ileum. The results demonstrated that accounting for the P-gp distributions enhanced PBPK predictions of bioavailability for the compound under study. Yet, a consensus as to the P-gp expression in the intestine using relative expression techniques has not been demonstrated (Bruyere et al., 2010; Abuasal et al., 2012; Harwood et al., 2013).

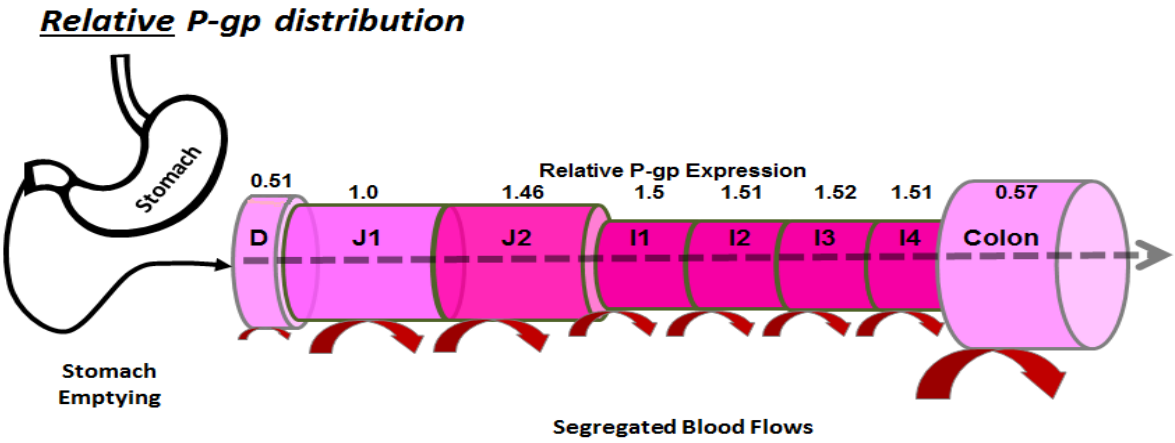

Figure 1-1. Schematic representation of the ADAM model, displaying the mechanistic segmentation of the GI tract into 9 sections with segregated blood flows to each section. The abundance of P-gp is highlighted by increasing segmental colour intensities with the relative P-gp expression having been normalised to the first jejunal segment (J1). D represents duodenum, J represents jejunum and I represents ileum. Normalised P-gp expression values are also provided above each compartment.

Predicting the impact of inter-individual variability in transporter expression and function within a population rather than in the individual human is advantageous in order to appreciate particular individuals who are at the greatest risk of adverse events. A weighted mean coefficient of variation (CV) is implemented into the ADAM model based on meta-analysis of relative expression techniques. However, where this relies on protein data alone, only relatively few data are incorporated, which may not be representative of a wider population (Harwood et al., 2013).

1.7.3 Relative Expression Factors (REFs) for Scaling

Expression based scaling factors have been used for many years in metabolic and transporter-based IVIVE (Proctor et al., 2004; Darwich et al., 2010). To account for any transporter expression differences in the *in vitro* system (Caco-2, MDCK-II) and the human jejunum, IVIVE scaling factors have been generated using immunoblot densitometry to provide REFs (Equation 1-3 for P-gp, MRP2 and BCRP (Harwood et al., 2013) that are utilised in published work (Darwich et al., 2010; Neuhoff et al., 2013). Indeed, a major limitation in using this REF, is that it is based on a single human jejunum that may not be representative of a population (Troutman and Thakker, 2003a).

$$REF = \frac{In\ Vivo\ Expression}{In\ Vitro\ Expression}$$

Equation 1-3

The REF scalar for transporters is not nearly as sophisticated the Inter-System Extrapolation Factor (ISEF) for metabolic scaling. The ISEF was devised to correct for differences in enzyme abundance and activity (per unit of Cytochrome (CYP)P450 isoform) in recombinant expression systems and human liver (Proctor et al., 2004). It is yet to be established if an expression-abundance scalar, such as the ISEF, is required for transporter IVIVE scaling. The limitations of immunoblotting have provided a barrier to the generation of transporter scalars utilising protein abundance data, *i.e.,* a lack of availability of transporter protein standards to enable transporter protein abundance determination. It is postulated that a substantial advancement in defining expression scaling factors, will arise from absolute transporter abundance data generated in both the human and the *in vitro* systems, where models can progress from this relative expression, semi-mechanistic approach (Harwood et al., 2013). An overview of transporter based IVIVE scaling factors discussed or utilised by other groups is provided in Figure 1-2.

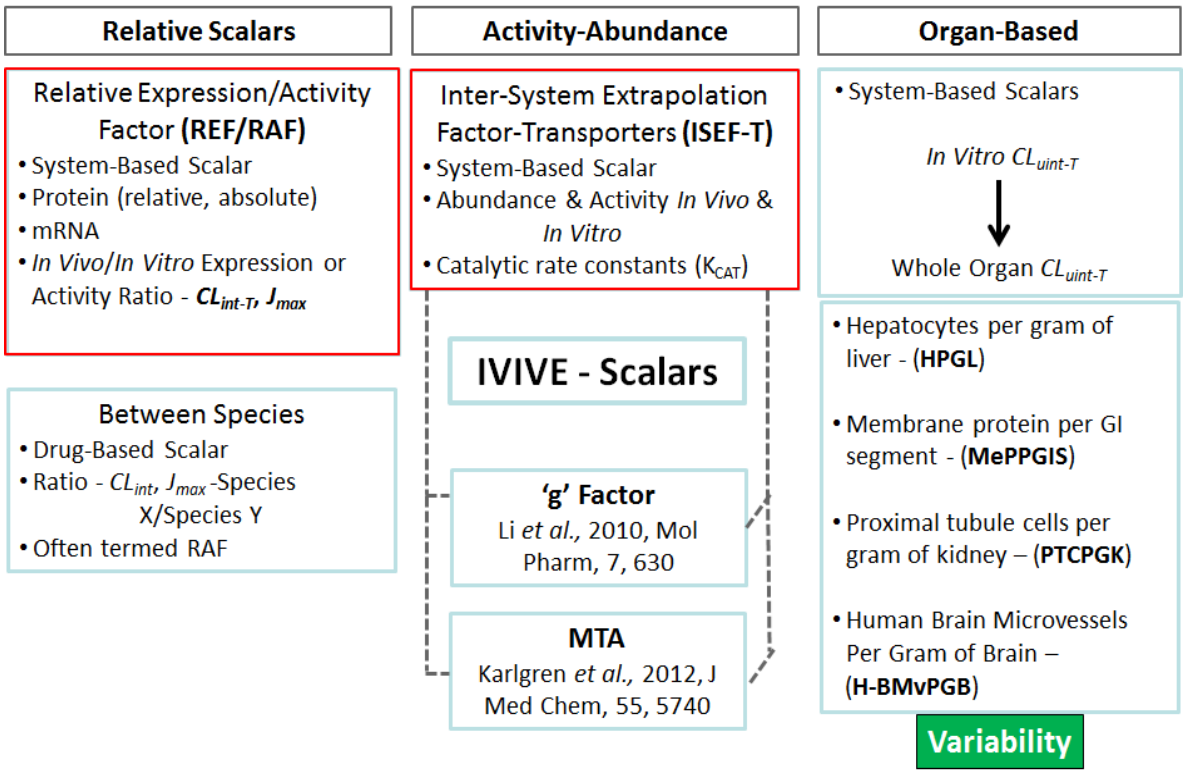

Figure 1-2. An overview the three categories of transporter-IVIVE scalars. The scalars boxed in red are the focus of this thesis. MTA is the maximal transporter activity scalar.

1.8 Transporter Abundance Determination by Mass Spectrometry

Since 2008, significant advances within proteomics using Liquid-Chromatography-Coupled to Tandem Mass Spectrometry (LC-MS/MS) (Kamiie et al., 2008; Li et al., 2008) and quantitative immunoblotting (Tucker et al., 2012) techniques, has enabled the determination of drug transporter protein abundances within human tissues (Li et al., 2009b; Li et al., 2009a; Niessen et al., 2010; Sakamoto et al., 2011; Shawahna et al., 2011; Uchida et al., 2011; Deo et al., 2012; Karlgren et al., 2012; Ohtsuki et al., 2012; Schaefer et al., 2012; Groer et al., 2013; Oswald et al., 2013; Prasad et al., 2013; Bosgra et al., 2014; Drozdzik et al., 2014; Prasad et al., 2014; Vildhede et al., 2014). To coordinate with mammalian tissue abundance measurements there has also been a focus on characterizing *in vitro* systems used routinely in drug development for determining the impact of drug transporters on drug disposition, for example Caco-2 (Miliotis et al., 2011b; Oswald et al., 2013), MDCK-II and LLC-PK_1 transfected cells (Kamiie et al., 2008; Li et al., 2008; Di et al., 2011; Zhang et al., 2011). With the exception of a single study (Tucker et al., 2012), quantifying absolute transporter abundances is achieved by LC-MS/MS based analysis.

1.8.1 LC-MS/MS Proteomic Techniques to Determine Transporter Abundances

The following sections principally focus on isotope labelled or ‘targeted’ proteomic strategies that are predominantly utilised for transporter protein absolute abundance quantification. However, relative estimates of protein quantities can be provided by employing label-free or ‘global’ proteomic techniques.

MS based absolute quantification techniques, or Quantitative Targeted Absolute Proteomics (QTAP), relies on the simultaneous analysis of an isotope labelled standard peptide and the equivalent non-labelled peptide derived from the biological matrix. The peak intensities of co-eluting equivalent standard and peptides from the biological sample can be utilised to quantitate the amount of protein within a sample. QTAP comprises 1), the selection of standard isotope labelled (SIL) proteotypic peptides used as surrogates of the whole protein for quantification of protein abundances in the sample and their subsequent isotopic labelling; 2), the purification of the subcellular fraction(s) that contain the proteins to be quantified; 3), the enzymatic digestion of the proteins into proteotypic peptides, and 4), simultaneous quantitation of the SIL and proteotypic peptides in the target biological matrix by LC-MS/MS (Ohtsuki et al., 2011; Harwood et al., 2014).

1.8.1.1 Selection and Labelling of Peptide Standards

The first stage within the QTAP strategy is to identify the transporter protein(s) to be quantified. In principal, any protein can be targeted for abundance quantification, if its entire amino acid sequence has been confirmed. This information can be sourced from databases such as www.uniprot.org. Proteins are typically too large to be separated and quantified by LC-MS/MS techniques therefore, targeted proteins require digesting into smaller peptide components using proteolytic enzymes such as trypsin. Numerous groups involved in quantifying transporter abundances by QTAP strategies employ in silico selection strategies, based on theoretical peptide yields after trypsin digestion. Furthermore, adherence to numerous additional criteria depicted as either, essential or favourable is also performed. The peptide standard selection criterion of numerous prominent research groups within the transporter proteomics field has already been expertly reviewed (Kamiie et al., 2008; Ohtsuki et al., 2011; Oswald et al., 2013; Uchida et al., 2013; Prasad and Unadkat, 2014; Qiu et al., 2014). The standard peptide selection criteria within our group includes selecting for uniqueness, size (7-25 amino acid residues), post-translational modifications, eliminating peptides containing residues prone to modification *i.e.,* methionine (oxidation), cysteine (alkylation) or asparagine (glycosylation) and avoidance of those in hydrophobic transmembrane spanning domains. A particular selection criterion which is not always centred upon is missed-cleavage by trypsin. Employing in silico tools such as 'conSEQUENCE' (Lawless and Hubbard, 2012), permits the selection of peptides that theoretically, possess a reduced incidence of missed cleavage events when undergoing trypsin digestion. This is employed at the University of Manchester (Russell et al., 2013). The suitability of the in silico selected peptides is subsequently confirmed in the laboratory with cost-effective non-labelled peptides with an equivalent sequence.

Within transporter proteomics, the selected peptides are either chemically labelled (*in vitro*), *i.e.,* the Absolute Quantification (AQUA) technique, or metabolically labelled (*in vivo*) using stable isotopes incorporating the Quantification Concatamer (QconCAT), Stable Isotope Labelling of Amino Acids in Culture (SILAC) or in Mammals (SILAM). The 'heavy' labelled sequence equivalent peptides undergo a mass shift, this distinguishes the standard peptides from the biologically derived peptide in the MS, even though the ionisation behaviour is similar.

1.8.1.2 Preparation of the Biological Sample

The measurement of integral membrane transporter protein abundance requires that the complexity of the biological sample is reduced (Huber et al., 2003). From a tissue and cellular

perspective, the heterogeneous nature of the intestine provides challenges to obtaining the intended membrane proteins for quantitation. The key transporters and metabolic enzymes reside within the enterocytes and are located in the mucosal layer; therefore homogenization of an intestinal tissue sample containing the entire tissue cross section is not appropriate for obtaining membrane protein preparations. The method of harvesting enterocytes from the underlying interstitial and muscle layers prior to membrane extraction can vary. Physical removal of enterocytes by crushing (Groer et al., 2013) or scraping the mucosa (Tucker et al., 2012) has been used in intestinal transporter abundance quantification. Chemical methods are also available utilising calcium chelation techniques to elute enterocytes (Galetin and Houston, 2006), however the utility of this approach for abundance quantitation has not been reported.

To measure transporter abundances, a further reduction in sample complexity is required due to their relatively low abundance within the proteome and to isolate the cells PM, in which the functionally relevant protein is localised. Membrane extraction procedures are employed to obtain a PM fraction by differential centrifugation (Kamiie et al., 2008). Alternatively, studies employ commercially available extraction kits that harvest a 'native' membrane protein fraction, that does not specifically purport to harvest a PM fraction (Li et al., 2009b), or kits that do propose to harvest the PM (Kumar et al., 2015). However, where tissue is sparse, transporter abundances have been obtaining in whole cell fractions (Uchida et al., 2011; Ohtsuki et al., 2013). An appraisal of the purity of the membrane fraction understudy is not routinely undertaken, therefore the proportion of contaminating components from other organelles than the PM is not known. A fraction used for endpoint abundance determinations containing a significant proportion of contaminating components will lead to a bias in abundance quantification.

1.8.1.3 Reduction, Alkylation and Proteolytic Digestion

The harvested membrane fractions are rich in hydrophobic integral membrane proteins which poses a problem for the application of subsequent in-solution proteolytic digestion procedures. Therefore, procedures to solubilise and denature the proteins are required prior to incubation with the proteolytic enzyme(s). Treatment with agents that disrupt membranes and solubilise the proteins are employed, examples are; sodium deoxycholate (DOC) (Balogh et al., 2013), urea (Karlgren et al., 2012) and commercially available surfactant preparations (Miliotis et al., 2011b). To denature and unwind the protein, di-sulphide bridge reduction at cysteine-cysteine residues is commonly undertaken with dithiothreitol (DTT) (Li et al., 2009b) or guanidinium hydrochloride (Kamiie et al., 2008). The free sulfhydryl groups are alkylated with iodoacetamide (IAA) to prevent

the reformation of disulphide bonds. The reduced and alkylated proteins are typically subject to proteolytic digestion overnight, with the endopeptidase trypsin, which favours cleavage at C-terminal side of arginine and lysine residues. However, some groups, including ours, have adopted the incubation of lysyl endopeptidase (Lys-C) prior to the trypsin stage (Karlgren et al., 2012; Achour et al., 2014). Lys-C cleaves only at lysine residues and may facilitate digestion to completeness in combination with trypsin.

1.8.1.4 Reverse-Phase LC

Prior to introduction to the MS, the digested peptides are separated by their hydrophobicity using reverse-phase LC. The LC separates out the analytes (peptides) over time with an increasing gradient of solvent, usually acetonitrile, from a highly aqueous to highly organic state, washing over a hydrophobic chromatography column consisting of silica with C18 side chains. This column configuration retains peptides until the acetonitrile concentration reaches a point in which the peptide is eluted. Hydrophilic peptides are eluted first with peptides consisting of increasing hydrophobicity following. Formic acid (0.1%) is maintained throughout the LC run to protonate basic residues as an ion source when entering the MS. Both nano and regular flow LC systems are used. However, nano-LC is particularly useful for low sample volumes and is also suggested to improve detection sensitivity (Qiu et al., 2014).

1.8.1.5 Peptide Mass Analysis

Triple quadrupole mass spectrometers are usually the instrument of choice for QTAP studies. The key attributes of triple quadrupole instruments is their selectivity and sensitivity, facilitating the quantification of pre-selected transition ions (fragmentation of peptide bonds between residues) for the peptides with a specific mass-charge ratio (m/z). This enables the quantification of low abundance peptides with a reduced likelihood of false positive events.

As alluded to in Section 1.8.1.1, non-labelled selected peptides are used to identify the most abundant ion transitions, typically 2-3, for each peptide, this is also known as selected or multiple reaction monitoring (SRM/MRM), which increases the selectivity of the system. A library of peptides containing the selected transitions is generated within suitable programs to direct the MS to select and monitor the relevant peptides separated by the LC system.

The peptides eluted by the LC system enter the ion source in liquid form (Figure 1-3), via a high voltage charged capillary needle. When combined with a nitrogen gas, nebulisation of the liquid ensues, forming a plume of predominantly positively charged peptides that are accelerated towards

to the entrance of a high vacuum mass analyser (Jonsson, 2001). The triple quadrupole instrument is composed of 3 quadrupoles in series, the first (Q1) and third (Q3) are mass analysers that also act as mass filters and the second (Q2) is a collision cell. A quadrupole is composed of 4 metal rods with alternating and opposing polarities, with the connection of the rods to a current to generate a radiofrequency (Jonsson, 2001). The setting of the current and radiofrequency permits a narrow range of m/z to pass through the quadrupole, therefore, the selectivity/specificity is high. In a triple quadrupole instrument, the Q1 selects the pre-cursor/parent ions. The precursor ion is subject to collision induced dissociation in Q2. Fragmentation of the precursor ion, is activated by collision when an inert gas is introduced into the cell generating product, predominantly b (C-terminal cleaved) or y (N-terminal cleaved) ions (Jonsson, 2001). The masses of the product ions are analysed in the Q3, the fragments that are not selected are discarded. This reduces ionic complexity prior to the detection of the selected ions at an electro-photomultiplier tube detection system, generating a current that is recorded as fragmentation spectra over the duration of the LC-MS/MS run. The problem with triple quadrupole mass analysis is that there is no relationship between the number of ions that make it through to the detector and the concentration of the starting material. Therefore, the QTAP strategy requires a calibrating standard.

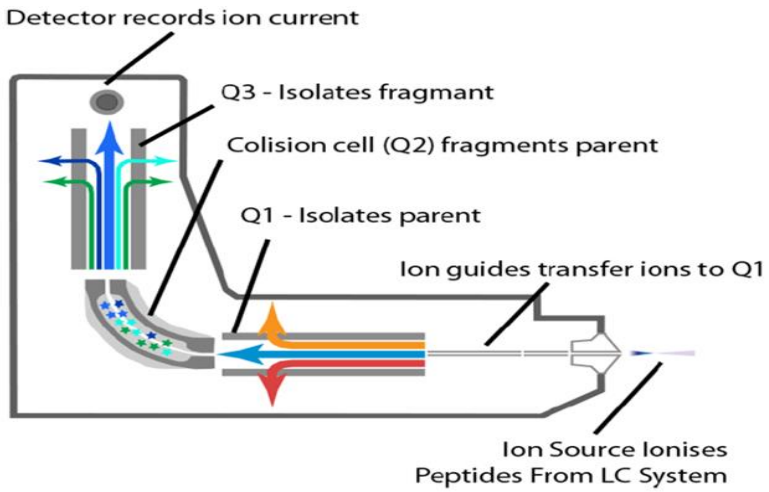

Figure 1-3. A representative illustration of the configuration of a triple quadrupole mass spectrometry instrument . Reproduced courtesy of Dr Matthew Russell, University of Manchester.

1.8.1.6 Absolute Quantification (AQUA) Standards

The AQUA approach to generate SIL standard peptides (Gerber et al., 2003) is the most commonly employed method to quantify transporter protein abundances (Kamiie et al., 2008; Li et al., 2008; Miliotis et al., 2011b; Deo et al., 2012; Groer et al., 2013; van de Steeg et al., 2013; Kunze et al., 2014; Vildhede et al., 2014). AQUA peptides can be chemically synthesised and purchased from

commercial suppliers. The standard peptides can be entered into the QTAP workflow prior to proteolytic digestion (Miliotis et al., 2011b), or more commonly post digestion (Kamiie et al., 2008; Groer et al., 2013). The peptide standards are run simultaneously with the peptides from the biological matrix, generating multiple co-eluting ion signal intensities. The standard-to-native signal intensity area ratio is calibrated against an external calibration curve to determine protein abundance.

1.8.1.7 Quantification Concatamer (QconCAT) Standards

The QconCAT technique is an alternative method for generating proteotypic SIL peptide standards for absolute protein quantification analysis (Beynon et al., 2005). The principle of the QconCAT technique is that selected quantification peptides (standards) are concatenated to form a string of peptides that are metabolically labelled within a host expression vector. The vector expresses the artificial construct containing the standard peptide labelled at the terminal lysine (K) or arginine (R) residues from labelled growth media. The artificial protein is extracted via a His-tag using affinity chromatography and is subjected to simultaneous proteolytic digestion with the biological matrix, to yield equimolar concentrations of standard peptides for quantification of target proteins (Simpson and Beynon, 2012; Russell et al., 2013). The construct is usually populated with two standard peptides per target protein and a host of non-naturally occurring peptides (NNOP) that enable the concentration of the QconCAT to be determined, in conjunction with the known concentration of the non-labelled ‘light’ NNOP. Similar to the AQUA method, the ratio of the area under the curve for the standard and native target peptides signal is required. Additionally, the ratio of ‘heavy’-to-‘light’ NNOP is required for QconCAT based quantifications. A distinct advantage of the QconCAT compared to AQUA is its cost-effectiveness when undertaking the analysis of multiple proteins. However, an important limitation for the QconCAT approach is access to expertise in recombinant molecular methods in order to generate the construct, and the potential of failure to express the construct, which can be time-consuming to resolve (Russell et al., 2013). Nevertheless, the construction of a QconCAT with the capability of quantifying transporter protein abundances is demonstrated by our group (Russell et al., 2013). Moreover, the utility of this approach to measure drug metabolising enzymes has been reported (Achour et al., 2014).

1.8.1.8 Label-Free MS Approaches

Label-free approaches for protein quantification do not possess calibrating standards to quantify the absolute abundance of target proteins. A large array of fragmentation spectra are generated which are submitted to databases such as MASCOT (www.matrixscience.com) to identify the

proteins responsible for fragment ion peaks. Label-free approaches are suitable for estimating the relative abundance of target proteins. However, a label-free approach has been undertaken in conjunction with an SIL approach to determine transporter abundances in human livers (Karlgren et al., 2012).

1.9 Absolute Transporter Abundances in IVIVE-PBPK

1.9.1 Between Laboratory Considerations

There is now a reasonable amount of transporter protein absolute abundance data available to harness within IVIVE-PBPK modelling, yet there is still relatively little data for the human intestine (Groer et al., 2013; Oswald et al., 2013; Drozdzik et al., 2014) or Caco-2 cells (Miliotis et al., 2011b) using LC-MS/MS or by quantitative immunoblotting (Tucker et al., 2012). However, caution should be exercised when implementing data into such models, therefore ascertaining potential confounding factors which could lead to any differences between laboratories requires appreciation. These differences may simply be based on inherent biological inter-individual variability; however, other biological factors may also require attention such as the influence of age, gender, disease and drug history, with particular relevance to induction of transporters due to drug exposure (Greiner et al., 1999). Another aspect requiring consideration are the differences in procedures employed throughout the QTAP workflow by different groups. To date, there has been no formal assessment of the potential bias imparted by the various methods used at each stage to obtain endpoint abundances between groups. This has recently been advocated using a matched sample approach (Harwood et al., 2014).

1.9.2 Absolute Abundance Generated REF

A REF scaling factor for P-gp using the intestinal abundance (Tucker et al., 2012; Groer et al., 2013; Oswald et al., 2013; Drozdzik et al., 2014) and Caco-2 cell monolayer data available in the literature can be generated (Miliotis et al., 2011b). The P-gp REF scalar can be potentially generated across the entire length of the intestine, given that the study of Drozdzik et al., quantified P-gp abundances in the most proximal intestinal region, the duodenum, and the distal region of the intestine, the sigmoidal colon (Drozdzik et al., 2014). At present, it is not evident if a bias in abundance generated between laboratories is apparent, therefore, using these data for IVIVE should be approached with caution. Ideally, the abundances of both the *in vitro* and *in vivo* systems should be measured in the same laboratory, generating an ‘in-house’ REF. It should be noted that transporter abundance data for flask-grown MDCK-II (Li et al., 2008; Zhang et al., 2011) and Caco-

2 cells (Oswald et al., 2013) are available, yet these preparations were not extracted from filters and therefore are also not appropriate for REF generation within IVIVE.

Table1-1. A summary of the available literature transporter abundance data in human intestinal regions.

Intestinal Region	Transporter Protein												Source
	P-gp	MRP2	MRP3	BCRP	ASBT	HPT1	PepT1	OATP2B1	OCT1	OCT3	OST-α	Na/K-ATPase	
Duodenum	✓	✓	✓	✓	✓	✓	✓	✓	✓	✓	**X**	**X**	(Tucker et al., 2012) (Groer et al., 2013)
Jejunum	✓	✓	✓	✓	✓	✓	✓	✓	✓	✓	✓	✓	(Oswald et al., 2013)
Ileum	✓	✓	✓	✓	✓	✓	✓	✓	✓	✓	✓	✓	(Drozdzik et al., 2014)
Colon	✓	✓	✓	✓	✓	✓	✓	✓	✓	✓	**X**	**X**	(Harwood et al., 2015)

1.9.3 Intestinal PBPK Models and Absolute Transporter Abundances

As shown in Figure 1-1, the relative approach provides segmental expression of transporters normalised to the first jejunal segment. Incorporating absolute abundances into the intestine changes the model structure, in that, segments become inter-dependent, therefore transporter expression is not reliant on normalisation to a given segment. Transporter abundances are given in concentrations per segment or unit area, rather than as unit-less scalars, enabling a more physiological approach. The study by Drozdzik et al., measured P-gp abundance in multiple segments along the GI tract (n=6 intestines) showing that the trend for increasing P-gp expression in the more distal regions of the small intestine agrees with the relative expression data for P-gp shown in Figure 1-1 (Drozdzik et al., 2014). Yet, for MRP2 and BCRP there is a discordance between the relative (Harwood et al., 2013) and absolute data (Drozdzik et al., 2014), in which a decrease in relative expression was demonstrated in the distal small intestine, while the absolute data shows a consistent proximal-to-distal small intestinal expression. Obtaining transporter abundances from further studies is required to establish region-specific transporter abundances and their associated inter-individual variability, from a larger cohort of donors based on data from numerous research groups.

1.9.4 Function *versus* Abundance Scalars

Due to the relative paucity of high quality kinetic data (Section 1.5.2) combined with absolute transporter abundances, it is not known if a transporter-based ISEF (Equation 1-4), akin to that for metabolic enzymes (Section 1.7.3), is required for transporters. Elucidating the amount of active transporter within the membrane, or the 'functional transporter abundance' can be obtained from such an approach. The ISEF permits the correction of transporter driven CLint or Jmax per unit of transporter isoform in both the enterocyte and the *in vitro*/recombinant system. This enables the calculation of a transporters catalytic rate constant (K_{CAT}) in both the enterocyte and recombinant system. At present, PBPK models utilising relative expression data neglect the extrapolation of activity per unit of transporter.

$$CLISEF_{,j} = \frac{CL_{\mathrm{int},j}(Ent) / Transporter_j\ abundance\,(Ent)}{CL_{\mathrm{int},j}(rhTransporter) / Transporter_j\ abundance(rhTransporter)} \qquad \text{Equation 1-4}$$

where CLISEF-$_J$ is the CLint Inter-System Extrapolation Factor for a transporter isoforms (*j*), enterocytic intrinsic clearance $CLint_j$ *(Ent)* (µL/min/cm^2) in, for example, an *ex vivo* intestinal

mucosal preparation within an Ussing chamber system, the transporter isoforms enterocyte abundance (pmol transporter/cm^2 mucosal tissue), the recombinant transporter (*rh Transporter*) isoforms intrinsic clearance CLint,$_j$ in a filter monolayer (µL/min/cm^2) and the transporter isoforms (J) enterocyte abundance (pmol transporter/cm^2 filter-grown cell monolayer).

The ISEF can then be incorporated into Equation 1-5 to calculate the unbound intrinsic clearance for a transporter isoform in any intestinal segment.

$$CLu_{GIS,\text{int}} = \left[\sum_{j=1}^{n} \left(ISEF_j \times \frac{J\max\ (rhTranspo\ rter_j) \times Transporte\ r\ Abundance_j(ent)}{Km(rhTranspo\ rter_j)} \right) \right] \times MePPGIS \times GIS\,S.A \qquad \text{Equation 1-5}$$

for each transporter isoforms (*j*); rhTransporter indicates recombinantly expressed transporter; MePPGIS is the amount of membrane protein per gastrointestinal segment and GIS S.A is the gastrointestinal segments surface area.

The exclusive transport of drug molecules by a single transporter protein is not necessarily commonplace, *i.e.,* overlapping transporter-substrate specificity (Lin et al., 2011). Therefore, establishing abundance-function scaling factors may be challenging in heterogeneous transporter expressing tissues, such as the human intestine. Therefore, the choice of probe compound should be selected carefully and the design of the experiment may warrant co-incubation with inhibitors, which is also fraught with issues due to inhibitor compounds' overlapping transporter specificity (Matsson et al., 2009). This is not a simple field in which to establish robust scalars.

In vitro systems engineered to over-express transporter proteins are routinely used in drug development. It has been demonstrated that the kinetic activity of vinblastine (VBL) decreases in relation to increasing P-gp expression given as, per unit of P-gp protein (Tachibana et al., 2010; Korzekwa and Nagar, 2014). Furthermore, the role of membrane composition is also shown to modulate substrate binding to P-gp and affect its activity (Romsicki and Sharom, 1999; Meier et al., 2006) and that microvillus membrane lipid composition changes along the length of the GI tract in rats (Kararli, 1995). Therefore, these complexities may require attention if we are to attain relevant mechanistic scaling factors.

Obtaining kinetic data in human intestinal *ex vivo* tissues is achievable (Stephens et al., 2001), yet the availability, tissue quantity/quality and technical assistance required to perform abundance and

kinetic studies may be prohibitive for establishing these scalars. In addition, membrane vesicle studies could be undertaken, however these system are suited to low permeability compounds, due to the potential issue of sink violation (Zamek-Gliszczynski et al., 2013).

1.10 Study Aims & Objectives

Upon commencement of this project, the only reports that quantified transporter abundances suitable for incorporation into an intestinal IVIVE strategy, were related to P-gp levels in Caco-2 cell monolayers (Miliotis et al., 2011b). Therefore, there was a clear need to develop techniques to measure transporter abundances in human intestine and *in vitro* cell systems relevant for intestinal transporter IVIVE, to generate more robust mechanistic scaling factors.

The overall objective of this project is to develop the methods to quantitatively analyse human intestinal and *in vitro* cell system transporter proteins and to identify the relationship between transporter abundance and function. As a side project, a small scale across laboratory comparison of matched samples was undertaken to establish whether methodological differences between laboratories leads to a bias in endpoint transporter abundances. The specific aims of the study to achieve this are:

1. To develop and validate a QTAP workflow to enable the quantification of human intestinal enterocytes and Caco-2 cells monolayers using a QconCAT approach.
2. To assess the relationship between transporter mRNA expression, protein abundance in Caco-2 cell monolayers over different cultivation periods, passages and drug treatments. Investigate mRNA-protein-activity relationships for P-gp and BCRP in Caco-2 cell monolayers.
3. To undertake a small scale cross laboratory comparison of human intestine and Caco-2 cell monolayer Sodium Postassium ATP-ase (Na/K-ATPase, ATP1A1), P-gp and BCRP abundances.
4. To generate a theoretical framework to account for procedural protein and peptide losses in QTAP strategies.

Chapter 2- Materials and Methods

This chapter describes in detail the finalised methods employed in conducting the work described in subsequent results chapters. In instances where methods are being developed and validated, (*i.e.,* where methodology is not finalised), a description of these methods will be provided in the accompanying results chapters.

2.1 Materials

2.1.1 Cell Culture & Transport Experiments

Caco-2 cells (HTB-37) were purchased from the American Type Tissue Culture Collection, (ATCC, Rockville, MD, USA) at passage 18 and MDCK-II wild type (WT) cells from The National Cancer Institute (NKI, Amsterdam Netherlands). ATCC Caco-2 high passage (Passage 100+) cells were taken from the cryogenic storage at The Biomedical Facility of Salford Royal Hospital. Cell culture reagents and transporter buffers, Dulbecco's Modified Eagle's Medium (DMEM), penicillin/streptomycin, L-glutamine non-essential amino acids and Hanks Balanced Salt Solution (HBSS) were purchased from Invitrogen Life Sciences (Paisley, Scotland). New-born foetal calf serum gold (heat inactivated) and trypsin- ethylenediaminetetraacetic acid EDTA were purchased from PAA Laboratories (Yeovil, UK). Tissue culture flasks (25, 75 and 175 cm^2) and Transwell filters (1.13 cm^2, 0.4 µM pore size, Cat. no. 3401) were purchased from Corning Life Sciences (Lowell, MA, USA). Roche c*O*MPLETE protease inhibitor cocktail was supplied by Roche Diagnostics (Mannheim, Germany). The test compound [^{3}H]-Vinblastine-Sulfate (VBL) (740 GBq/mmol) was supplied by American Radio-Chemicals (St Louis, MO, USA) and [^{3}H]-Estrone-3-Sulfate E-3-S) (185 GBq/mmol), Optima Gold Liquid Scintillation Cocktail (LSC) and 96 well black-opaque Optiplates were purchased from Perkin Elmer (High Wycombe, UK). All other materials were purchased from Sigma-Aldrich (Poole, UK).

2.1.2 Cell and Human-Based Membrane Extraction

Transwell® filters (44 cm^2, polycarbonate, 0.4 µM pore size, Cat. no.3419) were obtained from Corning Life Sciences (Lowell, MA, USA). Ultracentrifuge tubes suitable for a SW41ti rotor (13.5 mL) were purchased from Beckman Coulter (High Wycombe, UK).

For immunoblotting, a mouse monoclonal Mdr1 (D11) primary antibody and secondary goat anti mouse conjugated IgG horse radish peroxidase antibody were purchased from Santa Cruz Biotechnology (Santa Cruz, CA, USA) with the anti-human beta actin (SC 15 clone) primary

antibody from Sigma-Aldrich (Poole, UK). The Immobilon PVDF membrane and chemiluminescent detection kit was from Millipore (Billerica, MA, USA). All other reagents including the BCA protein and cytochrome c reductase (CCR) assay kits were purchased from Sigma-Aldrich (Poole, UK).

2.1.3 Protein Digestion

The proteolytic enzymes, lysyl endopeptidase (Lys-C) and trypsin were generated recombinantly and supplied by Wako (Osaka, Japan) and Roche Applied Sciences (Mannheim, Germany), respectively.

2.1.4 Proteomic Analyses

The QconCAT construct for the generation of peptide standards for transporter protein abundance quantification, 'the TransCAT' was developed by Dr Matthew Russell, a post-doctoral researcher based in The School of Pharmacy and synthesised in the protein expression facility at the Manchester Institute of Biotechnology, The University of Manchester. All other chemicals and reagents were supplied from Sigma-Aldrich, (Poole, UK). AQUA peptides were synthesised by Cambridge Research Biochemicals (Billingham, UK). The non-labelled (light) version of the Non-Naturally Occurring Peptide (NNOP) [Glu^1]-fibrinopeptide B (Glu-Fib) QconCAT calibrator peptide (EGVNDNEEGFFSAR) was synthesised to 95% purity by Severn Biotech Ltd (Kidderminster, UK). Non-labelled Maxi SpikeTide peptides were synthesised by JPT Peptide Technologies (GmbH, Berlin, Germany).

2.1.5 Gene Expression Analysis

A Transcriptor First Strand cDNA Synthesis Kit for reverse transcription of RNA to cDNA and hydrolysis probes (Universal Probe Library, spanning the entire human genome) for relative gene expression analysis were supplied by Roche Applied Biosciences (Burgess Hill, UK). Primer pairs for each gene were synthesised by Sigma-Aldrich (Poole, UK).

2.2 Methods

2.2.1 Cell Culture

Low and high passage Caco-2 cells (passage 25-35 & 105-115, respectively) were maintained in DMEM growth media containing 10% new born foetal calf serum, 45 U/mL penicillin ,45 µg/mL streptomycin, 1% non-essential amino acids and 1.1% L-glutamine in an humidified atmosphere of 95% air and 5% CO_2 at 37°C (Collett et al., 2004). The cells were fed every 2 days with fresh growth media until 90% confluent where they were sub-cultured routinely every 6 days with trypsin (0.05%)-EDTA and seeded into 75 or 175 cm^2 adherent tissue culture flasks at 12,000 cells per cm^2 after counting by trypan blue exclusion. VBL selected Caco-2 cells (Caco-2-VBL) were generated at Passage 100+ by routine culture with growth media containing 11 nM VBL (Anderle et al., 1998) for 5 passages (previously generated and cryogenically stored by Dr A Warhurst, University of Manchester). The cells were seeded into 75 or 175 cm^2 adherent tissue culture flasks at 15,000 cells per cm^2 to ensure the duration between sub-culturing was consistent with Caco-2 cells. MDCK-II-WT cells were seeded at 12,000 cells per cm^2 and maintained in similar growth media to Caco-2 without supplementation with glutamine or non-essential amino acids. The MDCK-II-WT cells were fed every 2 days and were routinely sub-cultured every 3-4 days.

2.2.2 Preparation of Membrane Fractions from Cultured Cells

Preliminary studies focussed on harvesting and extracting cell membrane proteins from 175 cm^2 tissue culture flasks, while subsequent studies employed harvesting proteins from filter-grown cells.

2.2.2.1 Flask-Based Membrane Extraction

Caco-2 (low passage) or MDCK-II-WT cells were grown to confluence and either scrape harvested or trypsinsed followed by homogenisation using a Dounce, hand-held Teflon-glass homogeniser. As flask-based membrane extractions were the cornerstone of developing robust membrane extraction methods, further details of these methods are provided in Chapter 3.

2.2.2.2 Filter-Based Membrane Extraction

The following method for filter-based membrane extraction of Caco-2 cells has previously been published (Russell et al., 2013) and is shown in Figure 2-1. Cells grown to 90% confluence on flasks were trypsinised and counted on a haemocytometer by a trypan blue exclusion method. All Caco-2 cell variants were seeded onto 44 cm^2 Transwell filters (n = 3 filters pooled per experiment) at a seeding density of 2.2 x 10^5 cells/cm^2 (Miliotis et al., 2011b). The growth media was replenished every 2 days. Low passage Caco-2 cells were grown for 10, 16, 21 and 29d, while high

passage and Caco-2-VBL cells were grown for 21d. Twenty four hours prior to harvest, the cells were fed fresh media to reduce the likelihood of development of a starvation phenotype.

The membrane extraction procedure is based on an adaptation of previously described methods (Zhang et al., 2004; Ohtsuki et al., 2012). On the day of harvest, tight junction formation was assessed after 2 x HBSS-4-(2-hydroxyethyl)-1-piperazineethanesulfonic acid (HEPES) (25 mM) washes (Hubatsch et al., 2007), by performing a monolayer integrity transport assay that assessed apical to basal (A-to-B) permeability of the paracellular transport marker Lucifer Yellow (LY; 50 µM in Hanks balanced salt solution (HBSS) containing 25 mM HEPES). Permeability was measured over 60 min at 37°C with donor (1 µL) and receiver samples (200 µL) taken in duplicate at the beginning and end of the transport assay. LY concentrations were calculated from a standard curve after reading on a Victor^2 plate reader (Wallac) at 485nm excitation and 535nm emission for 0.1s with a fluorescein filter. Any filters displaying an apparent permeability (Papp) of > 1 x 10^{-6} cm sec^{-1} were not included for subsequent membrane harvesting. The monolayers were washed twice with PBS (4°C) and 1 mM $NaHCO_3$ (pH 7.0) was added to the apical chamber and incubated for 10 min at 4°C to swell the cells. The cells were harvested by scraping with a cell scraper into 20 mL of 1 mM $NaHCO_3$ (pH 7.0) per filter (15 mL per filter for MDCK-II-WT cells) and lysed for 16h at 4°C with a protease inhibitor cocktail with agitation at 4 Hz. After 16 h, a 1 mL sample ('total protein', (TP)) was taken. The remaining TP lysate was centrifuged at 100,000 x *g* in a Beckman L7 ultracentrifuge for 30 min at 4°C in a SW41ti swing-out rotor and the supernatant containing the soluble fraction was discarded. The pellet was re-suspended in TSEM buffer (10 mM Tris-HCl, 250 mM sucrose, 0.1 mM EGTA, 0.5 mM $MgCl_2$, pH 7.4, (Zhang et al., 2004)) at 4°C and homogenised on ice with a Dounce hand-held homogeniser for 75-stokes. A sample (100 µL) termed the 'Insoluble Fraction' was taken. The insoluble fraction was centrifuged at 5,500 x *g* in a Sorvall SS34 rotor at 4°C, the supernatant was retained and the pellet was re-suspended in TSEM buffer and homogenised again for 50 strokes. The second homogenate was centrifuged at 5,500 x *g* and the supernatant retained. The supernatants were combined and spun at 100,000 x *g* for 60 min at 4°C in a SW41ti swing-out rotor and the pellet representing the total membrane (TM) fraction was re-suspended in TSE buffer (TSEM buffer minus $MgCl_2$) and a 200 µL sample was taken. The remaining TM fraction was layered onto a 38% sucrose cushion (Kamiie et al., 2008) and spun at 100,000 x *g* a SW41ti swing-out rotor for 30 min. The resultant turbid interface at the sucrose-buffer boundary containing PM was taken and re-suspended in TSE buffer and spun at 100,000 x *g* for 60 min at 4°C in a SW41ti swing-out rotor. The pellet representing the PM fraction was re-suspended

in TSE buffer. All samples were stored at -80°C with protein concentration subsequently determined by BCA assay where absorbance was measured at a wavelength of 560 nm, using bovine serum albumin (BSA) as a standard.

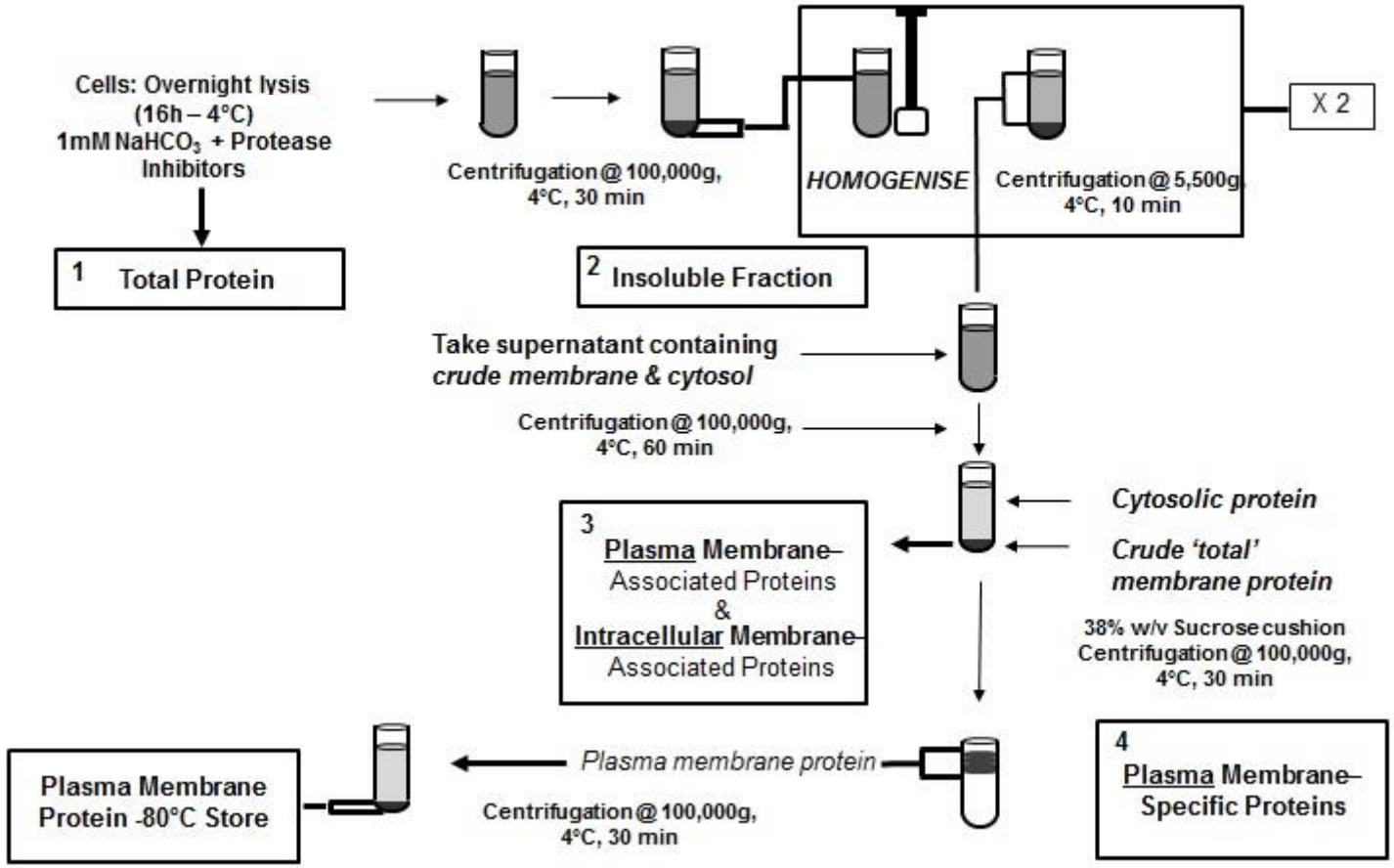

Figure 2-1. Schematic describing the plasma membrane extraction protocol from cells grown on filters. The routine sampling of fractions is highlighted by boxes numbered 1-4.

2.2.2.3 Human Intestinal Tissue Harvest & Membrane Extraction

Human intestinal tissue was obtained after informed consent from patients undergoing elective intestinal surgery at Salford Royal NHS Foundation Trust. Prior ethical committee approval had been granted by the North West Research Ethics Committee (REC No:-12/NW/0306, Trust R&D No: 2012/132GI). Patients undergoing procedures for a range of disorders including; pancreatic cancer; intestinal adhesions (fistulas) and diverticular disease were consented in this study. Patients suffering from inflammatory bowel disease (*i.e.,* Crohn's disease or ulcerative colitis) and/or known to be affected by hepatitis B were excluded from participation. Only macroscopically normal (upon visual inspection) tissues were used within this study. Immediately after resection, macroscopically healthy margins of resected intestinal tissue were opened by blunt dissection to expose the mucosa and were the washed in ice-cold 0.9% NaCl immediately after procurement. The tissue was transferred in ice-cold oxygenated small bowel ringer (NaCl (121 mM), $NaHCO_3$ (25.1 mM), $KHCO_3$ (1.6 mM), KH_2PO_4 (0.2 mM), K_2HPO_4 (1.2 mM), $CaCl_2$ (1.2 mM), $MgCl_2$ (1.2 mM) and D-glucose (10 mM)), which had been equilibrated to pH 7.4 by bubbling with 5% CO_2/95% O_2 (Stephens et al., 2001).

2.2.2.4 Enterocyte Chelation:

The rinsed mucosa was removed from the underlying bowel wall by blunt dissection and placed onto Perspex tissue adaptors (constructed by Salford Royal Hospital Medical Physics Department) with 8 or 16 cm^2 apertures to expose the mucosa to chelating solutions (Figure 2-2). The time from bowel resection to securing the tissue in adaptors was always less than 1 hour.

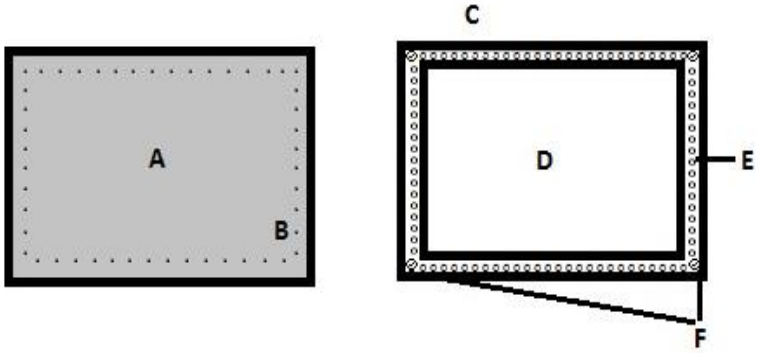

A – Base adaptor plate

B – Pins to secure tissue (serosa down)

C – Top plate

D – Aperture exposing mucosa (8 or 16 cm^2)

E – Pin holes for securing tissue

F – Corner screws to secure tissue and plates in position

Figure 2-2. Human tissue adaptor used for chelating and harvesting human enterocytes.

Optimisation of the human enterocyte chelation method took place on 5 separate human intestinal tissues where buffer composition, incubation times and agitation by flushing were all assessed for success in procuring enterocyte material of a sufficient quantity to allow the necessary downstream assays on membrane fractions to be performed. The final enterocyte chelation method adopted is as follows. All solutions used for eluting enterocytes were made in a base buffer consisting of NaCl (112 mM), KCl (5 mM), HEPES (20 mM), pH 7.1 (Tris) (Bowley et al., 2003). The adaptor-secured mucosa was rinsed twice in base buffer (4ºC) and immersed in a sodium citrate (27 mM) pH 7.1 solution with protease inhibitors at 4ºC for 30 min to destabilise cell-to-cell contacts (Weiser, 1973). The secured mucosal tissue was then rinsed twice in base buffer (4ºC) and immersed in an EDTA buffer, adapted from Dr Oliver Hatley, University of Manchester, (EDTA (30 mM), heparin (10 U/mL), dithiothreitol (DTT, 1 mM) and protease inhibitors), pH 7.1 at 4ºC and was placed on an orbital stirrer at 250 rpm for 40 min at 4ºC. After 40 min of stirring with 30 mM EDTA, the tissue was placed in a small beaker containing 50 mL of fresh EDTA solution, plus any material that was removed by chelation after orbital stirring. Whilst in the tissue adaptor, the mucosal surface was repeatedly flushed with the bathing EDTA buffer using a 10 mL syringe and 21g needle to further remove mucosal structures (*i.e.,* villus, crypts & enterocytes) for a maximum of 10 min at 4ºC. To confirm that the chelated material resembled mucosal structures, the enterocyte preparation was checked under an inverted light microscope. The chelated material was pelleted at 2000 x *g* for 10 min at 4ºC. After removal of the supernatant, the pellet was washed in base buffer and a further spin at 2000 x *g* for 10 min at 4ºC ensued. The pellet of enterocytes was stored at -80ºC for no longer than 3 days prior to membrane fractionation.

The enterocyte pellet was re-suspended in TSEM buffer at 4°C and homogenised on ice with a Dounce hand-held homogeniser for a minimum of 75-strokes. The homogenate was examined under an inverted light microscope and the absence of intact enterocytes confirmed and a sample of the 'TP' homogenate was taken and frozen at -80ºC. From this point on, the extraction procedure for human enterocyte TM or PM fractions was the same as that used for filter-grown cultured cells, with the exception that the sampling of the insoluble fraction did not occur. All samples were stored at -80°C and protein concentration was subsequently determined by BCA assay, using BSA as a standard.

2.2.2.5 Mucosal Crushing:

Where sufficient mucosal tissue was available, an adjacent section of mucosa to that taken for enterocyte chelation was harvested by blunt dissection, snap frozen and stored in liquid nitrogen.

The mucosal tissue was defrosted on ice and homogenised in TSEM buffer containing protease inhibitors at 4°C for 50 strokes. The homogenate was sieved to remove any remaining large mucosal pieces and a maximum of a further 150 strokes followed. The homogenate was checked to confirm the presence of intact enterocytes under an inverted light microscope and was spun at 5,500 x *g* in a Sorvall SS34 rotor at 4°C. The supernatant was retained and the pellet was re-suspended in TSEM containing protease inhibitors, homogenised for a maximum of 150 strokes and was spun at 5,500 x *g* and this second supernatant was retained. In a departure from previous methods to obtain a TM fraction, the two supernatants were not combined for subsequent ultracentrifugation. Thus, two separate TM fractions were obtained from each supernatant. This is due to concerns that the first supernatant retained (5,500 x *g,* spin 1) did not resemble a sufficiently homogenised sample as intact enterocytes were still present. Only the supernatant from the second homogenisation and spin was taken through for procurement of the TM and subsequently used for proteomic analysis. TM's were obtained and stored as previously described from pelleting the supernatants at 100,000 x *g* (Section 2.2.2.2), with the exception that sampling of an insoluble fraction did not occur.

2.2.3 Histological Assessment of Human Enterocyte Chelation

To visually confirm that enterocytes contained within mucosal structures such as crypts and villus were removed from the underlying lamina propria layer of the mucosa, pieces of mucosa taken before and after chelation were sliced into small sections (< 1 cm) and fixed in 4% formaldehyde. The fixed mucosal pieces were embedded in paraffin blocks, cut into 5 µM sections and stained by haematoxcylin and eosin and imaged by light microscopy (Leica Microsystems, Wetzlar, Germany) from a digital camera affixed to the microsope at 100 or 200x magnification.

2.2.4 Assessment Membrane Purity

The activity of the enzymes alkaline phosphatase (AP, (EC 3.1.3.1)) and cytochrome c reductase (CCR, (EC 1.6.2.4)), markers of the plasma and endoplasmic reticular membranes respectively, were measured to assess the purity of intermediate and end-point fractions obtained throughout the membrane harvesting.

2.2.4.1 Alkaline Phosphatase Activity Assay

The AP activity assay is a glycine-based method measuring the liberation of p-nitrophenyl + inorganic phosphate (p-NP+Pi) by alkaline phosphatase from the precursor substrate p-nitrophenylphosphate (p-NPP, 2.1 mM). The base assay buffer made fresh for each assay

consisted of Glycine (100mM), 1mM $MgCl_2$, pH 8.8 (buffer based on Abcam colorimetric alkaline phospahatse assay kit). The liberation of p-NP from p-NPP was quantified in samples containing 10 µg protein against a p-NP standard curve in 96 well plates for 60 min at 37ºC. The reaction was stopped by NaOH (1M) and was read on a plate reader at 405 nm for 0.1s.

2.2.4.2 Cytochrome C Reductase Activity Assay

The CCR kinetic activity assay kit is based on the conversion of the oxidised form of cytochrome c to the reduced form via the donation of hydrogen (reduction) from NADPH forming NADP. The assay was run based on kit instructions. Briefly, the working cytochrome c buffer consisted of potassium phosphate buffer (300 mM) containing EDTA (0.1mM), pH 7.8, plus 4.5 mg/mL cytochrome c and was combined with 10 µg of protein at 25ºC. The reaction was started by adding 100 µL NADPH (0.85 mg/mL) and measured at 10s intervals over 1 minute at 550 nM on a kinetic spectrophotometer, where the absorption spectrum of cytochrome c changes with its oxidation/reduction state.

2.2.5 Immunoblot Analysis of P-gp Expression

To determine the enrichment of P-gp throughout the membrane extraction procedure in Caco-2, various protein fractions were separated by sodium dodecyl sulphate polyacrylamide electrophoresis (SDS-PAGE) (Bannon et al., 2009). A 4% stacking gel containing 10 lanes was overlaid on a 7.5% SDS-acrylamide resolving gel. Protein samples (ranging from 0.3125 - 2.5 µg, equalised for volume (10.3 µL)) were denatured in bromophenol blue at 90ºC for 5 min and 15.3 µL were added to each well. A molecular weight 'rainbow' marker (Amersham Biosciences, Bucks, UK) was run alongside the proteins. Samples were run in SDS-PAGE buffer (1.5% Tris base, 0.7% glycine and 0.5% SDS) at 150V for 90 min. Gels were transferred by electrophoresis (100V) to an immobilon PVDF membrane (MerckMillipore, Billerica, MA, USA) over 60 min in electro-transfer buffer (3% Tris, 15% glycine and 20% methanol) at 4ºC. The membrane was incubated with rotational agitation overnight in 2% casein Tris-buffered saline and 0.1% tween (TBS-T) at 4ºC. After washing (3 x 10 min in TBS-T), the membrane was incubated with a mouse monoclonal mdr1 antibody (1/750 dilution in TBS-T) for 1 hour and a beta-actin (AC 15 clone) monoclonal antibody (1/4000 dilution in TBS-T) for 2 hours. A further series of 3 x 10 minute washes in TBS-T was followed by a 60 min incubation with a secondary horse radish peroxidase antibody (1/4000 dilution & 1/20000 dilution in TBS-T plus 5% powdered milk for P-gp & beta-actin, respectively) for chemiluminescent detection of protein bands. After another set of washes for 30 min, the

membrane was treated with a chemiluminescent horseradish peroxidase substrate ranging from 30 seconds to 2 min in a dark room for subsequent development onto photosensitive film.

The relative expression of protein bands was determined by blot densitometry using Image J analysis software (NIH, Bethesda, Maryland). After obtaining band densitometry with background subtracted, the ratio of P-gp to beta-actin was calculated to correct for bias in sample loading onto the gel. These ratios were normalised to the ratio of the initial starting TP (lysate) to gauge P-gp enrichment throughout the membrane fractionation procedure.

2.2.6 Generating Standard Peptides for Protein Abundance Quantification

To enable the quantification of absolute protein abundances within this study, two separate methods for generating SIL peptides standards were employed. The first was an AQUA approach and the second was the generation of a QconCAT construct.

2.2.6.1 Generation of AQUA SIL peptides:

AQUA SIL peptides for the enterocyte-apical membrane anchored protein Villin (AA-[**V**$^{13}C_5$ ^{15}N]PDTVVEPALK) and the basolateral membrane marker protein Na/K-ATPase I-[**V**$^{13}C_5$,^{15}N]EIPFNSTNK were selected based on preliminary digests of Caco-2 PM. The digested PM peptides were submitted for fragmentation by an Orbitrap mass spectrometer (Biomolecular Analysis Facility, Faculty of Life Sciences, the University of Manchester), in which peptides selected by label-free data-dependent acquisition (DDA) were ranked according to their relative abundance using Mascot (v2.4.1) search engine (Matrix Science, London, UK), see Appendix Figure B-1 for selected peptides. Searches revealed that the highest abundance peptide belonging to an apical and basal membrane marker, respectively, was for Villin (ranked # 42/335) and Na/K-ATPase (ranked # 116/335). The suitability of the selected Villin peptide was checked for mis-cleavage and ionisation efficiency using conSEQUENCE software program http://king.smith.man.ac.uk/CONSeQuence/ (Eyers et al., 2011). Practical validation of the selected villin proteotypic peptide for ionisation efficiency, including examination of potential transition schedules was undertaken with a synthesised, sequence equivalent, non-labelled peptide (Maxi SpikeTides). Upon satisfaction that the selected peptide was suitable for incorporation into an SRM schedule, the AQUA peptide was synthesised.

2.2.6.2 Generating the 'TransCAT' (QconCAT) construct:

As alluded to previously in Section 2.1.4, the TransCAT construct was developed by Dr Matthew Russell at The University of Manchester to quantify human drug transporter protein abundances

with a specific focus on those expressed in the liver (Russell et al., 2013). The construct consists of 8 ABC superfamily proteins and 13 SLC superfamily proteins, with potential for the utilisation of two peptide standards unique for each target protein, except for Organic Solute Transporter alpha OST-α (SLC51A) and Organic Anion Transporter 4 (OAT4, SLC22A9) for which only a single suitable peptide could be identified. The entire TransCAT sequence is provided in Appendix Figure C-1. Of note, is that the AQUA SIL peptide for Na/K-ATPase is the same as one of the Na/K-ATPase selected peptides in the QconCAT.

A comprehensive description of the TransCAT's construction is already provided (Russell et al., 2013). Briefly, the design of the TransCAT was based on identifying suitable proteotypic peptides that are unique to the target transporters proteins, would ionise efficiently and to exclude peptides that were susceptible to missed-cleavage on either terminal end during digestion using the www.srmatlas.org, conSEQUENCE and BLAST software programs. Further considerations for selection were the exclusion of (where possible); -

- peptides that were prone to post-translational modifications (www.uniprot.org)
- residues that can suffer side chain reactions such as methionine, cysteine, asparagine, glycosylated residues, poly & N-terminal glutamine sequences
- dibasic and tribasic tryptic sites, *i.e.,* sequential lysine or arginine residues or lysine and arginine side-by-side

To enable quantification of the QconCAT level, four 'calibrator' NNOP peptide sequences were incorporated into the construct. For this study however, only a single NNOP peptide was used for quantification, Glu-Fib (EGVNDNEEGFFSAR).

Validation of the theoretical peptides selected for inclusion into the TransCAT for ionisation efficiency, including examination of potential transition schedules for each peptide was undertaken with synthesised, sequence equivalent, non-labelled peptides (Maxi SpikeTides). Upon satisfaction that the selected peptides were suitable for incorporation into an SRM schedule TransCAT synthesis commenced.

Briefly, the TransCAT was synthesised after incorporating the genes corresponding to the QconCAT (including fusion protein NUSa to facilitate successful TransCAT expression) into the protease deficient JM109 (DE3) E.coli via a pET21 plasmid. The growth media was enriched with $^{13}C_6$-arginine and $^{13}C_6$-lysine for isotope incorporation into the selected peptides of the TransCAT and protein expression was induced by isopropyl β-D-1-thiogalactopyranoside. The TransCAT was

purified by nickel-sepharose and further purified by gel filtration; buffer exchange and on HiLoad superdex columns for subsequent reconstitution in 200 mM NaCl and Tris-HCl (pH 8) (Russell et al., 2013) and storage at -20ºC.

2.2.7 Protein Digestion

2.2.7.1 Protein digestion (AQUA & QconCAT - University of Manchester)

To digest the protein samples into the tryptic peptides required for absolute protein abundance quantification, an adapted in-solution digest was developed based on established methods (Balogh et al., 2013). Protein samples (typically, 50 µg) and the TransCAT (5 µL, 1/10 diluted stock) were suspended in protein digestion buffer (Ammonium Bicarbonate (25 mM), pH 8), denatured with a final volume of 10% (w/v) deoxycholate (DOC) and incubated at room temperature for 10 min. The TransCAT levels were based on the abundances of Na/K-ATPase in Caco-2 PM (~30 fmol/µg) after quantification by Bertin Pharma (BPh). For the AQUA assays, the TransCAT step was omitted from the procedure. Samples were reduced by DTT (60 mM) at 56°C for 20 min and subsequently alkylated by IAA (15 mM) in the dark at room temperature for 30 min. The concentration of DOC in the incubation was reduced to 1% (w/v) and 1 µL Lys-C (1 µg/µL) was added and the mixture was incubated at 30ºC for 4 hours. Recombinant trypsin (2.5 µL at 1 µg/µL) was added to the samples and incubated overnight (18h) at 37ºC. To precipitate the DOC and acidify the digest, trifluoroacetic acid was added (0.1–0.5% v/v) to achieve the optimal pH of 3 and was chilled at 4ºC for 30 min. After two 14,000 x *g* spins, the supernatant containing the peptides was removed from the pellet containing the precipitated material and evaporated to approx. 50 µL by vacuum centrifugation with adjustment to 0.1% formic acid and 3% acetonitrile and stored at -20ºC.

2.2.7.2 Protein digestion (AQUA – Bertin Pharma (BPh))

Frozen TM and PM protein samples were sent to BPh (Orleans, France) overnight on dry ice, for digestion and quantification of transporter protein abundances utilising an AQUA-based SRM LC-MS/MS strategy. The transporters selected for quantification in Caco-2 and human intestinal mucosal/enterocyte membranes were Na/K-ATPase, P-gp, BCRP and MRP2. Proteins were digested by the MS2 plex assay kits developed by BPh based on techniques developed in Prof. Terasaki's laboratory (Tohoku University, Sendai, Japan) that included reduction, alkylation and an overnight tryptic digestion step (Kamiie et al., 2008). The SIL proteotypic peptides selected for analysis were AAVPDA[**V**^{13}C,^{15}N]GK (Na/K-ATPase), FYDPL[**A**^{13}C,^{15}N)GK (P-gp), SSL[**L**$^{13}C_5$,^{15}N]DVLAAR (BCRP) and QLLNNI[**L**$^{13}C_5$,^{15}N]R (MRP2).

2.2.8 LC-MS/MS Analysis

2.2.8.1 Preparation of NNOP (Glu-Fib) Assay Mix for SRM Analysis

A typical mixture of: digested sample, standard (QconCAT) and NNOP (calibrator peptide) ('the sample') was prepared as follows: 18 µL of membrane protein and standard with 2 µL of stock Glu-Fib (25 pmol/µL) which was diluted 1/100,000 in 3% acetonitrile, to provide a final concentration of 0.238 fmol/µL after correction for Glu-Fib stock purity (95%).

2.2.8.2 Sample Analysis by LC-MS/MS

Samples were analysed by LC-MS/MS using a nanoACQUITY nano-HPLC system (Waters, UK) coupled to a TSQ Vantage triple quadrupole mass spectrometer (ThermoScientific, Pittsburgh, PA), as previously described (Russell et al., 2013; Achour et al., 2014). Samples (8 µL) were injected onto a trapping column (Symmetry C18, 180 mm x 20 mm; Waters), at flow rate of 5 µL/min for 3 min. The flow was then switched to bring the trap in line with the analytical column (1.8 µm HSS T3, 75 µm × 150 mm; Waters) maintained at 35 °C. Peptides were eluted with a 0.3 µL/min flow rate and a gradient of 3 to 60% acetonitrile over 40 min, followed by a ramp to 95% acetonitrile for 5 min, then a return to starting conditions to re-equilibrate the system before subsequent runs. The mass spectrometer was operated in the positive ionisation mode after electrospray ionisation to monitor the m/z of the selected standard and sample peptide transitions. Transition schedules were designed and the workflow was managed using Skyline version 2.5.0.6079 (MacCoss Lab Software, USA) (MacLean et al., 2010a). Transitions for 8 transporter proteins, Na/K-ATPase, Human Peptide Transporter 1 (HPT1), P-gp, MRP2, BCRP, OST-α, OST-β and Organic Anion Transporting Polypeptide 2B1 (OATP2B1) were selected from high-intensity *y*-ions of higher m/z than the parent, and where, available, a high intensity *b*-ion (Table 2-1). For each transition, the dwell time was set at 0.15 s. Collision energies were optimized for each transition using Skyline's in-built functionality (Maclean et al., 2010b). Data were acquired using Xcalibur version 2.0.6 SP1 and Tuneplus version 2.2.0 Eng2, configured with an Acquity driver (build 1.0) (Waters, U.K.).

2.2.8.3 Assay Quality Control - Establishing Linearity, Limits of Quantification & Precision

Linear regression analysis was employed to evaluate 1) the linearity of the calibrator NNOP and 2) the sample peptides in relation to the NNOP dilution factor (Achour et al., 2014). To assess NNOP linearity, a calibration curve was prepared using the synthetic 'light' Glu-Fib and a pre-digested TransCAT construct to calculate the light to heavy peak area under the curve ratio. The TransCAT-to-NNOP ratio was varied from 1-to-10 to 10-to-1 (100-fold range). A pool of 3 digested human

intestinal samples was generated to evaluate sample peptide to QconCAT dilution factor linearity. A fixed volume of assay mix (20 µL), containing variable volumes of pooled sample and diluent buffer were combined with digested QconCAT and Glu-Fib (1 in 10000 diluted) set to 1 and 3 µL, respectively (Achour et al., 2014). Assay precision was assessed in 5 human samples with 3 separate injections per sample, spanning 2 days for each selected transporter peptide. In addition, within day (intra-day) and between day (inter-day) precision was assessed for n=5 human intestinal samples. The impact of inter-operator differences when manually evaluating the co-elution profiles boundaries that enable Skyline to calculate the light-to-heavy peak area of selected peptides by Skyline was also assessed. Two independent operators performed this analysis.

2.2.8.4 Calculation of Transporter Abundance Values

The ratios of native (light) and standard (heavy) selected transitions for each peptide were calculated in Skyline. Transporter abundances were determined from TransCAT-derived proteotypic standards by Equation 2-1 (Achour et al., 2014):

$$A_{Transporter} = [NNOP] \cdot R_{\frac{H.NNOP}{L.NNOP}} \cdot R_{\frac{L.Peptide}{H.Peptide}} \cdot \frac{1}{F_{Sample}} . V_{Digest} \cdot \frac{1}{Protein\ Content} \qquad \text{Equation 2-1}$$

where $A_{Transporter}$ is the estimate of transporter protein abundance in the protein fraction under investigation in units of fmol/µg. The [NNOP] is the known concentration of the light NNOP peptide (fmol/µL) which was corrected for purity (95%) prior to incorporation in Equation 2-1. The ratio of the heavy to light NNOP ($R_{H.NNOP:L.NNOP}$), where the H.NNOP is the isotope labelled standard(s) derived from the TransCAT and the L.NNOP is the standard of known concentration, permits the calculation of the equimolar concentration of the TransCAT. $R_{L.Peptide:H.Peptide}$ describes the ratio of the light (derived from the sample) to heavy peptide (derived from the TransCAT), and, when combined with the previous terms, provides peptide concentration (fmol/µL) in the assay mix. The $R_{H.Peptide:L.Peptide}$ is corrected for isotope incorporation efficiency for lysine and arginine prior to integration into the equation (Russell et al., 2013). The $1/F_{sample}$ term describes the correction for dilution of the peptide digest by NNOP in the assay mix (18 µL digest in 20 µL) and converts the peptide concentration in the assay mix to the peptide concentration originating from the digest, also see Equation S9, Appendix 4. V_{Digest} is the volume of the digest in µL and converts digested peptide concentration to peptide abundance in fmol. The 1/Protein Content term reflects the protein fraction under study, which in the case of this study is either, TP (whole cell/homogenate), TM or a PM protein in µg. The ‘Protein Content’ term relates the abundance of the peptide in the digest to the abundance in the protein matrix under study. The ‘Protein Content’ term reflects the gravimetrically

determined protein content and not the nominal protein content entering the digestion procedure (Section 2.2.8.5). For the calculation of transporter abundances by AQUA, the deviations to the above calculation method are as follows: The concentration of the standard peptide is provided by the manufacturer and is therefore known, hence, the $R_{H.NNOP/L.NNOP}$ term is redundant. The [NNOP] term converts to [AQUA] standard.

2.2.8.5 Gravimetric Determination of Peptide Quantity for Abundance Determinations

During peptide denaturation, alkylation and digestion, there is the potential for peptide losses to the precipitated fraction (Section 2.2.7.1), while additional losses may also result from non-specific binding to preparatory/LC-MS/MS tubes and during pipetting (Prasad and Unadkat, 2014). Therefore, rather than use the nominal peptide content entering into the digestion strategy as the denominator in the protein abundance units (fmol/µg), the peptide content of each sample was calculated by gravimetric methods using an analytical balance with a sensitivity limit of 10^{-5} grams. Full details of the calculations to determine the peptide content in the LC vial for AQUA and QconCAT strategies are given in Appendix 4 as well an entire schematic overview of the workflow development (Appendix Figure D-1).

2.2.8.6 Bertin LC-MS/MS Conditions

Samples were analysed by LC-MS/MS using a normal flow series 200 autosampler/HPLC pump and a Flexar LC (Perkin Elmer, Waltham, MA, USA) coupled to a API5500 triple quadrupole mass spectrometer (AB Sciex, Framingham, MA, USA). Samples (40 µL) were injected into the LC system analytical column (X Bridge BEH130 C18, 100 x 1.0 mm, 3.5 µm, Waters) with column oven maintained at room temperature. Peptides were eluted with a 50 µL min^{-1} flow rate and a gradient of 2 to 60% acetonitrile over 60 min. The transition schedules were obtained by direct flow injection of peptide solutions. The [M+2H]+ ion was selected as parent ion and the 4 most intense ions obtained by collision in Q2 were selected as the Q3 transitions (Table 2-2). Data were acquired using AB Sciex Analyst 1.6 software and excel.

Table 2-1.Overview of the transition schedules and the respective ions selected for the native and isotope labelled peptides used for transporter quantification.

Protein	Peptide	Native/Standard	Mass† (amu)	Q1	Ion/z‖	Q3.1	Ion/z	Q3.2	Ion/z	Q3.3	Ion/z	Retention Time (min)	CE‡ (eV)
NNOP	EGVNDNEEGFFSAR	Native	1570.6	785.84	*y*14/2+	1056.47	*y*9/1+	813.39	*y*7/1+	n/a	n/a	28-30	27,29
		Standard	1576.6	788.85	*y*14/2+	1062.50	*y*9/1+	819.41	*y*7/1+	n/a	n/a		27,29
Na/K-ATPase	IVEIPFNSTNK	Native	1261.44	631.34	*y*11/2+	1049.53	*y*9/1+	920.48	*y*8/1+	807.40	*y*7/1+	31-33	All 19
		Standard	1267.44	635.35	*y*11/2+	1055.55	*y*9/1+	926.50	*y*8/1+	813.42	*y*7/1+		All 19
HPT1	AENPEPLVFGVK	Native	1299.49	650.35	*y*12/2+	985.57	*y*9/1+	759.48	*y*7/1+	n/a	n/a	34-36	20, 25
		Standard	1305.49	653.36	*y*12/2+	991.51	*y*9/1+	765.5	*y*7/1+	n/a	n/a		20, 25
P-gp	AGAVAEEVLAAIR	Native	1269.47	635.36	*y*13/2+	971.55	*y*9/1+	771.47	*y*7/1+	840.45	*b*9/1+	41-44	21,21,19
		Standard	1275.47	638.37	*y*13/2+	977.57	*y*9/1+	777.49	*y*7/1+	840.45	*b*9/1+		21,21,19
MRP2	LVNDIFTFVSPQLLK	Native	1734.07	867.50	*y*15/2+	1179.68	*y*10/1+	1032.61	*y*9/1+	1049.58	*b*9/1+	27-29	29,29,26
		Standard	1740.07	870.51	*y*15/2+	1185.7	*y*10/1+	1038.63	*y*9/1+	1049.58	*b*9/1+		29,29,26
BCRP	VIQELGLDK	Native	1014.18	507.8	*y*9/2+	802.43	*y*7/1+	674.37	*y*6/1+	545.33	*y*5/1+	40-42	15,16,21
		Standard	1020.18	510.8	*y*9/2+	808.45	*y*7/1+	680.39	*y*6/1+	551.35	*y*5/1+		15,16,21
OATP2B1	ATMGTENTPGGK	Native	1163.28	582.27	*y*12/2+	358.20	*y*4/1+	806.33	*b*8/1+	n/a	n/a	27-30	24, 23
		Standard	1169.28	585.28	*y*12/2+	364.23	*y*4/1+	806.33	*b*8/1+	n/a	n/a		24, 23
OST-α	YTADLLEVLK	Native	1164.37	582.83	*y*10/2+	900.54	*y8*/1+	829.50	*y*7/1+	601.39	*y5/1+*	40-42	21,20,22
		Standard	1170.37	585.84	*y*10/2+	906.52	*y*8/1+	835.52	*y*7/1+	607.41	*y5/1+*		21,20,22
OST-β	ETPEVLHLDEAK	Native	1380.53	690.85	*y*12/2+	1150.61	*y*10/1+	712.36	*y*6/1+	575.81	+2y10/+1	28-30	All 26
		Standard	1386.53	693.86	*y*12/2+	1156.63	*y*10/1+	718.38	*y*6/1+	578.82	+2y10/+1		All 26

† The mass in Daltons (amu) calculated with the online molecular weight calculator tool in Expasy http://web.expasy.org/compute_pi/, ‖ z, is the charge state of the selected ion pair, and ‡ CE is the optimised collision energy determined using non-labelled Maxi SpikeTides. The CE values are given sequentially for each product ion Q3.1, Q3.2, Q3.3

Table 2-2.Overview of the transition schedule and the respective ions selected for the native and isotope labelled peptides used for transporter quantification.

Protein	Peptide	Native/ Standard	Mass† (amu)	Q1	Ion/z	Q3.1	Ion/z	Q3.2	Ion/z	Q3.3	Ion/z	Q3.4	Ion/z
Na/K-ATPase	AAVPDAVGK	Native	826.4	414.2	*y*9/2+	685.4	*y*7/1+	586.3	*y*6/1+	489.3	*y*5/1+	374.2	*y*4/1+
		Standard	832.4	417.2	*y*9/2+	691.4	*y*7/1+	592.3	*y*6/1+	495.3	*y*5/1+	380.2	*y*4/1+
P-gp	FYDPLAGK	Native	909.4	455.7	y8/2+	763.4	*y*7/1+	600.3	*y*6/1+	485.3	*y*5/1+	275.2	*y*3/1+
		Standard	913.4	457.7	y8/2+	767.4	*y*7/1+	604.3	*y*6/1+	489.3	*y*5/1+	279.2	*y*3/1+
MRP2	QLLNNILR	Native	982.6	492.3	y8/2+	742.5	*y*6/1+	629.4	*y*5/1+	515.3	*y*4/1+	242.2	*y*3/1+
		Standard	989.6	495.8	y8/2+	749.5	*y*6/1+	636.4	*y*5/1+	522.3	*y*4/1+	242.2	*y*3/1+
BCRP	SSLLDVLAAR	Native	1043.6	522.8	y10/2+	870.5	y8/1+	757.5	*y*7/1+	644.4	*y*6/1+	529.3	*y*5/1+
		Standard	1050.6	526.3	y10/2+	877.5	y8/1+	764.5	*y*7/1+	651.4	*y*6/1+	536.3	*y*5/1+

The transition schedules given in the table have been previously published (Sakamoto et al., 2011, Kamiie et al., 2008).

2.2.9 Analysis of Transporter Gene Expression

2.2.9.1 RNA Isolation and cDNA Generation

Caco-2 cells (all variants) were seeded on 1.13 cm^2 polycarbonate Transwell filters at 2.2 x 10^5 cells per cm^2 and were grown for 10, 16, 21 and 29 days with monitoring for transepithelial electrical resistance (TEER). On the day of harvest, tight junction formation was assessed after two HBSS-HEPES (25 mM) washes at 37ºC by performing a monolayer integrity transport assay using LY at 50 µM in HBSS HEPES (25 mM) for 1 hour A-to-B at 37°C. Any filters displaying a LY Papp of > 1 x 10^{-6} cm sec^{-1} were not included for subsequent RNA isolation. The filters were washed twice in ice-cold HBSS-HEPES (25 mM). Tri Reagent® (150 µL) was added to the monolayers to extract total RNA. After incubating for 5 min at room temperature (22°C), the solubilised monolayers were mixed by pipette agitation (20x) and were subsequently stored at -80ºC for up to 4 weeks. After defrosting solubilised monolayer extracts on ice, a chloroform-based RNA extraction followed. Chloroform (300 µL) was added to the solubilised monolayer and mixed, left to incubate on ice for 10 min and spun at 13000 rpm for 10 min at 4ºC. The uppermost layer (above the median DNA interface) containing RNA was decanted into 500 µL isopropanol and left at -25ºC for 90 min. Samples were spun at 13000 rpm for 10 min at 4ºC and the supernatant was removed leaving pellet containing the RNA. The pellet was washed by centrifugation in 70% ethanol at 13000 rpm for 10 min at 4ºC, the ethanol was removed and the pellet was air-dried. The dried pellet was re-suspended in RNase/DNase free molecular biology grade water and the RNA quality (A260/A280 ratio) and content was determined on a nanodrop-lite spectrophotometer (Thermoscientific, Pittsburg, PA, USA). RNA preparations were stored at -80ºC. RNA samples that demonstrated an A260/A280 ratio of < 1.8 were not incorporated into further analyses.

RNA (3 µg) was reverse transcribed to cDNA with reverse transcriptase and random hexamer primers from a Transcriptor First Strand cDNA Synthesis Kit (Roche Applied Science, Burgess Hill, Sussex, UK) at 29°C (10 min), 50°C (60 min) and 95°C (5 min) on a temperature controlled heating block (Techne, Bibby Scientific, Staffs, UK). The reaction was stopped on ice.

2.2.9.2 Gene Expression Analysis by Real-Time PCR

Relative quantification of transporter gene expression was performed with a Light cycler 480 real-time Polymerase Chain Reaction (PCR) system (Roche Diagnostics, Burgess Hill, Sussex, UK) using gene-specific primer pairs combined with detection by hydrolysis probes that were FAM 5'-fluorescein-labelled and 3'-labelled dark quencher dye (Bannon et al., 2009). Gene-specific primers

were designed by the Probe Finder software (version 2.49 for human, http://lifescience.roche.com). The complementary hydrolysis probes for the selected primers were identified in the assay design centre application of the Probe Finder software. The primer pairs and complementary probes for the 8 selected genes are provided in Table 2-3.

Table 2-3. Primer sequence and complementary hydrolysis probes used for the 8 selected genes analysed for relative gene expression analysis by real-time PCR.

Gene	Primer Sequence	Hydrolysis Probe
Peptidyl-prolyl-isomerase A (PPIA, Cyclophilin A)	F – atgctggacccaacacaaat R - tctttcactttgccaaacacc	# 48
P-Glycoprotein (P-gp, MDR1, ABCB1)	F – gagtatcttcttccaagatttcacg R – tccccttcaagatccatcc	# 49
Breast Cancer Resistance Protein (BCRP, ABCG2)	F - tggcttagactcaagcacagc R - tcgtccctgcttagacatcc	# 56
Multidrug Resistance-Associated Protein 2 (MRP2, ABCC2)	F - agcatgcttcccatgatga R - tctagccgctctgtggaaac	# 1
Organic Anion Transporter Polypeptide B1 (OATP2B1, SLCO2B1)	F - ataccgctacgacaacacca R - tgagcagttgccattggag	# 57
Organic Solute Transporter A (OST-A, OST-α, SLC51A)	F - gctgtggtggtcattataagcat R - gtggctgcatcgtttctttt	# 75
Organic Solute Transporter B (OST-B, OST-β, SLC51B)	F – ctgaagaccaattacggcatc R - gagggcaagttccacagg	# 79

For the analysis of relative gene expression, the probe master mix supplied within the Light Cycler 480 Probes Master kit containing FastStart Taq DNA polymerase, reaction buffer, $MgCl_2$ and dNTP mix (Roche Applied Sciences, Burgess Hill, UK) was combined with 0.5 µL (20 µM) forward and reverse primers, 0.44 µL of hydrolysis probe, 1 µL cDNA and 8.36 µL of PCR-grade H_20 to provide a 20 µL assay mix aliquoted into a V-bottomed 96 well PCR plate. Negative control reactions without cDNA were carried out for each run. The PCR reaction was carried out under the following conditions on the Light cycler 480 apparatus. An initial cycle to activate the Taq DNA Polymerase at 95°C for 10 min followed by 45 cycles of 95°C for 10 sec, 55°C for 15 sec and the 72°C for 1 sec. The program ended with a cooling cycle of 40°C for 10 sec. The action of Taq DNA polymerase on the hydrolysis probe catalyses the cleavage and separation of the fluorescent reporter and quencher dyes, emitting a fluorescent signal which is detected at 530 nm by the light cycler system. The intensity of the fluorescence signal indicates the level of a particular genes expression. The calculation of gene expression is based on the ratio of the cycle threshold of the target to that of the reference. The assumption herein, is that the amplification efficiencies per

cycle, (*i.e.,* a doubling in the amount of material for each cycle, or 100% efficiency) for the reference housekeeper gene Peptidylprolyl Isomerase A (PPIA) and target (transporter) gene are the same. Therefore, if the expression of target gene is high, the target:reference ratio will approach 1.

2.2.10 Determining Transporter Function by Monolayer Transport Assays

In the following section, the general methods consistently applied to monolayer flux assays are described. Transport assay procedures that are specific to a particular aspect of the studies presented in this thesis will be described in detail in the relevant results chapter.

2.2.10.1 Bi-Directional Monolayer Transport Assay: General Methods

For bi-directional transport experiments (Apical-to-Basolateral: A-to-B & Basolateral-to-Apical: B-to-A), Caco-2 cells (all variants) were seeded on 1.13 cm^2 polycarbonate Transwell filters at 2.2 x 10^5 cells per cm^2 and were maintained in growth media for 10, 21 and 29 days in a humidified atmosphere of 95% air and 5% CO_2 at 37°C. Cells were fed every 2 days with monitoring of TEER run in parallel to assess tight junction formation. Cells were fed 24 hours prior to the commencement of the transport assay. The placement of transport buffers HBSS-HEPES (25 mM) pH 7.4 or HBSS-2-(N-morpholino)ethanesulfonic acid (MES) (10 mM) pH 6.5 (Neuhoff et al., 2003) in the apical or basolateral chambers was dependent on the experiment being performed. Transport buffers containing [^{3}H]-labelled test compounds (E-3-S at 0.01 µM and VBL at 0.03 µM for the tritiated compound) and concentrations in addition to up to 1000 µM of cold VBL stock for kinetic assays, LY (50 µM) and in certain experiments unlabelled inhibitors were warmed to 37ºC. For the flux assay, the monolayers were washed for 15 min at 37ºC in a calibrated rotating incubator (Stuart Scientific, Bibby Scientific, Staffs, UK) at 100rpm in HBSS-HEPES (25 mM) pH 7.4. After washing, TEER was measured and the bi-directional flux assay was initiated by addition of transport buffer containing the test compound to the designated donor chamber, with 0.4 mL added to the apical and 1.2 mL added to the basal chamber. The donor transport buffer was immediately sampled (100 µL) and replaced with the same volume of transport buffer containing the test compound. Monolayers were stirred at 100 rpm and 37ºC, with 1 x 100 µL sample withdrawn from the receiver chamber into a 4 mL LSC vial for subsequent ^{3}H counting and 1 x 100 µL sample aliquoted into a black 96 well Optiplate for monitoring monolayer integrity by LY transport. The appropriate transport buffer without test compound was used to replace the 200 µL sampled from the receiver buffer to maintain chamber buffer volumes. Sampling took place on a heating block set to 37ºC, at varying time intervals (dependent on the experiment) for up to 2

hours. At the end of the experiment, final donor samples were taken to assess mass balance over the experimental duration. To evaluate the monolayer content of test compound at the end of the transport assay, filters were washed three times in ice cold HBSS-HEPES (25 mM) pH 7.4 and filters were cut out with a scalpel blade and deposited into an LSC counting vial. Three mL of Optima Gold LSC cocktail was added to the samples and mixed vigorously by hand. Samples were left for 2 hours then counted on a 1211 Rackbeta liquid scintillation counter (Wallac, Milton Keynes, UK) for 5 min. The tritiated counts/min/pmol of probe compound was used to calculate monolayer content after correction for filter binding. LY fluorescence was determined as descrtibed in Section 2.2.2.2, monolayers displaying a LY Papp > 1 x 10^{-6} cm sec^{-1} were discarded. Experiments were performed under 'sink' conditions, *i.e.,* a less than 10% transfer of the test compound from the donor into the receiver compartment and mass balance was monitored over the duration of the transport assay (Equation 2-2). In instances where the sink was violated, the flux periods were omitted from final permeability analyses. Results from monolayers were discarded where mass balance was violated, *i.e.,* where a > 80% recovery of the test compound over the duration of the transport assay was observed. The Papp for test compounds and LY was determined using Equation 2-3.

$$R = \frac{(C_r(t) \cdot V_r + mono + C_d(t) \cdot V_d)}{(C_0 \cdot V_d)} \cdot 100 \qquad \text{Equation 2-2}$$

where R is the recovery of the test compound over the duration of the transport assay, C_r and C_d are the concentrations on the donor and receiver chambers at time (t), C_0 is the initial concentration in the donor compartment at t=0, mono is the concentration in the filter/monolayer at the end of the experiment with V_d and V_r, the volumes of the donor and receiver compartments, respectively.

$$\text{Papp} = \frac{(\frac{dC}{dT})}{C.A} \qquad \text{Equation 2-3}$$

where *dC*/*dT* is the flux of the test compound calculated from the slope of the appearance of the compound over time in the receiver compartment, C is the concentration of the drug in the donor solution at the start of the assay and A is the area of the filter.

In many transport experiments the presence of an assymetrical Papp in the B-to-A *versus* the A-to-B indicates the presence of an active efflux transport mechanism. In order to obtain information about the impact of transporter proteins on Papp, asymmetrical transport was assessed by

calculating the efflux ratio (ER), the ratio of transport (Papp) in the B-to-A and A-to-B directions (Equation 2-4).

$$\text{Efflux Ratio} = \frac{Papp_{(B-to-A)}}{Papp_{(A-to-B)}} \quad \text{Equation 2-4}$$

2.2.11 Analysis of E-3-S Protein Binding

A protein binding assay was employed to determine the extent of E-3-S binding to BSA in transport experiments with Centrifree® micropartition filter devices with a nominal molecular weight limit of 30,000 KdA (Millipore, Bedford, MA, USA). The Centrifree® device was warmed to 37°C together with HBSS-MES (pH 6.5) and HBSS-HEPES (pH7.4) with and without the addition of 0.05% (w/v) BSA. Additionally, 0.01 µM [$^{3-}$H]-E-3-S was spiked into each buffer with an accompanying non-labelled buffer acting as a control.

For background correction, samples of the blank buffer (pH 6.5 and 7.4) with and without BSA were taken. Initial donor samples with buffers containing 0.01 µM [$^{3-}$H]-E-3-S were sampled prior to filtration. The Centrifree® devices were spun-washed for 20 min in the appropriate buffer without BSA or [$^{3-}$H]-E-3-S at 2000 x *g* in a Heraeus cryofuge 5500i centrifuge with a swing out rotor at 37°C. Centrifree® devices were loaded with 0.5 mL of the BSA buffer with and without [$^{3-}$H]-E-3-S (n=3 devices per condition) and spun at 2000 x *g* for 20 min, with a swing out rotor at 37°C. After centrifugation, the filtrates were sampled. The sample radioactivities were determined in duplicate (100 µL) on two separate days after the addition of 3 mL LSC cocktail and determined over 5 min in a liquid scintillation counter (Wallac, Turku, Finland).

Correction for adsorption of [$^{3-}$H]-E-3-S to components of the Centrifree® devices was undertaken in buffer without BSA. The fraction of [$^{3-}$H]-E-3-S adsorbing did not exceed 12%.

The unbound fraction of E-3-S was calculated using Equation 2-5 and was subsequently used for determining in the unbound donor and receiver concentrations in the transport assay.

$$f_u = \frac{C_u}{C_{initial}} \quad \text{Equation 2-5}$$

2.2.12 Estimation of Transporter Kinetic Parameters by Compartmental Modelling

To obtain the intrinsic kinetic parameter estimates CLint, Jmax and Km, and $P_{passive}$ the simultaneous fitting of probe substrate concentrations (pmol/L) in donor and receiver compartments

from bi-directional transport assays was performed using R (version 3.1.1, R Foundation for Statistical Computing, Vienna, Austria). The model was developed by Dr Howard Burt, Simcyp Ltd (Sheffield, UK) for internal validation of a toolkit developed for *in vitro* assay kinetic parameter estimation. The base structure of the model describes the apical, cell and basolateral compartments of the filter-based Caco-2 monolayer system (Figure 2-3).

The permeation of the drug into each compartment over the duration of the transport assay was fitted by describing the $P_{Passive}$ of the P-gp probe substrate VBL across the apical and basolateral membranes and an active efflux component (P-gp) operating at the apical membrane (Equation 2-6, Equation 2-7 & Equation 2-8). It should be noted that the model generates permeability estimates in 10^{-4} cm sec^{-1} units, as these data can be directly input into Simcyp's population-based simulator as a P_{eff}, in units of 10^{-4} cm sec^{-1}. In this study, for the ease of translation to the *in vitro* experimental system data, $P_{passive}$ with SA corrections already applied when estimated by the model, will be reported as units of 10^{-6} cm sec^{-1}.

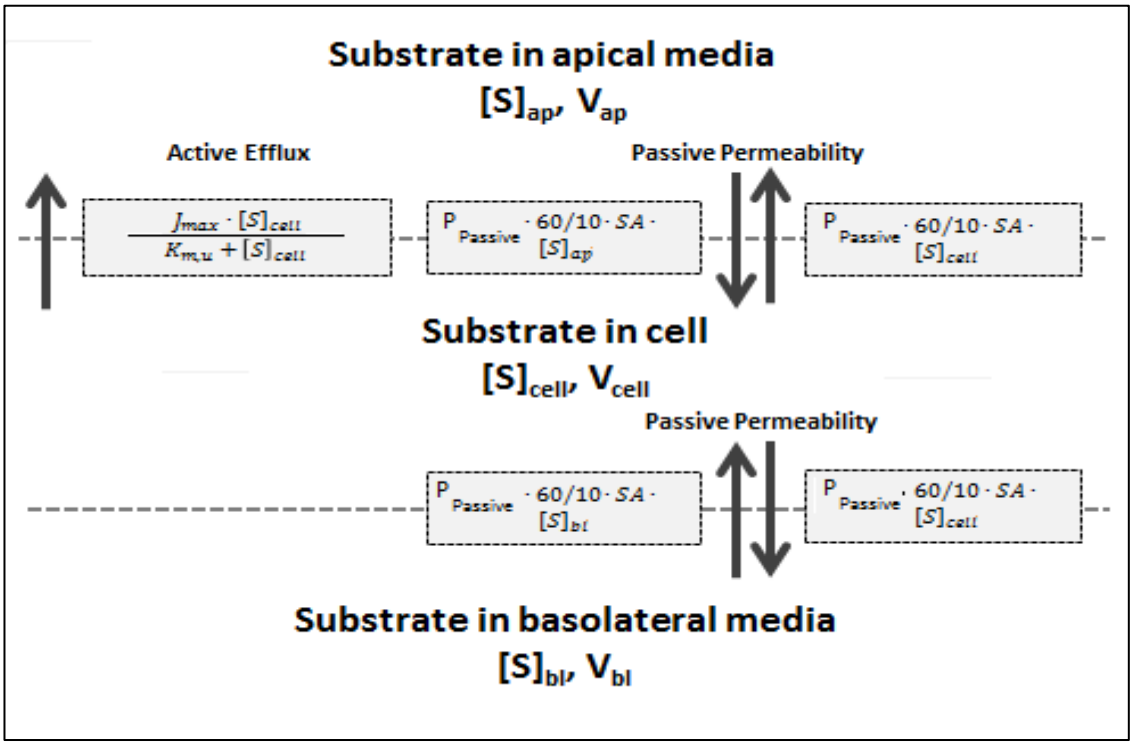

Figure 2-3. The structure of the three compartment model to estimate the transporter kinetic parameters from bi-directional transport assays. Jmax is the maximum rate of apical efflux transport (pmol/min), $P_{Passive}$ is the passive permeability and SA is the surface area of the apical or basolateral membrane (cm^2). A conversion factor (60/10) to convert min to seconds and permeability to 10^{-4} cm s^{-1}. This is an adaptation of an image produced by Dr Howard Burt, Simcyp Ltd (a Certara Company, Sheffield, UK).

$$V_{ap} \cdot \frac{d[S]_{ap}}{dt} = \frac{J_{max} \cdot [S]_{cell}}{K_{m,u} + [S]_{cell}} + P_{Passive} \cdot 60/10 \cdot SA \cdot \left([S]_{cell} - [S]_{ap}\right)$$ Equation 2-6

where substrate concentration in the apical compartment over the duration of the assay is estimated using the volume of apical media in microliters (V_{ap}), the substrate concentration [S] in the cell and the apical compartment (pmol/L), $P_{Passive}$, SA and the Jmax and Km of the active efflux process operating on the apical membrane. The 60/10 term converts minutes to seconds and permeability to 10^{-4} cm s^{-1}.

$$V_{cell} \cdot \frac{d[S]_{cell}}{dt} = -\frac{J_{max} \cdot [S]_{cell}}{K_{m,u} + [S]_{cell}} + P_{Passive} \cdot 60/10 \cdot SA \cdot \left([S]_{ap} + [S]_{bl} - 2[S]_{cell}\right)$$ Equation 2-7

where substrate concentration in the cellular compartment over the duration of the assay is estimated using the volume of cell in microliters (V_{cell}), the substrate concentration [S] in all compartments (pmol/L), $P_{Passive}$, SA, Km and Jmax of the active efflux process operating on the apical membrane.

$$V_{bl} \cdot \frac{d[S]_{bl}}{dt} = P_{Passive} \cdot 60/10 \cdot SA \cdot ([S]_{cell} - [S]_{bl})$$ Equation 2-8

where substrate concentration in the basolateral compartment over the duration of the assay is estimated using the volume of basolateral media in microliters (V_{cell}), the substrate concentration [S] in the cell and the basolateral compartment, $P_{Passive}$ and SA. The rate of transport (pmol/min) is combined within volume term providing the change in concentration (µM/min).
A series of assumptions are made within this model.

- There is negligible non-specific binding of the probe compound to the experimental system, buffer components or intracellular components.
- The compound is entirely available for active transport and passive permeability across both cell membranes without consideration for ionisation due to pH.
- An equal surface area is assumed at each pole of the cellular compartment
- Paracellular permeability is negligible
- The apical and basolateral unstirred boundary layer does not impact on substrate permeation across the monolayer

The model was built upon the selection of key structural 'fixed' parameters with known or experimentally determined values which include, the compartmental volumes, the SA's and for some fitting procedures drug-dependent parameters *i.e.,* $P_{Passive}$. In addition to the experimentally observed data and known parameters, initial parameter estimates for the unknown parameters

which required model estimation were provided based on experimental data or literature values. The model accounts for the removal of receiver compartment samples and the dilution in probe drug concentrations resulting from replacement with fresh probe-free transport buffer, to maintain buffer volumes within the transport assay.

The observed substrate concentrations within kinetic data sets spanned ~7 orders of magnitude. The larger values within the dataset are likely to bias the fitting procedure, therefore to estimate the goodness of model fit to the observed data, the weighted least squares regression method ($1/Y^2$) was employed. However, using $1/Y^2$ regression can provide too great a weight to the smaller numbers for the fitting procedure. The aim of the fitting procedure is to minimise the objective function (residual difference in the observed and fitted concentrations in the receiver compartment) to a global optimal minimum using a non-linear Newton-type algorithm (the function 'nlminb' available from the base R package). To gauge the goodness of model fit for both A-to-B and B-to-A transport simultaneously, the geometric mean fold error (GMFE), geometric mean fold bias (GMFB) and root mean square error (RMSE) were generated.

$$\mathrm{GMFE} = 10^{\frac{\sum\left|\log\frac{Predicted\ [Drug]}{Actual\ [Drug]}\right|}{\mathrm{N}}} \qquad \text{Equation 2-9}$$

$$\mathrm{GMFB} = 10^{\left|\frac{\sum log\frac{Predicted\ [drug]}{Actual\ [drug]}}{N}\right|} \qquad \text{Equation 2-10}$$

$$\mathrm{RMSE} = \sqrt{\frac{\sqrt{(\mathrm{Predicted\ [Drug]} - Actual\ [Drug]^2)}}{\mathrm{N}}} \qquad \text{Equation 2-11}$$

For data analysis, unless implicitly specified, all data analysis and statistics were performed in MS Excel (Redmond, WA, USA) and GraphPad Prism (San Diego, CA, USA) software packages.

Chapter 3-Development and Validation of Membrane Extraction Techniques for Quantitative Targeted Absolute Proteomic Studies

Declaration

Excerpts of text from this chapter are extracted from published articles:

1. *M.D. Harwood et al.,* (***2013)****, Biopharm Drug Dispos. 34, 2-28.*
2. *M.D. Harwood, et al., **(2014).** DMD. 42, 1766-1772.*

I wrote these manuscripts with editing undertaken by the co-authors. I retained editorial control for both these articles.

3.1 Introduction

Reducing the complexity of cellular material to obtain the desired organelle for functional studies has been undertaken for decades and is generally achieved by multistage centrifugation (Neville, 1960; Fleischer and Kervina, 1974). Quantification of transporter protein abundance by a QTAP strategy has used subcellular fractionation techniques to reduce sample complexity to prevent the muffling of targeted, low abundance membrane proteins, enhancing detection sensitivity in LC-MS/MS (Huber et al., 2003). Studies measuring the absolute abundances of transporters have used either homogenisation with differential centrifugation, or commercially available membrane extraction kits to obtain the total membrane (TM) or plasma membrane (PM) fractions for abundance quantification (Li et al., 2009c; Miliotis et al., 2011b; Ohtsuki et al., 2012). For each method, a differing number of homogenization, centrifugation and incubation steps are applied. Therefore, there appears to be no consensus as to the optimal methods to obtain an appropriate membrane fraction in which to measure transporter protein abundances (Harwood et al., 2014).

When reducing sample complexity, the purity of the targeted organelle fraction(s) is routinely assessed by undertaking activity assays in which an enzyme(s) that resides specifically within an organelle is used as a marker of purity. Assessment of the marker enzyme's activity in fractions derived throughout the enrichment procedure and comparison with activity in the whole cell component enables evaluation of enrichment or contamination. Furthermore, recovery and/or losses of target proteins within these organelle fractions may be assessed with enzyme activity balance sheets (Blitzer and Donovan, 1984). However, evaluation of a procedure's ability to enrich the membrane fraction by assessing the activity of key marker enzymes such as the apical membrane (brush border) alkaline phosphatase (AP), a marker of the PM (Ellis et al., 1992) or cytochrome c reductase (CCR), a marker of the endoplasmic reticulum (EnR) (Clark et al., 1969) has not been reported in QTAP studies (Harwood et al., 2014). This chapter aims to;

1) Optimise a PM extraction technique in Caco-2 and MDCK-II-WT cells. Membranes are characterised using marker enzyme activity together with P-gp, using immunoblotting, in order to provide a technique that enables the quantification of transporter proteins.
2) Develop a method to elute human intestinal enterocytes by a calcium chelation technique and obtain a TM fraction with AP activity enrichment characterisation.

3.2 Methods

The methods employed in this chapter include those described in Section 2.2.1 for Caco-2 and MDCK-II-WT cell culturing procedures, Section 2.2.4 for enzyme assay, Section 2.2.2.2 for membrane harvest of filter-grown cells and immunoblotting Section 2.2.5. Section 2.2.2.3 describes procurement of human tissue, Section 2.2.2.4 for enterocyte elution by chelation and membrane fractionation, Section 2.2.2.5 for preparation of membrane fractions after mucosal crushing and Section 2.2.3 describing histological assessment of human enterocyte chelation.

3.2.1 Preparation of Membrane Fractions from MDCK-II-WT and Caco-2 Cells

Two differential centrifugation methods were used to extract PM fractions.

3.2.1.1 Method 1

Method 1 is based on Tohoku University methodology (Kamiie et al., 2008; Ohtsuki et al., 2012).

Flask-grown cells were harvested by scraping or trypsin and were subjected to homogenisation by Dounce hand held homogenisation (30 strokes) on ice in Buffer A (0.1M KCl phosphate buffer, pH 7.4 plus protease inhibitors). In certain instances, 3 x 24 µA bursts of sonication were applied to the harvested cells. To check for the efficiency of cellular disruption, a 440 x *g* spin for 5 min at 4°C was run to pellet intact cells. A large pellet indicates ineffective cellular homogenisation, in these instances sonication re-commenced followed by homogenisation. The final homogenate was centrifuged at 10,800 x *g* (20 min, at 4°C) to pellet nuclear/mitochondrial fractions. The supernatant containing cellular membrane proteins was spun at 100,000 x *g* (20 min, at 4°C). The pelleted TM fraction was re-suspended in Buffer B (20 mM Tris-HCl, 250 mM Sucrose, 5.4 mM EDTA, pH 7.4) and layered on top of a 38% w/v sucrose cushion and centrifuged at 100,000 x *g* for 30 min at 4°C. The resultant turbid interface at the sucrose-buffer boundary containing 'PM' was harvested, re-suspended in Buffer B and centrifuged at 100,000 x *g* for 30 min at 4°C. The resultant pellet was re-suspended in 10 volumes of Buffer B. At various stages samples were taken and stored at -80°C to assess membrane enrichment by performing AP activity assays.

3.2.1.2 Method 2

Method 2 is described in Section 2.2.2 and Figure 2-1. Cells were harvested from flasks by scraping rather than by trypsinisation, due to the difficulty in harvesting a complete monolayer from filter-grown cells after trypsin incubation and concerns over proteolysis of target transporter proteins.

3.3 Results

3.3.1 Optimising Membrane Extractions in Flask-Grown MDCK-II-WT Cells

MDCK-II cells (passage 14-18) were chosen for initial membrane extraction experiments due their rapid growth characteristics and their previous usage in QTAP method development (Li et al., 2008; Zhang et al., 2011). Using Method 1, confluent MDCK-II cells grown in 75 cm^2 tissue culture flasks (~$15x10^6$ cells/flask) were harvested. Following homogenisation, a substantial pellet of whole cells was recovered post 440 x *g* spin (confirmed by microscopy), suggesting the cells were not disrupted effectively by homogenisation. This led to an absence of a TM fraction after the 100,000 x *g* spin. Tip-based sonication in conjunction with Dounce homogenisation was employed and cellular disruption was visualised by microscopy. The addition of sonication did yield a TM fraction however, a 'PM' fraction was not obtained, likely due to insufficient starting material.

Previous QTAP studies harvested MDCK-II cells from 162-175 cm^2 flasks to extract a 'native' membrane fraction using a membrane extraction kit (Li et al., 2008; Zhang et al., 2011). Therefore, the next set of experiments were conducted in 3x75cm^2 confluent flasks containing MDCK-II-WT cells (~$45x10^6$ cells) were extracted to increase the likelihood of obtaining a PM fraction. The homogenisation and sonication steps used previously were retained. Three separate extractions were performed on separate days. A consistent TM yield was achieved in experiments 2 and 3, with 1.77 and 1.81 µg/cm^2 protein obtained, respectively. The enrichment of the AP activity was determined in the starting and each harvested fraction (Figure 3-1). It is expected that the highest AP activity should be within the TM with the lowest activity in the nuclear/mitochondrial fraction. This data shows that using this extraction protocol, AP activity was not specifically enriched in the TM fraction, with only one of the three TM preparations showing a higher AP activity compared to the nuclear/mitochondrial fraction. The most likely explanation is that ineffective cellular breakage of the cultured cells using the homogenising and sonication protocol was leading to incomplete separation of plasma membranes from other organelles, particularly the nuclear/mitochondrial fraction. A further review of the literature for alternative strategies to effectively disrupt immortalised cells was undertaken.

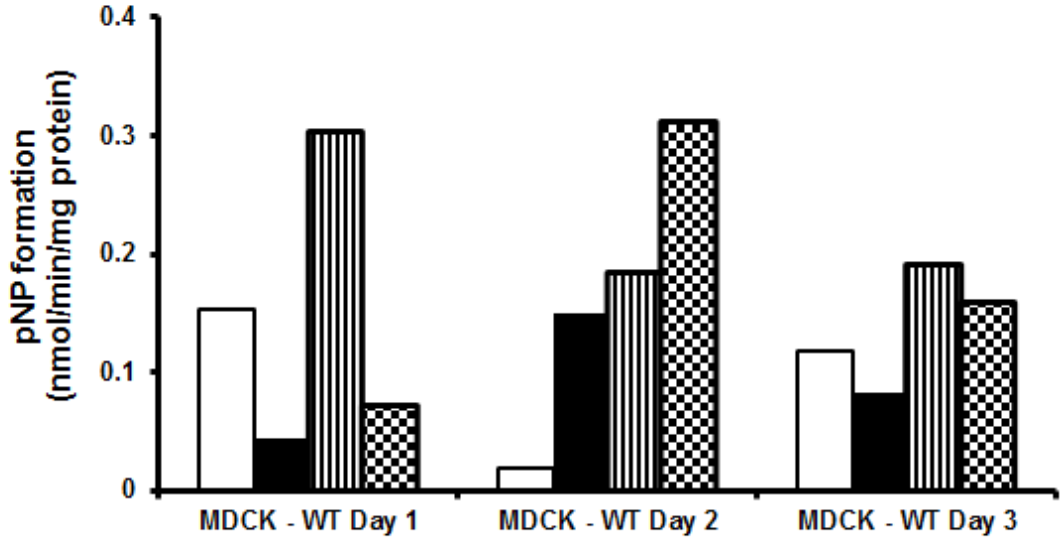

Figure 3-1. Alkaline phoshatase activity in various MDCK-II-WT cell fractions derived from method 1 membrane extraction protocol on 3 different days. MDCK-II-WT cells were grown to confluence in 3x75cm^2 flasks. The starting total protein (TP) and subsequent fractions in which alkaline phosphatase activity was measured are the; total protein (white bars), cytosolic and membrane containing supernatant (black), nuclear & mitochondrial fraction (vertical lined) and the total membrane fraction (chequered).

A study that specifically isolated a TM fraction from MDCK-II-MDR1 for subsequent transporter protein expression studies was identified (Zhang et al., 2004). The strategy for cellular breakage in Zhang et al., was an overnight lysing of cells in 1mM $NaHCO_3$ containing protease inhibitors followed by double homogenisation. Cellular swelling in hypotonic $NaHCO_3$ facilitates cell lysis. Further extractions ensued using the protocol of Zhang *et al*. (Method 2). Following personal communications with scientists from the Netherlands Organisation for Applied Scientific Research (TNO), the number of cells for membrane harvest increased. TNO used 70x10^6 to obtain abundance values in the PM fraction of MDCK-II cells (Verhoeckx et al., 2011).

Confluent MDCK-II cells were harvested by scraping from 3x175cm^2 flasks containing ~100x10^6 cells after overnight lysing in 1mM $NaHCO_3$ (n=3 experiments). A visual check using microscopy demonstrated that there was an absence of whole cells in the overnight lysate. To assess the composition of the fractions at each stage, samples were taken for analysis of AP activity. Based on initial experiments, the procedure from Zhang et al., was modified in light of AP activity loss from the discarded 4000 x *g* pellet, while the $MgSO_4$ stirring step was omitted as it is required for harvest of a brush border membrane fraction (Wilson and Webb, 1990). Both steps were omitted for future experiments. Consistent TM protein yields were obtained (1.75±0.16 µg/cm^2, n=3) and a PM fraction was obtained providing protein yield of, 0.6±0.32 µg/cm^2, (n=3).

AP activity was measured in the starting TP and each of the 3 subsequent fractions sampled (Figure 2-1) and summarised in Figure 3-2. AP activity increases throughout the procedure, although the degree of enrichment is modest from the TM (2.8-fold) to the PM fraction (3.8-fold).

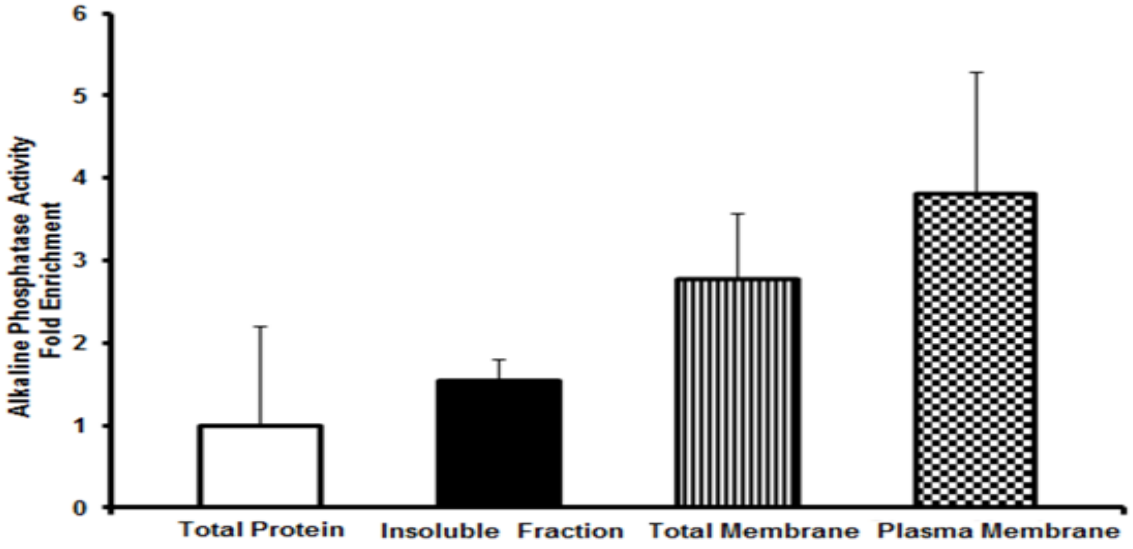

Figure 3-2. The enrichment in alkaline phosphatase activity in the starting TP and subsequent MDCK-II-WT cell fractions derived from membrane extraction method 2. MDCK-II-WT cells were grown to confluence in 3x175 cm^2 flasks (n=3). Values are given as Mean±SD from n=3 experiments.

To check for EnR membrane enrichment, the CCR activity assay was undertaken in matching samples to those in the AP activity assay. A limited enrichment in CCR activity in both the TM and PM fractions compared to the TP is shown (Figure 3-3). Unlike the plasma membrane marker AP, there was no further enrichment of the microsomal marker CCR in the PM fraction, suggesting a moderate reduction of EnR components.

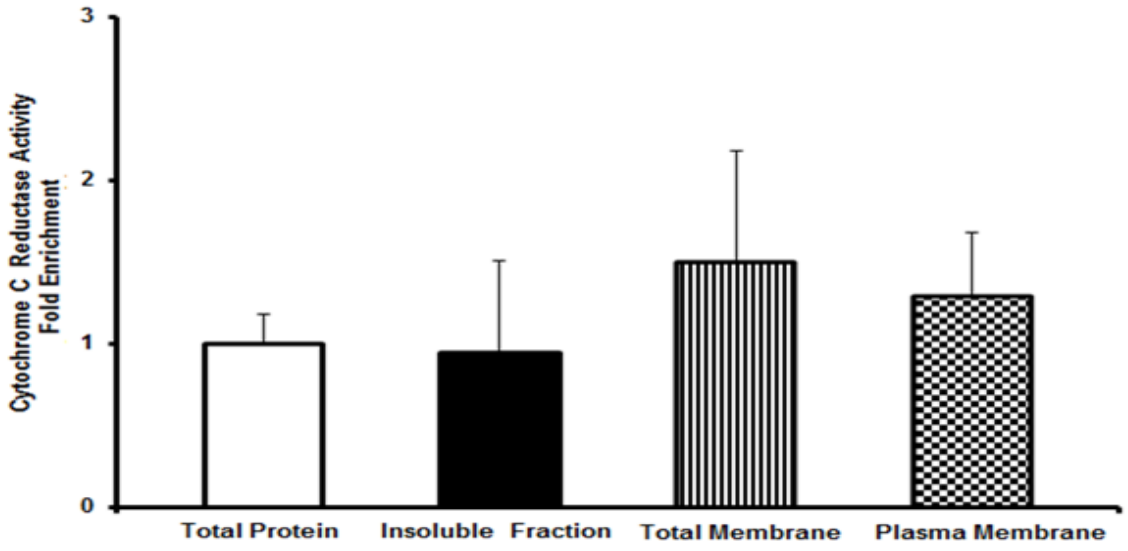

Figure 3-3. The enrichment in cytochrome c reductase activity in the starting TP and subsequent MDCK-II-WT cell fractions derived from membrane extraction method 2. MDCK-II-WT cells were grown to confluence in 3x175 cm^2 flasks (n=3). Values are given as Mean±SD.

On the basis that the AP activity enrichment for flask-grown MDCK-II-WT cells is 3.8-fold compared to the starting TP (Figure 3-2), a comparison of activity enrichment *versus* the expected enrichment, based on protein yield was performed. Figure 3-4 shows the yield of the protein in the TP and subsequent fractions from flask-grown MDCK-II-WT cells. Less than 4% of the total cellular protein constitutes the TM fraction. The PM fraction constitutes 1.4% of the TP and 36% of the TM fraction. Theoretically, if the purity of the PM fraction is 100% (*i.e.,* there are no contaminating organelles) and AP activity reflects the purity of the PM fraction, the expected enrichment in the AP activity should be ~70-fold which is clearly not observed (Figure 3-3). Therefore, it is likely there are contaminating organelle components in the PM fraction, such as the EnR, as demonstrated by CCR activity in the PM fraction. Thus, Method 2 provides TM and PM fractions with specific, yet modest, enrichment of PM protein in these relatively undifferentiated cells and this approach was adopted in subsequent experiments.

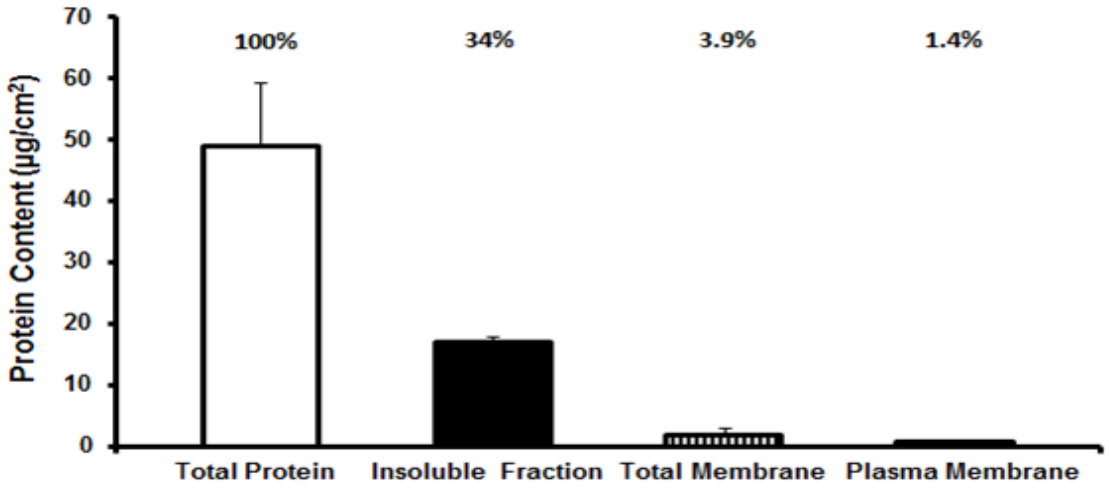

Figure 3-4. Protein content of various MDCK-II-WT cell fractions derived from membrane extraction method 2 as measured by the BCA assay. The text above the bars refers to the percentage yield of each fraction relative to the starting total protein fraction. Values are given as Mean±SD, n=3.

3.3.2 Optimising Membrane Extractions in Flask-Grown Caco-2 Cells

Having established a method to obtain TM and PM fractions in flask-grown MDCK-WT cells, method 2 was used for obtaining and characterising membranes from confluent flask-grown Caco-2 cells (Passage 23, 3x175cm^2, ~40x10^6 cells). Figure 3-5 shows comparable fold AP activity enrichment to MDCK-II cells of 3.21±0.13 and 3.4±0.09 (n=3) for the TM and PM, respectively *versus* the TP. Similar to MDCK-II cells, a lower fold enrichment in CCR activity was shown in the TM compared to PM fractions, 5 and 4.2–fold respectively (Figure 3-6) which is expected. However, it appears there is still contamination of the PM with EnR components.

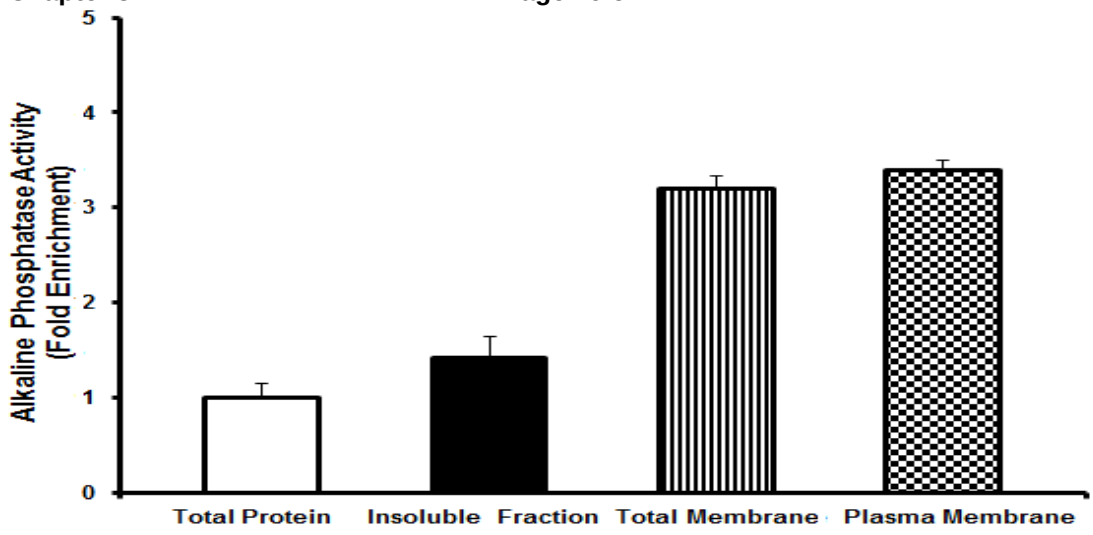

Figure 3-5. The enrichment in alkaline phosphatase activity in various Caco-2 cell fractions derived from membrane extraction method 2. Caco-2 cells were grown to confluence in 3x175 cm^2 flasks (n=3). Values are given as Mean±SD.

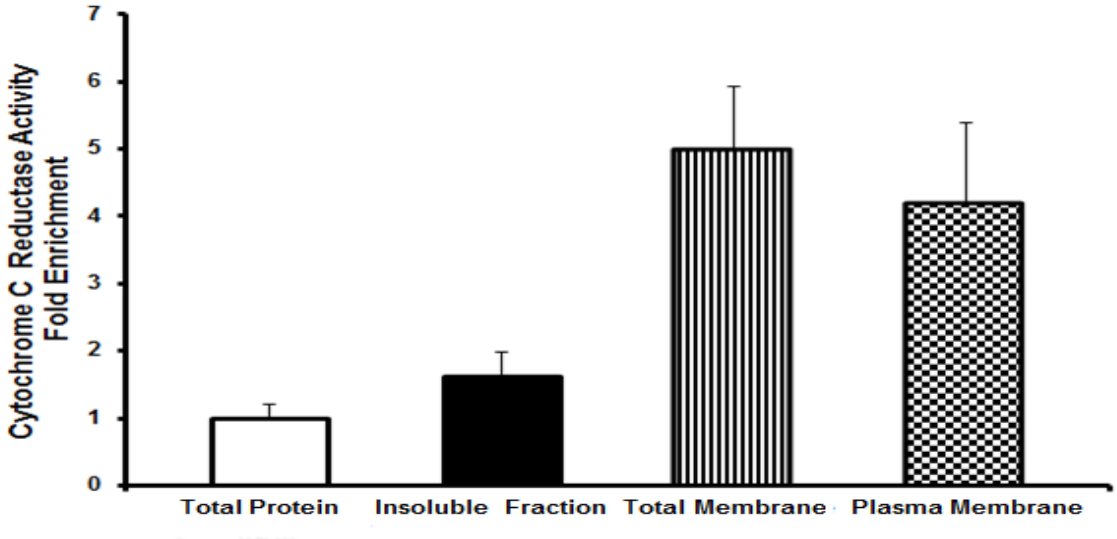

Figure 3-6. The enrichment in cytochrome c reductase activity in various Caco-2 cell fractions derived from membrane extraction method 2. Caco-2 cells were grown to confluence in 3x175 cm^2 flasks (n=3). Values are given as Mean±SD.

The protein yield in the starting material and fractionated samples from confluent flask-grown Caco-2 cells is shown in Figure 3-7. Similar to MDCK-II-WT cells, the TM and PM fractions constitute 3.4% and 1.4% of the total cellular protein, respectively.

Overall, method 2 yields similar enzyme marker activity enrichment and protein yield for flask-grown MDCK-II-WT and Caco-2 cells.

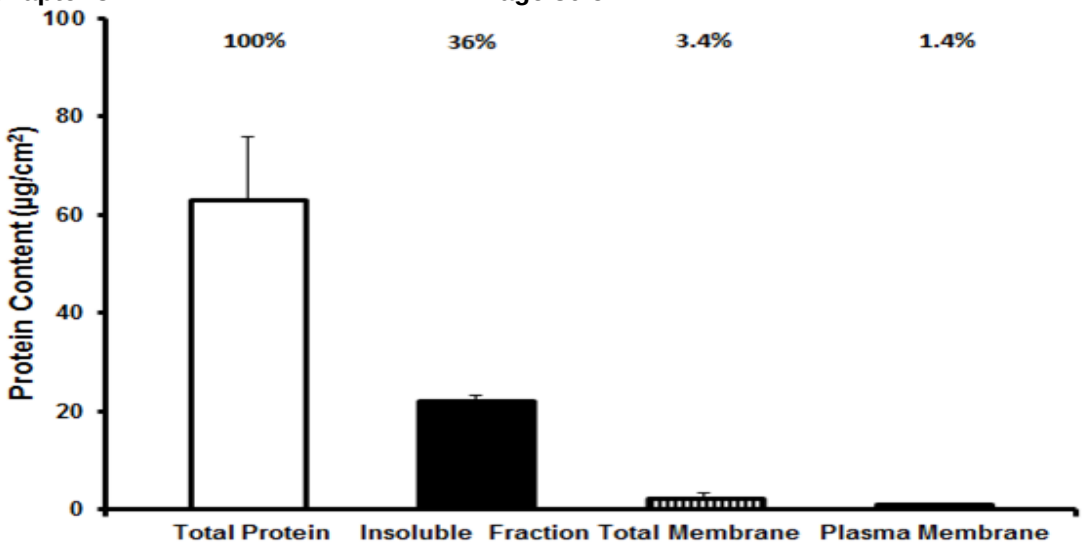

Figure 3-7. Protein content of various flask-grown Caco-2 cell fractions (n=3) derived from membrane extraction method 2 as measured by the BCA assay. The text above the bars refers to the percentage yield of each fraction relative to the starting total protein fraction. Values are given as Mean±SD**.**

3.3.3 Characterising Membrane Extractions in Filter-Grown Caco-2 Cells

Utilising cells cultured in flasks for method development purposes proved time and cost effective. However, employing downstream QTAP-based assays on membranes harvested from flask-grown cells has little utility for developing IVIVE scaling factors. Assessing a compounds' permeability and transporter protein interactions are routinely performed on filter-grown cell monolayers.

For each experiment, Caco-2 cells were grown on 3x44 cm^2 filters. The number of cells on each filter was assessed by trypan blue exclusion after trypsin-harvest on 10 and 29d cultured Caco-2 cells. Mean cell counts did not differ between 10 and 29d-grown Caco-2 cells (passage 25-35), being 32.4±5.21 $x10^6$ and 28.1±5.27 $x10^6$ cells/filter, respectively (n=3 filters, p=0.37, Unpaired t-test). It was therefore expected that approximately $90x10^6$ cells were harvested for membrane extractions. The purpose of growing Caco-2 cells for 10 and 29d (culture periods not typical for the performance of permeability assays) and using a seeding density of $2.2x10^5$ cells/cm^2 was to reciprocate the conditions employed in the study of Miliotis *et al*., 2011, thus enabling comparisons of their P-gp abundances to those subsequently generated in our laboratory (Miliotis et al., 2011b). In addition, Caco-2 cells grown for 16 and 21d (culture times typically employed for permeability assessments) were also used for membrane harvesting.

Monolayer integrity was assessed prior to monolayer harvest by LY transport (A-to-B transport, 60 min). The data provided in Figure 3-8 shows LY transport prior to harvesting the Caco-2 monolayers. There were no differences in LY transport between Caco-2 cell culture periods and Caco-2 cell variants (p=0.16, 1-way ANOVA) in a minimum of 3 experiments with triplicate filters.

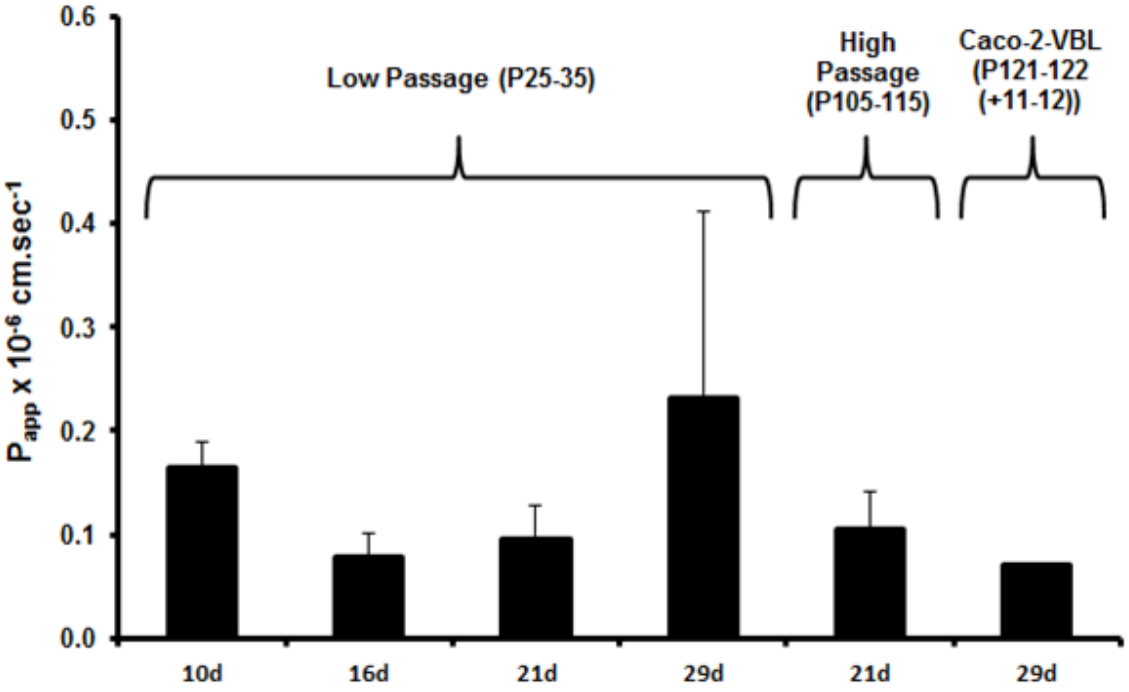

Figure 3-8. Assessment of monolayer integrity by lucifer yellow apparent permeability (Papp) in different Caco-2 cell variants (n=3 filters, N=3-6 experiments). Caco-2-VBL are cells cultured in 11 nM VBL. Values are given as Mean±SD.

Filter-grown Caco-2 cells were fractionated using method 2 developed in flask-grown cells. The cellular fractions were analysed for AP activity as before. To preserve membrane proteins for downstream assays, CCR assays were not performed on filter-grown monolayers. Figure 3-9 shows the AP activity in filter-grown Caco-2 cells for various time periods. As expected, and consistent with the more highly differentiated phenotype characteristic of filter-grown cells, AP activity enrichment in the TM and PM fractions is elevated compared to flask-grown counterparts. The range of AP activity fold-enrichment values for the PM *versus* the starting TP are 5.3±0.75 (21d Caco-2 cells) to 7.7±2.65 (10d Caco-2 cells) with a maximum of 36% AP activity loss (Equation 3-1). There are no differences in the fold AP activity enrichment when comparing matching fractions across the 4 culture periods (p=0.55, 1-way ANOVA). Interestingly, there are only marginal increases in AP activity enrichment between the TM and PM fraction, indicating a lack of purification of the PM from preceding TM fractions. It is expected that a robust marker PM fraction (*i.e.,* AP) is positively correlated to the protein yield from the putative PM obtained from each sample, reflecting the purity of the PM fraction. Therefore, if contaminating components are present in the PM, the correlation between protein and activity should weaken. The relationship

between AP activity and protein content of TM and PM is provided in Figure 3-10. There are no correlations between AP activity, TM and PM proteins (R^2=0.0118 & 0.0143, Figure 3-10 A & C, respectively). Removal of the single outlier (encircled data points, different samples for TM and PM) for the TM and PM fractions still did not produce significant correlations. These data may indicate a PM containing proteins originating from contaminating organelles. Overall, there appears to be limited enrichment in the PM fraction based on AP activity in filter-grown Caco-2 cells.

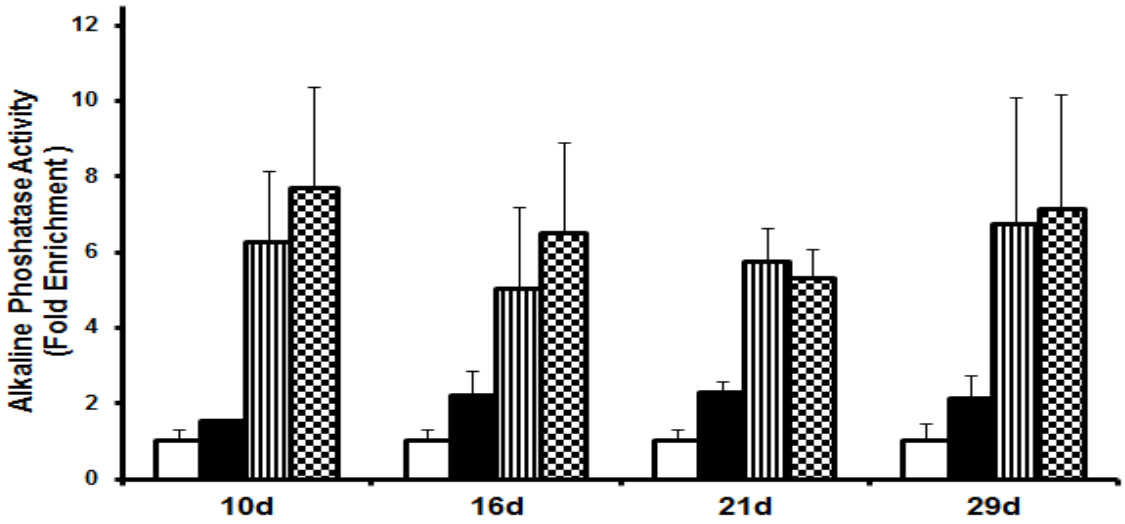

Figure 3-9. The enrichment in alkaline phosphatase activity in various Caco-2 cell fractions grown on filters for 10, 16, 21 and 29 days (n=3 filters, N=4 experiments). The bars represent, total protein (white), insoluble fraction (black), total membrane (vertical lined) and the plasma membrane fraction (chequered).

$$\text{AP activity loss } (\%) = \frac{(AP_{TP} - (\sum AP_{TI}, AP_{TM}, AP_{PM}))}{AP_{TP}} \qquad \text{Equation 3-1}$$

where AP_{TP} is the alkaline phosphatase activity in the total protein, AP_{Ti} is the alkaline phosphatase activity in the insoluble protein fraction, AP_{TM} is the alkaline phosphatase activity in the total membrane fraction, AP_{PM} is the alkaline phosphatase activity in the plasma membrane fraction.

The protein content of subcellular fractions from all variants of filter-grown Caco-2 cells is provided in Figure 3-11**.** For low passage Caco-2 cells a significantly higher TM protein content is observed in 29 *versus* 10d-grown cells (p=0.009, 1-way ANOVA). When comparing each Caco-2 variant grown for 21d (N=3-6), low passage cells showed a higher TP and TM protein content than Caco-2-VBL (p=0.028 & 0.008, 1-way ANOVA, respectively). The protein content of the final PM constitutes a range of 0.8-1.6% and the TM 4-6.1% of the TP fraction. The PM fraction ranges from 16-27% of the preceding TM fraction with a mean of 21±8%, resulting in a 5-fold enrichment in this final stage. Similar to flask-grown cells, a discrepancy between the expected PM enrichment from the protein yield and fold AP activity enrichment is shown for filter-grown cells.

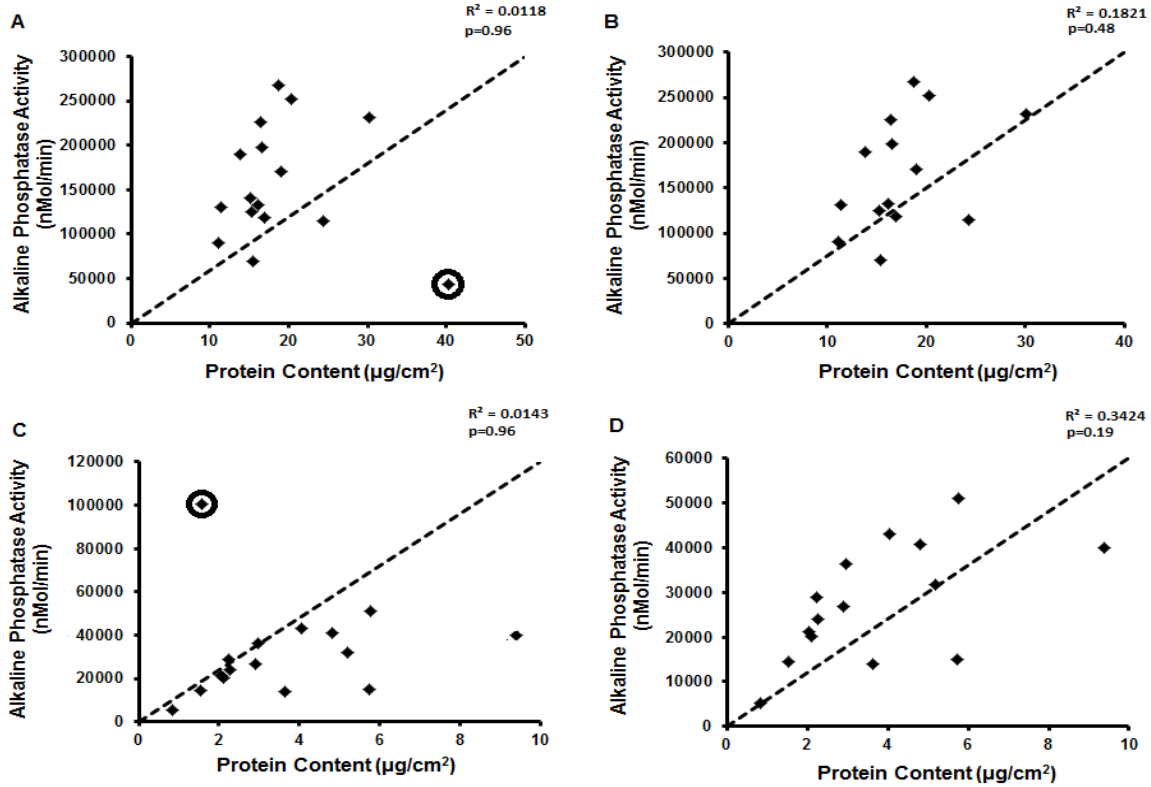

Figure 3-10. An assessment of the relationship between membrane protein content and alkaline phosphatase activity by correlation analysis (Pearson's correlation coefficient). A and C indicate total and plasma membrane fractions (n=16), respectively. The encircled data point indicates an outlier (the data point in A & C are not the same sample). Correlations with removal of the outlier are shown in B and D for total and plasma membrane fractions (n=15), respectively. The correlation coefficient R^2 and significance level (t-distribution) are indicated on each graph. The dashed line indicates the line of identity.

Having undertaken activity assays to assess membrane enrichment, immunoblotting techniques were employed to evaluate the enrichment of the transporter protein P-gp in various fractions of 10d-filter-grown Caco-2 cells (Figure 3-12). A standard curve to assess gel protein loading and blot densitometry in PM fractions (lanes 4-7) indicated that linearity was achieved between 0.625-2.5 µg. Therefore, the densitometry at 2.5 µg loading between fractions was assessed for enrichment after correcting against the actin and background. The blot demonstrates that there is a 23.8-fold enrichment in P-gp expression in the PM fraction (lane 4) , yet the TM fraction (lane 3) did not show enrichment *versus* the insoluble fraction (lane 2). This could be due to a heavy band of actin in this lane precluding the calculation of enrichment using densitometry *versus* the insoluble fraction.

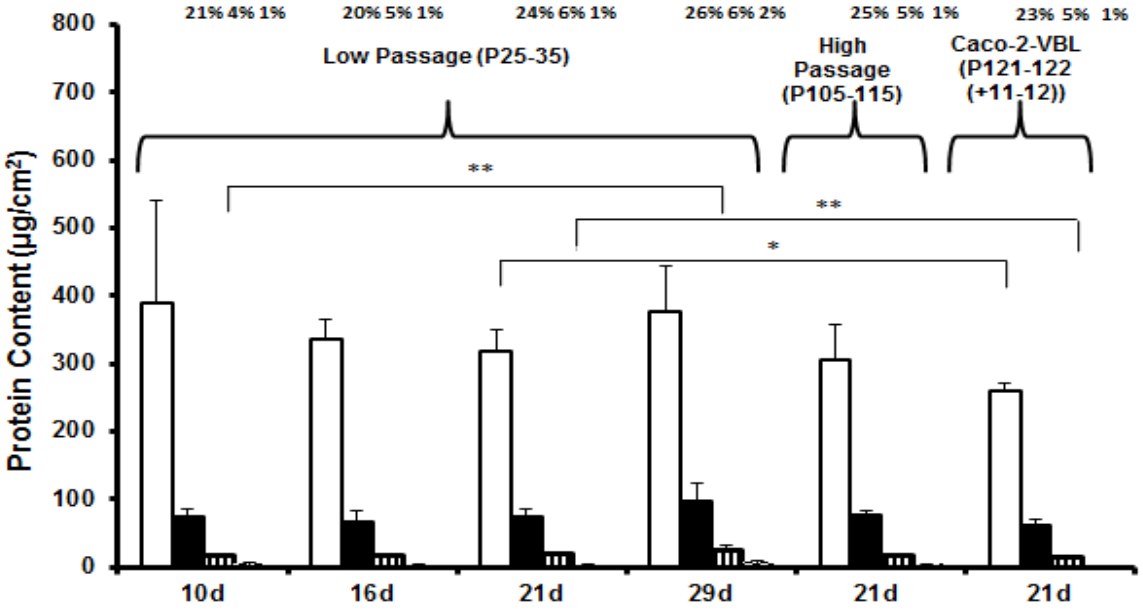

Figure 3-11. Protein content of various filter-grown Caco-2 cell fractions (n=3-6 experiments, triplicate filters per experiment) as measured by the BCA assay. The bars represent, total protein (white), insoluble fraction (black), total membrane (vertical lined) and the plasma membrane fraction (chequered). Caco-2-VBL are cells cultured in 11 nM VBL. Values are given as Mean±SD. The text above the bars refers to the percentage yield of each fraction relative to the starting total protein fraction which is set to 100%.* denotes p=<0.05, **denotes P=<0.01, 1-way ANOVA, with Bonferroni correction to test for differences between all groups.

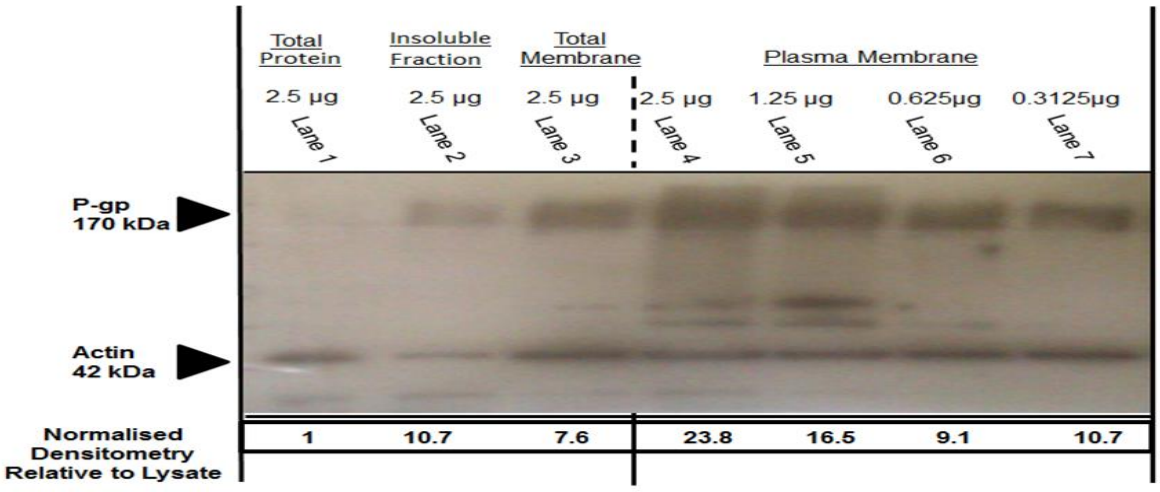

Figure 3-12. Assessing the enrichment of P-glycoprotein (P-gp) throughout the membrane fractionation procedure in 10d filter-grown Caco-2 cells using immunoblotting. The fraction and quantity of protein loaded into each lane is shown in text above the blot. A standard curve to assess the linearity of protein loading was run for the plasma membrane (lanes 4-7). A band resolving at 170 kDa indicates P-gp product and the actin housekeeper 'reference' protein band resolves at 42 kDa. Blot densitometry was used to assess enrichment of each fraction *versus* the total protein fraction. Enrichment is provided in text below the blot, corrected for background and actin densitometry.

3.3.4 Harvesting and Characterising Membranes from Eluted Human Enterocytes

When quantifying absolute protein abundances, it is desirable to isolate the constituent of the tissue in which the target protein is expressed (Shawahna et al., 2011). A calcium chelating agent EDTA was used to liberate enterocytes, from the basal lamina propria of the mucosa. To minimise the liberation of material from the serosal layer, only the luminal mucosal surface was exposed to EDTA using tissue adaptors (Figure 2-2). In a concurrent project undertaken at the Centre for Applied Pharmacokinetic Research, the University of Manchester, Dr Oliver Hatley pre-incubated thawed human intestinal tissues with a citrate buffer to prime the enterocytes for chelation (Weingartl and Derbyshire, 1993), then agitated with 5 mM EDTA (45 min, 4°C) to elute enterocytes. Preliminary experiments using 3 fresh jejunum samples secured in the tissue adaptors found that the 5 mM-EDTA regime provided a low yield of enterocyte and villus material after microscopy observations. Sufficient material to obtain a PM was obtained only when vigorous flushing was applied (needle & syringe) and mechanically brushing the mucosal surface with a scalpel blade. However, mechanical disturbance to harvest enterocytes was not continued due to concerns of liberating lamina propria. Furthermore, a PM fraction could not be established from the eluted colonocyte material (n=1 distal colon) using sodium citrate and EDTA (5 mM). A previous study to harvest colonocytes from distal colon used 30 mM EDTA (Sandle et al., 1994). Therefore, a subsequent experiment incubated distal ileum with 30 mM EDTA, resulting in obtaining a PM fraction. This protocol was employed for subsequent enterocyte harvesting (Section 2.2.2.4). However, the majority of tissues (7 of 9) presented in this study were limited to obtaining a TM fraction, due to insufficient tissue/surface area. A histological inspection of human distal ileal mucosa (Figure 3-13) showed that enterocytes/villus structures were successfully removed from the underlying lamina propria by sodium citrate and 30 mM EDTA elution.

For eluted material, a similar Dounce-homogenisation procedure to that described for Caco-2 cells, (75-125 strokes) was established by visual confirmation of cellular disruption by microscopy. The centrifugation steps then mirrored those used for obtaining a TM or PM in Caco-2 cells.

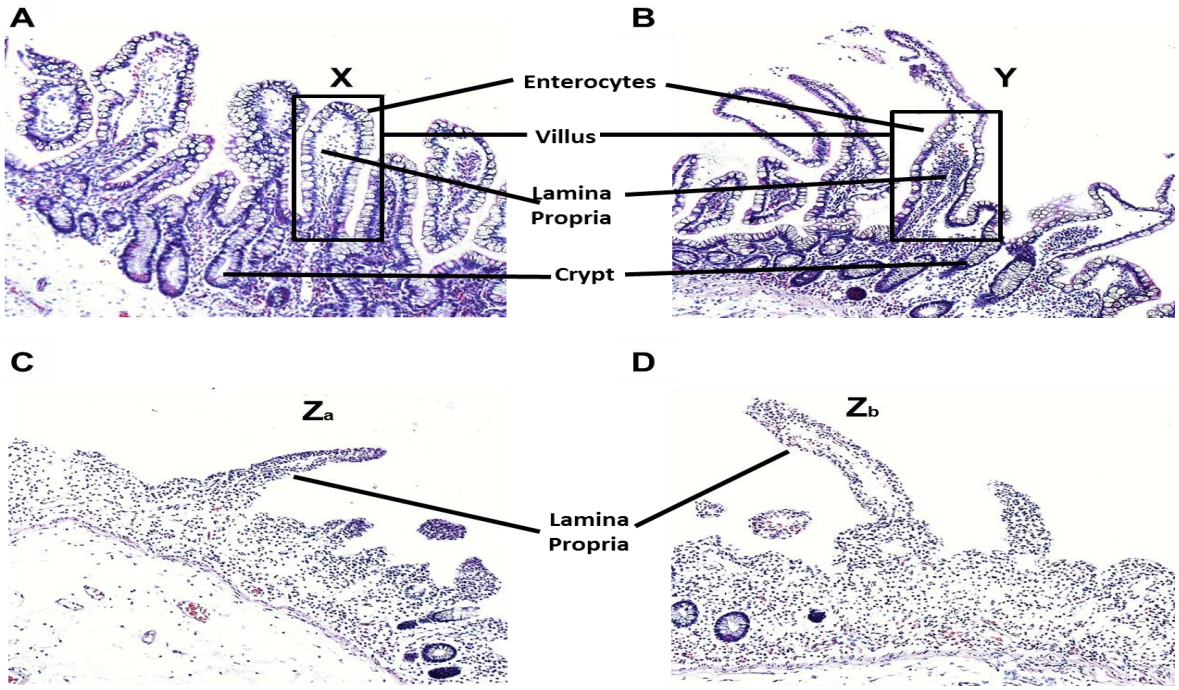

Figure 3-13. Histological assessment of enterocyte elution by the EDTA chelation method in haematoxylin and eosin stained human distal ileum. Sections were cut at a 6 µM diameter after fixation in formaldehyde (4%) and imaged at a 100x magnification. Figure 1A, represents distal ileum not subjected to EDTA (control), with an intact enterocyte-villus structure denoted by 'X'. Figure 1B, shows the process of enterocyte shedding, denoted by 'Y' as a result of EDTA incubation. Figures 1C and D, show the complete removal of enterocytes from the underlying lamina propria layer after EDTA incubation, denoted by Za and Zb.

To compare if different methods for harvesting enterocytes for proteomic analysis affect transporter abundance determinations, a mucosal crush technique on matched human intestinal mucosa was undertaken (where sufficient material was available, Section 2.2.2.5). This is a technique in which stripped mucosal tissue is crushed by homogenisation using the Dounce apparatus.

The protein content of the starting TP homogenate and the TM for jejunum (n=5), ileum (n=3) and colon (n=1) by the EDTA chelation are shown in Figure 3-14. The mean protein yield of eluted enterocytes in the starting homogenate for jejunum and ileum were not significantly different (p=0.62, Unpaired t-test) with mean yields of 583 ± 217 and 662 ± 180 µg/cm^2, respectively. For the single colon sample, a lower yield of 170 µg/cm^2 protein was found. For the TM fractions there were no differences when comparing the protein yields for jejunum and ileum (mean, 25±11 and 38±22 µg/cm^2, respectively, p=0.29, Unpaired t-test). The yield of TM protein relative to the TP homogenate was similar to that found for the filter-grown Caco-2 TM fractions (Figure 3-11).

Mucosal crushing was undertaken on thawed distal jejunum samples (n=3). Protein yield per mg of mucosal tissue rather than per cm^2 (these samples are not stretched across an adaptor) are provided in Figure 3-15. No significant differences were found in the yield (%) of TM protein from the original TP when matched eluted or crushed samples were compared (p=0.31, Unpaired t-test).

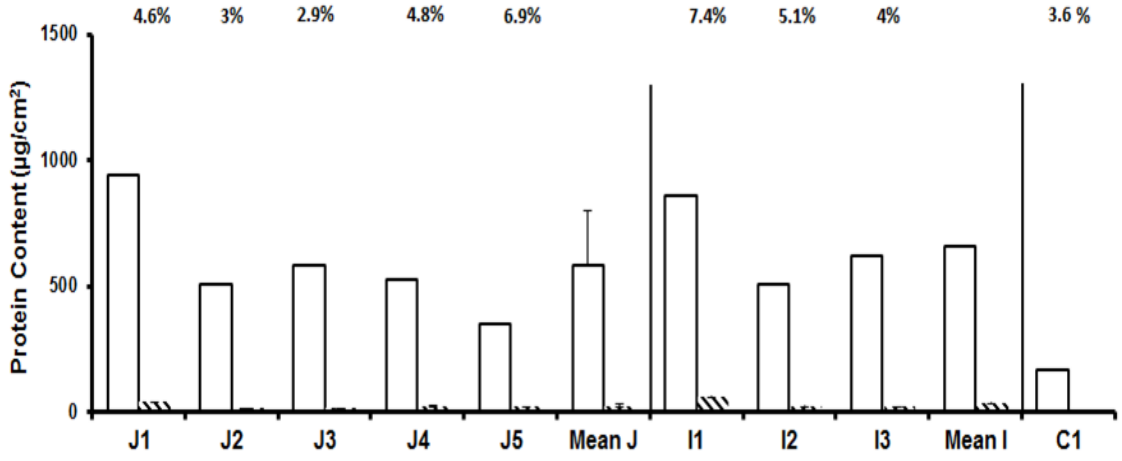

Figure 3-14. Human enterocyte protein content (µg/cm2) in homogenate and total membrane protein fractions after EDTA chelation (n=9). The percentage yield of total membrane (striped) relative to the homogenate (white) for each fraction are given above the bars. J1-5 signifies jejunal samples, I1-I3 signifies Ileal samples and C1 is a distal colon sample. Mean J and I, represent mean values ± SD for jejunum and ileum, respectively.

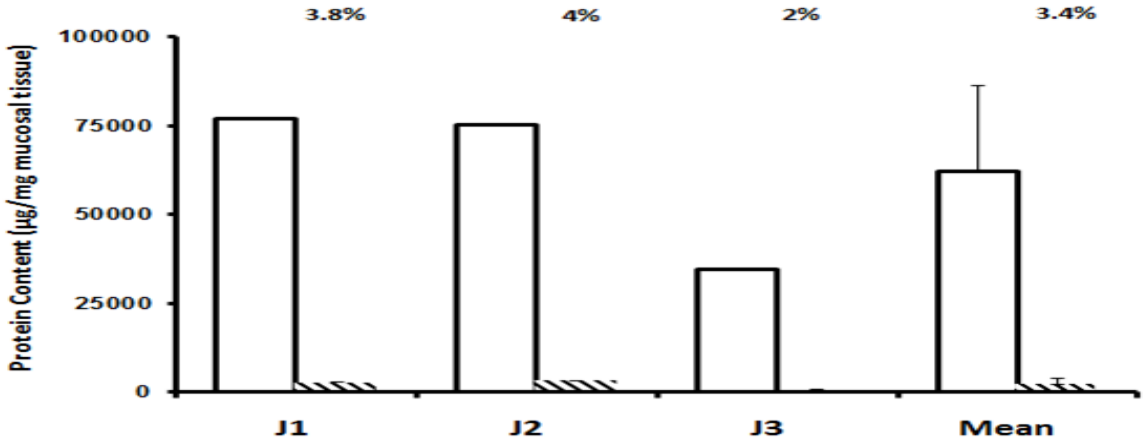

Figure 3-15. Human mucosal protein content (µg/mg mucosal tissue) in homogenate and total membrane protein fractions (n=3). The percentage yield of total membrane (striped) relative to the homogenate (white) for each fraction are given above the bars. J1-3 signifies each jejunal sample. The mean is provided ± SD.

In samples in which sufficient total membrane protein was available, an alkaline phosphatase activity assay was performed to assess the enrichment of PM components within a TM fraction from starting homogenates. From 7 enterocyte preparations (Figure 3-16), a mean fold increase of AP activity of 3.64 ± 1.74 was observed in the TM fraction *versus* the homogenate fraction.

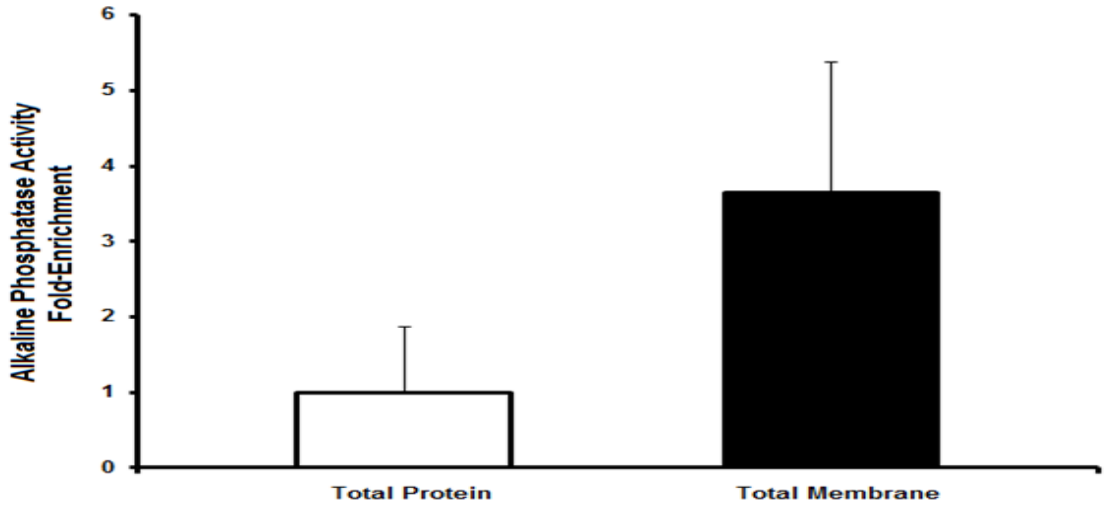

Figure 3-16. Alkaline phosphatase activity enrichment in the total membrane fraction compared to the original starting total protein fraction. The assay was performed with proteins from jejunum (n=3), ileum (n=2) and distal colon (n=2) during enterocyte chelation experiments (Appendix Table A-1 for human tissues).

3.4 Discussion

Transporter proteins are functionally expressed in the PM component of the cell. It is therefore important to measure the absolute abundance of transporter proteins in a fraction of the cell that adequately represents the PM. Numerous techniques have been employed to obtain a membrane fraction suitable for quantifying transporter proteins including differential centrifugation (Kamiie et al., 2008; Miliotis et al., 2011b; Tucker et al., 2012) and commercially available membrane extraction kits (Li et al., 2008; Deo et al., 2012; Groer et al., 2013; Vildhede et al., 2014). Until very recently (Kumar et al., 2015), an assessment of the enrichment or purity of the membrane fraction in which the protein abundances are measured has not been reported. Therefore, the work presented here, was undertaken to develop a robust fractionation procedure to obtain a PM with reasonable purity, in order to measure transporter protein abundances reliably in QTAP assays. To test for enrichment, organelle-specific marker enzyme activity assays were performed in various samples throughout the fractionation.

Initial work focussed on obtaining membrane fractions from MDCK-II-WT cells grown on flasks using a differential centrifugation technique (Kamiie et al., 2008) to obtain a PM. MDCK-II cells were chosen due to their rapid growth and the use of flask-grown MDCK-II cells for transporter QTAP assay development (Li et al., 2008; Zhang et al., 2011). The first phase of experiments highlighted the challenges to effectively homogenise MDCK-II-WT cells using hand-held 'Dounce'-type techniques and the requirement for a suitable quantity of starting material to obtain a consistent yield of membrane fraction. This led to inadequate protein yield and inconsistent enrichments of AP activity in target membrane, even when sonication steps were introduced, in addition to homogenisation, to facilitate cellular disruption. Therefore, an alternative method was sought. Cavitation methods are a strategy used to disrupt cells by inert gases, (Ohtsuki et al., 2012), however such devices are expensive and not readily available. A strategy incorporating overnight lysis of MDCK-MDR1 cells with hypotonic $NaHCO_3$ found a 38-fold enrichment for P-gp in a TM preparation *versus* the starting lysate after immunoblot analysis (Zhang et al., 2004). Based on this, a hypotonic lysing technique was developed. In addition, undertaking secondary homogenisations should improve the disruption of any remaining intact organelles after lysing, as adopted in this study and Zhang et al., 2004.

Application of the overnight lysing and secondary homogenisation strategy to MDCK-II-WT and Caco-2 cells, led to the highest AP activity enrichment in the PM fraction *versus* the TP lysate. In addition, a slight reduction in the enrichment of the microsomal marker CCR was observed when

obtaining the PM from the preceding TM fraction. The TM fraction can be characterised to contain EnR, golgi, lysosomal, PM and any other intracellular protein present when components originating from medium-speed spin sedimentation are discarded. Ideally, the PM fraction should not contain any intracellular components. Overall, the enrichment in AP activity in the TM and PM fractions was modest. However, this may be expected, as a study in which AP activity was used as a marker of brush border membrane maturation in plastic-grown MDCK-II cells showed that there is a substantial rise (5-fold) in AP activity between 6 and 13 days post confluence, which plateau's thereafter (Lai et al., 2002). This indicates that for these relatively un-differentiated cells, in which brush border membranes do not sufficiently mature in flasks, it might be reasonable to expect a low AP activity enrichment. Alternatively, obtaining a mixed plasma membrane containing both basal and apical membranes might lead to lower enrichment activity, 'a dilution effect' for this apical-brush border protein. It was anticipated that the peak enrichment of the EnR would occur in the TM fraction which was confirmed, yet there was only a modest non-significant reduction in CCR activity in the PM of both cell lines. A 2.5-fold enriched CCR activity in a mitochondrial/ER fraction was observed with a concomitant 2-fold activity reduction in the PM phase, compared to the starting homogenate in flask-grown MDCK-II cells (Geilen et al., 1994). In Geilens' study, the authors also allude to the PM fraction containing mitochondrial components (13%). It is clear that a PM fraction will be contaminated by components from the EnR and mitochondria and the methods used to obtain PM's in this study show that it is challenging to obtain pure organelles. This agrees with a recent study which found contamination of the PM fraction with golgi and mitochondrial proteins after using a commercially available kit (Kumar et al., 2015). When considering QTAP studies, the relative lack of cellular differentiation in flask-grown Caco-2 cells is supported by >10-fold higher P-gp levels in filter *versus* flask-grown Caco-2 cells (Miliotis et al., 2011b; Oswald et al., 2013).

Having undertaken methods to establish a PM fraction with enrichment of PM markers in un-differentiated flask-grown cells, the next stage focussed on harvesting filter-grown Caco-2 cells for various culture periods. The ability to obtain a sufficient quantity of high quality membranes from filter-grown cells is crucial, as it is these transporter protein abundances that are incorporated into IVIVE scaling strategies. To ensure sufficient yields of membrane proteins to run down-stream assays, including at least two trypsin-based digestion assays, a minimum protein quantity of 200 µg was required. Therefore, Caco-2 cells were grown on 44 cm^2 filters, manufactured with the same material (Polycarbonate) and pore density (0.4 µM) as those routinely used in transport assays (Hubatsch et al., 2007). Filter surface area is assumed not to affect transporter expression. Using

method 2 to extract TM and PM from filter-grown Caco-2 cells, as expected, provided a higher AP activity enrichment in filter-grown *versus* counterpart flask-grown Caco-2 cells. A study by Hidalgo *et al*., 1989, described an 8-to-10-fold enrichment of AP activity in brush border membrane preparations generated from filter-grown Caco-2 cells (Hidalgo et al., 1989). Another study, in which the brush border and basolateral membranes were separated in 7-to-9 day filter-grown Caco-2 cells, found a 15-fold AP activity enrichment in brush border fractions and 3-fold enrichment in the basolateral membrane fraction (Ellis et al., 1992). Overall, the 5.3-to-7.7-fold enrichment in AP activity in our mixed PM (*i.e.,* containing basolateral and brush border membranes) of filter-grown Caco-2 cells appears reasonably consistent with these other studies measuring AP activity enrichment in the more refined brush border membrane. The lack of AP activity enrichment from the TM to PM fraction is not ideal. It is expected that the dense EnR fraction migrates through the 38% sucrose layer. It is possible that the PM together with intracellular membranes are travelling through the sucrose during centrifugation, thus, the retained turbid interface at the sucrose-buffer boundary constituting the PM fraction is similar in composition before and after centrifugation.

An additional theoretical concern with the overnight lysis stage of this cell fractionation protocol is that it could result in transporter instability on the membrane, *i.e.,* during lysis the transporters sequester to intracellular components, move into a soluble phase, or degrade. While we have no direct evidence that this was occurring, future work should include time course studies to assess the effect overnight lysing on transporter protein abundances. Yet, evidence from immunoblots assessing P-gp enrichment across the various fractions of 10d filter-grown Caco-2 cells demonstrated a 3.1-fold enrichment in the PM fraction *versus* the TM fraction.

It appears that cultivation time had little effect on filter-grown Caco-2 cell TP protein content, but there was a higher TM protein in 29 compared to 10d cultured cells, possibly reflecting cell differentiation in older cells. Yet in Caco-2-VBL cells, protein content for the TP and TM fraction was lower than for 21d-filter-grown low passage cells. VBL is reported to affect the length of apical microvilli and disturb protein trafficking to the apical brush border membrane in mice (Achler et al., 1989). It is the action of VBL on microtubule structure and membrane protein organisation which could lead to the observed reduction in protein content for Caco-2-VBL cells. The TP contents found in the present study are slightly lower than those from a previous study which ranged from 470-550 µg/cm^2, although a different technique (Bradford assay) was used for measuring protein content (Inui et al., 1992). In addition, a personal communication with Professor Per Artursson (the University of Uppsala) via Dr. Sibylle Neuhoff (Simcyp Ltd), suggested total protein content in filter-

grown Caco-2 cells ranges from 200–300 µg/cm^2. Therefore, the results presented for the cells in this study appear to be reasonably consistent with previous work.

Until recently, it was not known if the PM yield was reasonable, *i.e.,* 1-2% of TP. However, in a recent study, the indirect calculation of the fractional yield constituting a PM fraction from liver and HEK293-transfected cells indicated typical PM yields of 1.1-to-1.9%, similar to those obtained with our extraction method (Kunze et al., 2014). In this study, approximately 20% of the TM fraction represents the theoretical PM fraction. However, it has been postulated recently that the PM accounts for 10% of the crude membrane fraction procured from a 'native' membrane protein extraction kit (Vildhede et al., 2014). Differences in extraction method may result in different yields of protein from sub-cellular fractions. Therefore, procedural differences such as harvesting procedures, buffer composition and membrane extraction technique differences may lead to methodological bias on endpoint abundances (Harwood et al., 2013). As yet, no formal assessment has been reported as to the impact of membrane extraction method on quantification of transporter protein abundances.

Considering that approximately 1-2% of the TP constitutes the PM fraction, it may be expected that if there were no losses of PM proteins throughout the procedure, the maximum AP activity enrichment likely to occur is 50-to-100-fold compared to the original TP, that is, if activity is directly proportional to AP protein levels. On this assumption, there is a greater than 10-fold disparity between protein enrichment and AP activity. It is known that AP requires the divalent cations Mg^{2+} and Zn^{2+} as co-factors and any loss of these could lead to sub-optimal catalytic activity (Igunnu et al., 2011). The AP assay here was performed without Zn^{2+} which could potentially lead to a reduced catalytic capacity of the enzyme (Olorunniji et al., 2007). AP activity is reasonably conserved i.e 0-15% activity loss, with a maximum loss of 36% in a single sample. Yet, there is a need to consider the basis on which the enrichment calculations are made. The fold enrichment calculations are based on AP activity (formation of p-NP) corrected for protein, *i.e.,* nmol/min/mg protein, rather than an absolute activity *i.e.,* nmol/min. Therefore, by correcting for protein content, there is a drop-off in activity throughout the procedure. This could be due to loss of co-factors from within the sample, or the inhibitory effects of components such as fatty acids (the proportion of lipid content will be high in membrane fractions) as observed for the enzyme CYP2C9 (Rowland et al., 2008), leading to a lower calculated enrichment based on marker enzyme activity assays. Therefore, if activity does not accurately reflect organelle enrichment, marker activity assays should only be used as a guide rather than an established quantitative means to assess the intrinsic purity

of a sub-cellular fraction. However, these assays are still a useful guide and should be undertaken routinely when establishing membrane extraction methods.

It is noteworthy that a human liver microsomal fractions are on average 40 mg/g liver for a 30 year old human (Barter et al., 2007). A similar protein yield for a TM fraction employed when measuring transporter protein absolute abundances has been reported as 35.8 and 41.6 mg/g liver, in Tucker *et* al., 2012 and Deo *et al*., 2012, respectively. Therefore, it is likely that abundances do not represent the PM component and any transporters, whether fully or part formed, that are associated in with intracellular structures/membranes (Bow et al., 2008; Choi et al., 2011) may be accounted for in these fractions. Caution is therefore advised when interpreting these data to represent the functional complement of a cells' transporter protein abundance.

The techniques developed for obtaining a PM fraction in human intestinal mucosal samples were based on obtaining enterocytes by elution. EDTA (a metal chelating agent) is routinely employed for harvesting enterocyte and colonocyte material from the underlying lamina propria layer (Zhang et al., 1999; Bowley et al., 2003; von Richter et al., 2004) . The action of Ca^{2+} binding by EDTA disrupts cell-to-cell adhesion mediated by calcium-dependent cadherin proteins (Panorchan et al., 2006). Incubations with sodium citrate were also performed prior to EDTA incubation to facilitate cell-to-cell destabilisation (Weiser, 1973; Weingartl and Derbyshire, 1993). Tissue adaptors were constructed to minimise the potential for procuring serosal cells and structures (Figure 2-2). The tissue adaptors comprise a solid base plate with pins at its periphery for securing the tissue. The tissue is placed serosal surface down on the plate. A second upper plate containing apertures of known surface areas harness the tissue to the base plate with reciprocal pin holes. This restricts exposure of the chelating agents to the mucosal surface to reduce serosal protein contamination.

Initial experiments with stripped jejunum and distal colon tissue using EDTA (5 mM) provided a low yield of enterocyte material insufficient to provide a PM fraction. The reasons for low yields are not clear, however it is postulated that EDTA may require access to the basal surface to facilitate calcium chelation and enterocyte elution. Work undertaken on a partner project by Dr Oliver Hatley, successfully procured enterocytes using sodium citrate-EDTA (5 mM) to stripped mucosal tissue pinned to a silicon base in a beaker. However, the tissue was thawed from cryopreservation potentially impacting on tissue integrity, enhancing the elution of enterocytes, possibly via freeze-fracture or enterocyte permeabilisation (Gronert et al., 1998). Applying an increased EDTA (30 mM) concentration provided assurances that during the 40 minute incubation, sufficient material

could be procured to provide membrane fractions. It is inevitable that an increase in the incubation time leads to an enhanced harvesting of enterocytes. However, this also brings an increased likelihood of procuring crypt-based enterocytes as opposed to those from the villus (Zhang et al., 1999). A preferential expression of OATP1A2 in the villus tip has been observed, whereas P-gp is expressed along the entire crypt-villus axis (Glaeser et al., 2007). Therefore, the location of the cells obtained by elution along the crypt-villus axis may be important for measuring transporter protein abundances. In this study, there was no attempt to exclude crypt enterocytes (Appendix Figure A-1). OATP1A2 has proven challenging to measure in the intestine by gene expression analysis (Tamai et al., 2000; Nishimura and Naito 2005; Hilgendorf et al., 2007; Meier et al., 2007) and also utilising proteomic techniques (Drozdzik et al., 2014). However, it is possible that transporters concentrated at the villus tip, such as OATP1A2, may be more difficult to quantify due preparation of whole intestinal/mucosal biopsies for gene expression analysis, or due to a dilution effect of crushing the whole mucosa as performed by Drozdzik et al., 2014, rather than isolating villus enteorcytes. Visual checks by microscopy were performed for each elution experiment and observations confirmed isolated enterocytes or villus tip structures were predominant within the eluent.

In a previous study in human duodenal tissues P-gp, MRP2 and BCRP abundances were quantified after mucosal scraping by quantitative immunoblotting (Tucker et al., 2012). However, it is postulated here that underlying lamina propria or basal layers might also be harvested. Studies to compare elution and scraping have been not been performed to assess intestinal transporter abundances. Yet, activity differences exist between numerous CYP450 enzymes in intestinal microsomes harvested by mucosal scraping and elution, which might result from crypt cell harvesting by scraping (Galetin and Houston, 2006). Other studies to quantify intestinal transporter abundances do so in membranes isolated after mucosal crushing and homogenisation (Groer et al., 2013; Oswald et al., 2013; Drozdzik et al., 2014). Studies to compare enterocyte harvesting techniques are warranted, therefore a small-scale study using 3 distal jejunum tissues in which both elution and mucosal homogenisation is proposed within the context of this work.

Assessing the protein content in intestinal samples (n=9) using the final elution protocol shows an approximate 2-fold higher homogenate protein content yield in the jejunum and ileum compared to filter-grown Caco-2 cells. This is expected given the highly folded nature of the human mucosa compared to Caco-2 cells. As anticipated, the distal colon sample demonstrated lower homogenate yields compared to jejunum and ileum. The yield of protein from the TM as a percentage of the

homogenate was similar to filter-grown Caco-2 cells. Compared to the scraping technique applied to human duodenum in Tucker et al., 2012, the yields of TM protein in this study are 54-fold lower (1344 vs. 25 µg/cm^2). Tucker et al., have not shown a histological evaluation of their mucosal tissue after scraping, therefore, the most likely explanation is that scraped preparations are contaminated with sub-epithelial layers. Figure 3-13, shows no evidence of significant enterocyte retention, therefore the lower protein content is unlikely to be due to incomplete enterocyte harvesting. Furthermore, in Tucker et al., it is understood that the mucosa was not stretched and their fractionation procedure omits a medium speed spin for nuclear/mitochondrial sedimentation, resulting in a particularly crude TM. Remarkably and for unknown reasons, the yields of the TP homogenate observed in this study are lower that the scraped TM protein content (Tucker et al., 2012).

Similar to immortalised cells, the AP activity in TM fractions was shown to be enriched compared to the starting homogenate fraction. There is little data in the literature by which to compare AP activity enrichments in a TM fraction. Studies instead focus on assessing AP activity enrichment for refined brush border membrane preparations which are typically range from 9-17-fold in small intestine (Lucke et al., 1978; Ward et al., 1980; Shirazi-Beechey et al., 1990; Blakemore et al., 1995). Appreciating that other studies measure abundances in a relatively crude membrane fraction, it is assumed that a TM fraction is sufficient to permit absolute abundance of transporter proteins for this study.

Considerable effort was invested in obtaining and characterising membrane fractions to enable the quantification of transporter abundances in QTAP assays. However, state of the art techniques in regard to LC-MS/MS systems, have been shown to possess sufficient sensitivity and resolution to enable the quantification of low abundance proteins such as plasma membrane transporters to be quantified in a total protein fraction using both a targeted approach, (Ohtsuki et al., 2013) and a label-free approach (Wisniewski et al., 2012), negating the requirement for quantification in an enriched membrane fraction. Under the assumption that the majority of the transporter protein is resident in the plasma membrane of the total protein fraction, this approach may provide a feasible means to quantify cellular/organ transporter protein abundance for the purposes of IVIVE, without requiring the consideration of losses or contamination of other sub-cellular organelles within these enriched fractions. However, the ability of research groups to perform these analyses may be hampered by the availability of suitable LC-MS/MS systems.

3.5 Conclusion

A step-wise approach to developing a membrane extraction method is described in this chapter using enzyme activity assays to classify the enrichment of target membrane fractions throughout the procedure in flask and filter-grown cell lines relevant to transport assays. This systematic approach has demonstrated that obtaining a pure PM, as assessed by marker enzyme activity assays is a significant challenge. However, protocols for the isolation of two membranes fractions, the TM and PM, from a host of Caco-2 cell variants have been developed which produce enzyme enrichments and PM protein yields that are consistent with the limited data in the literature. In addition, a method to harvest human intestinal enterocytes is also described with the generation of a TM fraction. There is the potential to compare two different methods for harvesting enterocytes by elution and mucuosal homogenisation in matched samples to investigate if this impacts on transporter abundance determinations. Overall, these data provide a sound basis for downstream evaluation of absolute protein abundances by QTAP assays.

Chapter 4 - Development of Digestion and Optimisation of LC-MS/MS Methods for Quantification of Human Intestinal Transporter Proteins' Absolute Abundance using a QconCAT Technique

Declaration

A summary of the work described in this chapter has been submitted for publication in the peer-reviewed Journal of Pharmaceutical and Biomedical Analysis as described below:

M.D. Harwood, B. Achour, M.R. Russell, G.L. Carlson, G. Warhurst, A. Rostami-Hodjegan. Application of an LC-MS/MS Method for the Simultaneous Quantification of Human Intestinal Transporter Proteins Absolute Abundance using a QconCAT Technique.

This article was written primarily by the candidate, Matthew Harwood with editing undertaken by the co-authors. I retained editorial control of this article.

Work described in this article was performed by the candidate in conjunction with Dr Matthew Russell and Dr Brahim Achour, post-doctoral scientists with the Systems Pharmacology Group at the University of Manchester. They provided specific expertise and training in proteomics and QconCAT analysis that facilitated development of the tools and approaches used in this chapter

In this chapter the selection and generation of the peptide standards via expression of the transporter QconCAT 'TransCAT' will not be described in detail but is alluded to. This aspect of the project was driven by Dr Matthew Russell and has been described in *Russell et al., (**2013**). J Proteome Res, 12, 5943-5942.*

4.1 Introduction

Drug transporter proteins functionally expressed in human enterocytes can facilitate or hinder drug absorption and influence drug disposition in instances of polypharmacy (Greiner et al., 1999). The impact of transporter proteins on these processes will depend on their expression level, location within the enterocyte membrane and function (Varma et al., 2010). To estimate the influence of transporter protein function on drug absorption, disposition and DDI's, strategies incorporating PBPK modelling approaches are used (Darwich et al., 2010; Varma et al., 2012). As alluded to in Chapter 1, PBPK models require incorporation of transporter protein expression in sub-models representing pharmacokinetically relevant organ systems, including the intestine, that are typically based on gene expression (i.e,. mRNA) or immuno-blotting analyses (Harwood et al., 2013).

Recently, studies have employed QTAP strategies, utilising unique proteotypic peptides combined with LC-MS/MS methods to quantify the absolute abundances of human intestinal transporter proteins (Groer et al., 2013; Oswald et al., 2013; Drozdzik et al., 2014). In these studies, an absolute quantification (AQUA) strategy was employed for generating the peptide standards. The QconCAT technique (Section 1.8.1.7), is an alternative method for generating isotope labelled peptide standards (Beynon et al., 2005). An artificial protein is constructed within an *E coli* vector and expressed, with stable isotope enrichment of growth media. The extracted artificial protein is subjected to proteolytic digestion strategies to yield equimolar concentrations of standard peptides for quantification of target proteins (Simpson and Beynon, 2012). A QconCAT method has recently been applied to simultaneously quantify several human hepatic drug metabolising enzymes (Achour et al., 2014). In addition, the construction of a transporter protein-specific QconCAT ('TransCAT') is described (Russell et al., 2013). However, the method validation and their application for quantification of several transporter proteins have yet to be reported. Having established methods to obtain human enterocyte TM fractions, efforts turned to protein digestion and LC-MS/MS method development to enable transporter protein abundance quantification.

The aim of this study was to develop and validate proteolytic digestion and LC-MS/MS methods to quantify the absolute abundances of Na/K-ATPase, HPT1; P-gp; MRP2; BCRP; OST-α/β and OATP2B1 in human enterocyte TM's using the TransCAT construct. The delivery of robust techniques to allow quantification of transporter abundance proved challenging and therefore concurrent to continued development of strategies for in-house abundance quantification, a contingency plan was sought, which is described.

4.2 Materials & Methods

The finalised methods for this Chapter are described in Section 2.2.2.2 for Caco-2 cell membrane fractionation, Section 2.2.2.4, for eluting human enterocytes, Section 2.2.6 for generating peptide standards, Section 2.2.7 for protein digestion, and Section 2.2.8 for LCMS/MS analysis.

4.2.1 Materials

Described are additional materials to those defined in Section 2.1. For initial protein digestion, Nvoy carbohydrate polymer was obtained from Expedeon (Cambridge, UK); Anionic Acid Labile Surfactant II (AALS II), Non-ionic Acid Labile Surfactant II (NALS II) and strong cation exchange (SCX) spin tips kit were obtained from Proteabio (Morgantown, West Virginia, USA); Tris(2-carboxyethyl)phosphine (TCEP) was supplied by Thermo-Fisher (Waltham, MA, USA); and C18 ZipTips were obtained from, Millipore, (Billerica, MA, USA).

4.2.2 Methods

4.2.2.1 Nvoy Proteolytic Digestion Protocol

Nvoy proteolytic digestion was based on protocols already described (Russell et al., 2013). Herein, digestion with either; 4% or 0.1% Nvoy was used. Protein (typically 50 µg), TransCAT (5 µL, 1/10 diluted stock) and NNOP-Glu-Fib were suspended in protein digestion buffer (Ammonium Bicarbonate (25 mM), pH 8; Nvoy 0.1% or 4% and acid-labile surfactants: NALS-II 0.01%, AALS-I 0.1%) and reduced with TCEP (12 mM final concentration, 37°C, 1h). Samples were alkylated by IAA (6 mM, 30 min) in the dark at room temperature. The alkylated mixture was diluted 2-fold prior to addition of 1 µL of Lys-C (1 µg) and subsequent incubation (37ºC, 3h). Recombinant trypsin (2.5 µL at 1 µg/µL) was added, followed by overnight incubation (18h, 37ºC). To improve binding to the chromatography column, the Nvoy and surfactants were dissociated from the peptides, HCl and DMSO were added to the digest mixture to obtain an optimal pH 2, incubated 37°C for 15 min, while addition of 30% acetonitrile provided an optimal pH of 3. SCX spin tips were used to recover digested peptides by washing peptides in SCX wash buffer (60% acetonitrile; 40% H_2O and 0.03% ammonium formate) and eluting by centrifugation in SCX elution solution (90% H_2O; 10% acetonitrile and 2.5% ammonium formate) twice. The eluted peptides were lyophilized and stored at -80°C until it was reconstituted in 3% acetonitrile and 0.1% formic acid for LC-MS/MS analysis. Where data dependent acquisition data (DDA) is described, this resulted from label-free analysis of fragmentation spectra generated from Orbitrap XL mass spectrometry (Section 2.2.6.1).

4.3 Results

4.3.1 Initial Development of Proteolytic Digestion and LC-MS/MS QTAP Assays

4.3.1.1 Preliminary Development of an In-Solution Proteolytic Digestion Strategy

Early work performed by Dr Matthew Russell involved attempting to digest PM proteins from a rat liver sample based on a guanidinium hydrochloride method (Kamiie et al., 2008). Prior to applying digestive enzymes, a viscose mix ('slurry') of membrane proteins was produced resulting from chloroform/methanol precipitation. The precipitate could not be effectively solubilised by application of 6M urea, therefore it was concluded that the complete digestion of precipitated peptides could not be guaranteed. An alternative digestion strategy was sought using Nvoy, a carbohydrate polymer, primarily used for reducing protein aggregation, at 4% initially and finally at 0.1%. The denaturing agent TCEP, which does not react with IAA, and can be used at a lower concentration than DTT, was also incorporated into the digestion protocol. The addition of surfactants (AALS II and NALS II) provided the potential for micellar formation in order to mask the hydrophobic regions of the proteins, reducing the likelihood of precipitation. SCX columns were employed to remove Nvoy which could be detrimental to chromatographical analysis (Russell et al., 2013).

4.3.1.2 Caco-2 Cell Plasma Membranes Digestion: The Initial Phase

Having defined an Nvoy-based digestion strategy, its application for generating peptides suitable for quantifying target protein absolute abundances using a TransCAT LC-MS/MS approach was required. To this point, the TransCAT was expressed and the LC-MS/MS conditions had been optimised based on the unlabelled sequence equivalent SpikeTide peptides (Section 2.2.6.2). A series of Caco-2 cell PM digests were performed over several months.

The initial aim of the digestion work was to identify if peptides relevant to the PM were being released into the digest. A DDA analysis was performed on Caco-2 cell PM digests, revealing that peptides relating to the basal membrane marker protein Na/K-ATPase and Villin, a high abundance apical membrane marker protein (that is not a constituent of the TransCAT construct), could be identified when submitting the fragmentation spectra obtained by orbitrap mass spectrometry to the MASCOT search engine (Figure 4-1). Two peptides selected for Na/K-ATPase quantification by the TransCAT are highlighted in Figure 4-1A by red boxes. These peptides however could not be detected via the MASCOT search, even though *in silico* digestion and other criteria were met (Section 2.2.6.2). This does not necessarily indicate that these peptides are not present in the digest. It is possible that they are of low abundance within the complex protein matrix. MASCOT

also identified PM peptide fragments for > 1000 relevant PM proteins from the digest with few missed-cleavage events, providing confidence the membrane extraction and digestion protocols could generate a refined protein sample for down-stream absolute abundance determination.

The next stage was to establish co-elution profiles for digested Caco-2 cell PM proteins and TransCAT standards via an LCMS/MS (triple quadrupole) QTAP strategy. For Na/K-ATPase, native and standard peptide co-elution was demonstrated (Figure 4-2). However, the levels of the native peptide are expected to show far greater signal intensity for this high abundance protein. For the majority of the native peptides analysed, the ion signals were either low, not detectable or the standard signals were too high to permit quantification. Therefore, the TransCAT levels required adjusting in order to obtain similar analyte-standard ion signal intensities.

Performing a digest with a 10-fold diluted stock of TransCAT construct was expected to result in a mirroring of peak signal intensities from the native and standard peptides. Yet, this failed to provide standards at sufficient levels when assessing targeted profiles. Of note, there was also a continuing trend for low native peptide ion signal peak intensities at 10^5 to 10^6 cpm range for Na/K-ATPase, where the expectation was a 10-fold greater signal than demonstrated (Figure 4-3). To identify if protein/peptide losses were occurring in various stages of the SCX column recovery, a protein mass balance assay was run.

To assess peptide losses in SCX column recovery, a cocktail of unlabelled SpikeTide peptides was processed throughout the procedure. At various stages, including the starting SpikeTide mixture, samples were taken and a BCA assay was performed. Only 31% of the SpikeTides were accounted for in the final eluent (Figure 4-4) with 69% of peptides lost to discarded wash steps or could not be accounted for when assessing mass balance from all retained samples. This led to the formation of an alternative strategy in the form of an in-gel digest. This approach had been successfully undertaken for the enzyme abundance analysis performed on liver microsomes (Achour et al., 2014).

Figure 4-1. Data-Dependent Acquisition (DDA) following the submission of orbitrap fragmentation spectra from a Caco-2 PM digest to the MASCOT search engine. A, represents Na/K-ATPase and B represents Villin. The text highlighted in red are the peptides which were successfully identified by MASCOT to be a constituent of their respective proteins. The red boxes in A, represent the peptides selected for inclusion into the TransCAT construct.

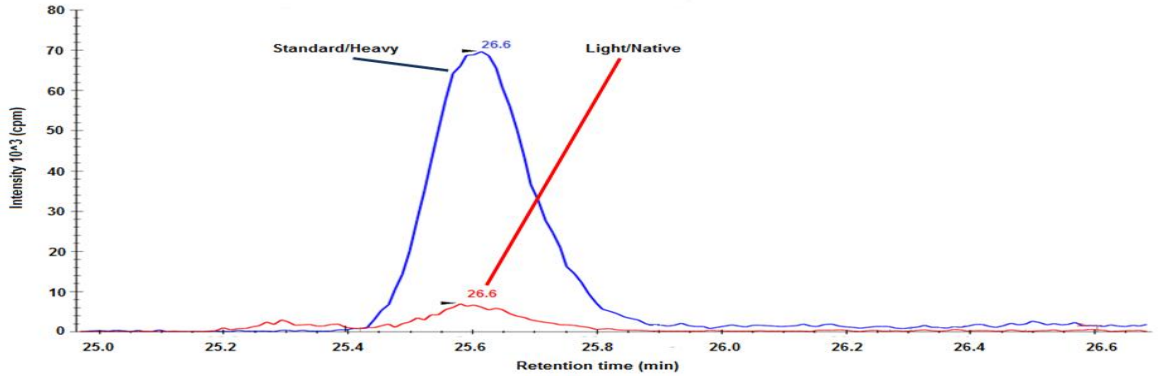

Figure 4-2. A co-elution profile for Na/K-ATPase (IVEIPFNSTNK) from a Caco-2 cell PM Nvoy-based digest. The blue and red peaks represent the standard and native peptides, respectively and were captured in the Skyline program.

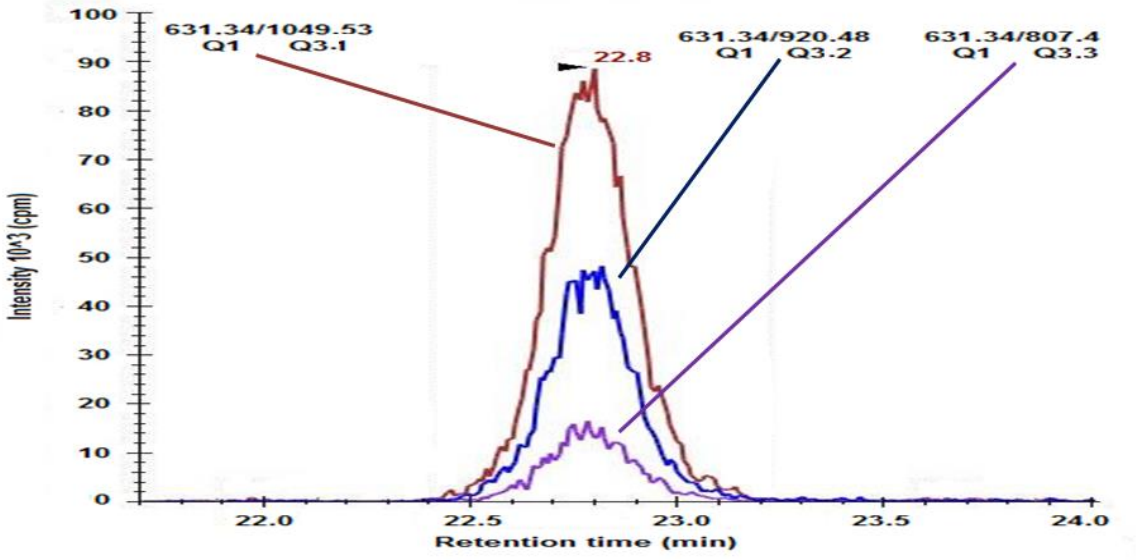

Figure 4-3. Ion intensity signals for the 3 selected transition of the peptide IVEIPFNSTNK selective for Na/K-ATPase from a Caco-2 cell PM digest.

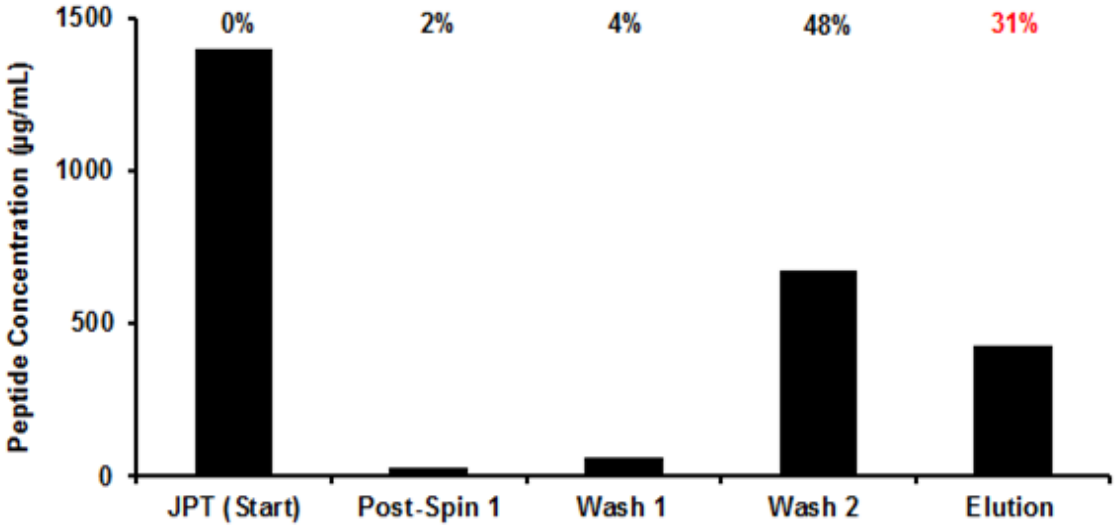

Figure 4-4. Assessment of peptide (SpikeTide) loss through the SCX peptide purification procedure by the BCA assay. The text in black above the bars relates to protein loss and the red text relates to the remaining peptides in the eluent. The peptides not accounted for after mass balance equated to 15%.

An in-gel digest performed (by Dr Matthew Russell) on Caco-2 cell PMs demonstrated reasonable success based on a DDA-based MASCOT search, ranking the plasma membrane markers villin and Na/K-ATPase 42nd and 116th of 335 peptide hits specific to the PM, respectively, (Appendix Figure B-1). For the key protein P-glycoprotein (P-gp), there was limited sequence coverage (9%, not shown) and fragmentation spectra did not yield peptides selected for QTAP. The in-gel approach did not provide satisfactory assurances that target peptides were present in the digest for subsequent LC-MS/MS analysis.

To summarise the work described, a schematic describing the workflow and decisions at each stage is provided (Figure 4-5).

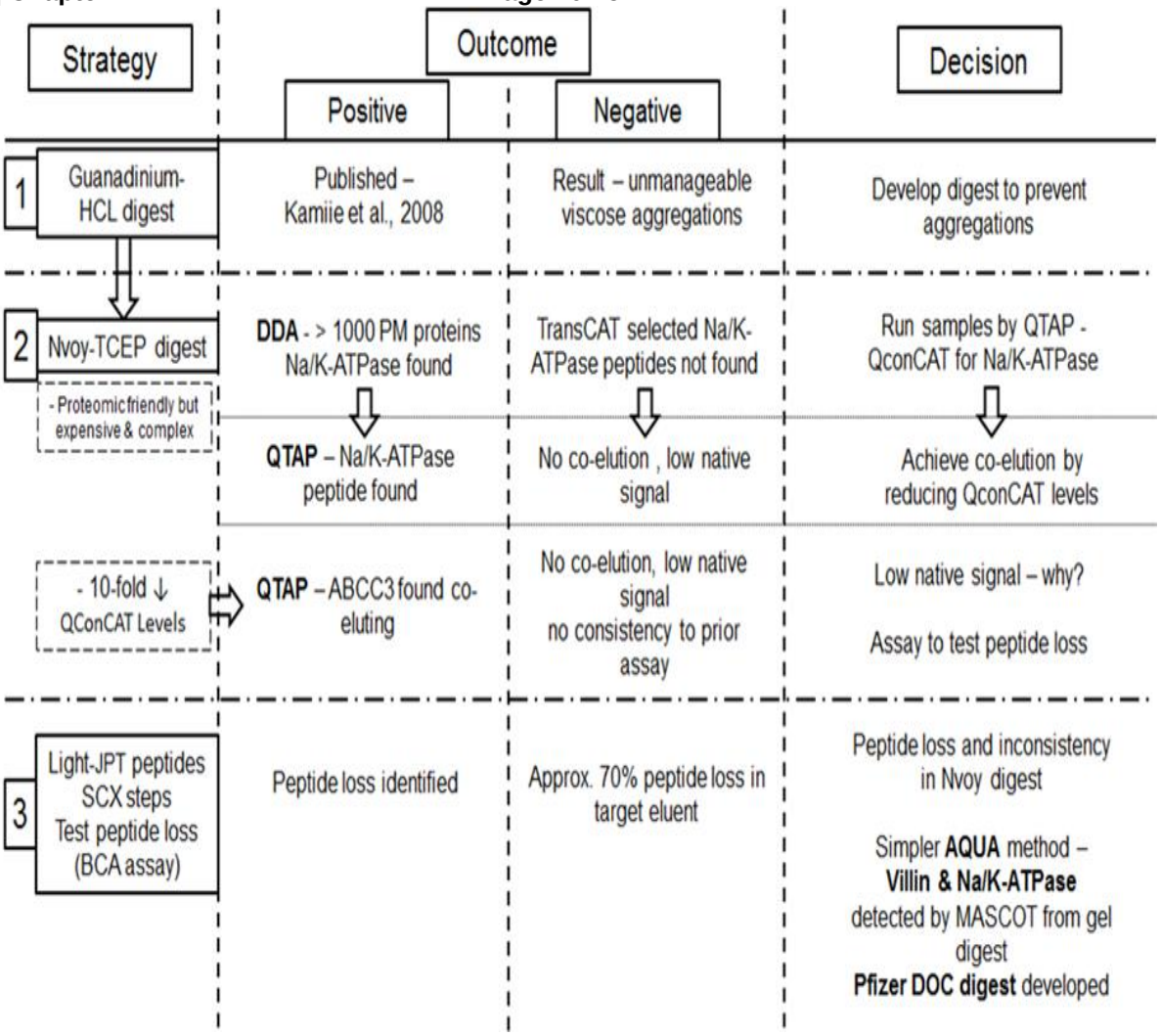

Figure 4-5. A schematic describing the digestion workflow and decision making for Sections 4.3.1.1 and 4.3.1.2. The initial phase used a guanadinium HCl digestion method published by The Terasaki group, Tohoku University, which provided an unmanageable mixture. A proteomic friendly digest Nvoy-TCEP was used to prevent protein aggregation, where peptide fragments relating to Na/K-ATPase were found, but not the specific peptides pre-selected for analysis by QTAP. Inconsistencies were found in co-elution even after reducing the QconCAT standard levels and native signals were low for the key high abundance marker protein Na/K-ATPase. A BCA assay found peptide losses were approximately. 70% in the SCX purification stage. Therefore, to simplify the system, an AQUA method focussing on previously detected (by gel digest) high abundance peptides for the membrane markers villin and Na/K-ATPase assay, *i.e.,* a 'low hanging fruit' notion, and development of a DOC digest by Pfizer was to be undertaken, see Section 4.3.1.3.

4.3.1.3 A Strategy Adaptation for Obtaining Absolute Transporter Abundances

Based on the previous inconsistencies in obtaining peptides relevant for quantification of transporter protein abundances, and a pressing requirement for functional cell model transporter assay developments, a divergent set of plans were pursued simultaneously.

4.3.1.3.1 University of Manchester Strategic Plans

1. Development of a sodium deoxycholate (DOC) based digestion strategy favoured by the proteomics group at Pfizer Limited (Groton, CT, USA) (Balogh et al., 2013) – Work performed by Dr Matthew Russell.
2. Identifying and commissioning the production of AQUA peptides for Villin and Na/K-ATPase. The proteotypic peptides were identified by DDA analysis of Nvoy based digests (Appendix Figure B-1) – Work performed by Matthew Harwood.

Firstly, the rationale for the DOC-based digest was fostered on links between the Centre for Applied Pharmacokinetic Research, the University of Manchester and Pfizer Limited. Communications with the proteomics group at Pfizer provided valuable information to develop an adapted version of their successful digestion protocol (Balogh et al., 2013). Secondly, the rationale behind the AQUA strategy was to simplify our QTAP design to obtain pilot data for peptides identified from DDA analysis in highly abundant PM proteins. Thus, if quantification of the highly expressed protein villin was not achievable, then a fundamental flaw exists in the ability of our digest to recover sufficient targeted peptides or; that the analytical equipment possesses insufficient sensitivity to measure this protein. Digestions using the QconCAT were temporarily postponed until AQUA strategies were assessed.

4.3.1.3.2 Contingency Plan – An External Source for Abundance Quantification

Bertin Pharma (BPh) (Orleans, France), a contract research organisation capable of measuring protein abundances (Kunze et al., 2014), were employed to perform analyses on a host of Caco-2 cell and human intestinal tissue samples. The techniques utilised by BPh are AQUA-based methods and linked to the techniques developed by the University of Tohoku, Japan (Kamiie et al., 2008). BPh were blinded as to the identity of the samples. In the forthcoming chapters data generated from BPh will be presented alongside in-house generated data.

4.3.1.3.3 AQUA-Based Villin and Na/K-ATPase Absolute Abundance Quantification

The DOC-based proteolytic digest (Section 2.2.7.1) was performed on Caco-2 cell PM proteins, with the notable omission of the recovery phase by SCX columns from the protocol. Initial work identified that native ion signal intensities of selected transitions for villin were in the 10^4-10^5 cpm range and that those for Na/K-ATPase (Appendix Figure B-2) were similar to those previously demonstrated (Figure 4-3). After analysis of ion intensity profiles, suitable spiking concentrations of AQUA peptides into the digest mixture for the villin and Na/K-ATPase were obtained. Native and standard peptide co-elution was achieved enabling the quantification of villin and Na/K-ATPase absolute abundances in filter-grown Caco-2 cell PM digests (Figure 4-6).

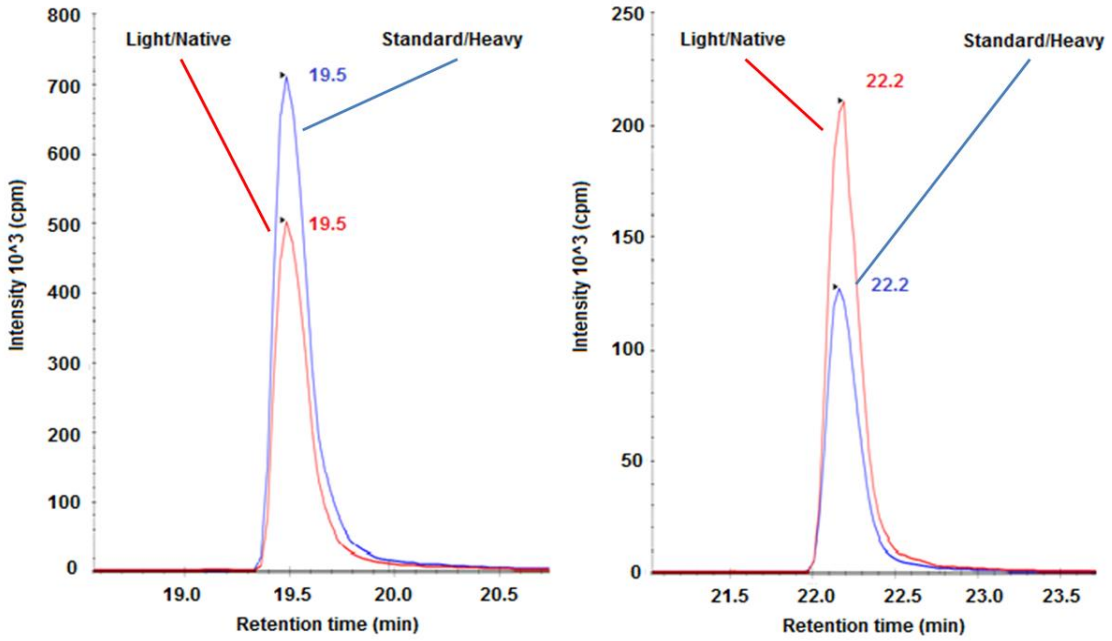

Figure 4-6. Co-elution profiles for Villin (AAVPDTVVEPALK) and Na/K-ATPase (IVEIPFNSTNK) peptides in a 16d grown Caco-2 PM digest. The blue and red peaks represent the standard and native peptides, respectively. Profiles were captured in the Skyline program.

This demonstrates the ability of the DOC digest to provide a sufficient yield of highly abundant proteotypic peptides for abundance determination using an AQUA approach. It is also important to note that gravimetric determination of peptide losses throughout the stages of digestion found a 24.6% loss of peptides from the nominal 50 µg of protein entering the digestion procedure. It is the peptide content in which losses are accounted for that is used to obtain protein abundances in fmol/µg protein and not the nominal concentration entering the digestion procedure. As expected, high abundances are exhibited for villin and Na/K-ATPase (Figure 4-7). Given these results, efforts turned to re-commencing the development of the QconCAT strategy by using the TransCAT construct with a DOC digest.

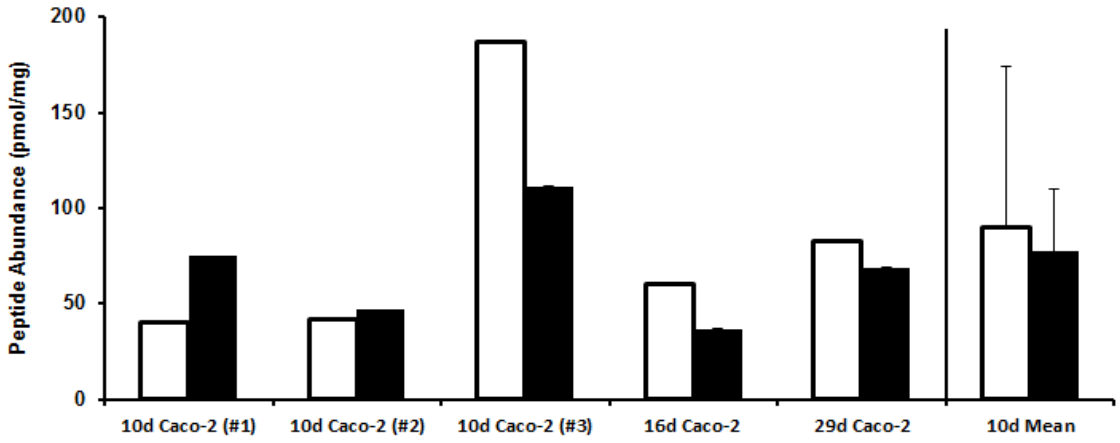

Figure 4-7. Villin and Na/K-ATPase absolute protein abundances in filter-grown Caco-2 cell PM digests for 10 (n=3), 16 (n=1) and 29 days (n=1). Villin (white) and Na/K-ATPase (black) abundances are provided for each Caco-2 cell preparation. The mean ± standard deviation is given for 10d grown cells.

4.3.2 Development of an LC-MS/MS Method for the Simultaneous Quantification of Transporter Proteins Absolute Abundance using a QconCAT Technique

4.3.2.1 Development of the LC-MS/MS Analysis

Prior to performing TransCAT-based LC-MS/MS analysis to quantitate transporter protein absolute abundances in biological systems, the parameters for LC-MS/MS were optimised for the proteotypic peptides expressed in the TransCAT construct. The 3 transitions providing the highest ion signal intensities for the sequence equivalent unlabelled MaxiSpiketides peptides were selected and MS conditions such as dwell time and CE were optimised (performed by Dr Matthew Russell).

For this study, 7 transporter proteins were selected for TransCAT-based LC-MS/MS method development. The selected transporters are; Na/K-ATPase; HPT1; P-gp; MRP2; BCRP; OST-α/β (specific peptides are required for quantifying the alpha and beta subunits of OST-α/β) and OATP2B1. Na/K-ATPase and HPT1 were theoretically selected as high abundance apical and basolateral membrane marker proteins. P-gp, MRP2 and BCRP are key apical efflux transporters with distinct pharmacological relevance in the intestine that are implemented within the Simcyp population-based simulator (Varma et al., 2010; Harwood et al., 2013). The dimeric basolateral membrane transporter protein OSTα/β (Ballatori et al., 2005), and the apical membrane expressed uptake transporter OATP2B1 (Kobayashi et al., 2003; Shirasaka et al., 2012) were selected due to their relevance to work in Chapter 5.

Preliminary work with Caco-2 cell PM and human intestinal total TM digests focussed on attaining an NNOP (Glu-Fib peptide) co-elution peak area ratio to enable robust quantification of the TransCAT concentration for defining the concentrations of the target peptide standards. The initial

series of analytical runs established the levels of synthetic Glu-Fib for addition to the digested peptide mix (Section 2.2.8.1). Subsequent SRM analyses were based on identifying previously optimised product ion transitions in intestinal TM digests. The peptides that did not exhibit consistent product ion signal intensities were not developed for the SRM schedules presented in this study. A single SRM method was developed to simultaneously detect the singly charged product ions of the selected peptides in a single analytical run. For the NNOP (Glu-Fib) and HPT1, two product ion transitions were of sufficient intensity to develop the finalised SRM method. The reverse phase gradient elution method for the nanoHPLC system was also optimised based on preliminary SRM runs. For each transition, the dwell time was set to 0.15 s. A representative chromatogram of the finalised SRM-based elution profiles for all the peptides in the digested intestinal TM matrix is provided (Figure 4-8). The profiles for the light and heavy peptides selected to quantify Na/K-ATPase and P-gp demonstrate a distinctive co-elution (Figure 4-9 A & D) for all selected transitions in the native (light, Figure 4-9 B & E) and heavy (standard, Figure 4-9 C & F) peptides which are suitable for abundance quantification. Further graphical representations of co-elution profiles for the other selected peptides are available in (Appendix Figure D-2).

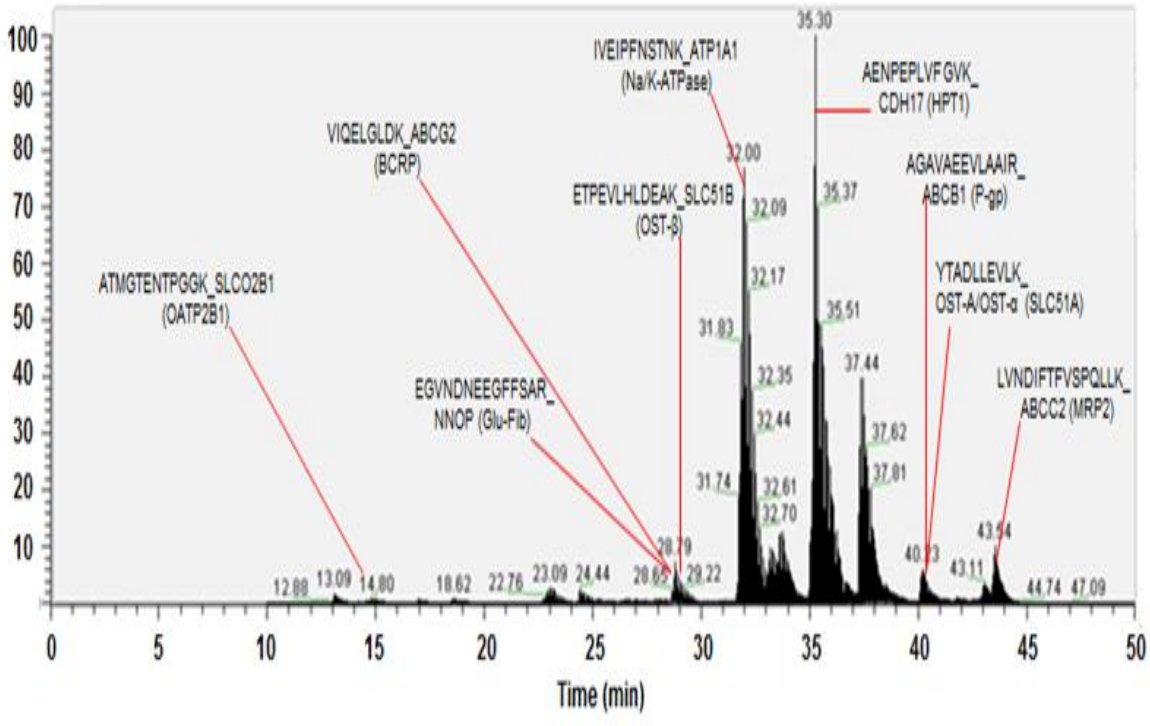

Figure 4-8. Total ion chromatogram demonstrating the developed LC-MS/MS SRM method for simultaneous quantification of the selected proteotypic peptides for the selected transporter proteins (Na/K-ATPase, HPT1, P-gp, MRP2, BCRP, OST-α, OST-β and OATP2B1) and the TransCAT calibrator peptide NNOP (Glu-Fib) and their isotope labelled standard peptides in a human intestinal TM digest.

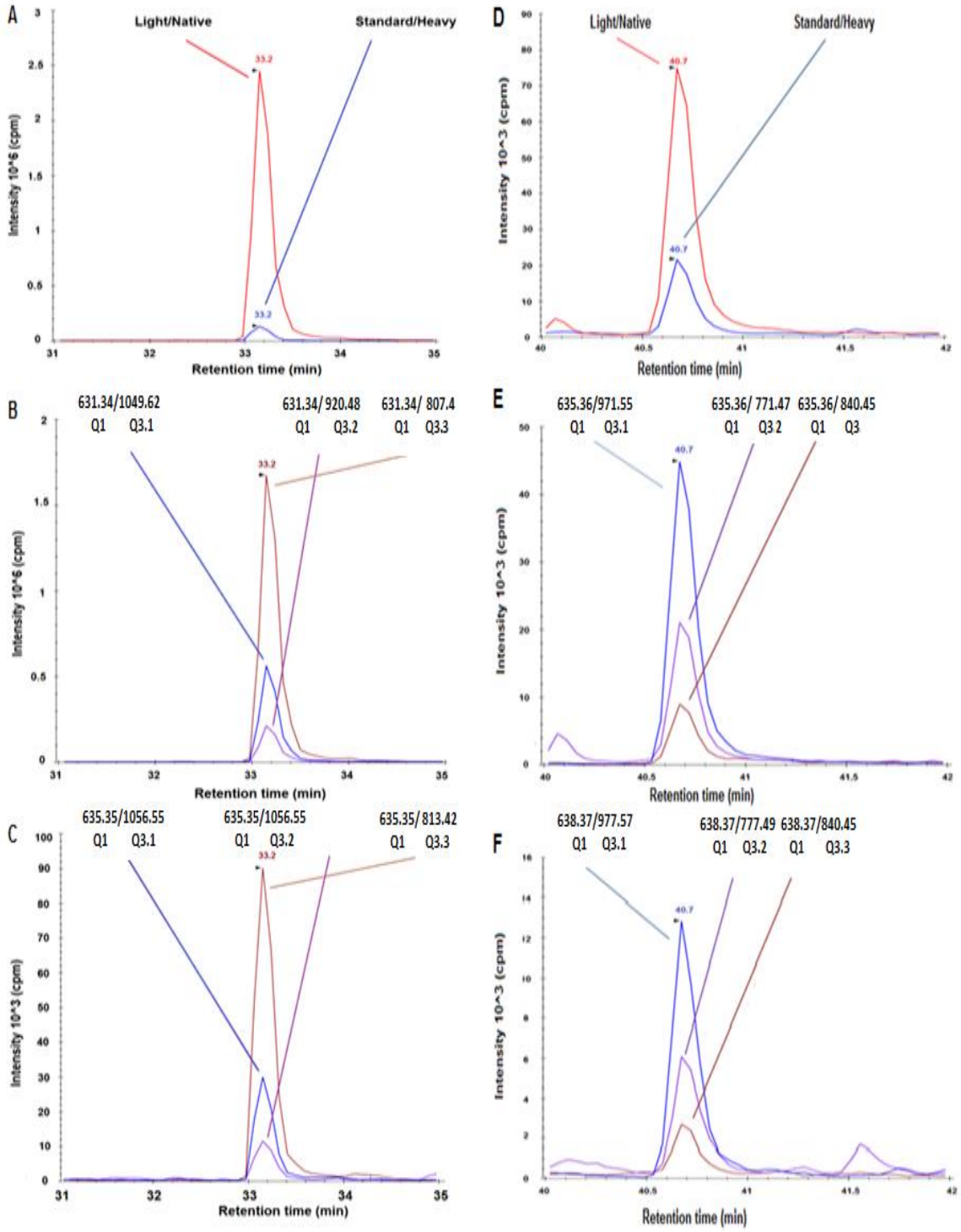

Figure 4-9. Co-elution and individual transition profiles for Na/K-ATPase (IVEIPFNSTNK, parts A-C) and P-gp (AGAVAEEVLAAIR, parts D-F) human intestinal TM digests., A & D, represent the cumulative profiles of the 3 product transitions selected for the native (light) and standard (heavy) peptides. B and E, represent the peak profiles for the 3 selected transitions for the light peptide and C and F, represent the peak profiles for the 3 selected transitions for the heavy peptide.

4.3.2.2 Method Validation – Linearity and Precision of the TransCAT Assay

To confirm that the developed TransCAT assay was quantitative, linearity and precision of the assay was established for calibration of the [TransCAT] (*i.e.,* via NNOP) and within biological matrices for the selected transporter peptides. For this aspect of the study, human intestinal TM's (distal jejunum (n=3), distal ileum (n=1) and a pooled intestinal TM sample (consisting of 3 samples, (Table 4-1))) were utilised. The internal standard-calibrator peptide (NNOP) selected for determining the equimolar concentrations of isotope labelled peptides released upon proteolytic co-digestion with the biological matrix was Glu-Fib (Simpson and Beynon, 2012). The NNOP peptide Glu-Fib permits quantification of both the standard and sample peptides.

The linearity of determining the QconCAT concentration from the co-elution of the NNOP peptide (EGVNDNEEGFFSAR) was tested. A series of pre-digested TransCAT constructs and synthetically synthesised light NNOP dilutions were analysed and the QconCAT concentrations were calculated from the ratios of the light and heavy peak intensities of the NNOP product ion transitions. Linearity was established over a greater than 100-fold range of QconCAT to NNOP ratio in the assay mix, with a correlation coefficient close to 1 (Figure 4-10A). The ability to measure target peptide abundances over a 14-fold range of sample protein injected onto the LC system was also tested. The masses of a pooled sample of 3 intestinal TM digests were varied in the assay mix with a fixed concentration of QconCAT. Equation 2-1 was employed to quantify the peptide abundances relative to the protein mass of the analytical run. For 6 of the 8 tested peptides, the linearity was established with correlation coefficients, $R^2 \geq 0.980$ (Figure 4-10B). However, the peptides selected for OST-β and OATP2B1 failed to demonstrate sufficient linearity (R^2=0.70 and 0.91, for OST-β and OATP2B1, respectively) over the sample concentration range tested (Figure 4-11). Therefore, any data relating to OST-β and OATP2B1 peptides presented are considered as data without quality control (QC) verification. In this study, the working range of the protein mass injected for LC-MS/MS analysis for the samples described in Table 4-1 were 2.49-3.56 µg protein injected. The lower limit of quantitation (LLOQ) was determined in the biological matrix at the lowest protein contents injected (0.23 µg) as 0.2 fmol/µg.

Table 4-1. Donor demographics of intestinal samples including recent drug history in which protein abundances were quantified.

Intestinal Region	Gender	Age	Ethnicity	Smoking Status	Disease/Complication/ Procedure	Drug History* [Human transporter Substrate (S) /Inhibitor (Inh) /Inducer (Ind)]	Mucosal Surface Area Chelated (cm^2)
Distal Jejunum (#1)	Male	65	Caucasian	Unknown	Incisional hernia & fistula	Codeine/ Loperamide (Inh)/ Omeprazole (S, Inh)	24
Distal Jejunum (#2) (> 130 cm proximal to the ileo-caecal valve)	Female	41	Caucasian	Non-smoker	Laparotomy, small bowel resection for enterocutaneous fistula	Cetirizine (S, Ind)/ Codeine/ Colestyramine/ Fentanyl (S, Inh)/ Fluticasone (S, Ind)/ Levothyroxine (Ind)/ Loperamide (Inh)/ Mebeverine Ondansetron/ Omeprazole (S, Inh)/ Salbutamol/ Salmeterol (Inh)	16
Distal Jejunum (#3)	Female	70	Caucasian	Non-smoker	Enterocutaneous fistula followed by laparascopic nephrectomy	Amitryptaline / Codeine/ Loperamide (Inh)/ Tramadol	24
Distal Ileum (Adjacent to the junction of the ileo-caecal valve)	Female	70	Caucasian	Non-smoker	Right hemicholectomy for displastic polyp removal	Budesonide (Inh)/ Cetirizine (S, Ind)/ Formatrol/ Furosemide (S, Inh)/ Monetelukast (S, Inh)/ Nitrofurantoin (Inh)/ Salbutamol /Tiotropium (S)	24

*For drug history, transporter Inhibitors are denoted (Inh), Inducers (Ind) and Substrates (S).

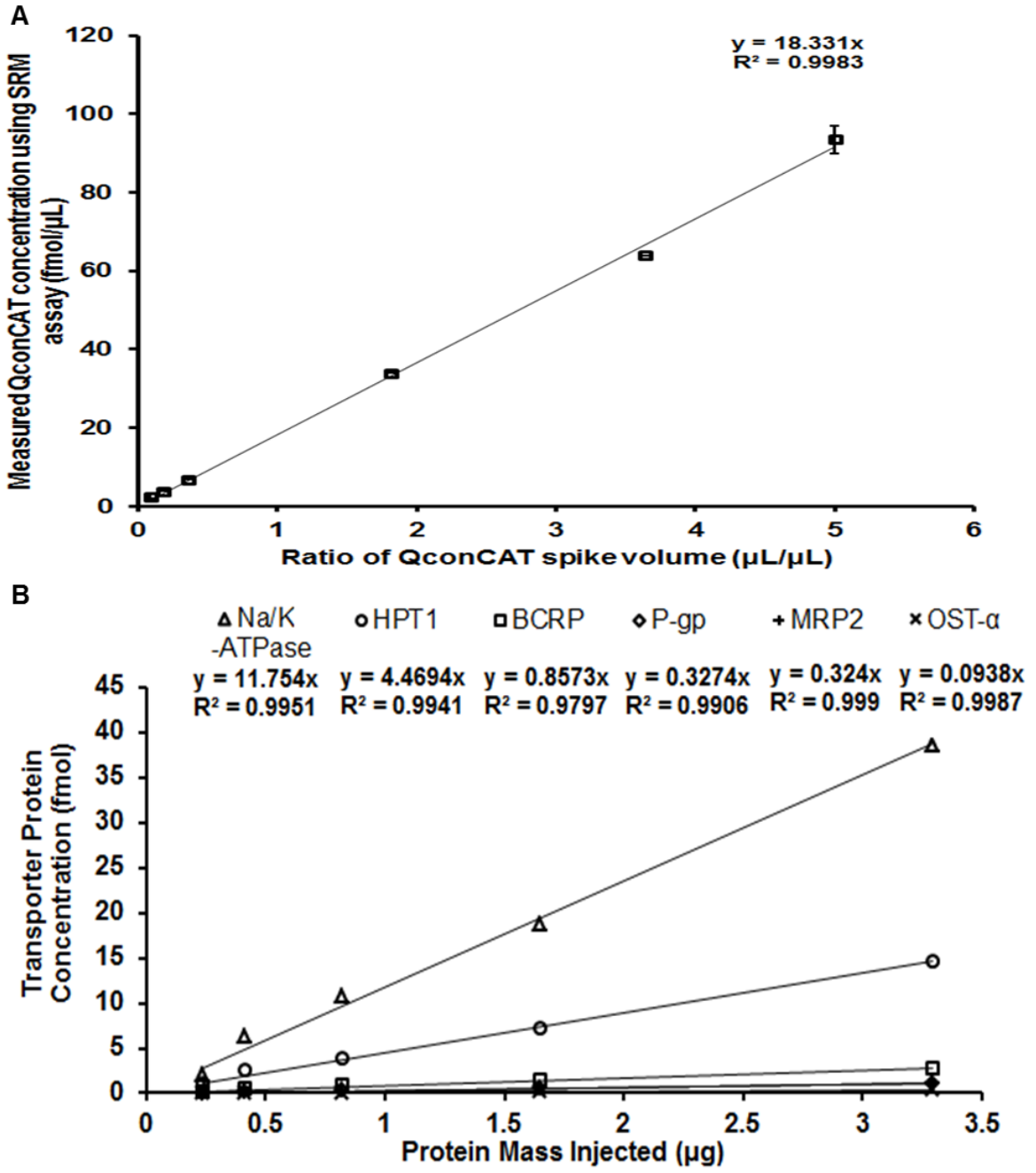

Figure 4-10 (A). Linearity of QconCAT quantification using the developed SRM assay for the NNOP peptide (Glu-Fib). The ratio of QconCAT spike volume signifies the dilution of spiked QconCAT (2 concentrations) and light Glu-Fib peptide (2.5 fmol/µL) in the assay mix. Linearity is displayed over a > 100-fold range for the QconCAT spike, demonstrating the dynamic range for which the QconCAT can be employed for abundance quantification. Error bars show the precision of measurements for one concentration of TransCAT based on two independent runs. B, demonstrates the linearity of transporter protein (Na/K-ATPase, HPT1, P-gp, BCRP, MRP2 and OST-α) concentrations quantified over a range of pooled human intestinal TM protein quantities. The total quantity of sample protein injected is plotted against the transporter protein amount as measured from the SRM assay for each protein. Linearity (R^2 = 0.980-0.999) is displayed for all proteins over a 14-fold range of injected human intestinal proteins.

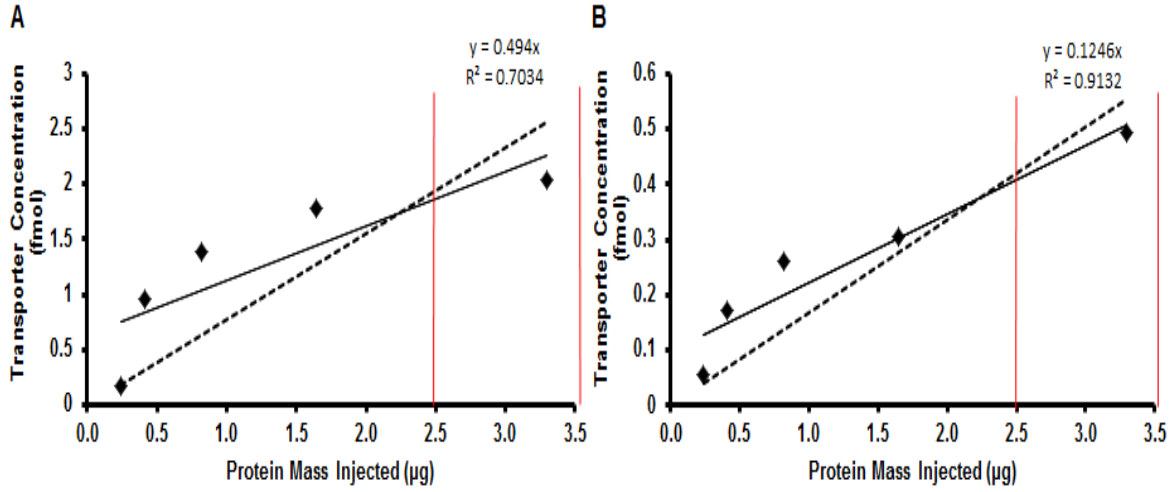

Figure 4-11. Linearity of transporter protein (OST-β (A) and OATP2B1 (B)) concentrations quantified over a 14-fold range of pooled human intestinal TM protein quantities. The total quantity of sample protein injected is plotted against the transporter protein concentration as measured from the SRM assay for each protein. The linearity (R^2 = 0.703-0.913) is provided in the graphs. The dashed trend line is forced through x and *y* coordinates 0, 0, representing unity). The red lines indicate the working protein range for the human intestinal membrane samples injected for the purposes of quantification in this chapter.

Within-day (intra-day) and between-day (inter-day) precision was assessed in 5 intestinal TM digests. The precision (coefficient of variation of the mean values) over 3 analytical runs between 2 separate days was <15%, which is within current FDA bio-analytical guidelines (FDA, 2013). The relative errors (RE) within-day and between-day for the linear peptides were <±15%, with the exception of MRP2 and OST-α that were below the LLOQ in some samples and displayed RE < 20% (Table 4-2). For the peptides not showing linearity (OST-β and OATP2B1), precision was <± 15% and within and between-day RE's were ≤20%. Due to the lack of transporter protein standards in biological systems, it is challenging to determine the accuracy within a biological context for quantitative assays. A commentary on the validity of performing accuracy determinations in QTAP assays is provided in the discussion (Section 4.4).

Losses of peptides during the digestion procedure, prior to loading into the LC-MS/MS stage of the workflow were accounted for by gravimetric methods (Appendix 4). The quantity of TM protein entering the digestion procedure was 50 µg for all samples. The gravimetric procedure determined peptide losses to be 36% (32.01 ± 3.37 µg TM protein, n=4) throughout this procedure, with the final mass measurement taking place after evaporation by vacuum centrifugation. It is the protein values that are corrected for losses that are used for corrected molar peptide abundances.

Table 4-2. Precision (CV%) analysis is provided for transporter proteins in human intestinal total membrane (TM) digests (n=5) over 3 sample runs, on 2 separate days. Within and between-day differences are provided as relative errors (RE, %) in two separate sample runs.

Protein	All runs	Within-day	Between-day
	Precision (%)	RE (%)	RE (%)
TransCAT	5.2-11.3	5.3 to 10.8	-8 to 12.5
Na/K-ATPase	5.4-12.7	6.7 to 13.1	-3.5 to 14.5
HPT1	1.4-11.4	-2.7 to 7.3	-10.4 to 10.2
P-gp	2.5-14.7	0.9 to 12.8	-2 to 13.9
MRP2*	4.3-10.3	4.8 to 18.6	-7.5 to 3.8
BCRP	2.3-8.0	-0.2 to 9.9	-11 to 10.3
OST-α	4.7-11.5	-8.7 to 15.4	-10.3 to 6.1
OST-β	7.2-14.2	-8.3 to 11.1	-13.6 to 20.0
OATP2B1	8.5-14.4	-18.7 to 17.4	-13.6 to 13.5

*Precision for one of the samples was based on two runs, as run 3 represented an outlier for MRP2.

Inter-operator differences in abundance quantification were assessed between 2 independent analysts for 104 co-elution profiles (7 peptides in 5 human intestinal samples). In >99% of cases, the abundance values determined by each operator were within a pre-defined threshold of 1.25-fold between-operators, highlighting the consistency in defining the co-elution peak area ratios in Skyline for incorporation into the abundance calculation (Equation 2-1).

4.3.2.3 Quantifying Absolute Transporter Protein Abundances in Human Intestine

The abundances for 6 transporter proteins are shown in (Figure 4-12). As expected, the basal membrane marker protein Na/K-ATPase shows considerably higher membrane abundances than the other proteins quantified. The cadherin-like transporter HPT1, was confirmed to be a relatively abundant apical membrane marker protein in our intestinal tissues. Of the apical efflux transporter proteins studied, the rank order of mean expression is BCRP>P-gp>MRP2 and in the single distal ileum sample MRP2 abundance was below the limit of quantification. The OST-α subunit was expressed at relatively low levels, and could not be detected in 2 of 3 jejunum samples, however its counterpart beta subunit was expressed at 6.7-to-9.7-fold higher levels. The abundance of OATP2B1 was also challenging to measure as only a single jejunal sample possessed abundances higher than the LLOQ (≥ 0.2 fmol/µg).

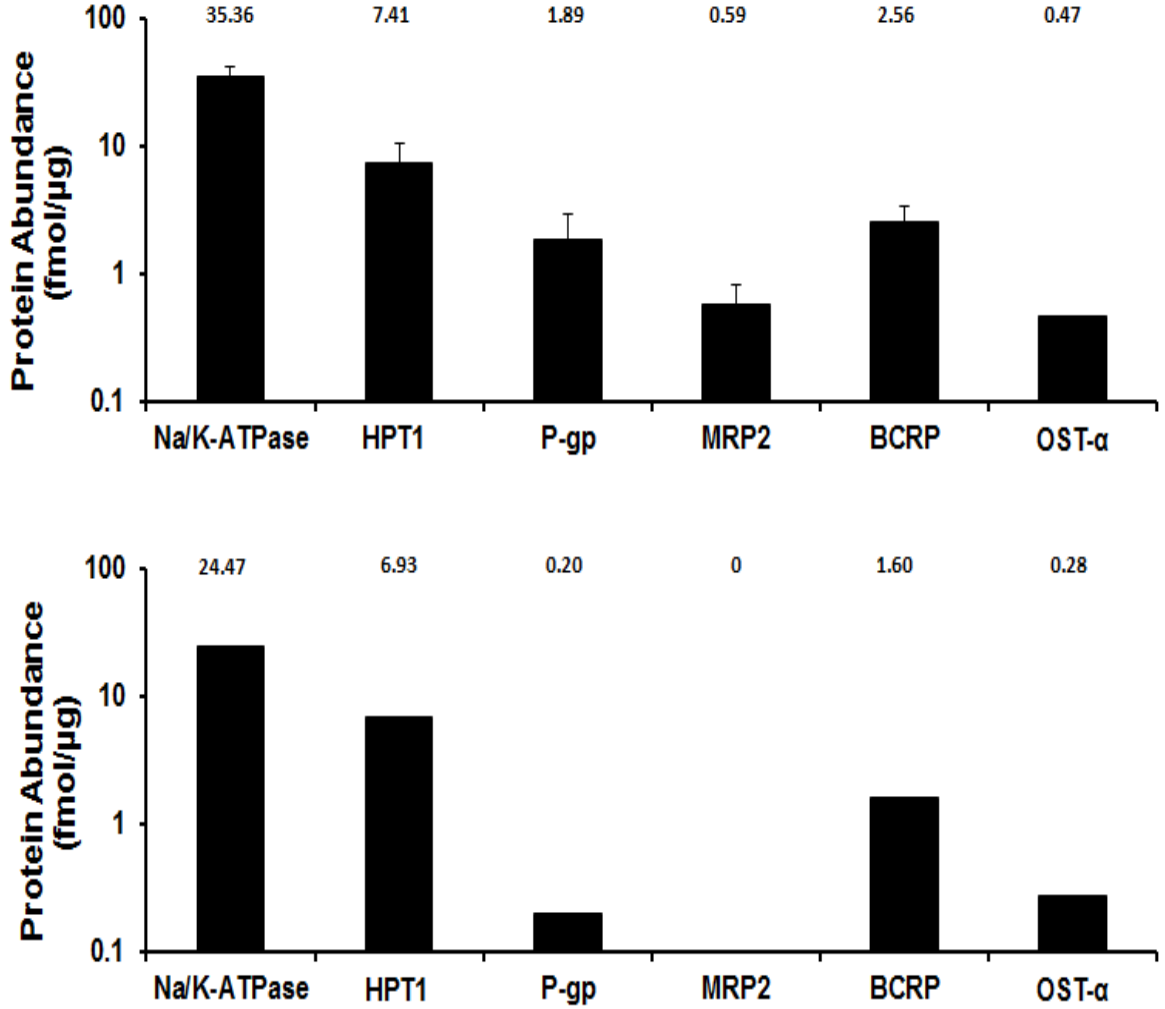

Figure 4-12. Absolute abundances of transporter proteins in human distal jejunum and ileum total membrane fractions. A, represents the transporter protein abundances in distal jejunum from 3 donors, measured in 3 separate analytical runs. B, represents the transporter abundances in distal ileum from a single donor, measured in 3 separate analytical runs. Data are expressed as Mean±SD. The text above the bars is the mean abundance of the transporter protein. BLQ denotes that the protein abundance was below the limit of quantification (< 0.2 fmol/µg membrane protein). For OST-α and OATP2B1, data for the jejunum is based on a single donor for the remaining 2 samples the abundance was below the limit of quantification.

4.4 Discussion

The aim of this study was to develop and validate a QconCAT-based LC-MS/MS method to quantify the absolute abundance of 8 key membrane transporter proteins in human intestinal samples. The challenges to developing a proteolytic digestion assay to enable robust transporter protein abundance quantification were also addressed. Due to the unexpected delays in development of a robust digestion protocol, a decision was taken to commission an external source to provide transporter abundance data from enterocytes and Caco-2 cells collected in this study. This was employed as an alternative strategy within this project to ensure that data generated from functional assays could be coupled to abundance data and would also provide unique cross lab comparison data as available.

A successful digestion strategy is critical to the QTAP workflow to provide the selected proteotypic peptides to enable the quantification of transporter protein abundances. Having undertaken guandinium hydrochloride-based digestion strategies (Kamiie et al., 2008) with limited success, a digestion assay with proteomic friendly reagents based on Nvoy and TCEP was developed (Russell et al., 2013). In practice, this assay was complex and care was required with regard to the digest mixture volumes generated. A purification stage (using SCX columns) was employed to reduce the likelihood of reagents liable for chromatography column contamination (*i.e.,* Tris, Nvoy).

Initial digests using Caco-2 cell PM proteins were analysed using a non-labelled, non-targeted DDA approach based on orbitrap MS-generated fragmentation spectra. These analyses were used to qualitatively define the presence of trypsin-derived proteolytic PM protein fragments, thus providing confidence in the applied digestion assay. The DDA analysis established that there were >1000 PM proteins that could be identified, however, the specific peptides selected for our PM marker protein Na/K-ATPase could not be distinguished. Based on identifying the presence of the Na/K-ATPase protein in our sample by DDA, we sought to identify whether a more selective targeted TransCAT approach using a triple-quadrupole MS could identify the proteotypic peptides for Na/K-ATPase. Although identification of a selected peptide was achieved, the native peptide peak ion signal intensity was <10^4 cpm. For other selected proteins there was little evidence of sufficient native peptide signal intensity to permit quantification and standard peptides were also at levels that were too high for quantification of peak area ion signal ratios. Inconsistencies in the digest persisted when altering QconCAT levels to reflect the lower signal intensities previously demonstrated. However, an improvement in native Na/K-ATPase signal intensity was observed

(10^4 cpm) which was considered to be consistent with the expected high abundance of this peptide. In addition, P-gp signal intensities for certain transitions were not reaching 10^3 cpm, which was concerning. On reflection, the signal intensities for Na/K-ATPase appear comparable with the subsequently developed DOC digest for similar samples using a TransCAT method, while for P-gp other proteomic groups demonstrate ion signal intensities ranging from 10^1 to >10^3 in a variety of biological matrices (Miliotis et al., 2011b; Zhang et al., 2011; Groer et al., 2013). Nevertheless, considerable losses of peptides may be responsible for the perceived low native peptide signal intensities observed. It was shown that nearly 70% of the peptides entering the SCX purification stage were not present in the final eluent. It is in our opinion that a quantitative assay for which the objective is to quantify absolute abundances cannot be based on procedures where approaching 70% losses of peptides occur.

After two years the project was not in a position to provide abundance data from membrane preparations and therefore alternative strategies were proposed. It was decided to obtain abundances in Caco-2 cell and intestinal samples through, BPh, the European partner to the proteomic technologies' led and established at the University of Tohuku, Japan (Kamiie et al., 2008) and possess the capabilities of performing transporter QTAP assays. Membrane protein samples obtained from Caco-2 cells and intestines were prioritised for distribution to BPh. Remaining protein samples were utilised for in-house assays which were to continue alongside measurements at BPh. The data provided by BPh is discussed in subsequent chapters.

Initiatives to establish a robust digestion protocol continued in-house by developing a DOC-based digest (Balogh et al., 2013). Within the study by Balogh et al., 2013, the impact of different denaturing agents on the quantification levels of OATP transporter proteins showed that a DOC digestion strategy provided an 8.6 and 33.5-fold higher abundance for OATP1B1 and OATP1B3 in HEK293 transfected cells, respectively compared to a guanidinium hydrochloride method. Communications between Pfizer and our group facilitated the development of a DOC digestion strategy. To simplify protein quantification, an AQUA-based approach was developed for Na/K-ATPase and villin, both high ranking proteins based on DDA analysis. In particular, the villin peptide should prove relatively simple to quantify if the digestion strategy provides effective yields of the selected standard peptide. This is based on villin's high ranking from in-house DDA analysis (42/335) which was also reciprocated in a separate label-free quantitative analysis from the Max Planck Institute in Caco-2 cells (Wisniewski et al., 2012).

Based on a small set of Caco-2 cell PM proteins, the abundances of Na/K-ATPase and villin were readily quantifiable from the high signal intensity co-elution profiles, obtained from a combination of DOC-based proteolytic digestion and AQUA proteotypic peptides. These findings provided assurances that further development of an TransCAT LC-MS/MS method should resume for transporter protein abundance quantification in intestinal tissues.

A TM protein fraction obtained from enterocytes chelated from freshly harvested intestinal samples from elective surgery was used for proteolytic digestion and absolute abundance quantification. Unlike the AQUA technique in which the standard peptide is typically added post-digestion, a QconCAT construct is typically added to the analyte protein matrix at the appropriate levels prior to digestion, enabling the concurrent digestion of the analyte proteins and QconCAT construct. This is advantageous, as processes intrinsic to the digestion strategy acting on the analyte and standard bearing QconCAT proteins are controlled for simultaneously. Furthermore, to quantify the levels of the standard peptides within a QconCAT construct, an NNOP calibrator peptide(s) is required. Isotope labelled NNOP's are built into the QconCAT construct and a synthetic-light 'analyte' non-isotope labelled calibrator peptide of a known concentration is added either prior to digestion, or post-digestion akin to the AQUA method. In this study, due to the limited amount of protein sample for in-house analyses, NNOP addition post-digestion was chosen. This safeguards the protein sample and potentially saves considerable time, as spiking the NNOP prior to digestion at levels that do not result in similar signal intensities to the standard, does not permit robust quantification of the standard peptides from the QconCAT, *i.e.,* within a 10-fold ratio, requiring a complete digestion re-run (Achour et al., 2014). Intially, it is critical to establish NNOP levels.

The NNOP dilution was established from co-elution profiles and optimisation of the SRM schedule for the selected peptides was undertaken. Co-elution profiles were then established for each target peptide. It is notable that the peptide selected to quantify the absolute abundance of P-gp in this study has also been employed in Caco-2 cells (Miliotis et al., 2011b) and human intestinal membranes (Oswald et al., 2013; Drozdzik et al., 2014), confirming the applicability of this peptide for determining P-gp abundances in enterocyte-like/intestinal systems.

When developing quantitative assays, it is necessary to perform validation of the LC-MS/MS method for linearity, precision and accuracy. The quantification of the TransCAT levels via the NNOP peptide Glu-Fib was linear over a 100-fold range of light to heavy ratios. For the targeted transporter proteins, linearity was established with precision for 6 of the 8 peptides used for

transporter quantification (R^2 >0.980). Linearity (*i.e.,* R^2 >0.95) was not achieved for OST-β and OATP2B1 selected peptides. Within the working range of peptide concentrations injected onto the LC for the intestinal digests (Figure 4-11, between red lines), there may be a small under-prediction in end point abundances (fmol/µg) as estimated from forcing the trend line through the *x-y* axis zero coordinates. Therefore, data relating to OST-β and OATP2B1 should be treated as values with partial QC verification. Similar linearity assessments have also been performed on a partner QconCAT for the purposes of measuring hepatic enzyme abundances, underpinning the capabilities of these constructs for quantifying target peptides over a wide-range of sample proteins (Achour et al., 2014).

Due to the limited availability of recombinantly expressed transporter proteins of known concentrations, establishing true biological accuracy in an AQUA or QconCAT assay is difficult to implement, particularly when the accuracy of the whole assay as opposed to only the LC-MS step needs to be confirmed. To determine the accuracy of peptide quantification for an AQUA assay, calibration curves and QC samples are prepared in digestion matrices in which the target proteins are absent (Groer et al., 2013) or are anticipated to be present at negligible levels (Miliotis et al., 2011b). However, the optimal approach to determine accuracy is to run biological matrices under study against samples containing a known concentration of the target protein. For transporter proteins, this approach is hindered by the limited availability of protein standards of a known concentration in suitable biological matrices and has only been demonstrated in a single study for proteo-liposomes containing P-gp (Prasad et al., 2014). Collectively, it is the lack of available standards of known concentrations, and the requirement for an internal standard to quantify the QconCAT concentration, that creates a significant challenge to implement the accuracy strategies employed in the literature for AQUA approaches, especially for drug transporter proteins. Recently, accuracy measurements for a QconCAT construct have been performed for CYP3A4 and CYP3A5 in commercially available liver microsomes, in which the enzyme abundances were measured by immunoblotting and ELISA (Achour et al., 2014). It could be countered that a comparison of techniques in matched samples does not constitute the determination of an assay's accuracy as each method may be inherently biased. Nevertheless, given the assumption that there is equimolar release of standard peptides during overnight digestion, accurate stoichiometric determination of light and heavy peak signal intensity should permit peptide quantification with sufficient accuracy.

Previous characterisation of the TransCAT (Russell et al., 2013) using the reported dual enzyme digestion strategy confirmed proteolysis reached steady state, providing further validation for this protocol. Another study using the same protocol reported the same result (Achour et al., 2014). Although most studies that quantified transporters in pharmacologically relevant tissues used trypsin as a digestive enzyme, recent studies have confirmed the utility of Lys-C as proteolytic enzyme for quantitative proteomics (Karlgren et al., 2012; Achour and Barber, 2013).

Protein abundances of pharmacokinetic relevance, *i.e.,* enzyme, transporter and receptor proteins are defined as moles of peptide corrected by the protein mass entering the digestion stage, routinely determined by standard protein assays. There are concerns that protein losses are inherent within the procedures leading to endpoint abundance quantification, therefore accounting for these losses is crucial for accurate abundance determinations (Uchida et al., 2013; Harwood et al., 2014; Prasad and Unadkat, 2014). To limit the downstream risk of contaminating the chromatography columns, the bulk of the protein denaturing agent, sodium deoxycholate was removed by precipitation following overnight digestion. Concerns, regarding the loss of digested peptides to precipitation were raised, as well as potential losses of peptides to sampling tubes and pipettes prior to loading into the LC-MS/MS system. Therefore, a gravimetric procedure (Appendix 4) was developed to account for these losses, in which sample tube masses, peptide solutions and precipitates were measured.

The developed SRM TransCAT assay was applied to measuring the absolute abundance of Na/K-ATPase; HPT1; P-gp; MRP2; BCRP andOST-α with reservations for partially verified OST-β and OATP2B1. For all tissues, Na/K-ATPase; HPT1; P-gp; BCRP and OST-β were quantifiable above the LLOQ (>0.2 fmol/µg). The ability to quantify membrane marker proteins is important for characterizing the quality of; the tissue, the membrane extraction procedure and the digestion protocol. For comparative purposes, as far as the candidate is aware no other data are available for Na/K-ATPase abundance in the intestine. However, Na/K-ATPase abundance is approximately 3-fold higher than expression in 17 human liver TM fractions (Ohtsuki et al., 2012). HPT1 is a peptide transporter that possess pharmacological relevance as it facilitates the proton-sensitive uptake transport of the antibiotic cephalexin in transfected Chinese hamster ovary cells (Dantzig et al., 1994). The peptide transport 1 (PepT1) protein has been quantified in 6 intestinal tissues exhibiting a 1.8-fold lower expression in the distal jejunum compared to HPT1 in this study (Drozdzik et al., 2014). However, for both studies these transporters are expressed at relatively

high levels compared to the SLC and ABC isoforms studied. For the apical membrane transporters BCRP, P-gp and MRP2, a similar rank order expression pattern to this study has also been observed in duodenal samples in which the absolute abundance was determined by an immunoblotting approach (Tucker et al., 2012). Yet, in a QTAP strategy, MRP2 was shown to possess the highest abundance compared to P-gp and BCRP in both duodenum and jejunum samples (Groer et al., 2013; Oswald et al., 2013; Drozdzik et al., 2014). The mean absolute levels of P-gp and BCRP in jejunum tissues are approximately 3 and 7-fold higher for samples in our study compared to the literature (Groer et al., 2013; Oswald et al., 2013; Drozdzik et al., 2014). These differences may arise from inter-individual variability or differences in the techniques applied to obtain abundances. Nevertheless, a cross laboratory comparison with matched tissues is required to determine whether these differences were indeed due to methodology or are genuine representations of the biological system (Harwood et al., 2014). The OST-α subunit forms a dimeric molecule with the OST-β subunit, which is functionally expressed as a dimer in the basal membrane of enterocytes and has been shown to participate in endogenous compound and digoxin transport (Seward et al., 2003; Ballatori et al., 2005). OST-α/β function is not conferred when subunit co-expression is absent (Seward et al., 2003). Furthermore, the localisation of the alpha subunit in the PM could only take place when the subunits are co-expressed (Sun et al., 2007). OST-α/β gene expression is regulated by farnesoid-X-receptor (Landrier et al., 2006). In addition, recent work has identified that the beta and not the alpha subunit is additionally regulated by a retinoic acid receptor-α and constitutive androstane receptors in human hepatoma cells (Xu et al., 2014), which may lead to a differential expression of the two subunits of OST-α/β seen in this study. However, it appears that the regulation of OST expression is complex and may be cell or organ specific (Khan et al., 2009). To quantify the abundance of a dimeric molecule such as OST-α/β, the lowest expressing subunit represents the absolute abundance of the functionally relevant protein co-localised in the plasma membrane. However, the limitation with any study that does not measure transporter abundance in a highly purified PM fraction risks measuring non-functionally relevant intracellularly sequestered OST subunits that are not co-expressed or co-localised in the PM, resulting in difficulties in applying this data to translational models. Finally, due to the role of OST-α/β in bile acid reabsorption, further studies focussing on terminal ileum expression may also provide greater opportunities to measure OST-α/β at the site in which it is most physiologically relevant.

The influence of recent drug administration should also be considered when determining transporter abundances. The 4 donors had all been administered a variety of drugs in the recent past which may influence transporter expression and potentially lead to abundance differences between studies. Characterising protein abundances in tissues originating from a diseased population is critical to generating PBPK models in clinical sub-populations for which the drugs are primarily indicated.

4.5 Conclusion

This study describes the challenges and development of a proteolytic digestion strategy together with an LC-MS/MS targeted proteomic method for quantifying drug transporter protein absolute abundance in human intestinal tissues using a QconCAT strategy. The methods were applied to measure Na/K-ATPase, HPT1, P-gp, BCRP, MRP2, OST-α in eluted enterocyte total membrane fractions. The beta subunit of OST-α/β and OATP2B1 abundances were obtained but did not adhere to stringent bioanalytical recommendations for LC-MS/MS validation. This study provides the basis to develop further SRM methods for quantification of numerous other transporter proteins of in pharmacokinetically relevant tissues for on-going projects focussing on human liver, brain and kidney at the University of Manchester.

Chapter 5 - Breast Cancer Resistance Protein Abundance Correlates better than mRNA Expression with Estrone-3-Sulfate Bi-directional Transport Activity

Declaration

Work presented in this chapter was performed by the candidate Matthew Harwood and where indicated Caco-2 abundance data was generated by Bertin Pharma, Orleans, France.

5.1 Introduction

Permeability screening assays routinely employ filter-grown Caco-2 cell monolayers to assess the ability of drug molecules to cross cellular barriers (Artursson, 1990; Hubatsch et al., 2007). When grown on permeable filter supports, Caco-2 cells slowly differentiate to provide a phenotype with similar morphologies (Hidalgo et al., 1989), and transporter protein expression profiles as human intestinal enterocytes (Hilgendorf et al., 2007). A correlation between the apparent permeability (Papp) of numerous compounds to the effective permeability (Peff) in man (Lennernas et al., 1993) has been studied in Caco-2 cell monolayers under different transport conditions, for example with a pH gradient operating across the cell monolayer (apical pH 6.5: basal pH 7.4) or without a pH gradient (apical pH 7.4: basal pH 7.4) (Sun et al., 2002) and is used to predict drug absorption in PBPK models (Yang et al., 2007; Darwich et al., 2010). Caco-2 cells are, therefore, an appropriate tool for studying the impact of transporters on drug permeability and data generated from these assays can be directly linked to models that can extrapolate to predict *in vivo* drug absorption.

Studies in Caco-2 and MDCK-II cells have shown that P-gp activity, as assessed by bi-directional transport and kinetic assays, correlate to protein expression after immunoblot densitometry analysis (Taipalensuu et al., 2004; Kamiyama et al., 2009; Tachibana et al., 2010). Further work has also established a protein abundance-activity correlation for P-gp using bi-directional transport and QTAP assays using a limited number of samples (Miliotis et al., 2011b). Currently, data on the relationship between protein expression and activity for BCRP, another key intestinal efflux transporter (Urquhart et al., 2008), is limited. Studies in Caco-2 cells using the BCRP probe substrate Estrone-3-Sulfate (E-3-S) showed a concomitant decrease in the relationship between BCRP expression and the secretory efflux ratio (ER) elicited by BCRP (Xia et al., 2005). However, in another study, the relationship for the E-3-S ER and the level of BCRP protein expression level was not as convincing (Kamiyama et al., 2009). Neither of these studies used a QTAP approach to assess BCRP protein expression. To investigate the effect of protein expression-activity relationships, the majority of these studies performed the transport assay on Caco-2 cells cultured on filters for varying time periods. There are conflicting data in the literature regarding the effect of Caco-2 cell culture period on transporter protein expression using a range of approaches to determine transporter protein expression (Hosoya et al., 1996; Anderle et al., 1998; Uchida et al., 2007; Kamiyama et al., 2009; Miliotis et al., 2011b). Therefore, there is a need to determine the

protein abundance profile of key transporters in Caco-2 cells using QTAP assays and to establish the relationship between BCRP abundance and function.

Sulfated conjugates of oestrogen, particularly E-3-S (Figure 5-1), have been used to probe the activity of BCRP (Imai et al., 2003; Suzuki et al., 2003; Poirier et al., 2014). As is the case for many compounds considered as probes for transporter proteins, E-3-S an organic anion, also exhibits overlapping transporter protein specificities (Figure 5-2 & Table 5-1). However, mechanistic kinetic modelling of E-3-S vectorial transport in Caco-2 cells has shown that basal to apical efflux is the dominant transport process in operation (Rolsted et al., 2011) (Figure 5-2).

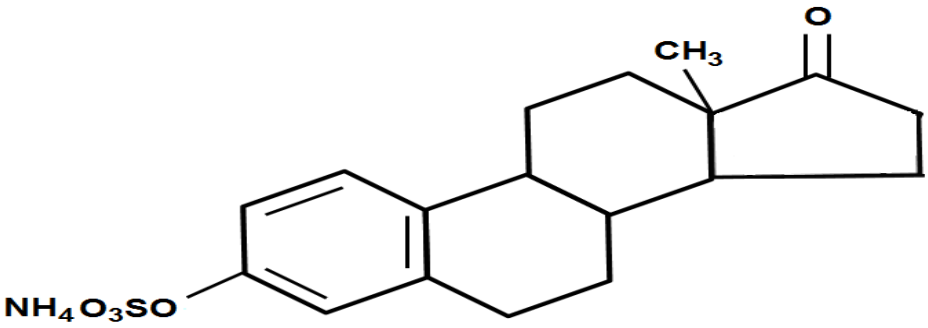

Figure 5-1. The chemical structure of Estrone-3-Sulfate (ammonium salt).

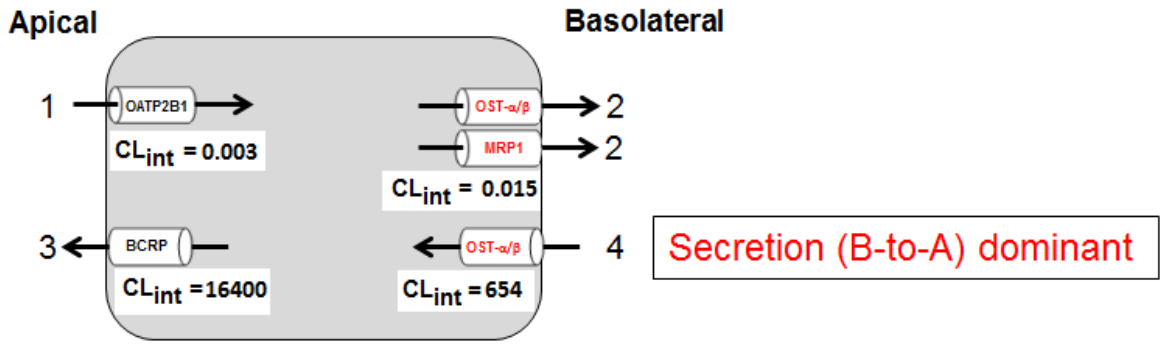

Figure 5-2. Postulated transport pathways for E-3-S at the apical (A) and basaloteral (B) membranes in Caco-2 cells. The estimated intrinsic clearance (CLint) is given as pmol/min/cm^2. Pathway 1 (apical uptake) and Pathway 3 (apical efflux) are postulated to transport E-3-S by OATP2B1 and BCRP, respectively, based on experimental evidence in Caco-2 cells (Gram et al., 2009). The transporter proteins mediating E-3-S transport via basolateral efflux (pathway 2) and uptake pathways (pathway 4) have not been established experimentally in Caco-2 cells. It is postulated that OST-α/β transports E-3-S bi-directionally (Seward et al., 2003; Ballatori et al., 2005; Sun et al., 2007) on the basolateral membrane and MRP1 also contributes to the basolateral efflux of E-3-S (Maeno et al., 2009).

Table 5-1. Physico-Chemical Properties of E-3-S, Metabolism & Transport Specificities.

Parameter	Value/Description	Source	Comments
Molecular Weight (g/mol)	365	http://www.webqc.org/mmcalc.php	Ammonium Salt
pKa	2.2	(Gram et al., 2009)	Unknown derivation
Compound Type	Acid (anion)	http://www.ebi.ac.uk/chebi CHEBI – ID 17474	
LogP	0.84	http://www.molinspiration.com/cgi-bin/properties	Calculated
Metabolism Km (μM)	Arylsulfatase Km 3.4 Steryl-Sulfatase Km 1.2	(Prost et al., 1984)	Back-conversion to estrone – not transported (Imai et al., 2003)
Transport			
Apical Uptake	Jmax – 0.08 Km,u – 28.9	(Rolsted et al., 2011)	OATP2B1-mediated*
Basal Efflux	Jmax – 0.15 Km,u – 9.7	(Rolsted et al., 2011)	MRP1-mediated*
Apical Efflux	Jmax – 19700 Km,u – 1.2	(Rolsted et al., 2011)	BCRP-mediated*
Basal Uptake	Jmax – 8640 Km,u – 13.2	(Rolsted et al., 2011)	OST-α/β-mediated*

*Postulated transporters mediating the directional flux of E-3-S. Jmax is in units of pM/min/cm^2

The primary aims of this study are to assess the gene expression and protein abundance of key drug transporters in low passage Caco-2 cells grown on filters from 10 to 29 days. Bi-directional transport of the BCRP probe E-3-S will be evaluated in respect to mRNA levels and protein abundance in 10 and 29d Caco-2 cells. As a secondary objective, the effect of altering pH conditions in the transport assays will also be investigated.

5.2 Methods

The finalised methods employed here, are described in detail in Section 2.2.1 for basic cell culture conditions, Section 2.2.2.2 for obtaining Caco-2 cell membrane fractions, Section 2.2.6 for generating peptide standards, Section 2.2.7 for protein digestion, Section 2.2.8 for LC-MS/MS analysis and section 2.2.9 for analysis of transporter gene expression. BPh protein abundance analysis is described in Section 2.2.8.6. The basic protocol for the monolayer transport assays are described in Section 2.2.10. E-3-S binding to BSA was performed as described in Section 2.2.11.

5.2.1 Bi-directional Monolayer Transport Assay: E-3-S Transport

The standard methods for the Caco-2 cell monolayer transport assays provided in 2.2.10 are built upon for E-3-S transport, with the following modifications.

[^{3}H]-E-3-S transport was assessed in 10 and 29d filter-grown Caco-2 cells (ATCC-HTB-37, passage 25-35) with similar culture conditions to those described in the study of Miliotis et al., (Miliotis et al., 2011b). The basolateral transport buffer consisted of HBSS-HEPES (25 mM) pH 7.4 or HBSS-MES (10 mM) pH 6.5 (pH gradient conditions), or without pH a gradient, pH 7.4/7.4 or 6.5/6.5. To improve E-3-S recovery, 0.05% (w/v) BSA was added to the transport buffer in each chamber (Grandvuinet and Steffansen, 2011). Monolayer integrity was monitored by LY transport (50 µM) bi-directionally (Section 2.2.10). E-3-S was estimated to possess a Km of 1.2 µM (Rolsted et al., 2011), therefore E-3-S transport at 0.01 µM concentrations was monitored under sub-saturating transport conditions. To assess the specificity of BCRP-mediated E-3-S transport, Ko143 (2 µM), a potent BCRP inhibitor (IC50, 0.2 µM) (Matsson et al., 2009), was added to both sides of the monolayer throughout the assay. Ko143 was shown to possess the capacity to inhibit OATP2B1 at concentrations greater than 5 µM (Karlgren et al., 2012). Based on this observation, it is anticipated that Ko143 (2 µM) retained its specificity for BCRP inhibition. The impact of apical uptake by OATP2B1 was also assessed in E-3-S transport experiments by the addition to both sides of the monolayer of the OATP2B1 inhibitor montelukast (100 µM) (Shirasaka et al., 2012). Transport was initiated by addition of the [^{3}H]-E-3-S-laden transport buffer to the requisite side of the monolayer and insertion into the orbital rotating incubator at 100 rpm and 37°C. The duration of the assay was 120 min. Donor samples (100 µL) were taken separately for LSC counting of [^{3}H]-E-3-S and fluorescent monitoring of LY at the start and end of the experiment, with replacement of the donor buffer immediately. Receiver chamber samples were also taken at 5, 15, 25, 50, 80 and 120 min for LSC and LY monitoring (100 µL for each) and the relevant transport buffer (200 µL)

was replaced immediately. The Papp were calculated after correction for E-3-S binding to BSA (*i.e.,* the unbound concentration, Equation 2-3).

A weighted mean analysis was used to assess the mean in the absence of abundance data above the limit of quantification for the QconCAT derived absolute transporter abundance quantification. To enable a weighted mean to be calculated Equation 5-1 was used.

$$W_{\bar{X}} = \frac{n_j \cdot \bar{X}_j}{n} \qquad \text{Equation 5-1}$$

where $W_{\bar{x}}$ is the weighted mean, n_j is the number of samples in which abundances are above the lower limit of quantitation, the $\bar{x}_j$ is the mean of the samples above the limit of quantification and n is the total number of samples in the data set.

5.3 Results

5.3.1 Characteristics of Caco-2 Monolayers

As a QC, the integrity of the monolayers was routinely monitored by TEER over the cultivation period and by the paracellular marker LY throughout the transport assay. A TEER plateau was typically reached at 7 days, indicating confluence was reached (Figure 5-3).

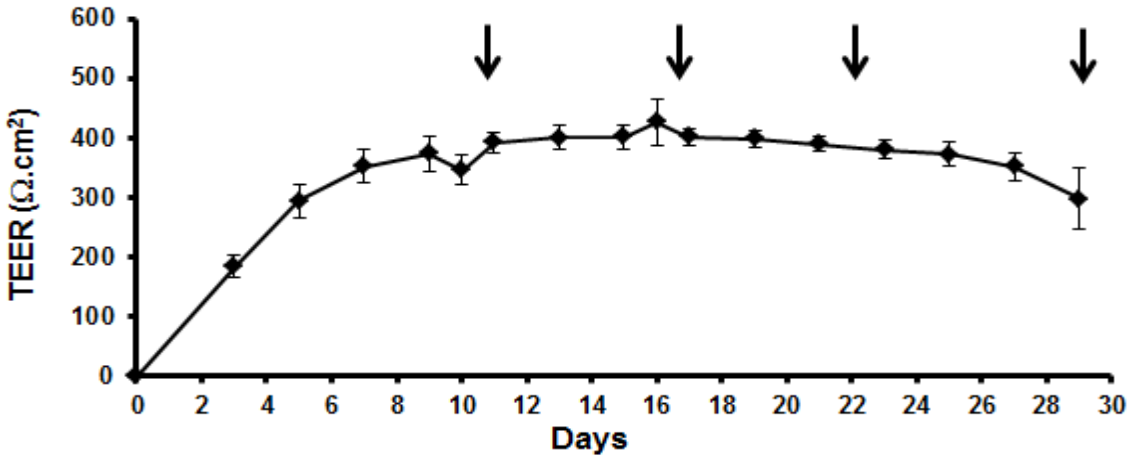

Figure 5-3. Assessment of monolayer integrity and growth by TEER for all cultured Caco-2 cells monolayers N=32 plates. Note, no transport assays were undertaken at 16 or 21d in Chapter 5, therefore data at 16 and 21d reflects TEER prior to RNA harvesting. The arrows indicate cell transport assay or RNA harvest points.

The mean end point TEER and LY Papp for Caco-2 monolayers are provided in Table 5-2. Caco-2 cell monolayers cultivated for 29 days showed significantly lower TEER's than the other groups (p=<0.001, 1-way ANOVA). There is also a significantly higher TEER in 16d monolayers compared to 10d monolayers (p=<0.01, 1-way ANOVA). The 10d monolayers exhibit significantly higher LY permeability than for 16 and 21d (p=<0.05, 1-way ANOVA) and 29d LY permeability is significantly higher than at 21d (p=<0.05, 1-way ANOVA), although these are within integrity cut-off limits for TEER and LY transport.

Table 5-2. Endpoint TEER and LY permeability in filter-grown Caco-2 cell monolayers.

	Culture Period (days)			
	10d	16d*	21d*	29d
TEER ($\Omega.cm^2$)	340 (± 70)	397 (± 61)‡	357 (± 19)	294 (± 49)†
LY Papp	0.32 (± 0.27)§	0.2 (± 0.16)‖	0.16 (± 0.09)	0.31 (± 0.21)
(x 10^{-6} cm sec^{-1})	N=13 (n=116)	N=3 (n=22)	N=3 (n=32)	N=15 (n=165)

*RNA filters only. †, significantly lower (p=<0.001) than all other periods. ‡, 16d monolayers higher than 10d monolayers (p=<0.01). §, significantly higher than 16 and 21d (p=<0.05) and ‖, significantly lower than 10d (p=<0.05). Differences between groups tested by 1-way ANOVA with Bonferroni (all group) post-hoc analysis to test for differences between groups. N denotes experimental plates and n denotes filters. Plates were typically seeded on different days from 5 batches of frozen stocks, all sourced from the ATCC at P18.

5.3.2 Age-Dependent Transporter Gene Expression Analysis in Caco-2 Cells

For the analysis of relative gene expression, mRNA levels for two commonly used endogenous 'housekeeper' proteins Glyceraldehyde 3-phosphate dehydrogenase (GAPDH) (Bannon et al., 2009) and PPIA (Seithel et al., 2006), were checked for the proximity of their cycle thresholds to the target transporter genes of interest in flask-grown Caco-2 cell monolayers. The mean cycle thresholds for GAPDH, PPIA and MDR1 were 17.00 ± 0.23 (CV=1.3%), 18.53 ± 0.26 (CV=0.8%) and 23.51 ± 0.25 (CV=1.1%). In further experiments with filter-grown Caco-2 cells of all ages, the proximity of PPIA was also found to be closer to that of MDR1 compared to GAPDH. There was no effect of cultivation time on PPIA gene expression (p=0.83, 1-way ANOVA) in 10-to-29d filter Caco-2 cells (Appendix Figure E-1). Based on the proximity of PPIA's cycle threshold to MDR1, the PPIA housekeeper gene was selected for relative expression analysis.

The relative gene expression levels of the ABC transporters MDR1, MRP2 and BCRP over a 29 day culture period are provided in Figure 5-4. The rank order of gene expression is MDR1>BCRP>MRP2 which is consistent across culture periods. For all transporters, the highest gene expression is consistently observed at 21 days and is significantly higher (p=<0.01, 1-way ANOVA) than the 10d culture period which shows the lowest expression levels for all three transporters. For both MDR1 and BCRP, there were no significant differences in expression between 16, 21 and 29 day cultured monolayers (Figure 5-4). However, MRP2 expression, in 21d cultured monolayers was significantly higher than those cultured for 16d (p=<0.01, 1-way ANOVA).

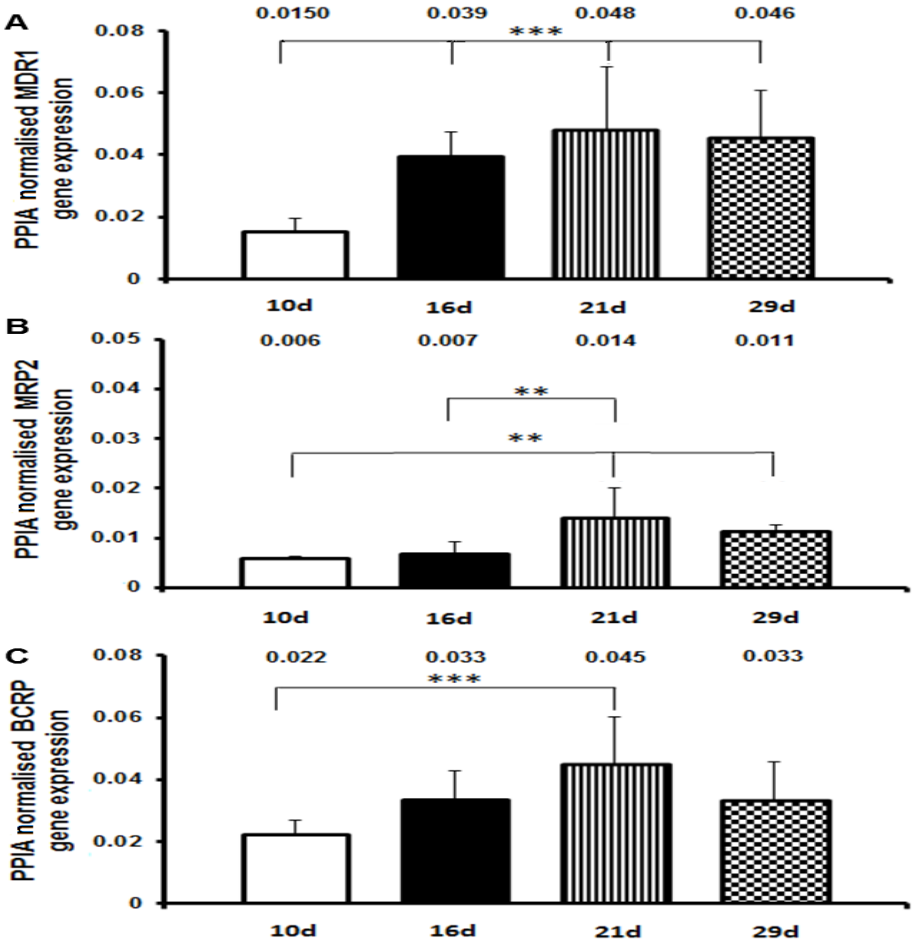

Figure 5-4. mRNA gene expression of MDR1, MRP2 and BCRP in 10 to 29 day cultured Caco-2 cells normalised to the housekeeper protein PPIA. A, represents MDR1, B, represents MRP2 and C represents BCRP. Each bar represents n=3 separate mRNA extractions. Assays were conducted on 2 separate days in duplicate. The values are given as Mean±SD, with the text above the bars representing expression mean levels. ** = p=< 0.01, *** denotes p=<0.001 as determined by a 1-way ANOVA with Bonferroni (all group) comparisons post-hoc analysis to test for differences between groups.

The relative gene expression levels of the SLC transporters OATP2B1, OST-A and OST-B in 10 and 29 day grown Caco-2 cells are provided in Figure 5-5. Measurements of SLC gene expression were focussed on cells grown for 10 and 29d due to the performance of bi-directional E-3-S transport assays in cells of these ages. A significantly higher (p=< 0.001, Unpaired t-test) gene expression is observed for all transporters in 29d cells. The overall rank order of the gene expression of the 6 transporter proteins being studied after 10 days is OATP2B1>OST-B>BCRP>OST-A>MDR1>MRP2 and for 29 days of culture is OATP2B1>OST-B>MDR1>OST-A>BCRP>MRP2. Taken together, these data suggest that MDR1 is most sensitive to the duration of culture period (Figure 5-6).

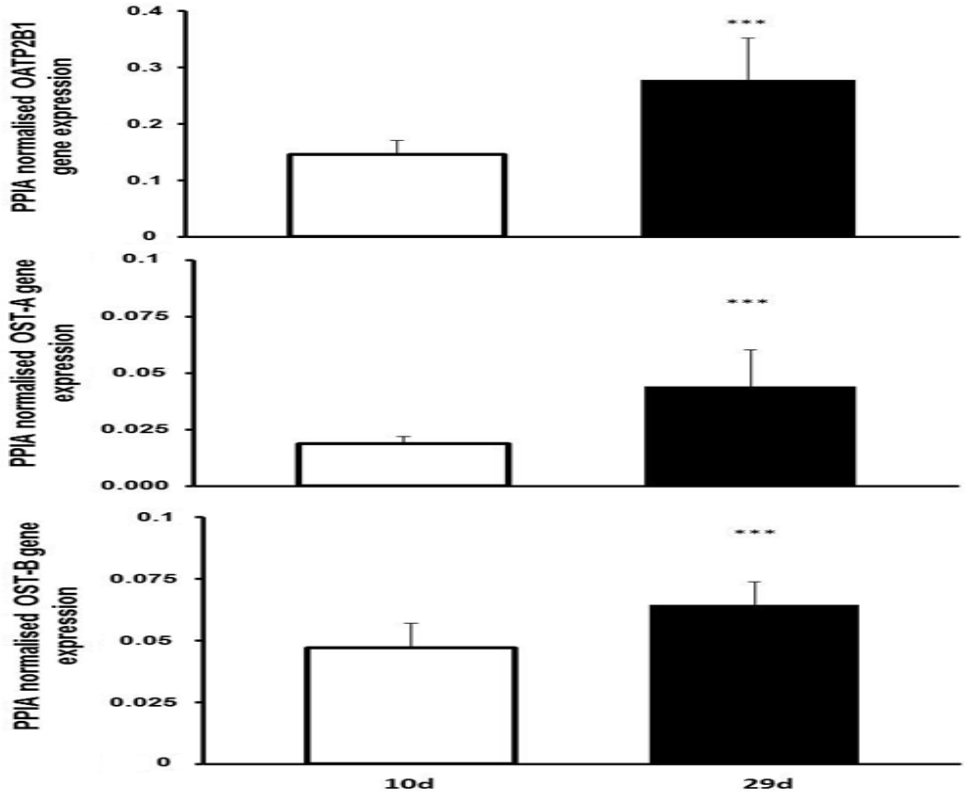

Figure 5-5. mRNA gene expression of OATP2B1, OST-A and OST-B in 10 and 29 day cultured Caco-2 cells normalised to the housekeeper protein PPIA. A, represents OATP2B1, B, represents OST-A and C represents OST-B. Each bar represents n=3 separate mRNA extractions. Assays were conducted on 2 separate days in duplicate. The values are given as Mean±SD, with the text above the bars representing mean expression levels. *** denotes p=<0.001 as determined by an Unpaired t-test.

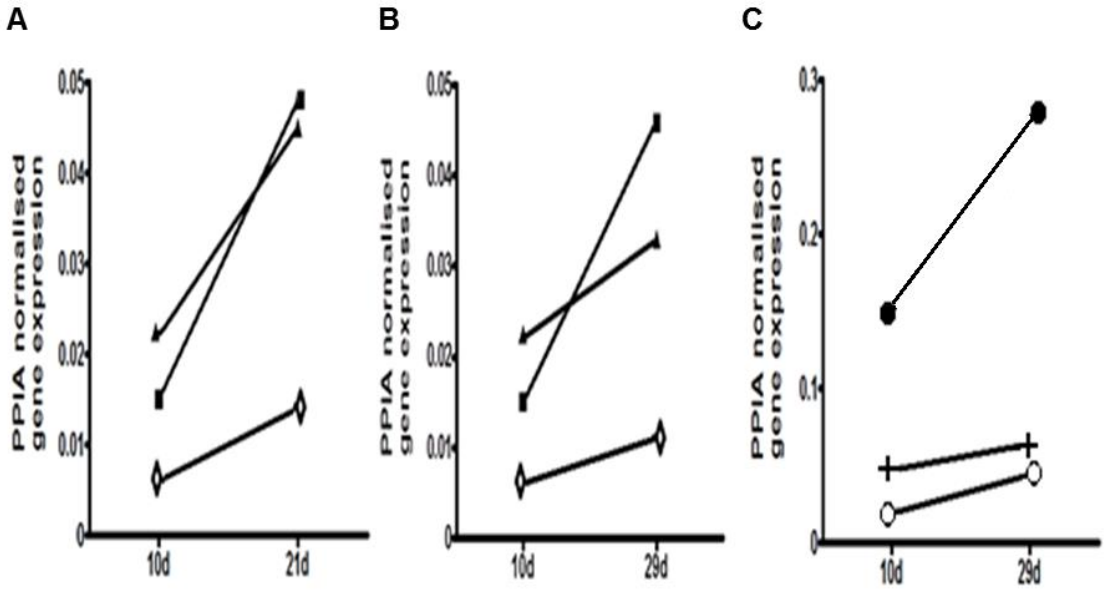

Figure 5-6. Plots showing the change in gene expression over Caco-2 cell cultivation time for all transporters. A & B, represent MDR1, MRP2 & BCRP at 10 & 21 and 10 & 29 day culture times, respectively. C, represents OATP2B1, OST-A and OST-B at 10 and 29d culture times. Symbols represent MDR1 (squares), MRP2 (diamonds), BCRP (triangles), OATP2B1 (filled circles), OST-A (cross) and OST-B (open circles).

5.3.3 Age-Dependent Transporter Protein Abundance Analysis in Caco-2 Cells

The protein abundance data described in this section was generated by analyses at BPh and the University of Manchester (UoM). It should be noted that protein abundances from matching samples analysed in both laboratories are represented. In certain instances, there was insufficient protein content to enable all samples to be analysed in both laboratories therefore, data from BPh represents a full data set, while, UoM samples represents a partial data set. A decision to focus on 10, 21 and 29d cultured Caco-2 cells was taken due to subsequent functional assays being undertaken in these cells. All data presented is from a single analytical LC-MS/MS QTAP run.

As a QC for TM and PM fractions, Na/K-ATPase abundances are described for BPh generated data in 10, 21 and 29 day cultured Caco-2 cells (Figure 5-7). The abundances from individual experiments are provided in Appendix Table E-3. There was no effect of culture time on Na/K-ATPase abundance for TM and PM fractions. On average, Na/K-ATPase abundances were higher in the PM compared to the TM fraction, but this was not significant (p=>0.05, Paired t-test). If Na/K-ATPase is entirely expressed in the PM fraction (*i.e.,* Na/K-ATPase is not found in intracellular locations), these results indicate a negligible enrichment in the PM fraction and agree with the AP activity data described in Chapter 3.

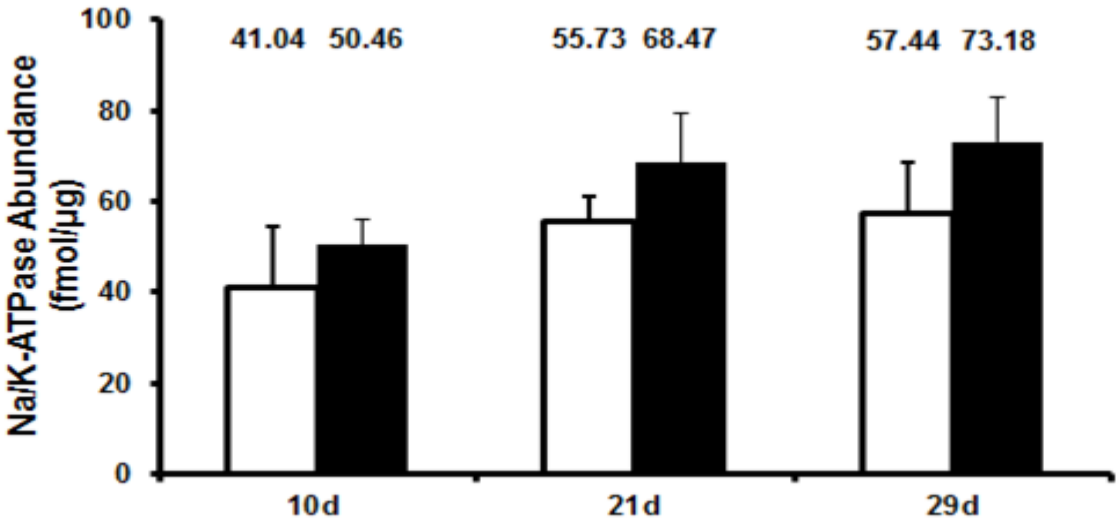

Figure 5-7. The absolute Na/K-ATPase protein abundance determined by BPh analysis in 10, 21 and 29d cultured Caco-2 cell monolayers. The text above the TM (white) and PM (black) represents the mean values of n=3 experiments, except for the 21 and 29d TM groups which are represented by n=6 experiments. Values are given as Mean±SD.

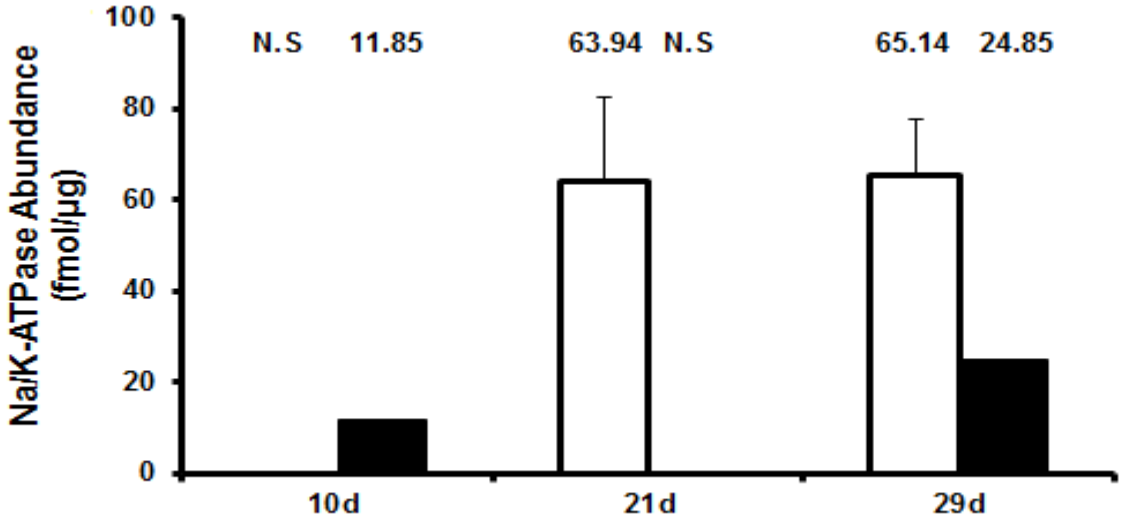

Figure 5-8. The absolute Na/K-ATPase protein abundance determined by analysis at The University of Manchester in 10, 21 and 29d cultured Caco-2 cells. The text above the TM (white) and PM (black) represents the mean values of n=3 experiments for the TM fractions and n=1 per group for the PM fractions. N.S denotes no samples available. Values are given as Mean±SD. Note, that the PM fractions in this data set are not derived from the same experiment as the TM fractions of the same age.

The 21 and 29 day cultured Caco-2 cell Na/K-ATPase abundances from the TM fraction using the QconCAT approach (n=3) (Figure 5-8) are consistent with those from BPh. The individual experimental values are provided in Appendix Table E4. However, there is a reduction in the PM abundances when comparing UoM to BPh; the solitary 10d sample showing 45.62 &.11.85 fmol/µg, and the 29d samples showing 63.66 & 24.85 fmol/µg for BPh and UoM, respectively. This could have resulted from degradation during sample storage, since sample preparation and analysis at the UoM was undertaken 8 months after BPh for the same PM samples. In contrast, the preparation and analysis of the TM samples between laboratories occurred in parallel (*i.e.,* ± 1 month).

The abundances of P-gp in 10, 21 and 29 day cultured Caco-2 cells are described after analysis by BPh (Figure 5-9). Data for individual experiments is provided in Appendix Table E5. The abundance of P-gp was greater than 10-fold lower than those found for Na/K-ATPase in the same samples. There was no significant effect of culture time on P-gp abundances in both membrane fractions and there were no abundance differences between the TM and PM fractions in matched samples.

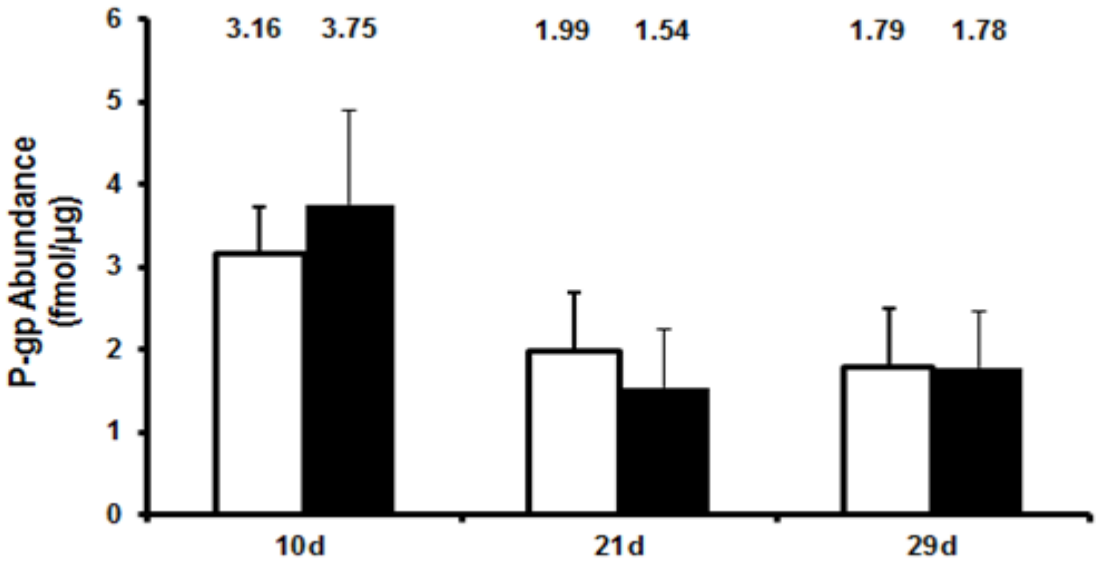

Figure 5-9. The absolute P-gp protein abundance determined by Bertin Pharma (BPh) analysis in 10, 21 and 29d cultured Caco-2 cell monolayers. The text above the TM (white) and PM (black) represents the mean values of n=3 experiments, except for the 21and 29d TM groups which are represented by n=6 experiments. Values are given as Mean±SD.

The abundances of P-gp in 10, 21 and 29 day cultured Caco-2 cells analysed by the QconCAT approach at the UoM, the BPh analysis and data generated by AstraZeneca in their own 10 and 29d Caco-2 monolayers (Miliotis et al., 2011b) are shown as a comparison in Figure 5-10. The individual experimental values are provided in Appendix Table E6 for the UoM data. The abundance of P-gp in 29d Caco-2 cells TM fractions was higher than for 21d cells (p=0.046, Unpaired t-test). However, there was also a tendency for higher abundance values in the 29d Caco-2 cells in the UoM analysis which was not observed in the same 29d samples analysed by BPh. At present the reasons for this discrepancy are not clear. Unlike the disparate abundances observed for the 10 and 29d Caco-2 PM samples for Na/K-ATPase measured between laboratories, similar values were quantified for P-gp, 2.87 &.2.97 fmol/µg, for the 10d sample, and 1.20 & 1.64 fmol/µg for the 29d sample, for BPh and UoM, respectively. If the duration of storage does result in sample degradation, it is not apparent for P-gp quantification in these samples.

The source and passage of Caco-2 cells and the feeding and seeding regimen for cultivation in flasks and filters is also similar to that of AstraZeneca in this study (Seithel et al., 2006), therefore it is reasonable to compare the data generated by AstraZeneca in 10 and 29d Caco-2 monolayers (Miliotis et al., 2011b), to the data from UoM and BPh. In addition, the standard peptide selected for P-gp abundance quantification is the same for this study and AstraZeneca's. Data shows that in 10d Caco-2 monolayers abundance values between laboratories is similar and the relationship becomes more divergent as Caco-2 monolayer cultivation time increases when comparing P-gp

abundances between BPh and the UoM/AstraZeneca studies. This could be due to the differences between laboratories in the standard peptide used for quantification.

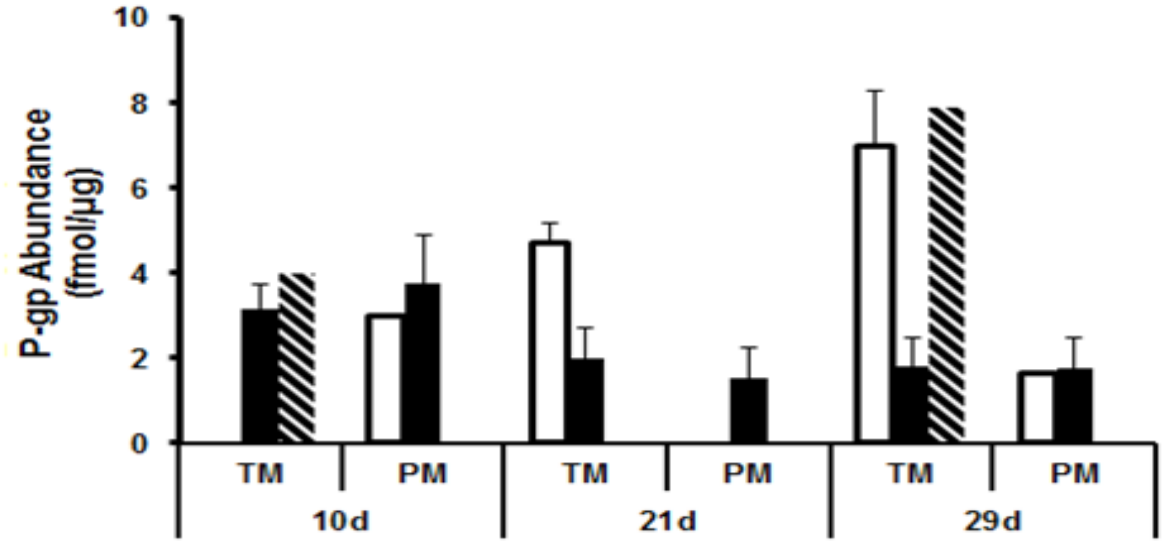

Figure 5-10. Comparison of P-gp protein abundances between Caco-2 cell monolayers across laboratories. Caco-2 cell monolayer P-gp abundances in TM and PM fractions were grown at the UoM are compared to those from AstraZeneca (Miliotis et al., 2011b). UoM Caco-2 cell P-gp abundances were analysed at BPh (Figure 5-9) and UoM. The mean abundances ± SD are provided for BPh (black), UoM (white) and AstraZeneca (Diagonal striped). UoM data for 10d PM and 29d PM and all AstraZeneca values are (n=1) experiment, otherwise values are from n=3-6 experiments. Note, that the PM fractions in this data set are not derived from the same experiment as the TM fractions of the same age.

The abundances of BCRP in 10, 21 and 29 day cultured Caco-2 cells are described after analysis by BPh (Figure 5-11). The abundances of the individual experiments are provided in Appendix Table E7. There is an effect of culture time on BCRP expression as abundances were higher in 10d compared to 21 and 29d Caco-2 cells (p=<0.001, 1-way ANOVA) in both TM and PM fractions. Analysis by BPh shows that BCRP abundances were at comparable levels to those for P-gp, with the exception of 29d TM fractions which exhibit a higher P-gp abundance (p=0.03, Paired t-test).

The abundances of BCRP in 10, 21 and 29 day cultured Caco-2 cell monolayers are described after analysis by the QconCAT approach (Figure 5-12). The abundances of the individual experiments are provided in Appendix Table E8. The abundance values for BCRP were no different between 21 and 29d TM fractions, suggesting a steady state expression was reached in cells grown for 21 days or longer. BCRP abundances were higher (p=0.048, Paired t-test) for BPh compared to UoM analysis for 21 but not 29 day cultured Caco-2 cell TM fractions. Of particular interest is the solitary sample quantified at the UoM in the 29d PM fraction which showed higher abundances than the matched counter-part analysed by BPh (see Appendix Table E8). However,

sample storage duration for this sample may have led to instability and caution is advised when interpreting this data.

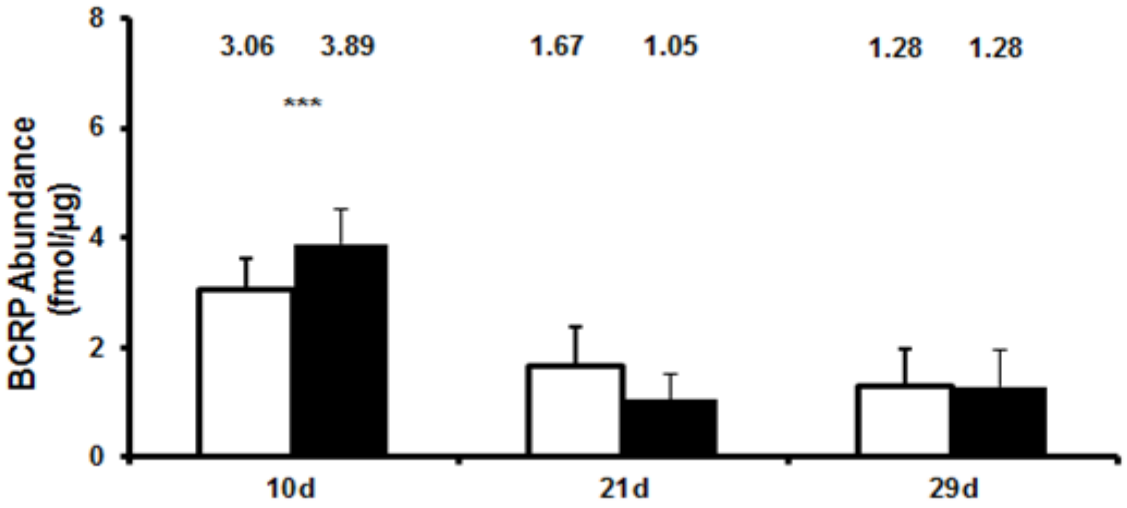

Figure 5-11. The absolute BCRP protein abundance determined by Bertin Pharma (BPh) analysis in 10, 21 and 29d cultured Caco-2 cells. The text above the TM (white) and PM (black) represents the mean values of n=3 experiments, except for the 21 and 29d TM groups which are represented by n=6 experiments. Values are given as Mean±SD and *** denotes p=<0.001.

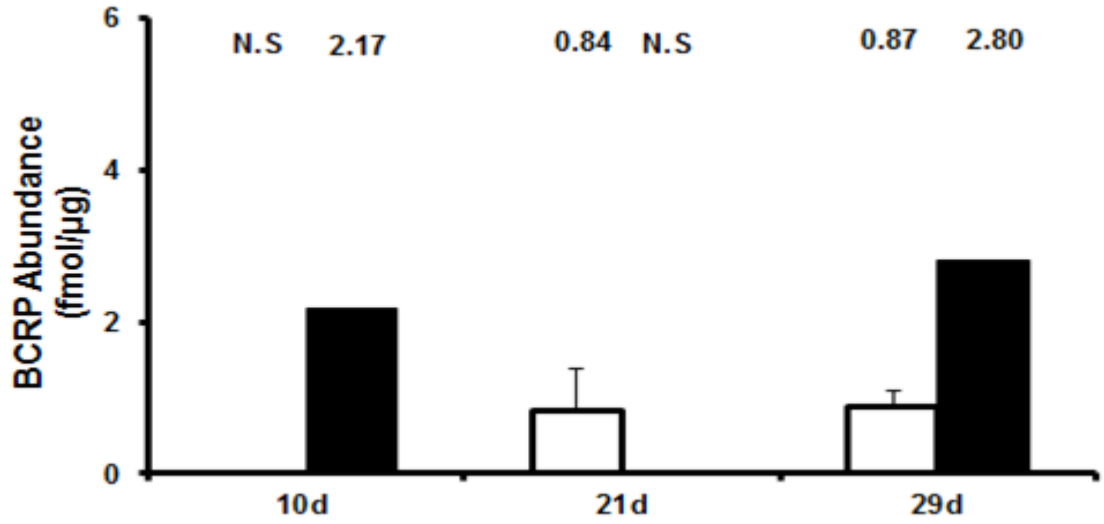

Figure 5-12. The absolute BCRP protein abundance determined at the University of Manchester in 10, 21 and 29d cultured Caco-2 cells. The text above the TM (white) and PM (black) represents the mean values of n=3 experiments for the TM fractions and n=1 per group for the PM fractions. N.S denotes no samples available. Values are given as Mean±SD. Note, that the PM fractions in this data set are not derived from the same experiment as the TM fractions of the same age.

Based on the protein abundance data from BPh, a disconnection in mRNA gene and protein expression for P-gp and BCRP as culture time increases is clear. To confirm these observations, TM fractions were generated from three additional preparations of 21 and 29d Caco-2 cells. These fractions were incorporated into the second sample batch sent to BPh for analysis and allow the consistency of Caco-2 cell long term culture to be assessed. This is because, the experiments in

which the TM fractions were harvested for analysis in batches 1 and 2 by BPh, were undertaken at least 7 months apart. The data from Batch 2 are embedded within the previously described results. However, in isolation there were no differences in P-gp or BCRP abundances between batches 1 and 2, demonstrating a stable protein expression over long-term cultivation (*i.e.,* months) from a single operator (Appendix Table E9) for individual data and comparisons between batches.

The abundances of OATP2B1, OST-α, OST-β and MRP2 in 10, 21 and 29 day cultured Caco-2 cells are described after analysis by the QconCAT approach (Figure 5-13 & Figure 5-14). The abundances of the individual experiments are provided in Appendix Table E10. The protein abundance values provided in the analysis (Figure 5-14) are weighted means according to Equation 5-1. This was necessary as some samples exhibited abundances below the lower limit of quantification. The rank order of protein abundances in 21d Caco-2 were P-gp>BCRP>OST-β>OST-α>OATP2B1 and MRP2, while for 29d Caco-2 cells, the rank order only differed with OST-α and OATP2B1 switching positions. When comparing the rank order for all transporters in 29d Caco-2 cells based on mRNA, there are notable disparities for MDR1/P-gp and OATP2B1 (Figure 5-14). However, for MDR1/P-gp which was ranked 3 of 6 for mRNA gene expression there was a 2.4-fold rise in mRNA expression and 3.1-fold rise in protein abundance from 10 to 29d, therefore is in reasonable agreement. Furthermore, based on mRNA expression, OATP2B1 was clearly the highest expressed transporter being studied, yet, when protein abundance was measured its rank dropped to 4 of 6.

There are clearly some disparities with translating mRNA expression data to protein abundances and differences between laboratories, particularly for P-gp abundances in Caco-2 cells. Nevertheless, the relationship between the mRNA and protein expression and function require establishing.

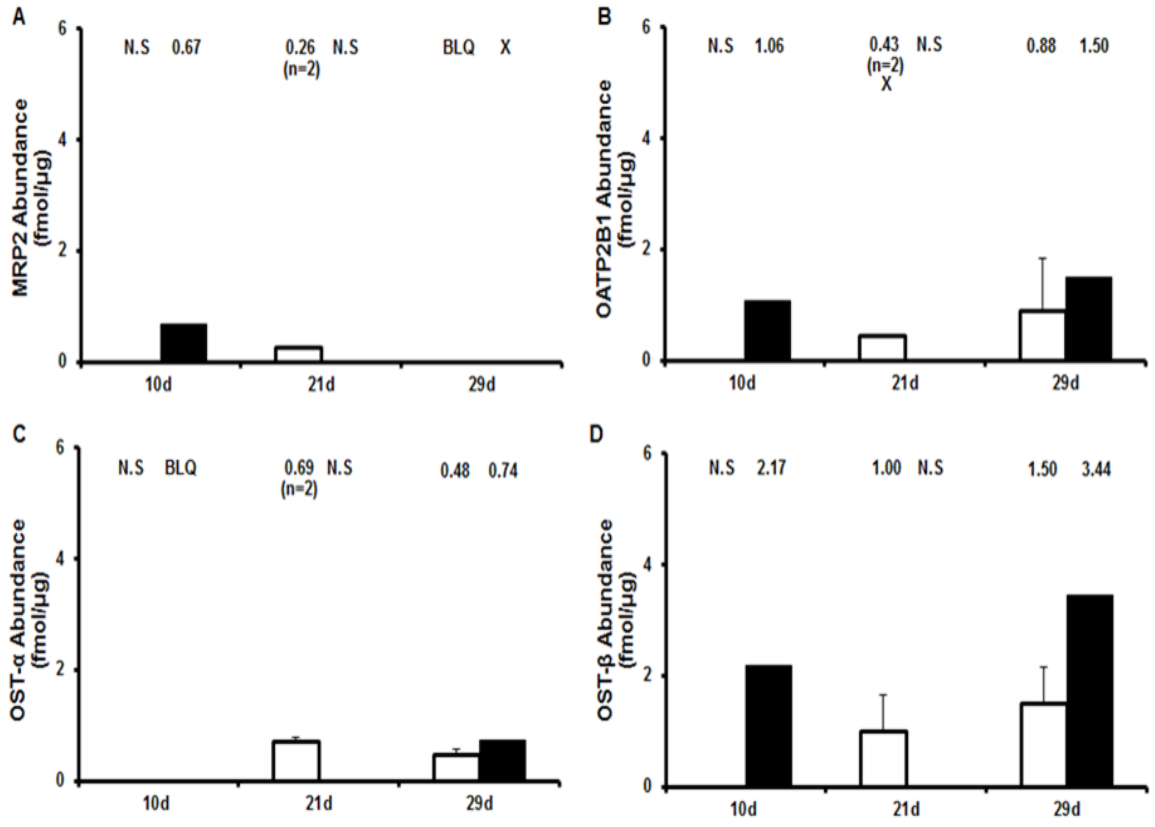

Figure 5-13. The absolute protein abundance of MRP2 (A), OATP2B1 (B), OST-α (C) & OST-β (D) determined at the University of Manchester in 10, 21 and 29d cultured Caco-2 cells. The text above the TM (white) and PM (black) represents the mean values of n=3 experiments for TM fractions and n=1 per group for PM fractions, unless stated. N.S denotes no samples available, X denotes an issue with the co-elution profile & BLQ is below the limit of quantification (<0.2 fmol/µg). Values are given as Mean±SD. Note, that the PM fractions in this data set are not derived from the same experiment as the TM fractions of the same age.

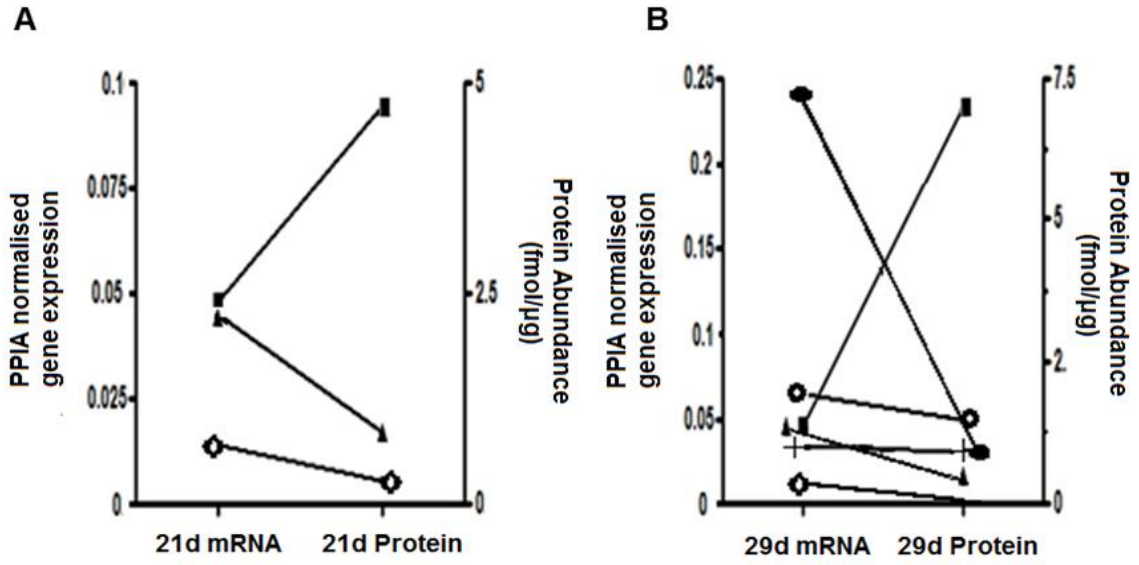

Figure 5-14. The relative levels of transporter mRNA gene expression and protein abundance in 21 and 29 day Caco-2 cells. A represents 21 day cells for MDR1/P-gp, MRP2 & BCRP and B represents all transporters being studied in 29 day cells. Symbols represent MDR1 (squares), MRP2 (diamonds), BCRP (triangles), OATP2B1 (filled circles), OST-A (cross) and OST-B (open circles). Values are given as means. The MRP2 protein abundances in 29 day cells were all below the limit of quantitation; therefore the values were set to zero.

5.3.4 Assessing BCRP Abundance-Transport Relationships in Caco-2 Cells

Having determined that BCRP expression was different in 10 and 29d Caco-2 cells after BPh analysis, experiments to test if there were relationships between BCRP expression and its probe compound E-3-S were performed. Initially, the transport of E-3-S in 10 and 29d Caco-2 cell monolayers was run with a pH gradient (apical pH 6.5, basolateral pH 7.4) to reflect the acid microclimate adjacent to the enterocytes (Lucas et al., 1978) and luminal bulk pH of the proximal small intestine (Fallingborg et al., 1989). Additionally, OATP2B1 is postulated to contain a low affinity pH-sensitive binding site, (Shirasaka et al., 2012), suggesting that pH might directly influence active apical substrate uptake via OATP2B1. Therefore, the increased hydrogen ion concentration when using pH gradient conditions may activate the low affinity binding site to facilitate OATP2B1-dependent apical uptake of E-3-S.

Preliminary experiments identified that E-3-S recovery was not consistent (in 2 of 4 experiments) displaying >20% loss at the end of the experiment due to non-specific binding, therefore low levels of BSA (0.05% (w/v)) was added to the assay buffer on both sides of the monolayer to improve recovery. Only 3 filters from >25 experiments showed a loss >20% at the end of the experiment.

5.3.4.1 Determining E-3-S Binding to BSA

The binding of [^{3}H]-E-3-S (0.01 μM) to BSA (0.05% (w/v)) in pH 6.5 and 7.4 transport buffers was assessed after correction for adsorption (12% in pH 6.5 buffer and 10% in pH 7.4 without BSA) to plastic and filter constituents of the Centrifree devices (Table 5-3). A concentration-dependent E-3-S binding to BSA was observed, with a greater binding displayed in the higher concentration donor buffers (at both pH's p=<0.01, 1-way ANOVA). In addition, a pH-sensitive effect was also observed in the donor (p=<0.001, 1-way ANOVA) but not the receiver buffers. Permeability was subsequently calculated under 'sink' conditions (<10% drug in the receiver compartment) based on the unbound concentrations in donor and receiver compartments under the assumption that only the unbound compound can permeate the membrane (Neuhoff et al., 2006).

Table 5-3. Determining the binding of [3H]-E-3-S to BSA in transport buffer.

	Unbound fraction (fu)			
	pH6.5 [donor]	pH6.5 [receiver]	pH7.4 [donor]	pH7.4 [receiver]
[^{3}H]-E-3-S (0.01 μM)	0.54 (± 0.05)	0.59 (± 0.03)	0.44 (± 0.03)	0.56 (± 0.03)

The receiver fu was determined by reserving receiver transport buffer at the end of transport assays. Donor fu was determined in freshly made transport buffer as per transport assays. N=2 experiments, in triplicate filtration devices. Donor [E-3-S] was >150-fold higher than in the receiver samples.

5.3.4.2 E-3-S Transport in 10 and 29d Caco-2 Monolayers

The bi-directional transport of E-3-S (apical: pH 6.5-basal: pH 7.4) in 10 and 29d cultured Caco-2 cell monolayers with the addition of the potent BCRP inhibitor Ko143 is shown in Figure 5-15. In control assays there was a net secretory E-3-S transport (B-to-A). The addition of the BCRP inhibitor Ko143, resulted in a reduced B-to-A transport (p=<0.001, unpaired t-test) in 10 and 29d monolayers, indicating the likely involvement of BCRP in E-3-S efflux. Interestingly, in 10d monolayers, Ko143 did not completely abolish E-3-S secretory transport, yet, in 29d monolayers a small net absorptive transport was observed, which is consistent with an apical uptake mechanism in operation, *i.e.,* OATP2B1. Under control conditions there was no effect of culture time on A-to-B (p=0.9, unpaired t-test) or B-to-A transport (p=0.06, unpaired t-test). An increase in A-to-B transport (p=0.003, unpaired t-test) in 10d, but not in 29d monolayers (p=0.32, unpaired t-test) was observed upon Ko143 incubation.

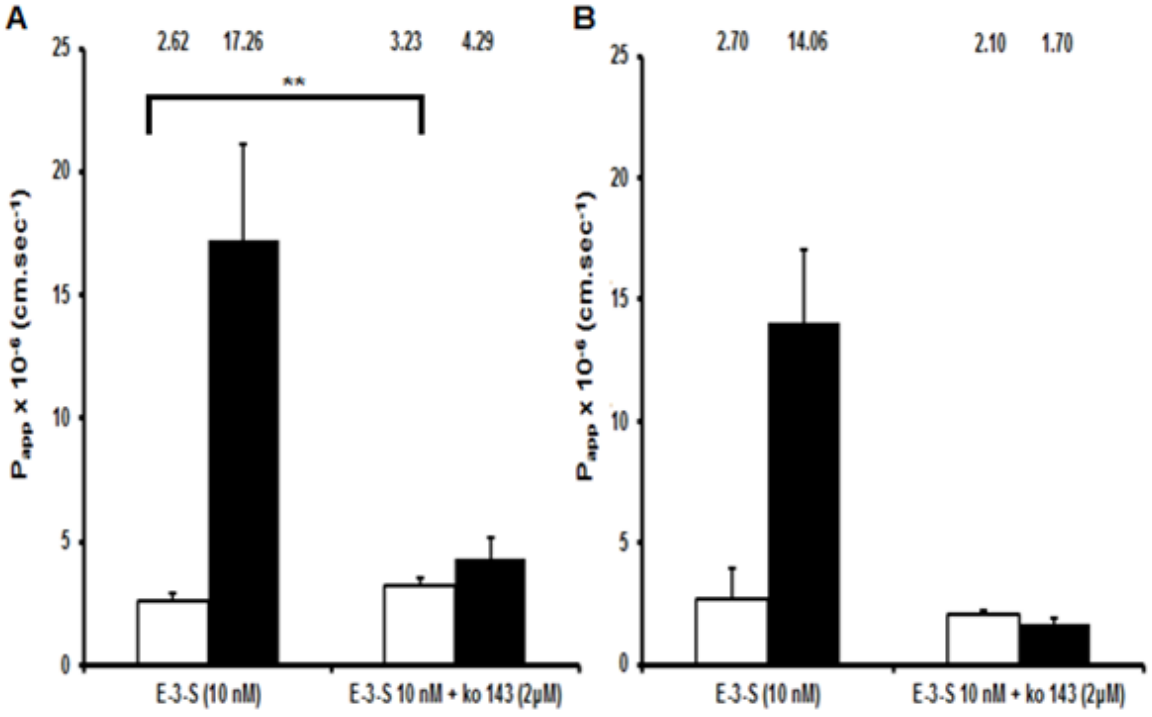

Figure 5-15. Transport of E-3-S (0.01 μM) in A-to-B (white) and B-to-A (black) transport directions across 10d (A) and 29d (B) cultured Caco-2 cell monolayers in the presence and absence of Ko143 (2 μM) at pH 6.5/7.4. The text above the bars is the mean Papp under each condition. The values are mean±SD of a minimum of n=6 filters of N=2 experiments. ** p=<0.01.

To investigate if the residual absorptive Papp in 29d Caco-2 cell monolayers after Ko143 incubation was due to OATP2B1 activity, the OATP2B1 inhibitor montelukast (100 μM) (Shirasaka et al., 2012) was added to both sides of the monolayer with and without Ko143. As shown in Figure 5-16A, absorptive Papp was reduced (p=0.001, unpaired t-test) by montelukast. However, a striking reduction in secretory permeability (10.85 x 10^{-6} cm sec^{-1} in control conditions and 0.59 x

10^{-6} cm sec^{-1} with montelukast incubation) was observed which was not anticipated. In addition, co-incubation of Ko143 and montelukast further reduced the absorptive (p=0.005, unpaired t-test) but not the secretory transport (Figure 5-16B). The content of E-3-S in monolayers suggests montelukast may have an impact on basal membrane uptake processes (Figure 5-17). The low E-3-S monolayer content after B-to-A transport observed with montelukast suggests it may act to restrict E-3-S access to the monolayer via the basal membrane. Overall, montelukast does not appear to exhibit sufficient selectivity to OATP2B1 to enable its contribution to absorptive transport to be defined.

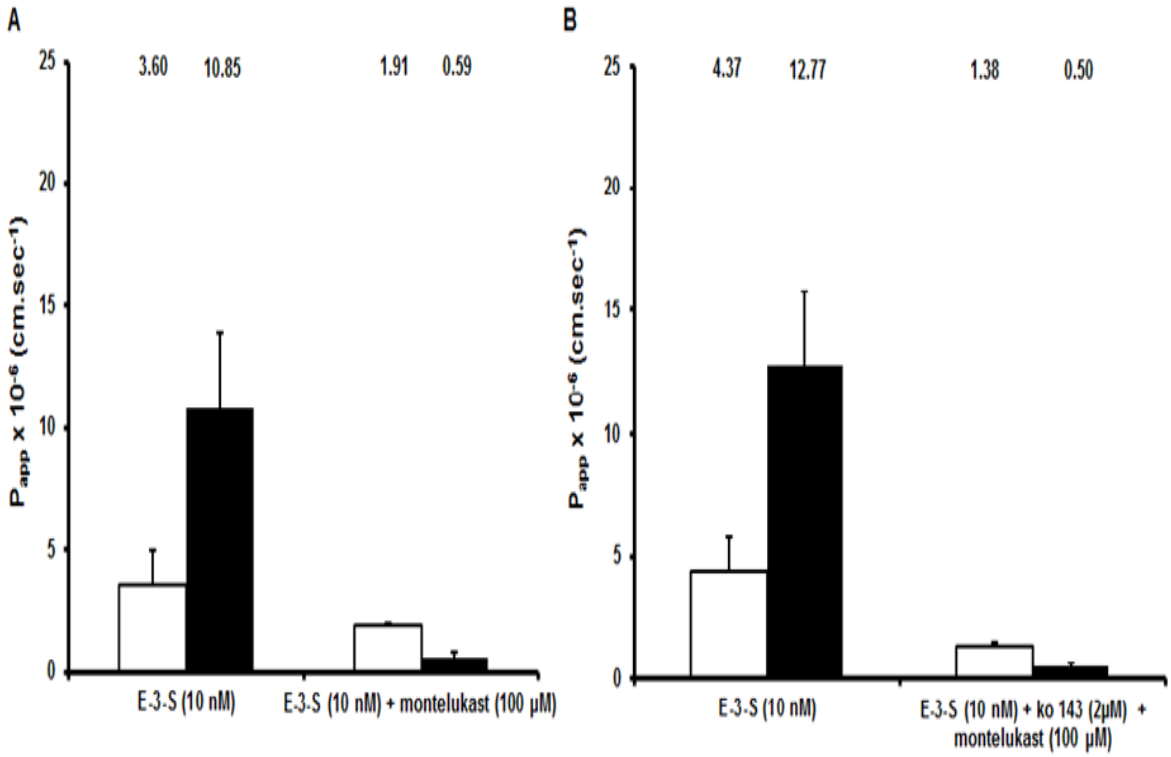

Figure 5-16. Transport of E-3-S (0.01 µM) in A-to-B (white) and B-to-A (black) transport directions across 29d cultured Caco-2 cell monolayers in the presence and absence of montelukast (100 µM) (A) and in the presence and absence of montelukast (100 µM) and Ko143 (2 µM) co-incubated at pH 6.5/7.4 (B). The text above the bars is the mean Papp under each condition. The values are Mean±SD of n=3 filters.

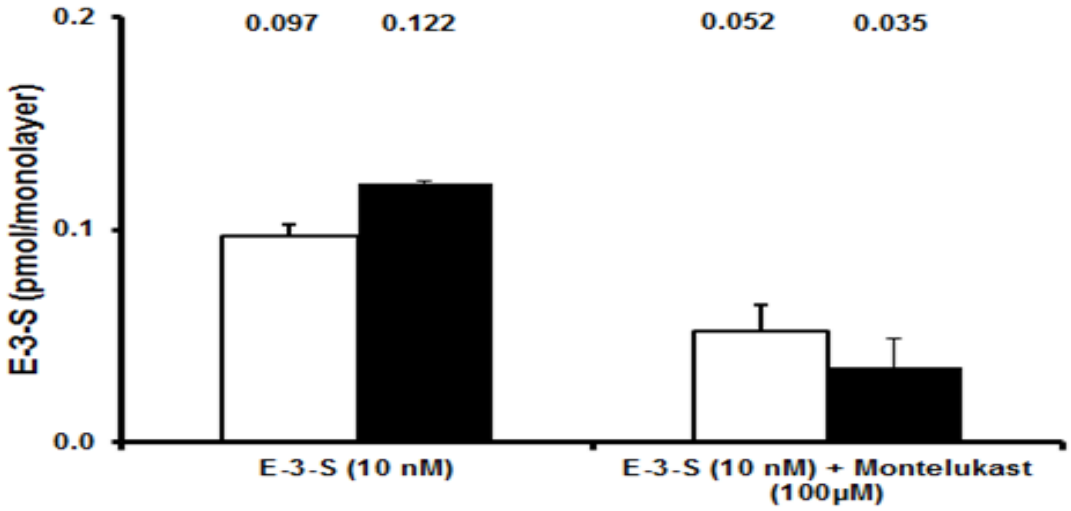

Figure 5-17. E-3-S monolayer content in the presence and absence of montelukast at pH 6.5/7.4. The A-to-B (white) and B-to-A transport (black) directions. The text above the bars is the mean Papp under each condition. The values are mean±SD of n=3 filters.

An imbalance in compound ionisation between compartments of a Transwell system is postulated to affect the passive and active processes acting on a compound, leading to a pH-dependent or 'false' asymmetry (Neuhoff et al., 2003). Therefore, the effect of pH on ionisation requires consideration within monolayer transport assays. However, this is unlikely to affect E-3-S permeability, as E-3-S is a strong acid (pKa 2.2) where the ionised fraction is calculated to be > 99.99% at pH 6.5 and 7.4. However, BCRP activity has been shown to be influenced by pH in transfected vesicle and monolayer systems (Breedveld et al., 2007). To assess the impact of the pH gradient and alteration of pH on E-3-S transport, assays were run with transport buffers at either pH 7.4, or pH 6.5, on both sides of the monolayer.

The effect of pH on monolayer integrity was assessed for 10 and 29d cultured monolayers (Table 5-4). At pH 6.5/6.5, an increased LY Papp (p=<0.05, 1-way ANOVA) was observed compared to pH 6.5/7.4 and pH 7.4/7.4 assays at 10 days. At 29 days, pH 6.5/7.4 monolayers showed lower LY Papp's than the other conditions. The anionic dye LY has a pKa is <0.7 (Stewart, 1978), therefore at the transport assay pH's it is expected that it is 100% ionised. It is therefore anticipated that LY ionisation is not affected by the pH used in these assays. However, all monolayers were within LY cut-off limits and there was no correlation (R^2 = 0.24) of E-3-S bi-directional transport with LY Papp's at 10 or 29d.

Table 5-4. The effect of pH on monolayer integrity after lucifer yellow permeability assessment.

	LY Apparent Permeability (x 10^{-6} cm sec^{-1})	
Assay Condition	10d	29d
pH 6.5/7.4	0.19 (± 0.12, n = 27)**	0.22 (± 0.19, n = 60)
pH 7.4/7.4	0.25 (± 0.24, n = 42)*	0.32 (± 0.19, n = 40)*
pH 6.5/6.5	0.41 (± 0.33, n=18)	0.35 (± 0.23, n = 42)**

* p=<0.05; ** p=<0.01. 10d cells – pH 6.5/6.5 higher LY Papp, 29d cells - pH 6.5/7.4 lower Papp

The bi-directional transport of E-3-S (apical: pH 7.4-basal: pH 7.4) in 10 and 29d cultured Caco-2 cell monolayers with the addition of Ko143 is shown in Figure 5-18. In 29d cells, an increased absorptive and a reduced secretory transport (p=<0.01, unpaired t-test) was observed for 29d compared to 10d monolayers. Similar to the pH gradient assay (Figure 5-15), Ko143 did not completely abolish E-3-S secretory transport in 10d monolayers, yet, in 29d monolayers a net absorptive flux was observed.

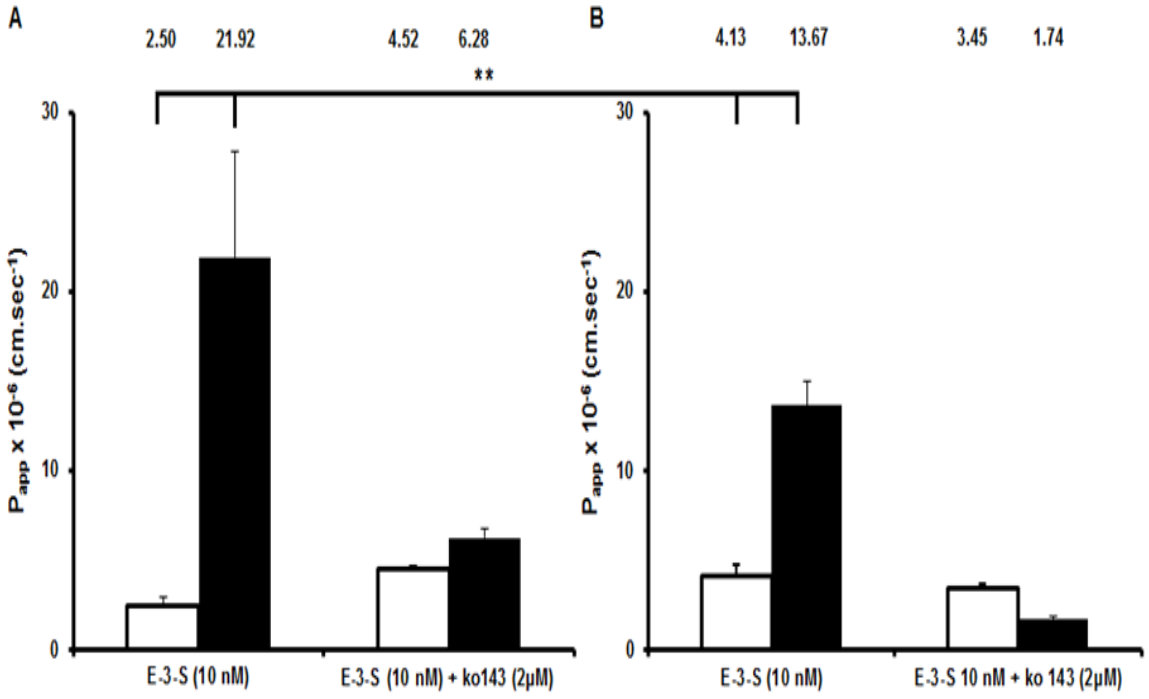

Figure 5-18. Transport of E-3-S (0.01 µM) in A-to-B (white) and B-to-A (black) transport directions across 10d (A) and 29d (B) cultured Caco-2 cell monolayers in the presence and absence of Ko143 (2 µM) at pH 7.4/7.4. The text above the bars is the mean Papp under each condition. The values are mean±SD of a minimum n=6 filters of N=2 experiments. **p = <0.01.

The bi-directional transport of E-3-S (apical: pH 6.5-basal: pH 6.5) in 10 and 29d cultured Caco-2 cell monolayers with the addition of Ko143 in 29d monolayers is shown in Figure 5-19. A significantly lower secretory transport (p=<0.05, unpaired t-test) was observed in 29d compared to

10d monolayers under control conditions. Consistent with the pH 6.5/7.4 and pH 7.4/7.4 assay, a net absorptive transport was found after Ko143 incubation in 29d monolayers. Overall, a consistently lower secretory transport was observed for E-3-S transport (without inhibitors) in 29d monolayers across different pH conditions. This was most pronounced under pH 7.4/7.4 conditions. Given that the potent BCRP inhibitor Ko143 consistently elicited a significant reduction in E-3-S secretory transport in all pH conditions, these data suggest that the likely mechanism responsible for the lower E-3-S transport is lower BCRP protein content in 29d vs 10d monolayers. There are no differences across pH conditions for absorptive or secretory E-3-S transport in 10d monolayers ($p=<0.05$). However, in 29d cells, secretory transport at pH 6.5 is higher ($p=<0.05$, 1-way ANOVA) than other conditions, consistent with the notion of lower pH's resulting in higher BCRP activity. In these assays consideration for alterations in intracellular pH were not accounted for, which may also impact on transporter functionality.

The pH 7.4/7.4 assay permits the assessment of E-3-S transport to define ER without any bias due to pH gradients. At pH 6.5/6.5 a pH gradient is still in operation as Caco-2 intracellular pH is 7.4-7.6 (Thwaites et al., 1993; Neuhoff et al., 2005). Therefore, pH 7.4/7.4 is the only system being studied that permits assessment without a pH gradient. The ER between 10 and 29d monolayers was assessed at pH 7.4/7.4 (Table 5-5). This shows that there was a significantly higher ER in 10d (ER = 9.0, $p=<0.01$, unpaired t-test) than 29d monolayers (ER = 3.3). No ER differences were found for 10 and 29d monolayers in other conditions. The relationship between BCRP abundance in the TM fraction and E-3-S ER (Table 5-6), shows a similar reduction in E-3-S ER and BCRP abundance in 29 compared to 10d Caco-2 cells monolayers. However, the relationship between mRNA expression and E-3-S ER was not similar for 29 and 10d Caco-2 cells, suggesting that BCRP protein abundances are a better indicator of BCRP-mediated E-3-S ER than mRNA expression.

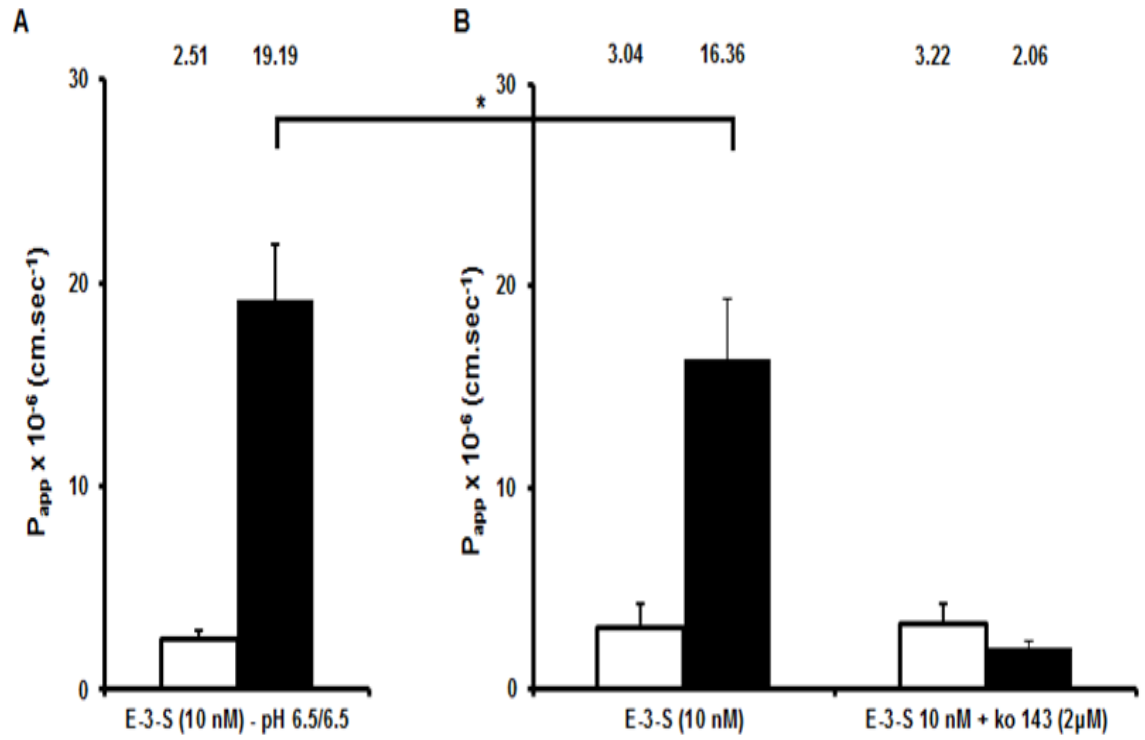

Figure 5-19. Transport of E-3-S (0.01 μM) in A-to-B (white) and B-to-A (black) transport directions across 10d (A) and 29d (B) cultured Caco-2 cell monolayers. 29d monolayers were also incubated in the presence and absence of Ko143 (2 μM) at pH 6.5/6.5. The text above the bars is the mean Papp under each condition. The values are Mean±SD of a minimum n=7 filters of N=3 experiments. *p = <0.05.

Data describing E-3-S monolayer content across conditions can be viewed in Appendix 6.

Table 5-5. Transport of E-3-S and secretory efflux ratio in 10 and 29d Caco-2 cell monolayers at pH 7.4/7.4 under control conditions (without inhibitors).

	10d Caco-2 Monolayers			29d Caco-2 Monolayers		
	Apparent Permeability (Papp)		Efflux Ratio†	Apparent Permeability (Papp)		Efflux Ratio
Condition	A-to-B ($\times 10^{-6}$ cm sec^{-1})	B-to-A ($\times 10^{-6}$ cm sec^{-1})	B-to-A Papp/ A-to-B Papp	A-to-B ($\times 10^{-6}$ cm sec^{-1})	B-to-A ($\times 10^{-6}$ cm sec^{-1})	B-to-A Papp/ A-to-B Papp
pH apical 7.4/ cell 7.4/basal 7.4	2.5 (± 0.5)	21.92 (± 5.89)	**8.97 (± 2.51)****	4.13 (± 0.66)	13.67 (± 1.32)	**3.32 (± 0.67)****
pH apical 6.5/ cell 7.4/basal 7.4	2.62 (± 0.25)	17.26 (± 3.88)	6.56 (± 1.22)	2.7 (± 1.39)	14.06 (± 3.01)	7.33 (± .4.67)
pH apical 6.5/ cell 7.4/basal 6.5	2.51 (± 0.43)	19.19 (± 2.7)	8.02 (± 0.76)	3.04 (± 1.19)	16.36 (± 2.97)	5.9 (± 3.18)

Data represent a mean ± standard deviation of a minimum of 6 monolayers for each condition for at least 2 experiments. ** indicates significant difference $p = < 0.01$ (unpaired t-test) in 10 and 29d monolayers. †The efflux ratio is calculated as the ratio of means for paired monolayers, rather than the mean of the ratios of B-to-A and A-to-B. The cellular pH is assumed in this case not to be affected by the extracellular pH.

Table 5-6. The relationship between BCRP mRNA, total membrane protein abundance and E-3-S efflux ratio in 10 and 29d Caco-2 cell monolayers.

Culturing Time	[^{3}H] E-3-S Efflux Ratio (pH7.4/7.4)	BCRP mRNA Expression (Relative to PPIA)	BCRP Protein Abundance (fmol/µg)
10 days	8.97 (± 2.51)	0.022 (± 0.004)	3.06 (± 0.22)
29 days	3.32 (± 0.67)	0.033 (± 0.013)	1.28 (± 0.33)
Fold Difference (10 days/29 days)	2.7	0.67	2.39

5.4 Discussion

To date, for filter-grown Caco-2 monolayers, only a single study has characterised the relationship between transporter gene (mRNA) and protein (QTAP-LC-MS/MS) expression and function (digoxin ER), (Miliotis et al., 2011b). In this study, the influence of culture period on Caco-2 cell monolayer transporter mRNA expression and protein abundances were measured in Caco-2 cell monolayers cultured over various time periods. The protein abundances for Na/K-ATPase, P-gp and BCRP in the TM and PM fractions of Caco-2 cells were also quantified in both the TM and PM fractions, and a comparison of transporter abundances in matched Caco-2 fractions between two laboratories was also performed for a limited number of samples. Finally, the relationship between the BCRP probe E-3-S and transporter expression was investigated in bi-directional permeability assays with 10 and 29d Caco-2 monolayers.

This study shows there was an effect of Caco-2 cultivation time on mRNA levels for all transporters investigated. For protein abundances, there was a disparity in the levels of P-gp measured in Caco-2 cells between two analytical laboratories. The protein levels of P-gp and BCRP did not correspond to the changes observed for mRNA expression with increasing cultivation times. However, the rank orders of mRNA and protein expression were in reasonable agreement, except for OATP2B1. The activity of the BCRP probe E-3-S determined by the ER in bi-directional transport assays did correlate to the lower levels of BCRP protein abundance observed in 29 compared to 10d Caco-2 cells.

Transporter proteins postulated to be relevant for E-3-S transport (Rolsted et al., 2011) were investigated for mRNA gene and protein expression in 10 to 29 day Caco-2 cell cultures. The endogenous control housekeeper protein used to normalise transporter gene expression requires stability between samples and analytical runs (Seithel et al., 2006), with expression levels in reasonable proximity to the target genes (Hilgendorf et al., 2007). Our studies agreed with previous work in Caco-2 cells showing that PPIA exhibited the greatest stability and cycle thresholds closer to the target genes than another housekeeper gene GAPDH. Cultivation time did not affect PPIA expression levels. However, the PPIA cycle thresholds in this study were approximately 4-fold higher (2 cycle thresholds lower) than the study of Seithel et al., 2006, which may lead to differences in relative expression levels observed for target genes between studies. Both PCR assays rely on Taq DNA polymerase technology, but use different probe and primer sequences which may result in the observed differences. For all the transporters studied, the highest

transporter expression was observed in cells cultivated for 21 days. The study by Seithel et al., 2006, found that MDR1, MRP2 and BCRP expression increased in a step-wise manner from 1-5 weeks cultivation and also confirmed that the increases in ABC transporter expression over cultivation time were also most prominent for MDR1 (Seithel et al., 2006). A general agreement was shown for the rank order of transporter gene expression between studies, with the exception of MRP2, which was the lowest expressed transport gene in this study. There is a consensus across laboratories that MRP2 is the highest expressed ABC transporter in Caco-2 monolayers (Hayeshi et al., 2008; Ahlin et al., 2009). Given the similarity in the source of the Caco-2 cells, their passage number and culturing conditions, including the use of heat inactivated serum from the same supplier (Seithel et al., 2006), it is postulated that these study elements will not contribute to the observed difference. At present, the reason for the disparity in MRP2 gene expression between studies is not clear.

To date, there is surprisingly little data in the literature quantifying the abundances of transporter proteins in the IVIVE-relevant Caco-2 cell line. Nevertheless, the protein abundance of P-gp has been reported in the TM, but not a PM fraction of filter-grown Caco-2 cell monolayers and correlated with mRNA gene expression (Miliotis et al., 2011b). In the present study, 7 transporter proteins were quanitfied in Caco-2 cell monolayers, with Na/K-ATPase, P-gp and BCRP quantified in TM and PM fractions for a selection of samples in separate laboratories. The two laboratories used different digestion conditions, peptide standards and analytical systems. No enrichment was demonstrated for Na/K-ATPase, P-gp and BCRP in the PM compared to the TM fractions for all transporters, irrespective of Caco-2 cell cultivation time. Immunohistochemical analysis has confirmed that P-gp is predominantly localised on the PM in Caco-2 cells, with lower staining intensities at intracellular sites (Ahlin et al., 2009). Nevertheless, if transporter proteins are predominantly localised at the PM, these findings suggest that there is a failure to enrich the PM in the sucrose cushion step of the membrane enrichment procedure, which accords with the AP activity data in Chapter 3. Yet, the protein content of the PM fraction diminishes 5-fold with regard to the TM fraction without the expected enrichment in protein abundance. This is likely to indicate a loss of proteins when attempting to obtain a PM fraction. As alluded to previously, there is little data to compare protein abundances in the TM and PM fractions, with the exception of Na/K-ATPase in human liver, which showed a higher abundance in the TM compared to the PM fraction (Ohtsuki et al., 2012). BPh suggested that a 3-4-fold enrichment in protein abundance should be observed for Caco-2 cells when comparing TM and PM fractions and that increasing the time for the sucrose

cushion centrifugation stage may enhance PM enrichment. The increased centrifugation time should be investigated in future studies to determine whether this delivers the additional 3-4-fold enrichment in the PM fraction.

The expression of Na/K-ATPase and P-gp was not influenced by Caco-2 cell cultivation time when analysed by BPh, although there was a tendency for a lower P-gp abundance at 21 and 29d compared to 10d grown cells. This is in agreement with immunoblot, confocal laser scanning microscopy and QTAP studies investigating the effects of cultivation time on transporter protein expression in Caco-2 cell monolayers (Hosoya et al., 1996; Anderle et al., 1998; Uchida et al., 2007). Interestingly, in Hosoya et al., 1996, the net secretory transport of verapamil increased from 1 to 4 weeks showing a disparity between protein expression and function. In Miliotis et al., 2011, a 2-fold higher P-gp abundance was observed at 29 *versus* 10 day Caco-2 cells with a concomitant increase in digoxin ER. The P-gp abundances using the QconCAT approach in this study use the same standard peptide as Miliotis et al., 2011 and show evidence of increasing P-gp abundances and similar absolute levels from 10 to 29 days, with Transwell culture conditions virtually identical to their study. These data suggest that peptide differences may have a significant impact on the quantification of transporter abundance (see Chapter 6). Activity-abundance correlations of P-gp in different laboratories using digoxin ER analysis in 10 and 29d cells would also be useful in determining which laboratory provides functional abundances that are most relevant to IVIVE. There was an effect of culture time on BCRP protein abundance when analysed by BPh showing BCRP expression at 10d being higher than later cultivation times. Uchida et al., 2007 described no effect of culture time on BCRP expression in Caco-2 cells, which may be due to differences in Caco-2 cultivation. Uchida et al., 2007 also reported absolute levels of BCRP exceeding 1 fmol/µg, which is consistent with data from BPh and slightly higher than UoM analysis in this study. For the other transporters quantified at the UoM, MRP2 abundances were ranked as the lowest and could not be quantified in 29d Caco-2 cells, whereas in accordance with human jejunum (Section 4.3.2.3), OST-β levels were higher than OST-α. OATP2B1 levels were similar to those found in Uchida et al., 2007. It was also demonstrated that there was a consistency in Na/K-ATPase, P-gp and BCRP abundances in 21 and 29d Caco-2 cell monolayers cultivated up to 12 months apart after blinded analysis by BPh. Routine checking of immortalised cell line phenotypic traits, such transporter expression levels are important procedures that should be employed for successful long-term IVIVE strategies within any laboratory.

The current study suggests that sample storage conditions may impact on abundance quantification. The single 10d PM fraction presented in the UoM abundance analysis was cryo-stored for 10 months prior to protein digestion and the subsequent digested peptide mix was cryo-stored for further 6 months prior to performing the final analysis at the UoM. The Na/K-ATPase abundances in this sample were 4-fold lower than obtained by BPh whose peptide storage conditions were less than 1 month. After personal communication with BPh it was suggested that membrane fractions stored for an extended time (e.g. 1 year or more) are susceptible to deterioration, with a potential for similar effects from long term storage of peptide digests. For the matched TM samples analysed by both laboratories there was only 1 month lag between sample preparation and analysis and good consistencies in Na/K-ATPase abundance determination was achieved between laboratories. This serves to highlight that sample storage should be considered as a potential factor influencing the quantification of abundances inherent to the sample. Further studies investigating sample stability over shorter (*i.e.,* days) and longer periods (*i.e.,* months), including freeze-thaw effects, are needed to define the effects of storage on abundance quantification. This would form part of the quality assurance procedures (Groer et al., 2013), to be implemented in future studies in our, and other laboratories.

Literature data indicates determining a consistent relationship between mRNA and protein transporter data is difficult (Siegmund et al., 2002; Taipalensuu et al., 2004; Berggren et al., 2007; Urquhart et al., 2008; Ahlin et al., 2009; Shirasaka et al., 2009; Prasad et al., 2013). Furthermore, it has been found that for approximately 60% of proteins mRNA data cannot explain the abundance of the corresponding protein (Vogel and Marcotte, 2012). This is borne out by the findings of this study, in which a different relationship for mRNA and protein levels were found between laboratories. The BPh analysis tends to suggest that there is no correlation between gene expression and protein abundance for P-gp and BCRP when considering Caco-2 cell cultivation time, as it is expected from the mRNA data, showing higher abundances at 29 compared to 10 days, that P-gp and BCRP protein expression would increase. For the UoM protein data, there was generally a good agreement between mRNA and protein abundance. The lowest ranking analysed protein abundance was shown for MRP2 which corresponds to the low levels of mRNA expression. The reduced ranking of OATP2B1 protein abundance relative to its high mRNA expression could be due to the peptide used in this analysis only being partially verified from a QC perspective, therefore this could be deemed as sub-optimal. There is also reasonable evidence in human liver tissues that OATP2B1 mRNA-protein correlations are at best weak, demonstrating R^2 values of

0.11-0.38 (Nies et al., 2013). The differences between laboratories require further investigation (Chapter 6). The challenges in relating mRNA to protein abundance are covered in a review (Vogel and Marcotte, 2012), which attributes the lack of mRNA-protein correlation observed due to the undervalued role of translation and neglecting the differences between mRNA and protein synthesis and degradation rates.

At present, there are no reports in the literature studying BCRP protein absolute abundance-function relationships in Caco-2 cells. To investigation this, the bi-directional transport of the BCRP probe E-3-S was investigated in 10 and 29d Caco-2 cell monolayers. pH has been shown to be important for BCRP activity (Breedveld et al., 2007) and OATP2B1 (Shirasaka et al., 2012), therefore assays were conducted with and without a pH gradient. Due to inconsistent recoveries of E-3-S at the end of the transport experiments, low levels of BSA were required to reduce non-specific binding. An assessment of E-3-S binding to BSA was therefore required to determine permeability based on the free fraction of E-3-S in the assay (Neuhoff et al., 2006). Approximately, 50% binding of E-3-S to BSA was observed which increased in a more alkaline pH. This is in agreement with data for the anion tenoxicam (pKa 5.3), which also displayed greater binding at a more alkaline pH. It was suggested that a conformational change in HSA, resulting from electrostatic forces was responsible for the enhanced binding (Bree et al., 1993). However, a more alkaline pH is expected to increase the negative charges on albumin, which should repel the binding of anionic molecules, which does not occur for both E-3-S and tenoxicam.

A meta-analysis of data on bi-directional E-3-S transport in Caco-2 cells found a mean absorptive and secretory Papp of 2.7 and 26.8 x 10^{-6} cm sec^{-1}, respectively (Xia et al., 2005; Wang et al., 2008; Ahlin et al., 2009; Kamiyama et al., 2009; Zhang et al., 2009; Grandvuinet and Steffansen, 2011; Rolsted et al., 2011; Varma et al., 2011; Mease et al., 2012; Segawa et al., 2013) which is consistent with the E-3-S, data presented in this study. There was little effect of pH on absorptive transport in either 10 or 29d Caco-2 cell monolayers in agreement with Grandvuinet & Steffansen 2011. Varma et al, 2011, did report pH-sensitive E-3-S transport in Caco-2 cells, but their studies were performed with a 50-fold higher E-3-S concentration than used in this study and by Grandvuinet & Steffansen 2011, suggesting they were studying both the lower affinity pH-sensitive and higher affinity pH insensitive binding sites (Shirasaka et al., 2012). Consistent with other studies using BCRP inhibitors, a small net absorptive transport after BCRP inhibition was observed (Xia et al., 2005; Wang et al., 2008; Kamiyama et al., 2009; Grandvuinet and Steffansen, 2011).

The impact of absorptive transport by OATP2B1 could not be definitively established using montelukast, an inhibitor of both OATP2B1 binding sites in transfected-oocytes (Shirasaka et al., 2012). Instead, montelukast appeared to inhibit E-3-S uptake into the Caco-2 cell monolayer, which may be due to inhibition of a basal uptake process, possibly mediated by OST-α/β. These observations suggest that this compound may not be suitable for inhibition studies in a heterogeneous expression system such as Caco-2 cells.

BCRP mediated E-3-S transport in the secretory direction was confirmed by the BCRP inhibitor Ko143. Furthermore, there was a pH sensitive secretory transport (pH 6.5/6.5) which could be attributed to a pH-sensitive BCRP activity and may arise from a short term lowering of intracellular pH from proton transport into the cell over the experimental duration (Thwaites et al., 1993; Breedveld et al., 2007). The short term lowering effect of enterocyte pH may be observed *in vivo*, upon the emptying of the acidic contents of the stomach into the duodenum. In line with the lower BCRP protein abundances measured in 29d Caco-2 cells, the secretory transport was consistently lower in the 29d monolayers. Due to the complex effects of pH on E-3-S binding to BSA and on transporter functionality, the simplest system in which to interpret abundance-function relationships is the pH 7.4/7.4 system. There was good agreement between protein abundance and E-3-S ER, but not for mRNA expression in 10 and 29d Caco-2 monolayers. Another study, Zhang et al., 2009, showed an increasing E-3-S ER over cultivation time (25d). It is difficult to compare the results of this study to that of Zhang et al., 2009, as E-3-S concentrations are 500-fold lower for this study (0.01 µM vs. 5 µM) and sub-saturating for BCRP (Km 1.2 µM, (Rolsted et al., 2011)), the sampling regime was different, the cells used were expression vector control Caco-2 BBe1 cells and no correlation to protein abundances were made. It is clear further work in other laboratories investigating abundance-function relationships is required.

Identifying transporter function is challenging in heterogeneous expression systems like Caco-2. E-3-S is postulated to be transported bi-directionally by proteins expressed at both poles of the cell. Therefore, a mixture of short course (1-5 min) and longer course (150 min) incubations over multiple concentrations will allow the estimation of intrinsic kinetic parameters by mechanistic kinetic models describing the Caco-2 Transwell system (Ahlin et al., 2009; Rolsted et al., 2011). CLint per pmol or K_{CAT} for the transporter protein can then be established when combining kinetic data with QTAP generated protein abundances to facilitate a mechanistic IVIVE approach (Harwood et al., 2013). Utilising, other BCRP transporter probes should also be undertaken to

reinforce these relationships for generating robust scaling factors. However, there are few compounds that specifically probe a transporters function selectively which was recently highlighted for another typical BCRP probe mitoxantrone, in LLC-PK1-MDR1 transfected cells, where a 5.8-fold secretory ER was demonstrated (Poirier et al., 2014).

5.5 Conclusion

This study investigated the relationship between gene and protein expression for several intestinal epithelial transporters using a QTAP approach in TM and PM fractions of Caco-2 cell monolayers. Furthermore, an assessment of the relationship between gene and QTAP generated protein expression, and BCRP activity using a bi-directional transport assay was described for the first time. The challenges in obtaining enriched PM fractions were shown when assessing 3 transporter proteins in both TM and PM fractions. Further methodological developments are required to obtain a more enriched fraction, with separation of brush border and basal membranes being the goal. For many of the proteins there was a reasonable agreement of protein and mRNA gene expression levels, however this may be dependent on the peptide standard used, which also warrants considerable further investigations. The activity also correlated with protein expression for BCRP measured by BPh, but not with mRNA data. However, the heterogeneity of transporter expression in Caco-2 cells and the issue of transporter probes interacting with multiple transporters complicate the assessment of abundance-function relationships. Therefore, obtaining ER's for input into IVIVE strategies is generally not performed. To understand the impact of transporters on drug disposition, generating intrinsic kinetic parameters permits the modelling of saturable transporter functionality by mechanistic IVIVE-PBPK. From the abundance data generated in the intestine and Caco-2 cell monolayers, the REF transporter scaling factor can be generated. Obtaining transporter kinetic parameters and REF's specific for each laboratory is needed. The generation of REF's and transporter kinetics from the UoM will be described in subsequent chapters.

Chapter 6 - A Cross Laboratory Comparison of Human Intestinal and Caco-2 Drug Transporter Protein Abundances

Declaration

Work presented in this chapter was performed by the candidate Matthew Harwood and by Bertin Pharma, Orleans, France.

6.1 Introduction

Numerous laboratories utilising a diverse range of techniques are quantifying the absolute abundance of drug transporter proteins by QTAP strategies in mammalian tissues and *in vitro* cell systems. Up to ten-fold differences in absolute abundances have been observed for specific transporter isoforms in non-matched samples between laboratories, for example, hepatic OATP1B1 (Prasad et al., 2014; Vildhede et al., 2014), summarised in a recent meta-analysis (Badee et al., 2015). Differences in the techniques applied to obtain endpoint absolute abundances include those required to:

- generate an enriched membrane fraction
- denature and digest the proteins
- select and generate the peptide standard(s)
- separate the peptides by chromatography and the mass analysis of the selected peptide fragments (LC-MS/MS)

Studies have investigated the effect of manipulating the methods associated with quantifying transporter protein absolute abundances. For example, the impact of the chaotropic agent used prior to protein digestion has been shown to have a considerable impact on the absolute quantification of OATP proteins (Balogh et al., 2013). Therefore, differences in the agent selected may be a source of variability between studies. The selection of the peptide standard may be important and has been investigated for P-gp, BCRP, OATP1B1, OATP1B3 and OATP2B1 (Kamiie et al., 2008; Prasad et al., 2014). In these studies, peptide selection was shown to have a limited impact on endpoint abundance quantification. Yet, in a recent study, standard peptide choice was considered to bias endpoint abundance quantification of hepatic OATP1B1 (Terasaki et al., 2014). The digestion strategy employed might also influence the capacity to quantify protein abundances and to generate peptides that are mis-cleaved. The potential shortcomings of the digestion strategy employed was recently demonstrated in a study comparing the choice of proteolytic enzymes and an in-solution compared to filter-aided protocol when undertaking global proteomic analyses (Chiva et al., 2014). Studies have also been undertaken to compare different proteomic approaches within a laboratory, such as those conducted at Tohoku University, Pfizer and The University of Washington (Kamiie et al., 2008; Qiu et al., 2013; Prasad and Unadkat, 2014). These studies found when comparing immunoblotting or SILAC/SILAM techniques that there was a reasonable agreement within the same samples to the AQUA method routinely employed. Establishing if

differences in abundances reported across laboratories are derived from inter-individual variability; the variability associated with assay-specific techniques and/or specific data analysis methods within each laboratory are crucial for generating robust PBPK models that accurately represent *in vivo* abundances. Therefore, a multi-centre study evaluating the consistency and comparability of the preparation steps and analytic outcome has been advocated (Harwood et al., 2014). At present, studies comparing the quantification of absolute transporter protein abundances between laboratories have not been reported.

The principal aim of this study was to compare the absolute transporter abundances for 3 proteins; Na/K-ATPase, P-gp and BCRP in the same Caco-2 cell and human intestinal membrane fractions, quantified by 2 independent laboratories, The University of Manchester (UoM) in the UK and Bertin Pharma (BPh) in France. Furthermore, additional intestinal samples (TM fractions, from eluted enterocytes) in which there was not sufficient protein material for analysis in both laboratories, were quantified by BPh and are also presented in this chapter. In addition, the only group who have performed QTAP transporter studies on human intestinal samples, crushed the tissue prior to immersing it in extraction buffer and performing a homogenisation to extract a 'native membrane' (Groer et al., 2013; Drozdzik et al., 2014). In order to reduce the risk of incorporating sub-epithelial components into the membrane extraction procedure, *i.e.,* to reduce contamination or a 'dilution effect' on abundances, the study presented in here, principally eluted enterocytes by chelation. However, it is not known if the method used to harvest the enterocytes prior to membrane extraction affects endpoint transporter protein abundances. Therefore, the effect of enterocyte harvesting method on transporter abundances was assessed by means of a pilot study using 3 distal jejunal samples that were either crushed by homogenisation, or the enterocytes were eluted by chelation.

6.2 Methods

Membrane fractions were prepared from Caco-2 cell monolayers and eluted enterocytes from human intestinal tissues as previously described (Section 2.2.2.2 and 2.2.2.4). For the pilot study assessing the effect of mucosal crushing compared to enterocyte elution by chelation, n=3 matched jejunal samples either; underwent elution by EDTA chelation (Section 2.2.2.4), or mucosal crushing by homogenisation in TSEM buffer (Section 2.2.2.5).The protein content of the membrane fractions was measured by BCA assay. Frozen membrane fractions (approx. 50 µg) were shipped overnight on dry ice to the laboratories of BPh. Samples were confirmed to have remained in a frozen state upon receipt at BPh. Membrane fractions stored at -80°C within Salford Royal Hospital Trust, were transferred (duration, ~45 min) to the Manchester Interdisciplinary Biosciences Centre, UoM, on ice, where the samples were immediately stored at -80°C. Samples underwent the proteolytic digestion (Section 2.2.7.1 and 2.2.7.2) and subsequent LC-MS/MS analysis routinely employed within each laboratory (Section 2.2.8). A summary of the key methods employed by each laboratory is supplied in Table 6-1. For this study the absolute protein abundance of Na/K-ATPase, P-gp and BCRP in 11 samples (Caco-2 cell monolayers (n=7), distal jejunum (n=3), and distal ileum (n= 1)) were compared. For some intestinal samples, there was insufficient membrane protein available for abundance quantification in both laboratories. For these samples, quantification was performed by BPh alone. MRP2 was also quantified in these samples by BPh.

Abundance data from each laboratory were compared by a Wilcoxon matched pair analysis to test for mean differences. To test for sample abundance correlations, a Spearman's Rank analysis was used. The non-parametric Wilcoxon test was chosen as the P-gp data was shown to be non-normally distributed after testing by the Kolomogorov-Smirnov test for normality. In statistical analyses an $\alpha = <0.05$ indicated a significant difference.

Table 6-1. An outline of the methods specific to each laboratory for the absolute quantification of Na/K-ATPase, P-gp and BCRP.

Table 6-1a. The University of Manchester.

Criteria	The University of Manchester
Peptide Selection	*In Silico* – UoM – ConSEQUENCE program
Standard Generation	Quantitative Concatenation (QconCAT)
	Na/K-ATPase – IVEIPFNSTN[**K**^{13}C]
Selected Peptides	P-gp – AGAVAEEVLAAI[**R**^{13}C]
	BCRP - VIQELGLD[**K**^{13}C]
Digestion	Deoxycholate denaturation, Lys-C + trypsin digest
LC-MS/MS	Nano flow LC – nanoAcquity (Waters) with TSQ Vantage (Thermo), SRM

Table 6-1b. Bertin Pharma.

Criteria	Bertin Pharma
Peptide Selection	*In Silico* – Tohoku University
Standard Generation	Absolute Quantification (AQUA)
	Na/K-ATPase – AAVPDA[**V**^{13}C,^{15}N]GK
Selected Peptides	P-gp – FYDPL[**A**^{13}C,^{15}N]GK
	BCRP - SSL[**L**^{13}C,^{15}N]DVLAAR
Digestion	MS2Plex-based process including trypsin-based digestion
LC-MS/MS	Normal flow LC – Flexar LC (Perkin Elmer) with API5500 (AB SCIEX) Vantage (Thermo), SRM

6.3 Results

6.3.1 Human Intestinal Transporter Abundance Quantification by Bertin Pharma

The absolute protein abundances of Na/K-ATPase, P-gp and BCRP from 9 intestinal samples from various regions were quantified by BPh (Figure 6-1). As expected, the abundance of the highly expressed PM marker Na/K-ATPase, was consistent across the samples range (30.76-56.99 fmol/µg). The abundance of BCRP was greater than P-gp in all samples, with the distal jejunum samples (n=4) possessing abundances of 2.59±1.4 and 0.91±0.4 fmol/µg, for BCRP and P-gp, respectively. In the solitary sample from the colon P-gp abundances were below the lower limit of quantification. The abundances of MRP2 were also measured, however only a single sample (distal jejunum #2) exhibited an abundance (0.33 fmol/µg) above the LLOQ (>0.125 fmol/µg). Due to the limited number of samples from each region of the gastrointestinal tract, it is difficult to assess the relationship between anatomical site and transporter abundances.

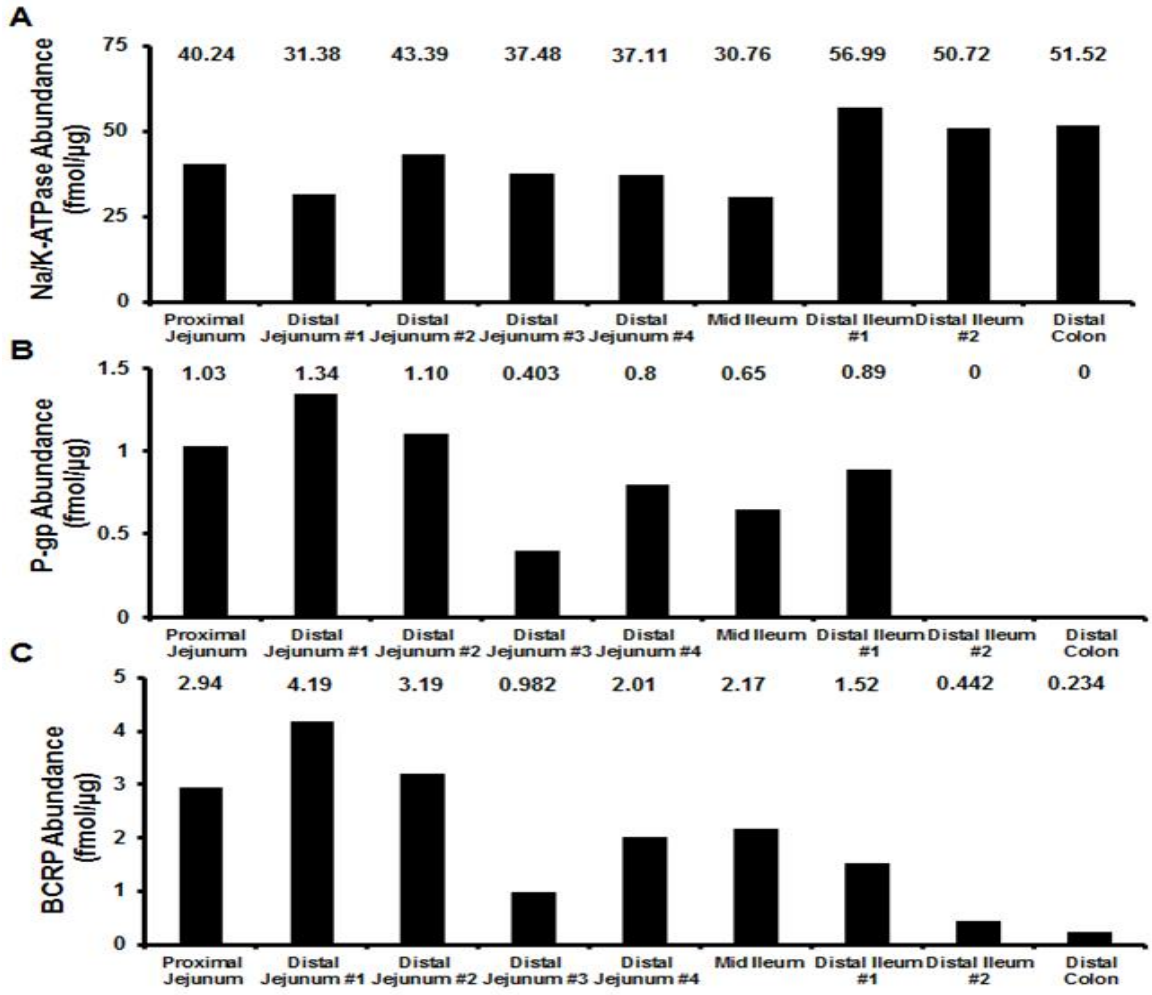

Figure 6-1. The absolute protein abundance of Na/K-ATPase (A), P-gp (B) and BCRP (C) in intestinal samples (n=9) from various regions of the gastrointestinal tract. The samples represent abundances from TM protein from eluted enterocytes. The text above the bars represents the abundance (fmol/µg TM protein) of each protein within the sample.

6.3.2 Method Comparison Across Groups Quantifying Transporter Protein Abundances

An analysis of the literature was undertaken to obtain an overview of the general differences in the methods used for sample preparation, peptide selection, digestion strategies and analytical systems by laboratories involved in quantifying absolute transporter abundances in mammalian tissues and *in vitro* systems. Table 6-2 provides a perspective on the diversity of techniques reported. Thirteen laboratories have reported quantification of transporter abundances in mammalian tissues or *in vitro* systems. The analysis shows that across the groups very few laboratories utilise identical methodology to quantify transporter abundances. The predominant methods used are those that employ a synthetically synthesised (AQUA) isotope labelled standard peptide. However, a combination of label free and targeted (labelled) approaches have been linked within the same study (Karlgren et al., 2012). Tohoku University and BPh laboratories are connected, therefore share many similarities. Furthermore, numerous laboratories have also fostered links with the forerunning developers of these methodologies, *i.e.,* Tohoku University and Pfizer Ltd, (Groton, CT, USA). Peptides that are used as surrogates for the quantification of the complete protein are selected based on a variety of criteria, the general details of which are described elsewhere (Ohtsuki et al., 2011; Oswald et al., 2013; Prasad and Unadkat, 2014; Qiu et al., 2014). However, for the frequently quantified transporter protein P-gp, 3 peptides are routinely employed to quantify human P-gp, highlighting a lack of consensus among groups. In-solution trypsin-based overnight digestion strategies dominate, but the utility of Lys-C to facilitate protein digestion prior to incubation with trypsin has also found favour at The Max Planck Institute and the UoM. Normal flow chromatography systems are commonly employed for separation of peptide digests, however nano flow systems are also currently utilised at Tohoku University, The Max Planck Institute and the UoM. The triple quadrupole MS system is routinely employed for labelled approaches, however the manufacturer and models differ between laboratories. To undertake studies with different LC-MS/MS systems within a laboratory requires the availability of at least two suitable systems, which may not be readily achievable due to the prohibitive cost of these instruments. For comparative purposes, the use of quantitative immunoblotting is also incorporated, which does not employ peptide selection strategies, protein digestion and LC-MS/MS systems for analysis, but does rely on suitable antibodies being available for target transporters (Tucker et al., 2012).

Table 6-2. A comparative analysis of methods used for quantification of transporter protein absolute abundances across research groups.

Group	Peptide Selection Method	Standard Generation (P-gp Standard)	Tissue/Cell Fractionation (DC/KIT/FASP)	Chaotropic/reducing agent	Digestion strategy	Standard Pre/Post Digestion	LC-MS/MS system	Source
Tohoku University (Study with *Boehringer Ingelheim, JP included)	*In silico* – In-house & MS/MS verification	AQUA Isotope Label (FYDPLAGK)[1]	DC - PM fraction; whole brain capillaries	Guanidinium hydrochloride	In-solution Trypsin (16h, 37°C) E:S-1:100	Post digestion	Multiplex HPLC – normal & nano flow MS - API5000 /QTRAP5500 (AB SCIEX) or 4000 Q trap (Applied Biosystems)	(Ohtsuki et al., 2012) (Sakamoto et al., 2011)*[1] (Uchida et al., 2014)
Pfizer	Prospector – UCSF & MS/MS verification	AQUA Isotope Label (NTTGALTTR)[2]	Kit extraction – native membrane (Calbiochem)	DTT; DOC	In-solution Trypsin (16h, 37°C) E:S-1:20-50	Pre-digestion or post digestion	Single & multiplex HPLC – normal flow MS - API4000 (Applied Biosystems) †	(Li et al., 2009a) (Zhang et al., 2011)[2] (Balogh et al., 2013)‖ (Qiu et al., 2013)
University of Paris Descartes	Linked to Tohoku University	AQUA Isotope Label (NTTGALTTR)	Whole brain capillaries	Guanidinium hydrochloride	In-solution Trypsin (16h, 37°C) E:S-1:100	Post digestion	HPLC – normal & nano flow MS – 4000 QTRAP/API 5000 (Applied Biosystems)	(Shawahna et al., 2011)
AstraZeneca	MS fragmentation – MASCOT search & MS/MS verification	AQUA Isotope Label (AGAVAEEVLAAIR)	DC – TM fraction	PPS	In-solution Trypsin (6h, 37°C) E:S-1:20	Pre-digestion	Single UHPLC – normal flow MS – 6460 (Agilent Technologies)	(Miliotis et al., 2011b)
TNO	See Tohoku University entry	AQUA Isotope Label (NTTGALTTR)[3]	DC - PM fraction	DTT	In-solution Trypsin (o/n, +2h, 37°C) E:S-1:100	Post digestion	Multiplex UHPLC – normal flow MS – Xev-TQ-S (Waters)	(Verhoeckx et al., 2011)[3] (van de Steeg et al., 2013)
The University of Washington	Prospector – UCSF & Skyline & MS/MS verification Links to Pfizer's proteomic laboratory	AQUA Isotope Label (NTTGALTTR)[4]	Kit extraction – native membrane (Calbiochem)	DTT	In-solution Trypsin (14-24h - 37°C) E:S-1:25	Pre-digestion (Deo et al., 2012) or post digestion	Multiplex UHPLC – normal flow MS – See Pfizer† or 6460A (Agilent Technologies)	(Deo et al., 2012) † (Prasad et al., 2014)
The University of Uppsala	Links to Pfizer & Max Planck Institute proteomic laboratories §	AQUA Isotope Label P-gp quantification not reported to date	Kit extraction – native membrane (Calbiochem)	DOC	In-solution Trypsin (16h, 37°C) E:S-1:20	Post digestion	See Pfizer entry.	(Karlgren et al., 2012) (Vildhede et al., 2014)

Table 6.2. Continued

Group	Peptide Selection Method	Standard Generation (P-gp Standard)	Tissue/Cell Fractionation (DC/KIT/FASP)	Chaotropic/ reducing agent	Digestion strategy	Standard Pre/Post Digestion	LC-MS/MS system	Source
Max Plank Institute	Total protein non-targeted	DDA Label free	DC – TM fraction	SDS	In-solution FASP Lys-C (o/n) room temp Trypsin – (2h - 37°C)	n/a	Total protein array HPLC – nano flow Orbitrap LTQ (Thermo Scientific)	(Karlgren et al., 2012) (Wisniewski et al., 2014)
The University of Greifswald[a]	Linked to Tohoku University	P-gp quantification not reported to date	DC - PM fraction	Not stated	In-solution Trypsin (16h, 37°C) E:S-1:100	Post digestion	Multiplex HPLC – normal & nano flow MS - QTRAP5500 (AB SCIEX) or 4000 Q trap (Applied Biosystems)	(Niessen et al., 2010)[a]
The University of Greifswald[b]	Expasy program & MS/MS verification	AQUA Isotope Label (AGAVAEEVLAAIR)	Kit extraction – native membrane (Calbiochem)	DTT	In-solution Trypsin (16h, 37°C) E:S-1:40	Post digestion	Multiplex HPLC – normal flow MS - API4000 (Applied Biosystems)	(Groer et al., 2013)[b]
Bertin Pharma	Linked to Tohoku University	AQUA Isotope Label (FYDPLAGK)[1]	DC – PM fraction	Unknown‡	In-solution‡ Trypsin	Post digestion	Multiplex HPLC – normal flow MS - API5000 (AB SCIEX)	(Kunze et al., 2014)
The University of Manchester	SRM Atlas ConSEQUENCE – program – UoM & MS/MS verification	QconCAT Isotope Label (AGAVAEEVLAAIR)	DC – PM fraction	DOC-DTT	In-solution Lys-C (4h - 30°C) Trypsin – (16h - 37°C) E:S-1:20	Pre-digestion	Multiplex HPLC – nano flow MS – TSQ Vantage (Thermo Scientific)	(Russell et al., 2013)
The University of Dundee**	n/a	S-tag – Antibody Label free	DC – TM fraction	n/a	n/a	n/a	n/a	(Tucker et al., 2012)

*Boehringer Ingelheim, Japan collaborated with Tohoku University. ** Professor Coughtrie's group are now based at The University of British Columbia. †Deo et al., 2012, performed LC-MS/MS analysis at Pfizer Ltd. ‡ An 'off the shelf' MS2Plex kit is used. §The targeted proteomic strategy at the University of Uppsala used the Pfizer laboratory and techniques described in Balogh et al., 2013. Differential Centrifugation (DC); Filter Aided Sample Preparation (FASP); Plasma Membrane (PM); Total Membrane (TM), Data-Dependent Acquisition (DDA). E:S is the enzyme substrate ratio for trypsin. PPS is a silent surfactant. The University of California, San Francisco (UCSF) n/a – not applicable, o/n - overnight.

6.3.3 Cross Laboratory Comparison of Absolute Protein Abundances

Linearity (R^2=≥0.994), precision (CV≤15%), accuracy (relative error, 71-112%) and the lower limit of quantification (LLOQ) were determined as 0.125 fmol/µg for all proteins by BPh and 0.2 fmol/µg by UoM (Harwood et al., 2015). In addition to seven Caco-2 monolayers, three human distal jejunum samples (#2, #3, #4) and one distal ileum (#2, Figure 6-1) were analysed by both BPh and UoM and are incorporated into the cross-laboratory comparison analyses. The comparative absolute abundances and the correlations between BPh and UoM for Na/K-ATPase, P-gp and BCRP are provided in Figure 6-2 and Figure 6-3. The individual abundance data for each sample is provided in Table 6-3. An additional two Caco-2 samples were initially incorporated into the analysis, however these were subsequently removed as the storage of the digested proteins differed by greater than 6 months between analyses from one laboratory to another, which was thought likely to confound comparative analyses. The removal of these samples did not affect the findings of this study. For the remaining samples described here, the digestion and analysis took place within a 1 month period between laboratories, a time period considered unlikely to impact on end point abundance determinations (Sakamoto et al., 2011). For Na/K-ATPase and BCRP, there was no difference in the mean abundances (p=0.36 & 0.76, respectively, Wilcoxon matched pairs) and no correlation (rs=0.42 & 0.29, respectively) across all samples between laboratories. There is a systematically higher BCRP abundance (ranging from 20 to 129% in individual samples) quantified by BPh than UoM in 21 and 29d cultivated Caco-2 cells (Table 6-3) which was not reciprocated in the intestinal BCRP abundances, which were on average 17% higher (-40 to 72%) in the UoM analysis. A systematically higher (63%, p=0.001, Wilcoxon matched pairs) P-gp abundance is quantified by UoM than by Bertin Pharma across all samples. P-gp sample abundances showed a high correlation (rs=0.42, p=0.04) (Figure 6-3). For the single distal ileum sample, P-gp abundance was below the limit of quantification (<0.125 fmol/µg) in BPh determinations but measurable by UoM. In both laboratories, lower mean abundances of P-gp were observed in the human intestinal samples than Caco-2 cell monolayers, irrespective of cultivation time. This is in contrast to BCRP, in which the opposite relationship is observed. It should be noted that peptide losses were accounted for within abundance determinations by the UoM being 36% for human tissues and 11% for Caco-2 cells and that no losses of peptide occur in BPh digestion strategies.

The potential impact of these results on IVIVE scaling was investigated by generating a REF-based scaling factor (Equation 1-3) for human distal jejunal samples and 21d cultivated Caco-2 cell monolayers (n=3) (Table 6-3). Due to the high correlation observed between laboratories when quantifying P-gp abundances, the systematically higher P-gp levels measured by the UoM had no effect on the jejunal-REF between laboratories (BPh-REF 0.37, UoM-REF 0.4). For BCRP however, there were distinct differences with the UoM jejunal-REF being 2-fold higher than the BPh jejunal-REF (Ref 2.22 vs. 1.10). This is due to the systematically lower Caco-2 cell abundance levels measured at UoM.

Table 6-3. Individual abundances of human intestinal and Caco-2 cell monolayer with jejunal REF scaling factors.

	Na/K-ATPase Abundance (fmol/µg)			P-gp Abundance (fmol/µg)			BCRP Abundance (fmol/µg)		
Sample	Bertin Pharma	University of Manchester	Relative Error (%)	Bertin Pharma	University of Manchester	Relative Error (%)	Bertin Pharma	University of Manchester	Relative Error (%)
Human Distal Jejunum 1	43.39	41.93	-3	1.10	3.07	64	3.19	2.28	-40
Human Distal Jejunum 2	37.48	34.58	-8%	0.40	0.98	59	0.98	1.92	49
Human Distal Jejunum 3	37.11	29.58	-25	0.80	1.62	51	2.01	3.49	42
Human Distal Ileum	50.72	24.47	-107	BLQ	0.2	-	0.44	1.6	72
Caco-2 21d (# 1)	51.56	82.47	37	1.89	5.21	64	1.7	1.19	-62
Caco-2 21d (# 2)	56.75	47.16	-20	2.27	4.5	50	1.94	1.16	-67
Caco-2 21d (# 3)	65.86	56.75	-16	2.07	4.31	52	1.94	1.12	-74
Caco-2 29d (# 1)	49.3	77.43	36	1.64	8.27	80	1.34	1.12	-20
Caco-2 29d (# 2)	74.81	54.32	-38	2.29	6.78	66	1.64	.72	-129
Caco-2 29d (# 3)	52.45	58.83	11	1.98	6.78	65	1.51	.75	-100
Caco-2 21d HP	90.43	52.33	-73	7.84	5.71	37	2.73	1.64	-67
Mean Human Distal Jejunum	**39.3 (±3.5)**	**35.4 (±6.2)**	**-12***	**0.8 (±0.3)**	**1.9 (±1.1)**	**58***	**2.1 (±1.1)**	**2.6 (±0.8)**	**17***
Mean Caco-2 21d	**58.1 (±7.24)**	**62.1 (±18.26)**	**-0.4***	**2.1 (±0.19)**	**4.7 (±0.48)**	**55***	**1.9 (±0.14)**	**1.2 (±0.04)**	**-62***
Mean Caco-2 29d	**58.9 (±13.91)**	**63.5 (±12.25)**	**3 ***	**1.97 (±0.32)**	**6.92 (±1.28)**	**71***	**1.5 (±0.15)**	**0.9 (±0.22)**	**-83***
Overall Mean	**55.4 (±16.12)**	**50.9 (±18.12)**	**-19***	**2.0 (±2.08)**	**4.8 (±3.51)**	**63***	**1.8 (±0.76)**	**1.5 (±0.89)**	**-34***
REF (Jejunum: Caco-2 -21d)	**0.68**	**0.58**	**-**	**0.37**	**0.4**	**-**	**1.11**	**2.22**	**-**

SD are given in parentheses. * denotes mean relative error when accounting for individual samples

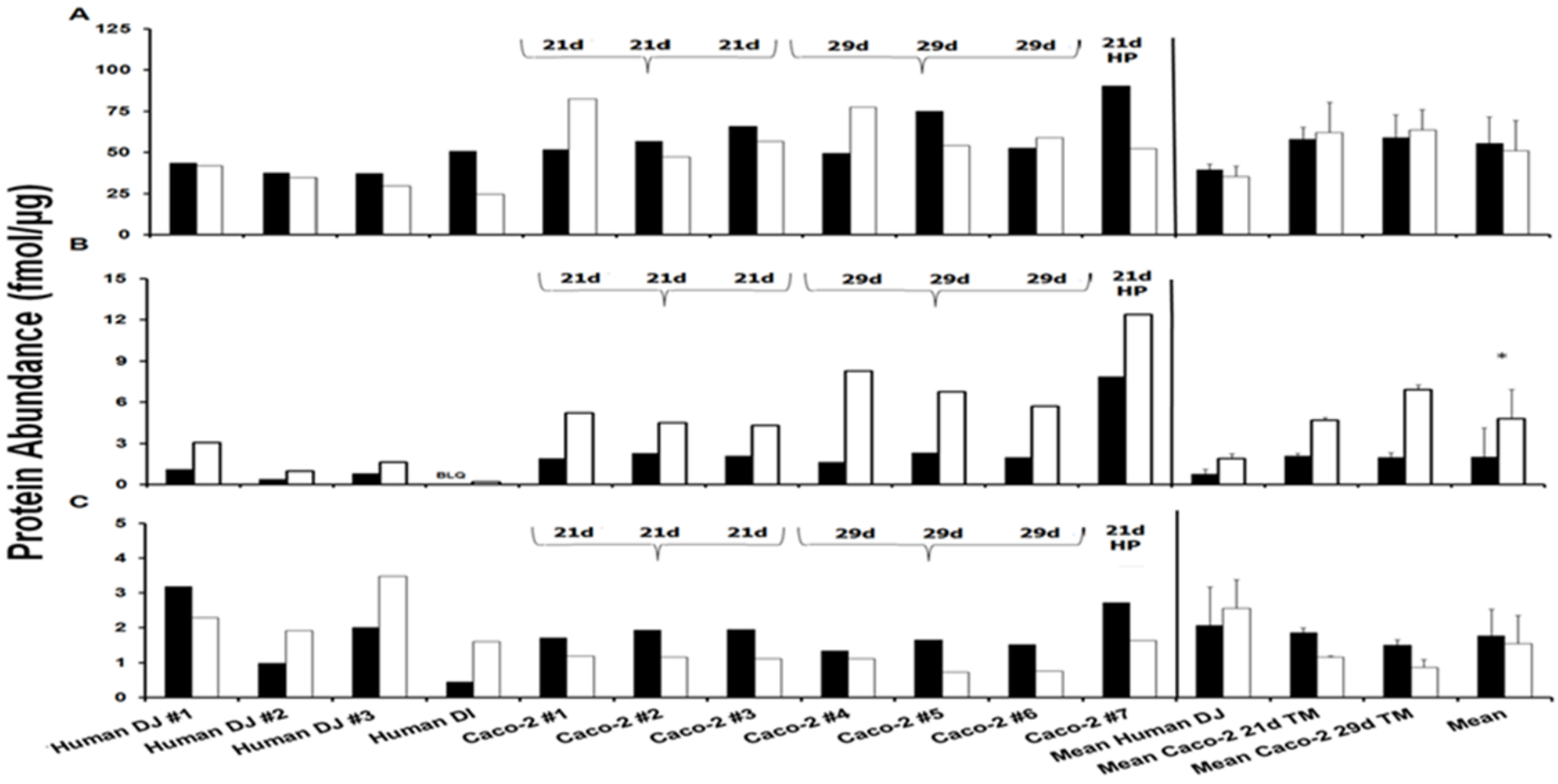

Figure 6-2. Absolute protein abundances of Na/K-ATPase, P-gp and BCRP determined by Bertin Pharma (black) and the University of Manchester (white) in Caco-2 cell monolayers (n=7) and human intestinal TM fractions (n=4). The text above the bars indicates Caco-2 monolayer cultivation age and HP is high passage Caco-2. Distal Jejunum (DJ) and Distal Ileum (DI). Below the Limit of Quantification (BLQ) * p = <0.05.

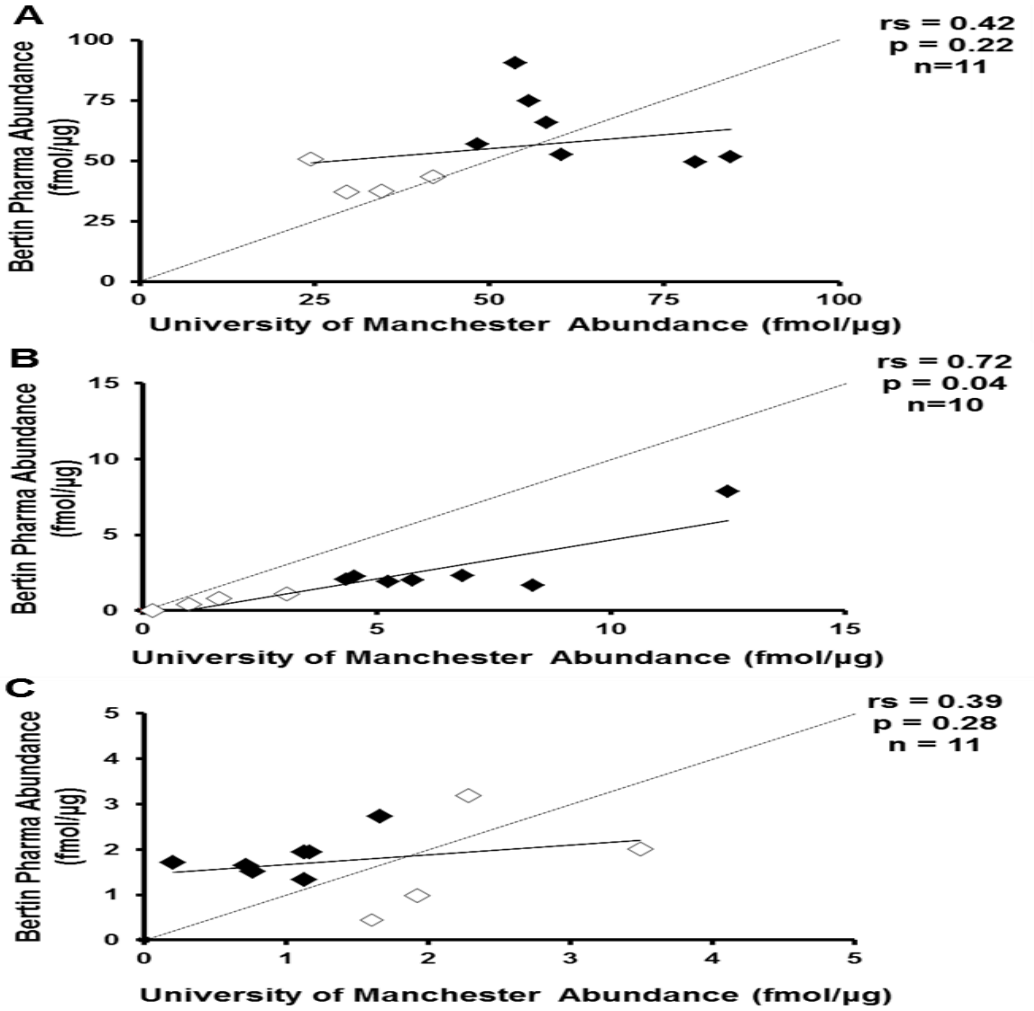

Figure 6-3. Correlation analysis (Spearman's Rank) of the absolute protein abundances of Na/K-ATPase (A), P-gp (B) and BCRP (C) between Bertin Pharma and the University of Manchester. Diamonds denote human (white) and Caco-2 cell monolayers (black). Spearman's rank correlation coefficients (rs) are provided as text on the plot, as are the p values representing the T-distribution for assessing the significance of the correlation. Note, a single sample from BPh for P-gp was not above the limit of quantification.

6.3.4 An Appraisal of Selected P-gp and BCRP Peptides

The proteotypic standard peptides selected by each laboratory for quantification of Na/K-ATPase, P-gp and BCRP are based on criteria described in publications from Tohoku University and The University of Manchester (Kamiie et al., 2008; Russell et al., 2013). The position of the selected standard peptides within P-gp and BCRP protein structure is provided (Figure 6-4). The selection criteria defined by Tohoku University would not have chosen the UoM peptide for P-gp, as a single nucleotide polymorphism (SNP) is present at position 261 (I261V - A781G). This SNP has an allelic frequency in African Americans of 0.6% (Kroetz et al., 2003) and 6.9% in Ugandans (Mukonzo et al., 2010). However, this SNP was not detected in the other populations studied; Caucasians, Asian Americans, Mexican Americans, Pacific Islanders and Japanese (Kroetz et al., 2003; Ozawa et al., 2004). The standard peptide selected for P-gp quantification by BPh was flagged by the ConSEQUENCE program developed at the UoM (Lawless and Hubbard, 2012) as a peptide prone to mis-cleavage by trypsin. This is due to the presence of aspartic acid (E) at the N-terminal flanking region of the selected peptide which is associated with missed cleavage events (Lawless and Hubbard, 2012). If missed cleavage was occurring, the selected peptide would be elongated, changing its mass, resulting in the first mass filter (Q1) of a triple quadrupole MS, rejecting its selection for subsequent analysis. This would result in a lower native peptide signal and a lower biological abundance.

For the BCRP peptides selected by both groups, no SNP's were detected. Tohoku University peptide selection criteria are unlikely to have scored the UoM peptide highly due to the presence of glutamine (Q) which has the potential to suffer a deamidation post translational modification. This event was judged tolerable at the UoM, given that the rate of glutamine deamidation is considerably lower than that for asparagine (N), with a reaction half-life of 660 days (Li et al., 2010b). In contrast, the UoM did not select the BPh BCRP peptide standard due to the perceived difficulty of efficient trypsin cleavage at dibasic and tribasic tryptic sites, *i.e.,* sequential lysine or arginine residues or lysine and arginine side-by-side at the N-terminal region of the BPh selected peptide (Lawless and Hubbard, 2012). For similar reasons outlined for P-gp, mis-cleavage may result in non-selection at the Q1 mass impacting on the native peptide signal.

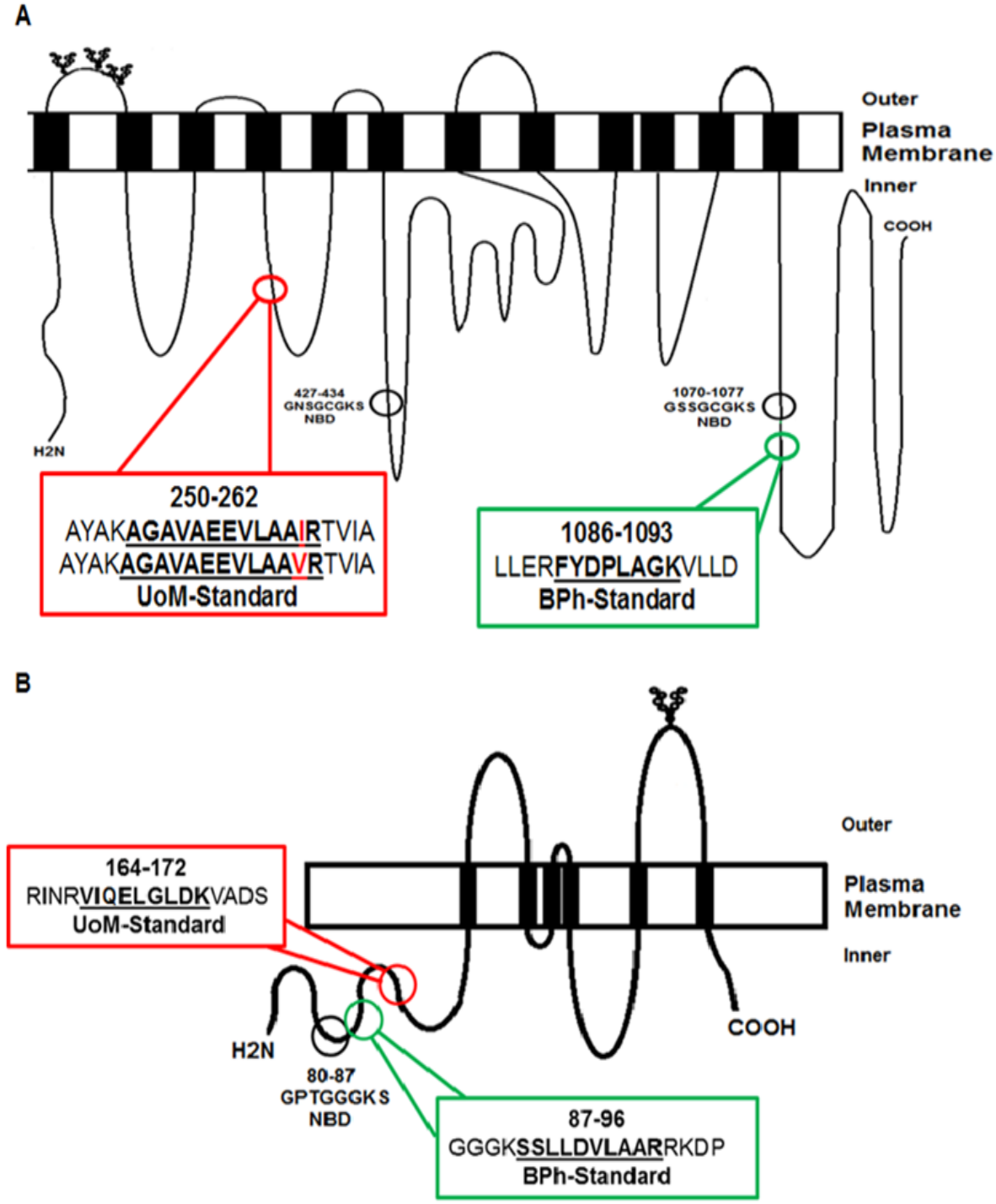

Figure 6-4. The location and nomenclature of the selected peptides for quantifying P-gp (A) and BCRP (B) absolute protein abundances. BPh selected peptide sequences (bold & underlined) are in the green boxes and the UoM (bold & underlined) are in the red boxes. The amino acids immediately flanking the selected peptides are in plain text. The UoM selected peptide contains the potential to harbour an SNP I261V (A781G) for P-gp which is given as red text. The variant 'V' peptide is also provided. The nucleotide binding region is given as NBD and N-glycosylated sites are shown in the first extracellular loop of P-gp and the third extracellular loop of BCRP.

6.3.5 A Comparison to Published Data: UoM *Versus*. The University of Greifswald Transporter Abundances

With the transporter abundance data already provided from the UoM tissues by two independent laboratories, a comparison was made with absolute abundance values obtained for P-gp, BCRP and MRP2 in non-matched distal jejunal samples from The University of Greifswald (UoG) (Groer et al., 2013; Drozdzik et al., 2014) (Figure 6-5). When comparing data from tissues in the UoG studies with UoM tissues analysed in both BPh and the UoM, there is a trend for higher P-gp (2.9-fold) and BCRP (5.8-fold) abundances in the UoM obtained tissue. For MRP2, only 1 of 4 samples were above the LLOQ when measured by BPh. However, there is reasonable agreement (<2-fold difference) between the UoM abundance analysis and the UoG tissues. From the current data set, it not possible to determine if these differences are due to biological, technical or analytical bias.

6.3.6 The Impact of Enterocyte Harvest Method on Transporter Abundances

To investigate whether different methods of harvesting enterocytes affect transporter abundance, Na/K-ATPase, P-gp and BCRP abundances were quantified by BPh in samples generated by mucosal crushing or enterocyte elution (Figure 6-6). A significantly higher ($p=<0.001$) Na/K-ATPase abundance was found after enterocyte elution by chelation compared to mucosal crushing by homogenisation. However, there were no differences in abundances for P-gp and BCRP between enterocyte harvest methods. This suggests that protein abundance determination in the intestine may depend on enterocyte harvest method for certain proteins or is dependent on the membrane in which the transporter is expressed, *i.e.,* basal (Na/K-ATPase) or apical (P-gp or BCRP).

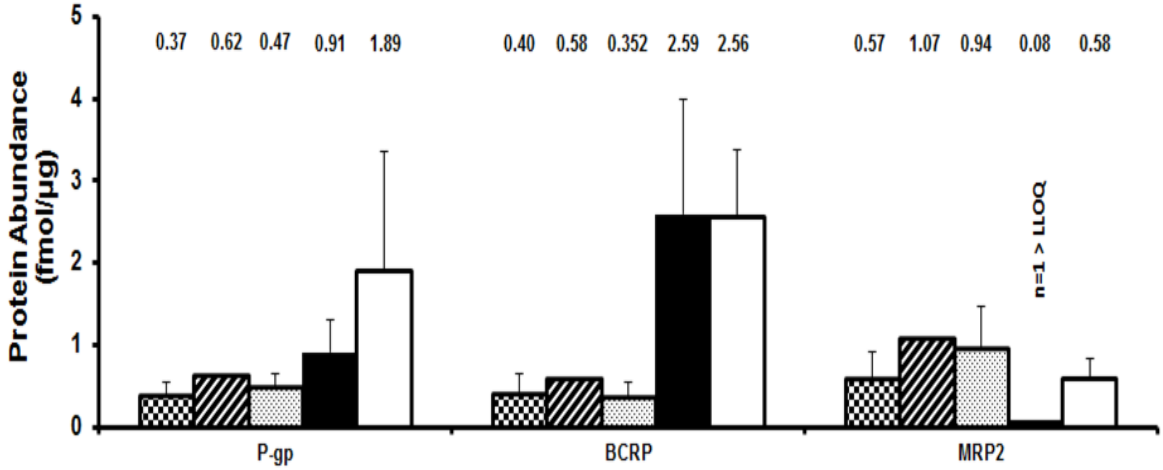

Figure 6-5. The absolute protein abundances of P-gp, BCRP and MRP2 in distal jejunum measured at the University of Greifswald (UoG), the UoM and BPh. The abundances are measured in digested total/native membrane fractions. UoG data is from 3 studies (Oswald et al., 2013) (n=4, chequered), (Groer et al., 2013) (n=1, diagonal line) & (Drozdzik et al., 2014) (n=6, dotted). The data from these studies was extracted by graphical digitization (Get Data program). BPh (n=4, black) and the UoM (n=3, white) samples are matched. The samples from the UoGare not matched to the BPh/UoM samples. BPh MRP2 data is a weighted mean as only a single sample was > LLOQ. Means are given as text above each bar and error bars represent ± SD.

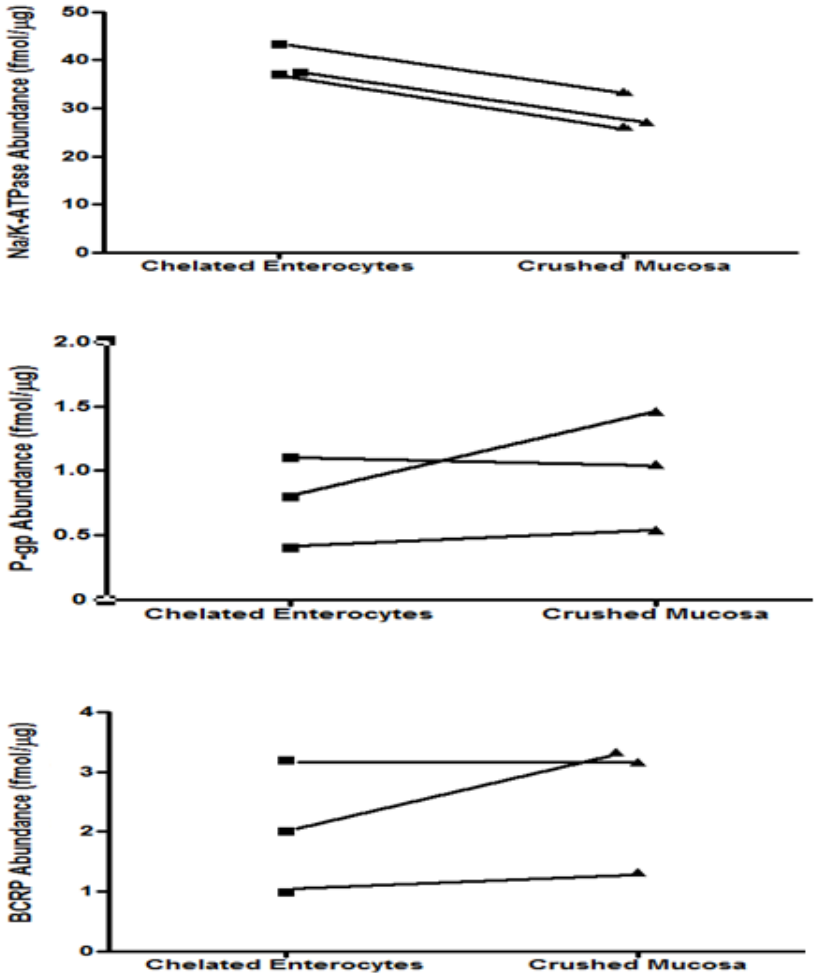

Figure 6-6. A comparison of Na/K-ATPase, P-gp and BCRP protein abundances in matched human distal jejunum TM protein samples after enterocyte chelation or mucosal crushing.

6.4 Discussion

A number of groups have developed, validated and applied protocols for quantifying the absolute abundances of transporter proteins in mammalian tissues and *in vitro* systems using proteomic approaches. With this raft of abundance data being generated across multiple laboratories now being incorporated into IVIVE-PBPK strategies (Bosgra et al., 2014; Kunze et al., 2014; Prasad et al., 2014; Vildhede et al., 2014), it is critical to establish if differing methods employed by each laboratory contribute to a bias in end point abundance determination. By utilising the TM proteins from human intestinal and Caco-2 cell monolayers we show that for P-gp there is a systematic bias in endpoint abundances when comparing two independent laboratories, BPh and the UoM. For both Na/K-ATPase and BCRP, the similarity when considering the mean endpoint abundances across all samples is encouraging. However, the lack of correlation when quantifying Na/K-ATPase and BCRP in individual samples suggests that there is an influence of technical and/or analytical variability in post-membrane fractionation stages.

Integral membrane transporter proteins are notoriously challenging to digest due to their poor solubility (Mirza et al., 2007). Therefore, chaotropic agents are often used to enhance protein solubility to facilitate the effective reduction, alkylation and digestion of target proteins. A considerable difference was found when determining the abundances of OATP proteins in HEK293-transfected cells, which resulted from the chaotropic agent used (Balogh et al., 2013). Based on the findings of Balogh et al., 2013, sodium deoxycholate (DOC) was employed as the chaotropic agent by the UoM. It is recognised that differences in agents employed for these processes require appreciation when comparing methodology across studies. Aside from the use of trypsin for proteolytic digestion, it is difficult to evaluate the effect of the potential differences in the procedures employed to denature, reduce, alkylate and digest the proteins between laboratories, as the components of the MS2Plex kit were not disclosed by BPh.

The determination of absolute transporter protein abundances requires that numerous assumptions are met, including that enzymatic digestion is complete (Ji et al., 2012). Numerous studies have investigated the efficiency of digestion for the selected peptides to varying degrees of complexity (Kamiie et al., 2008; Li et al., 2008; Zhang et al., 2011; Ji et al., 2012; Balogh et al., 2013; Groer et al., 2013; van de Steeg et al., 2013). Due to the limited availability of entire transporter proteins, an assessment of the completeness of digestion is a challenge. However, if a purified protein does become available, this permits an assessment of peptide recovery throughout the digestion procedure based on known amounts of whole protein (Prasad et al., 2014). However, the instability

of peptides over the duration of proteolytic digestion may also require consideration and could be a factor in reducing the MS signal (van den Broek et al., 2013).

In addition to the selection of peptides uniquely identifying the targeted protein based on trypsin digestion, programs that also score the peptide in regards to the potential for missed cleavage events may also be advantageous (Lawless and Hubbard, 2012). This is particularly pertinent given that in a recent relative quantification analysis, it was revealed that up to 46% of peptides generated, possessed mis-cleaved events when an in-solution trypsin digestion was performed in *E. coli* (Chiva et al., 2014). Analysis within our laboratory, found that both the peptides selected for P-gp and BCRP quantification at BPh (based on Tohoku University criteria) are prone to suffering missed cleavage events. The presence of N-terminal flanking glutamic acid (E) 2 positions from the conventional trypsin cleavage sites, arginine-lysine (R-K), is found to be particularly prone to missed cleavage, therefore the P-gp peptide selected at Tohoku University did not score as favourably as other P-gp peptides selected for the QconCAT construct used by the UoM in this study (Russell et al., 2013). The selection of peptides through the triple quadrupole mass spectrometer is based on pre-defined masses of selected peptides, where any violation of these masses, *i.e.,* by missed cleavage of target peptide, will lead to the exclusion of the peptide in mass filter 1 (Q1), resulting in lower abundances quantified in the samples. Therefore, these events may explain the differences in P-gp abundance quantification between laboratories shown in this study. The inclusion of mis-cleaved peptides within abundance quantitation has been advocated in order to obtain absolute abundances that more accurately reflect the genuine biological abundances within a system (Chiva et al., 2014). However, for this approach to be valid, an essential requirement is that the mis-cleaved peptide(s) are unique to the target protein. Furthermore, it is still critical to confirm that the *in silico* peptide selections are suitable for quantifying target proteins by experimental analysis to assess factors such as, co-elution and ionisation efficiency.

In a recent study, the choice of peptide was demonstrated to be critical for the quantification of human liver OATP1B1 (Terasaki et al., 2014). In the original study from this group, human liver OATP1B1 abundances were analysed and 9 of 17 samples were found to possess levels below the limit of quantification (Ohtsuki et al., 2012). This is unexpected given that OATP1B1 is the transporter protein exhibiting the highest absolute abundance of all transporters quantified in livers across studies (results of a meta-analysis by the candidate for Simcyp Ltd, data not shown). The original peptide selected by the group is located in the ninth transmembrane spanning domain of OATP1B1. Since the efficiency of tryptic digestion is thought to be compromised in these regions

(Kamiie et al., 2008), a re-evaluation of the original peptide against 4 other peptides located in intracellular or extracellular loop domains for human hepatic OATP1B1 quantification was performed. The study found that the original peptide under-estimated the mean abundance across 15 livers by greater than 20-fold in comparison to the best performing peptide. A methodological bias of this magnitude is a concern and will require consideration when incorporating transporter abundances into population libraries in PBPK models (Harwood et al., 2013). Clearly, a 20-fold greater abundance of hepatic OATP1B1 in individuals represented in PBPK models will have a substantial effect on transporter-mediated drug disposition.

In this study, there was a consistently lower BCRP abundance in all Caco-2 cells when analysed by UoM. This does not appear to be a peptide-specific issue since BCRP abundance in 3 of 4 human samples was higher at the UoM. It is possible that the Caco-2 cell membrane matrix may affect the digestion of the selected BCRP peptide and impact on end point abundance quantification. There is also a possibility that these differences could be due to chromatographical effects. A peptide commonly used peptide to quantify P-gp (Table 6-1), NTTGALTTR, was found to interfere with the chromatography when analysing human intestinal samples at the UoG, therefore it was not selected for further analysis (Groer et al., 2013). However, the source of the observed lower BCRP abundances in Caco-2 cells is unlikely to be founded on chromatographical interference within this study as co-elution profiles of native and standard peptides were generated. However, the methodological validation of these peptides was initially performed in human intestinal samples (Section 4.3.2). Therefore, further studies to assess the optimal digestion conditions for the selected BCRP peptides in Caco-2 cells are required.

Together with the requirement of obtaining transporter abundances in tissues of individuals for incorporation into PBPK models, absolute abundance data from mammalian tissues and *in vitro* systems can also be used to generate IVIVE scaling factors (Li et al., 2010a; Karlgren et al., 2012; Vildhede et al., 2014). Having established that there is a higher P-gp abundance across all samples and a lower abundance of BCRP in Caco-2 cells after quantification by the UoM, it is important to establish if laboratory-specific bias exist when generating IVIVE scaling factors. By generating a REF scaling factor (Equation 1-3), based on the ratio of distal jejunum transporter abundances to 21d cultivated Caco-2 cell monolayers for a specific transporter, it was shown that P-gp REF's were the same between laboratories, yet for BCRP this REF was 2-fold higher at the UoM. This suggests that if there is a consistent bias in abundance determination across both *in vivo* and *in vitro* systems, *i.e.,* as is the case for P-gp, the REF will not be affected. However, if bias

in abundance quantitation occurs selectively within a biological system between laboratories, the REF scalar will be influenced *i.e.,* Caco-2 cell BCRP abundances. An intestinal REF scalar for P-gp based on human jejunum and Caco-2 cells expression was used to build an IVIVE-PBPK model for digoxin (Neuhoff et al., 2013). A REF of 2 was incorporated into the model after analysis of immunoblotting densitometry data from homogenates from a single human jejunum and three 21d cultivated Caco-2 monolayers (Troutman and Thakker, 2003a). It is clear that the UoM-P-gp-REF scalar is lower than found in the study of Troutman & Thakker, due to the higher abundances measured in Caco-2 cells. This difference could be due to a number of factors including; differences in the methods used for quantifying expression; the use of homogenates compared to a total membrane fraction, the method of enterocyte harvest, differences in Caco-2 cell cultivation or the variability in the abundances inherent to the human samples. This emphasises the need to introduce standardisation into the determination of absolute abundances and subsequent generation of scaling factors. However, complete standardisation across laboratories is perhaps unrealistic, and therefore at the very least, scaling factors should be defined on a laboratory-specific basis to account for the variability in Caco-2 cell phenotype described between laboratories (Hayeshi et al., 2008). There is an obvious need to generate further scaling factors within various research groups in order to understand how the selected methods can impact on REF calculations.

The UoG are the only group to have reported intestinal transporter abundances at present using QTAP methods. The comparisons drawn between tissues from the UoM and the UoG highlight the potential variability in transporter abundances between laboratories/tissues. However, from this data set it is not possible to identify if the differences, which are particularly marked for P-gp and BCRP, are inherent to the biology of the tissue or based on differences in the methods employed for quantification. Similarities do exist between the studies described, such as choice of peptides for P-gp for the UoM and BCRP for BPh. However, differences in source of the tissues *i.e.,* cadaveric or surgically resected tissue at the UoG compared to surgical resection at the UoM, the membrane enrichment technique, the QTAP method, drug history and harvesting of enterocytes, may lead to the different abundances observed. It's shown that the method of enterocyte harvest, *i.e.,* elution of enterocytes by calcium chelation, or homogenising the mucosa, the latter of which is routinely employed at the UoG, does affect Na/K-ATPase abundances but not those of P-gp or BCRP. Therefore, this aspect of the methods may not be responsible for the differences observed between the studies for P-gp and BCRP.

This study does not control for differences in membrane fractionation technique which could be a source of variability across studies and within studies (Heikkinen et al., 2014). To test for within laboratory variability, repeated membrane extraction, protein digestion and subsequent abundance quantification is required on the same frozen tissue over multiple days. However, within our laboratory when employing an entire QTAP workflow for Caco-2 cells spanning a 7 month period of single operator cell culturing ('the candidate'), consistent abundance determinations for Na/K-ATPase, P-gp and BCRP were found when analyses was performed by BPh (Chapter 5).

6.5 Conclusion

As the use of techniques to measure transporter absolute abundances becomes more widespread, an appreciation of the limitations of the methods for accurately determining protein abundances, that are inherent to the biological system are required. Cross laboratory comparisons on the same samples, can reveal methodological biases that are integral to a particular laboratory or step within the workflow employed by each laboratory to determine abundances. This is critical when performing rigorous analysis of biological data sets from across laboratories, as is performed by scientists employing IVIVE strategies and builiding population-based PBPK models. Within this study, there are plans to perform further investigations between the UoM and BPh, by exchanging the peptide standards used within each laboratory, thus, permitting the parallel analysis of peptides in matched human intestinal samples. Furthermore, a multiple cross laboratory comparison, with matching samples, is required to enable the comparative evaulation of the entire proteomic workflow specific to each laboratory on the generation of absolute protein abundances. Studies are underway to perform such analyses, coordinated by the University of Upsalla, for execution in the coming year.

Chapter 7 - Efflux Ratio and Intrinsic Clearance of Vinblastine are Associated to P-gp Abundance in Caco-2 Cells

Declaration

Work presented in this chapter was performed by the candidate Matthew Harwood and Caco-2 abundance data was generated by Bertin Pharma, Orleans, France. The three compartment kinetic model used for estimating transporter kinetic parameters and passive permeability was developed by Dr Howard Burt, Simcyp Ltd, Sheffield, UK.

Excerpts of text from this chapter are extracted from published articles:

M.D. Harwood, *et al., (**2013**), Biopharm Drug Dispos. 34, 2-28.*

7.1 Introduction

To devise an effective mechanistic IVIVE strategy for transporters, incorporation of separate elements for the $P_{Passive}$ and transporter-mediated flux is necessary together with scaling factors to bridge any mechanistic differences between the *in vitro* and *in vivo* system. The 'drug parameters' are defined for each process within appropriate *in vitro* experiments and used in conjunction with the 'system parameters' *i.e.,* demographic, physiological or genetic parameters, to predict the behaviour of the drug *in vivo*. When integrating drug parameters into a model, the key processes including active kinetics, are often described by Michaelis-Menten model parameters (Km, Jmax or CLint). Applying active transport models to the *in vitro* data can take place only after deconvoluting the effects of $P_{passive}$. Ideally, the effects of the unbound fraction at the transporter binding site require delineation before using models (Harwood et al., 2013).

Expression-based scaling factors have been utilised in IVIVE and incorporated into PBPK models for many years (Proctor et al., 2004). The ISEF was devised to correct for differences in enzyme abundance and activity (per unit of CYP450 isoform) in recombinant expression systems and human liver. However, transporter expression scaling factors at present are not nearly as sophisticated due to the relative lack of transporter abundance data and paucity of good quality kinetic data. This is due to a number of factors including lack of transporter-specific substrates, poor definition of experimental set ups and their interpretation and limited information on the effects of transporter abundance on activity (Harwood et al., 2013). Therefore, a common approach to incorporating transporter functionality into IVIVE strategies is to assume there is a linear relationship between expression and activity (Neuhoff et al., 2013; Vildhede et al., 2014). In these studies, the REF scaling factor was incorporated into the IVIVE strategy under the assumption that Jmax is proportional to transporter expression (Harwood et al., 2014). In a study in which cell lines with increasing levels of P-gp expression were developed (Shirasaka et al., 2008), kinetic analyses of the P-gp probe compound Vinblastine (VBL) showed that the activity (Jmax) relative to the level of P-gp expression as measured by immunoblotting, decreased as P-gp expression increased (Tachibana et al., 2010; Korzekwa and Nagar, 2014). This suggests for VBL, that there is a redundancy in transporter function, such that the activity per unit of transporter protein decreases as protein expression levels increase. Therefore, the utility of linear scaling factors solely based on expression, *i.e.,* REF, may not be appropriate if *in vitro* systems expressing high levels of transporter protein are incorporated into an IVIVE strategy. In addition, it has also been shown that

P-gp expression increases in higher passages of Caco-2 cells grown in flasks (Anderle et al., 1998). If the increased Caco-2 expression is also observed when growing Caco-2 cell monolayers grown on permeable filter supports, a consequent increase in P-gp-mediated transport might be expected. If consistent across multiple laboratories, this observation warrants the development of expression-based scaling factors that are tailored to the effects of long term cell culture on transporter expression levels.

VBL is an alkaloid originating from the Madagascan Periwinkle (Catharansus Roseus) and is widely used for the treatment of many cancers (Lu et al., 1983). It has been known for many years that VBL is transported by P-gp in MDCK-II-MDR1 and Caco-2 cells (Horio et al., 1989; Hunter et al., 1993) and mammalian intestinal tissues (Stephens et al., 2001). However, the role of MRP2 has also been implicated to be responsible for VBL transport in MDCK-II-MRP2 and Caco-2 cell lines (Evers et al., 1998; Tang et al., 2002a; Taipalensuu et al., 2004) and multidrug resistant breast cancer cell line MCF-7 (Litman et al., 2000). VBL was selected as a P-gp probe compound for this study due to the observed redundancy in P-gp activity with increasing P-gp expression levels described previously (Tachibana et al., 2010; Korzekwa and Nagar, 2014). The structure, physico-chemical properties metabolism and transport protein specificities of VBL are provided in Table 7-1 and Figure 7-1 .

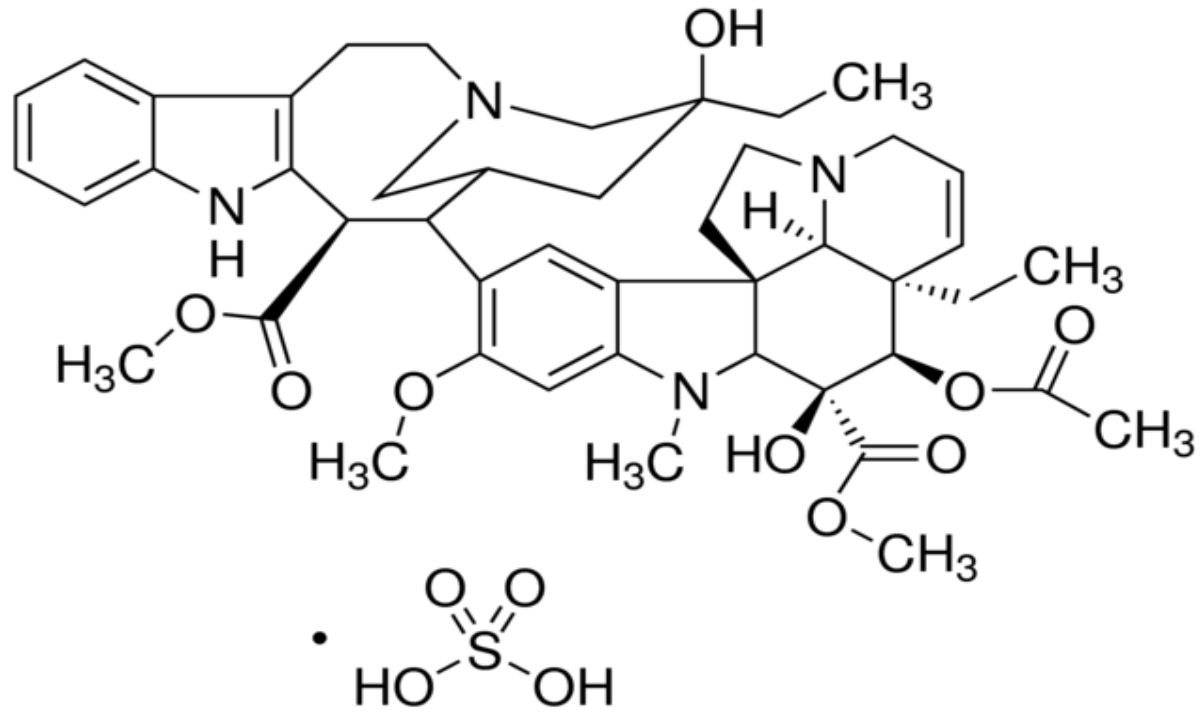

Figure 7-1. The chemical structure of Vinblastine sulphate (image courtesy of Sigma-Aldrich).

Table 7-1. Physico-Chemical Properties of VBL, Metabolism & Transport Specificities.

Parameter	Value/Description	Source	Comments
Molecular Weight (g/mol)	909	http://www.webqc.org/mmcalc.php	Sulfate Salt
pKa	5.4 7.57	(Sun and Avdeef, 2011)	Experimental
Compound Type	Base (Cation)	(Sun and Avdeef, 2011)	
LogP	1.97	(Juliano and Stamp, 1978)	Experimental
Metabolism	Deacetyl-VBL Km (ND) Km (μM) = 6.82* (CYP3A) V_{max} (nmol/min/mg) 0.64 Four metabolites found* Km (ND)	(Owellen et al., 1977) (Zhou-Pan et al., 1993) (Zhou et al., 1994)	Human (*in vivo*) Human liver microsomes Human hepatocytes
Transport			
P-gp	Jmax – 1.7 Km (μM)– 89.2	(Tang et al., 2002b)	Caco-2†
MRP2	Jmax – 0.54 Km (μM)– 71.8	(Tang et al., 2002a)	Caco-2‡

*single metabolite, structure not identified. † kinetic parameters may be influenced by MRP2 activity ‡measured in the presence of GF120918. ND – not determined. Jmax is in units of pmol.cm^2.s.

The key aims of this chapter are to quantify the P-gp abundances using QTAP techniques in Caco-2 cells postulated to possess different levels of P-gp, and to determine if the relationship between P-gp activity and abundance is linear for the P-gp probe compound VBL in each Caco-2 cell variant. In addition to low and high passage Caco-2 cells, this study also uses cells which are cultured in the presence of VBL within the growth media. This culturing regimen has been consistently shown to select Caco-2 cells possessing higher levels of P-gp, while those cells with lower P-gp levels do not survive the cytotoxic effects of VBL treatment (Anderle et al., 1998; Laska et al., 2002; Shirasaka et al., 2006; Siissalo et al., 2007). A compartmental modelling approach to describe the three-compartment Transwell system in which VBL transport is performed will be used to determine 'drug parameter' estimates. Establishing if linear/non-linear relationships between transporter activity and abundance exist, should provide invaluable information as to whether the commonly employed linear scaling approach (REF) is sufficient for transporter-based IVIVE.

7.2 Methods

The finalised methods employed in Chapter 7 are described in detail in Sections 2.2.1 for basic cell culture conditions, Section 2.2.2.2 for obtaining Caco-2 cell membrane fractions. Bertin Pharma (BPh) protein abundance analysis is described in Section 2.2.8.6. Section 2.2.9 describes the analysis of transporter gene expression. The basic protocol for the monolayer transport assay is described in Section 2.2.10. The estimation of active transport kinetic parameters and the $P_{Passive}$ of VBL in Caco-2 cells by simultaneous fitting in a three-compartment model are described in Section 2.2.12. Additional methodological details for VBL transport assays are given in Section 7.2.1.

7.2.1 Bi-directional Monolayer Transport Assay: VBL Transport

[^{3}H]-VBL transport was assessed in three Caco-2 cell monolayer variants:

1. ATCC-HTB-37, passage 25-35, purchased at passage 18 and cultivated solely by the 'candidate'.
2. High passage Caco-2 cells (passage 100+) were revived from cryogenic storage at passage 100 for use in studies presented in this chapter.
3. Caco-2-VBL cells were generated as described in Section 2.2.1 and cryogenically stored in Dr Geoffrey Warhurst's laboratory until revival for usage in studies presented in this chapter.

The transport buffers consisted of HBSS-HEPES (25 mM) pH 7.4 or HBSS-MES (10 mM) pH 6.5 and were performed with a pH gradient, *i.e.,* pH 6.5 in the apical chamber and pH 7.4 in the basolateral chamber, or without a pH gradient with transport buffer at pH 7.4 in both chambers of the Transwell system. As described in Section 2.2.10, monolayer integrity was monitored by LY transport (50 µM) bi-directionally. Bi-directional transport of the P-gp probe VBL was undertaken at 9 concentrations (0.03-to-1000 µM). For transport assays carried out at 0.03 µM VBL, [^{3}H]-VBL stock was solely used, with DMSO (0.1% v/v) as a vehicle control. For all higher concentration VBL experiments, the [^{3}H]-VBL stock and VBL dissolved in DMSO was used to achieve the starting VBL concentrations. DMSO did not exceed 0.2% (v/v) in any transport experiment. The maximum nominal concentration of VBL in the B-to-A direction (donor pH 7.4) was 250 µM due to the solubility limitations at high concentrations. At pH 6.5 no solubility limits were reached. To assess the specificity of P-gp-mediated VBL transport and to estimate the $P_{Passive}$, transport experiments performed with 0.03 µM VBL, were also incubated with the P-gp inhibitor verapamil (100 µM). Monolayers were pre-incubated with verapamil for 30 min prior to initiation of the transport

experiment with VBL. The transport assay was initiated by the addition of the [^{3}H]-VBL-laden transport buffer to the requisite side of the monolayer and insertion into the orbital rotating incubator at 100 rpm and 37°C. The duration of the assay was 60 min. Donor samples (100 µL) were taken separately for LSC counting of [^{3}H]-VBL and fluorescent monitoring of LY at the start and end of the experiment, with replacement of the donor buffer immediately. Receiver chamber samples were also taken at 5, 15, 25, 40, and 60 min for [^{3}H]-VBL and LY monitoring (100 µL for each) and the relevant transport buffer (200 µL) was replaced immediately. The Papp and monolayer contents were calculated as described in Section 2.2.10.1. The concentration of VBL (pmol/L) was obtained from calculating the activity of VBL in the initial donor sample in counts/min and correcting for the notional micromolar concentration of VBL (tritiated and non-tritiated) in the donor solution. The resulting counts/micromolar, was used to calculate the VBL concentration (pmol/L) for each chamber which was used for obtaining $P_{Passive}$ and kinetic parameter estimates in a three-compartment model (described in Section 2.2.12).

7.3 Results

The low passage Caco-2 cell line (P25-35) previously described in Chapter 5 together with a high passage (P105-P115) and VBL-selected Caco-2 cells (Caco-2-VBL, P113(+11)-P120(+18)) were used investigate the effects of long term culture and the promotion of transporter selection via cytotoxicity using the P-gp probe VBL.

7.3.1 Characteristics of Caco-2 Monolayers

As a QC, the integrity of the monolayers was routinely monitored by TEER over the cultivation period and by the paracellular marker LY throughout the transport assay. A TEER plateau was typically reached at 7 days, indicating confluence was reached (Figure 7-2).

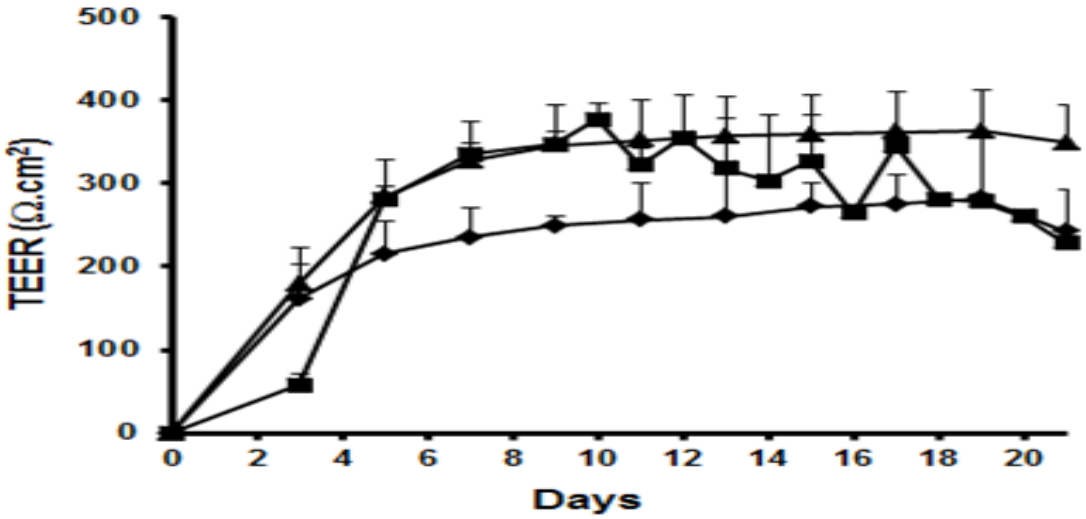

Figure 7-2. Assessment of monolayer integrity and growth by TEER for all variant Caco-2 cell monolayers N=29 plates. This includes the TEER prior to RNA harvesting in addition to transport experiments. Low passage (triangles), high passage (diamonds) and Caco-2-VBL (squares).

The mean end point TEER and LY Papp for Caco-2 monolayers are provide in Table 7-2.

Table 7-2. Endpoint TEER and LY permeability in filter-grown Caco-2 cell monolayers at 21 days.

	Caco-2 Cell Variant (all 21d cultivated)		
	Low Passage	High Passage	VBL-Selected
TEER ($\Omega.cm^2$)	346*** (± 36)	231 (± 47)	230 (± 67)
LY Papp	0.23 (± 0.13)	0.15*** (± 0.13)	0.25 (± 0.23)
(x 10^6 cm sec^{-1})	N=9 (n=78)	N=9 (n=78)	N=11 (n=65)

***, significantly different (p=<0.001) from other groups. Differences between groups tested by 1-way ANOVA with Bonferroni (all group) post-hoc analysis to test for differences between groups. N denotes experimental plates and n denotes filters.

Low passage Caco-2 cell monolayers showed significantly higher TEER's than the other groups (p=<0.001, 1-way ANOVA). In contrast, the high passage Caco-2 cell monolayers demonstrated

significantly lower LY permeability than the other groups (p=<0.001, 1-way ANOVA), although all three groups were within integrity cut-off limits for LY transport (Section 2.2.10.1). It should be noted that verapamil incubation elicited a rise in TEER, likely to be due to its Ca^{2+} channel blocking effects.

7.3.2 Transporter Gene Expression Analysis in Caco-2 Cell Variants

Transporter mRNA gene expression levels were compared to the housekeeper protein PPIA as described in Section 5.3.2. The expression of PPIA between the Caco-2 cell variants was stable (cycle threshold range-19.6-to-20.1, for all cell variants) confirming the utility of this housekeeper protein for analysis of relative transporter mRNA gene expression in these cells.

The relative gene expression levels of the ABC transporters MDR1, MRP2 and BCRP in the 21 day grown Caco-2 cell monolayer variants are provided in Figure 7-3. As expected, the MDR1 mRNA levels in Caco-2-VBL cells are significantly higher (p=<0.01, 1-way ANOVA) than either the normal low or high passage Caco-2 cells. The mRNA expression of BCRP in the low passage cells is 4-fold higher than the high passage Caco-2 cells and 10-fold higher than the Caco-2-VBL cells (p=<0.001, 1-way ANOVA), suggesting that culturing Caco-2 cells with VBL down-regulates BCRP transcription. MRP2 mRNA levels are reasonably consistent across the Caco-2 cell variants, with the low passage Caco-2 cells showing a 1.4-fold higher (p=<0.05, 1-way ANOVA) expression compared to high passage Caco-2 cells. There were no transcriptional effects of culturing with VBL on the levels of MRP2 mRNA.

7.3.3 Protein Abundance Analysis in Caco-2 Cell Variants

The protein abundance data for Na/K-ATPase and P-gp described in this section was generated by analyses performed by BPh. As a QC for TM and PM fractions, Na/K-ATPase abundances are described for all Caco-2 cell variants (Figure 7-4). There were no differences in Na/K-ATPase abundances between the Caco-2 cell variants. Only a modest enrichment in the proposed PM fraction was observed, which is consistent with data shown in Chapter 5 for low passage Caco-2 cells grown over varying periods. These data indicate that long term culture and VBL selection does not influence Na/K-ATPase abundance.

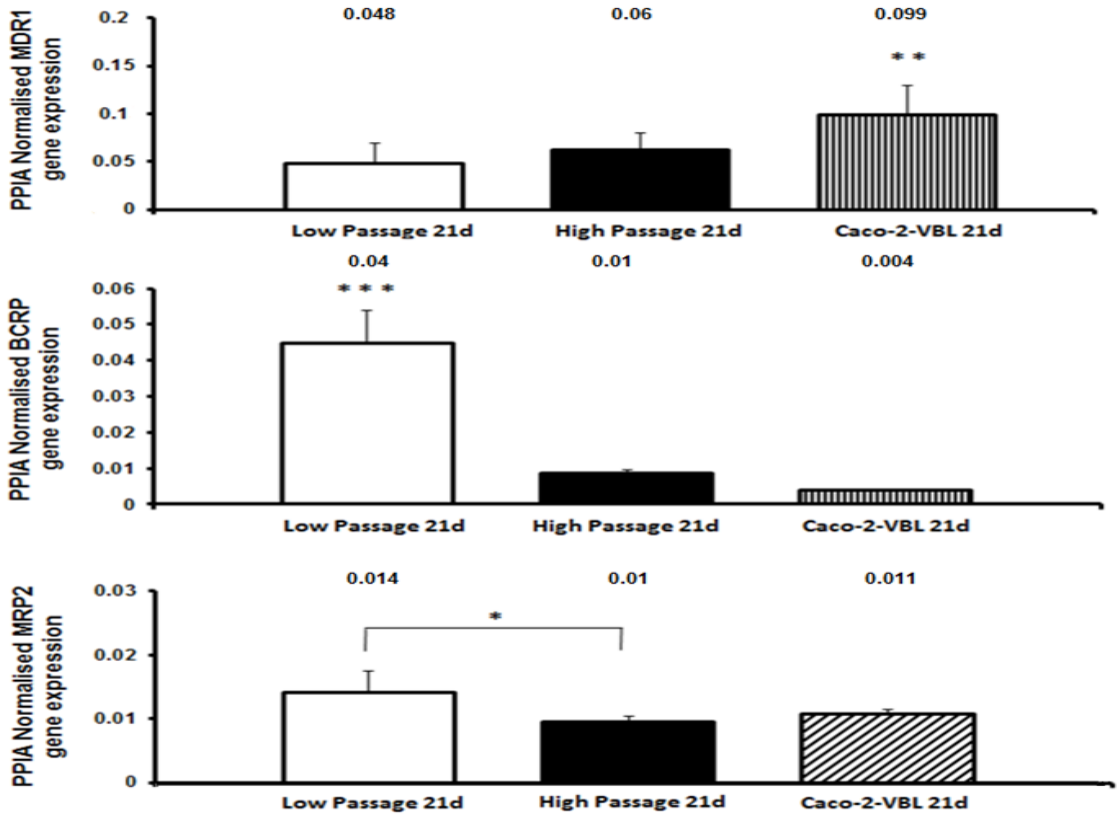

Figure 7-3. mRNA gene expression of MDR1 (A), BCRP (B) and MRP2 (C) in 21d cultured Caco-2 cells variants normalised to the housekeeper protein PPIA. Each bar represents n=3 separate mRNA extractions. Assays were conducted on 2 separate days in duplicate. The values are given as Mean±SD, with the text above the bars representing mean expression levels. * denotes p=<0.05, ** denotes p=< 0.01, *** denotes p=<0.001 determined by 1-way ANOVA with Bonferroni (all group) post-hoc analysis to test for differences between groups.

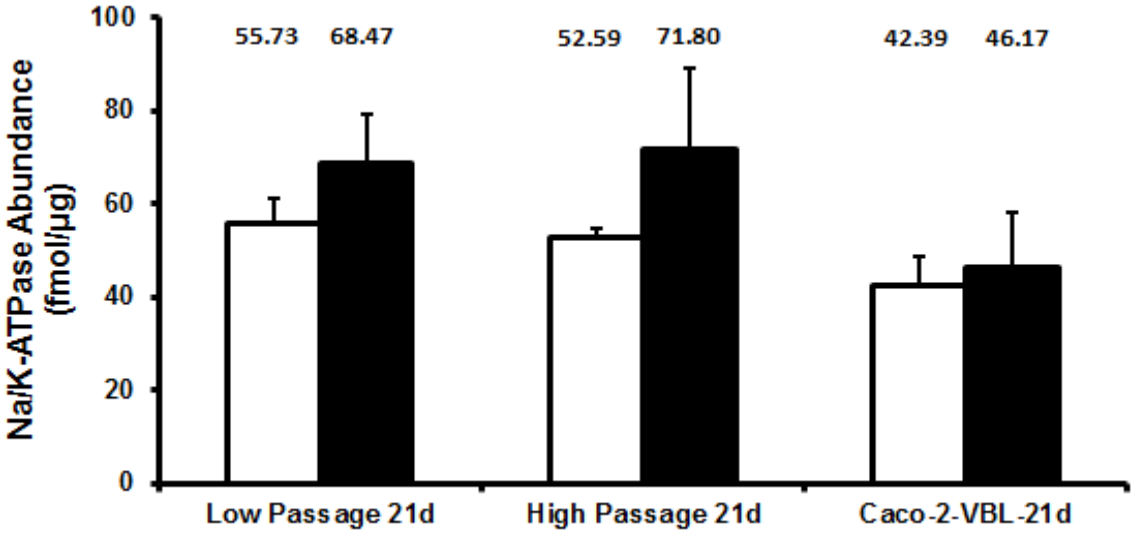

Figure 7-4.The absolute Na/K-ATPase protein abundance determined by Bertin Pharma analysis in all 21d cultured Caco-2 cell monolayers variants. The text above the TM (white) and PM (black) bars represents the mean values of n=3 experiments, except for the low passage 21d TM group which are represented by n=6 experiments. Values are given as Mean±SD.

The abundances of P-gp in 21 day cultured Caco-2 cells variants are described after analysis by BPh (Figure 7-5). There is a significantly higher P-gp abundance in Caco-2-VBL cell TM fractions

(p=<0.001, 1-way ANOVA), confirming the influence of culturing Caco-2 cells with VBL on promoting P-gp protein expression by cytotoxicity-based selection. These findings also match the higher mRNA expression observed in Caco-2-VBL cells compared to normal Caco-2 cells (Figure 7-3). However, from the mRNA data, it might be expected that the P-gp levels would be similar in low and high passage cells. Interestingly, the abundance of P-gp in high passage cells was significantly higher than low passage cells (p=<0.001, 1-way ANOVA). Unexpectedly, there was a significantly lower P-gp abundance (p = <0.01, Paired t-test) in the PM fraction of Caco-2-VBL cells that did not correlate to the membrane marker protein Na/K-ATPase, which was previously shown not to be difference in both these fractions (Figure 7-4). The full data set of Na/K-ATPase and P-gp abundances is provided in Appendix Table G-1 & Appendix Table G-2.

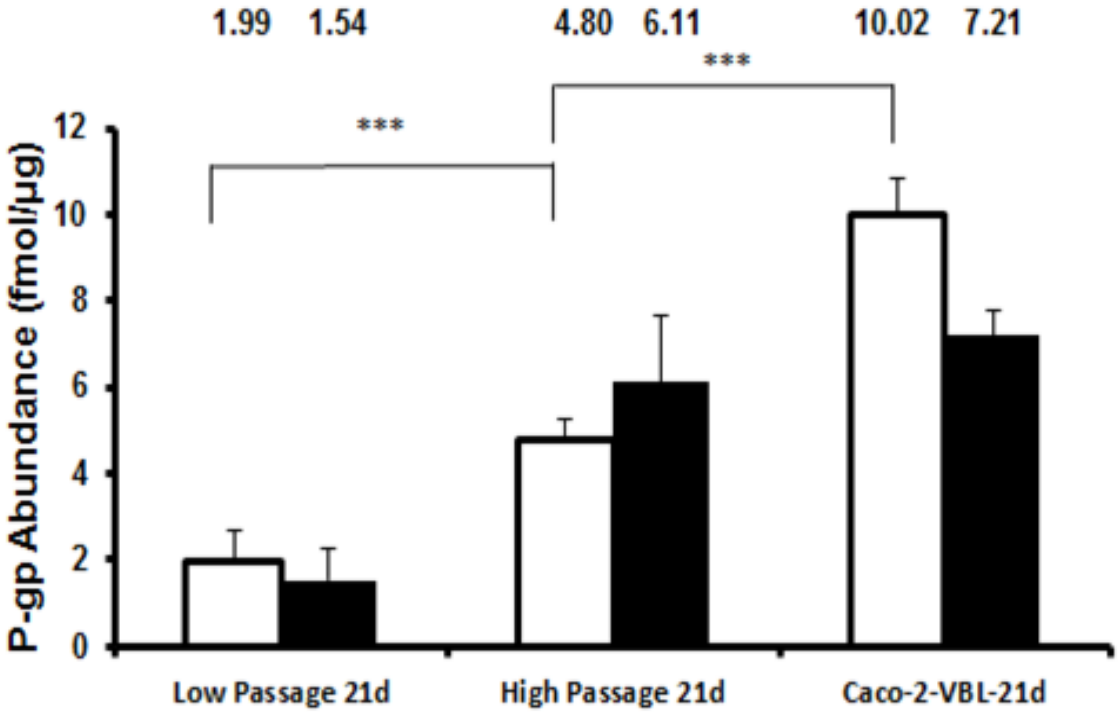

Figure 7-5. The absolute P-gp protein abundance determined by Bertin Pharma analysis in all 21d cultured Caco-2 cell monolayers variants. The text above the TM (white) and PM (black) bars represents the mean values of n=3 experiments, except for the low passage 21d cells TM group which are represented by n=6 experiments. Values are given as Mean±SD. *** denotes p=<0.001 as determined by a 1-way ANOVA with Bonferroni (all group) comparison post-hoc analysis to test for differences between groups.

7.3.4 VBL Transport in Caco-2 Cell Variants

Preliminary experiments focussed on determining bi-directional VBL transport in the presence of the P-gp inhibitor verapamil. The bi-directional permeability of VBL (0.03 µM), in the presence and absence of verapamil (100µM) performed for 120 min (6 samples taken over experimental duration) at pH 7.4 in both Transwell chambers is shown for 21d-grown cells (Figure 7-6). A 4.8-fold higher permeability in the secretory (B-to-A transport) when compared to the absorptive

direction (A-to-B transport) is observed. This ER is abolished in the presence of the P-gp inhibitor verapamil, suggesting that P-gp is responsible for driving the secretory process in Caco-2 cells. This data also suggests that if verapamil inhibits all active processes responsible for VBL transport across Caco-2 cell monolayers, the $P_{Passive}$ is approximately 10.5 x 10^{-6} cm sec^{-1}.

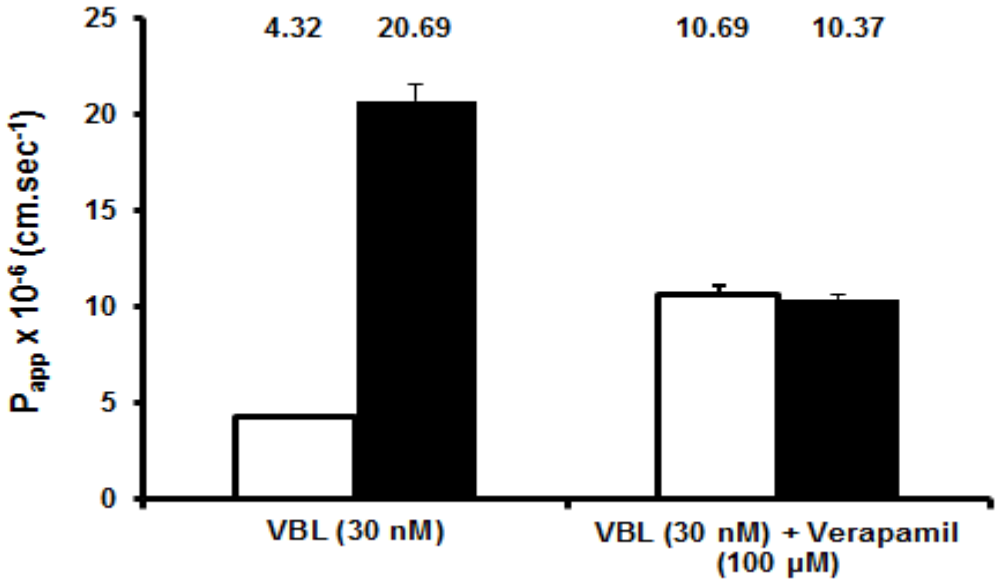

Figure 7-6. Transport of VBL (0.03 µM) in A-to-B (white) and B-to-A (black) transport directions across 21d cultured Caco-2 cell monolayers in the presence and absence of verapamil (100 µM). The text above the bars is the mean Papp under each condition. The values are Mean±SD of n=3 filters for each condition.

The transport of VBL (0.03 µM, over 60 min) in the presence and absence of verapamil (100 µM) was undertaken for all Caco-2 cell variants in a pH gradient system (apical pH 6.5, basolateral 7.4) as performed by Shirasaka and colleagues (Shirasaka et al., 2008). The observed VBL (0.03 µM) ER for Caco-2 cell variants was 2.86, 5.81 and 11.61 in low, high and Caco-2-VBL cells, respectively (Figure 7-7). The ER's approximated more closely to the different protein abundances of P-gp in each variant cell line (Figure 7-5, Table 7-3), rather than P-gp mRNA expression. In contrast to the pH 7.4/7.4 assay (Figure 7-6), verapamil incubation did not completely abolish VBL efflux, ranging from a residual ER of 1.3-fold in low passage cells to 2.45-fold in VBL-selected cells (Figure 7-7). This may indicate that a pH gradient has an effect on VBL transport due to the greater ionisation of this dibasic compound in the apical pH 6.5 buffer to limit $P_{passive}$ in the absorptive compared to the secretory direction, according to the pH-partition hypothesis (Neuhoff et al., 2003). Moreover, MRP2 may also play a smaller role in VBL efflux after verapamil inhibition.

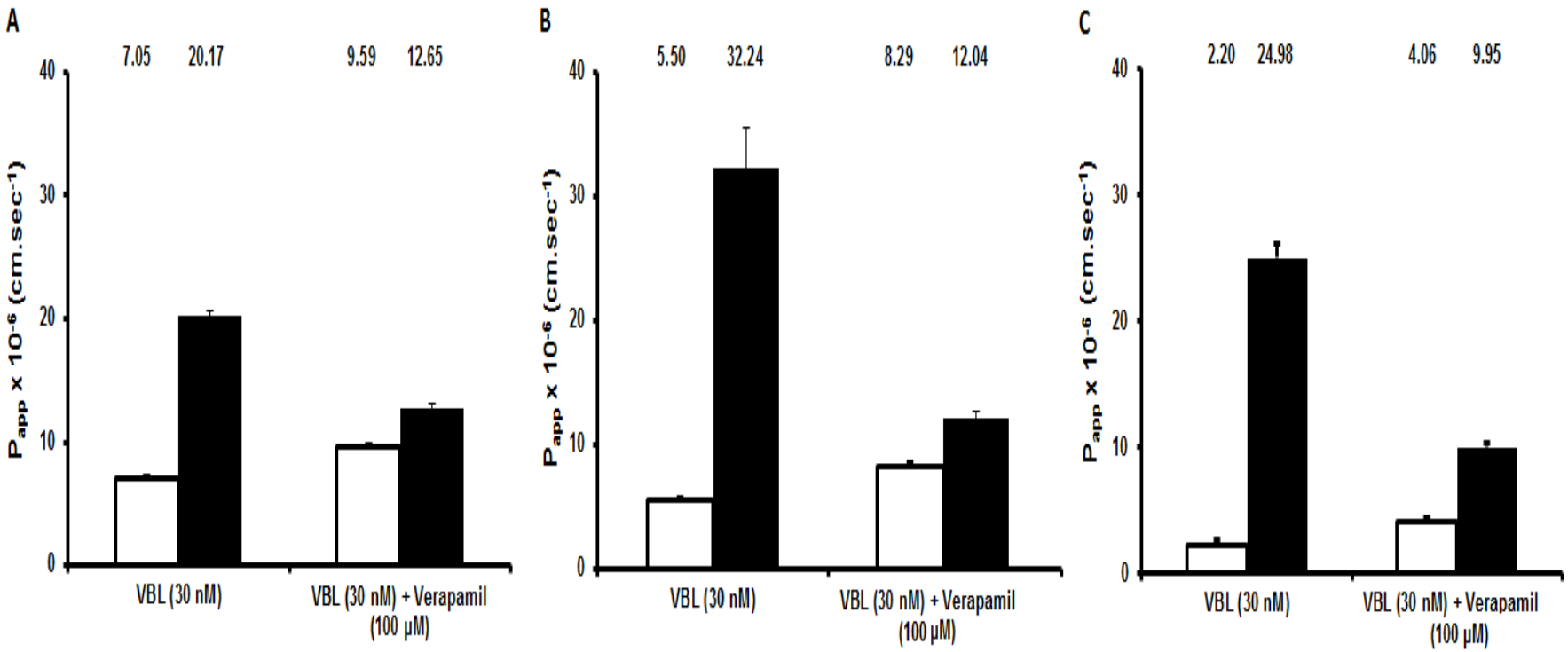

Figure 7-7. Transport of VBL (0.03 µM) in A-to-B (white) and B-to-A (black) transport directions across 21d cultured Caco-2 cell monolayers (all variants) in the presence and absence of verapamil (100 µM). A, low passage, B, high passage and C, VBL-selected Caco-2 cell monolayers. The text above the bars is the mean Papp under each condition. The values are Mean±SD of n=3 filters per condition.

Table 7-3. The relationship between VBL efflux ratio, P-gp total membrane protein abundance and mRNA expression in all Caco-2 cell variants.

Caco-2 Cell	[^{3}H] VBL Efflux Ratio (pH6.5/7.4)	P-gp mRNA Expression (Relative Units to PPIA)	P-gp Protein Abundance (fmol/µg)
Low Passage	2.86 (±0.15)	0.048 (± 0.021)	1.99 (± 0.71)
High Passage	5.87 (±0.66)	0.06 (± 0.018)	4.8 (± 0.48)
VBL-Selected	11.61 (± 2.52)	0.099 (± 0.031)	10.02 (± 0.84)
Fold Difference			
High/Low	**2.05**	1.25	**2.41**
VBL/Low	**4.06**	2.06	**5.04**
VBL/High	**1.98**	1.65	**2.09**

To ascertain whether MRP2 was responsible for the residual ER after verapamil incubation, the specific (*i.e.,* does not inhibit P-gp or BCRP) MRP2 inhibitor lansoprazole (Matsson et al., 2009), was incubated with VBL and verapamil in low passage Caco-2 cells. The VBL ER, when incubating with both verapamil (100 µM) and lansoprazole (100 µM), actually increases, ER of 2.64, (Figure 7-8) when compared to the residual ER of 1.32, (Figure 7-7). Interestingly, the A-to-B transport was not affected by incubations with both inhibitors. These findings suggest that MRP2 has little involvement in the transport of VBL at the low concentrations given in these experiments and may indicate that lansoprazole impacts on another transporter with an, as yet, unidentified role in the transport of VBL.

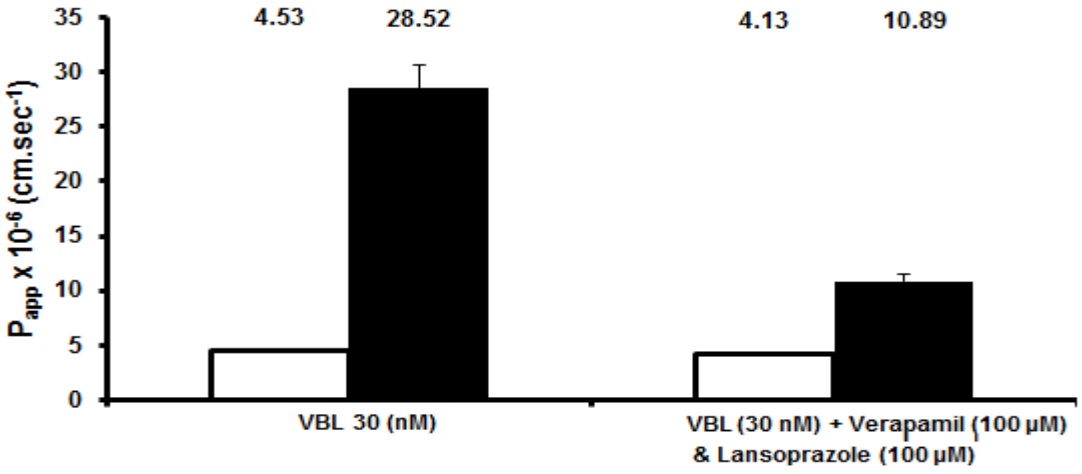

Figure 7-8. Transport of VBL (0.03 µM) in A-to-B (white) and B-to-A (black) transport directions across 21d cultured Caco-2 cell monolayers in the presence and absence of verapamil (100 µM) and lansoprazole over 60 min. The text above the bars is the mean Papp under each condition. The values are Mean±SD of n=3 filters for each condition.

To enable the relationship between mRNA, protein and the kinetic parameters for VBL to be established, each Caco-2 cell monolayer variant was incubated with increasing concentrations of VBL (0.03–to-1000 µM) with bi-directional transport monitored. For the B-to-A transport, the upper VBL concentration limit was found to be 250 µM; above this concentration VBL was insoluble. The permeability profile of each Caco-2 cell variant with increasing VBL concentrations is provided in Figure 7-9. A similar bi-directional concentration dependency was shown for low and high passage Caco-2 cells, whereas the Caco-2-VBL cells while showing a saturable effect in both transport directions failed to yield a unity in bi-directional permeability with a residual ER of 8.2 at 250 µM. Under the assumption that active transport is saturated at concentrations of 250 µM and above for the low and high passage cells, the $P_{passive}$ is estimated to be 10.7 and 8.25 x 10^{-6} cm sec^{-1} similar to that for the pH7.4/7.4 VBL transport assay with verapamil incubation (Figure 7-6). The saturation of active transport was more evident in the B-to-A compared to the A-to-B direction, in which an increase in the apparent permeability of VBL of less than 2-fold was determined over the concentration range. It is also noticeable that for both the low and high passage cells at VBL concentrations less than 10 µM are approximately 5-6 fold higher than those in Shirasaka et al., which may have resulted from the absence of stirring in their study (Shirasaka et al., 2008).

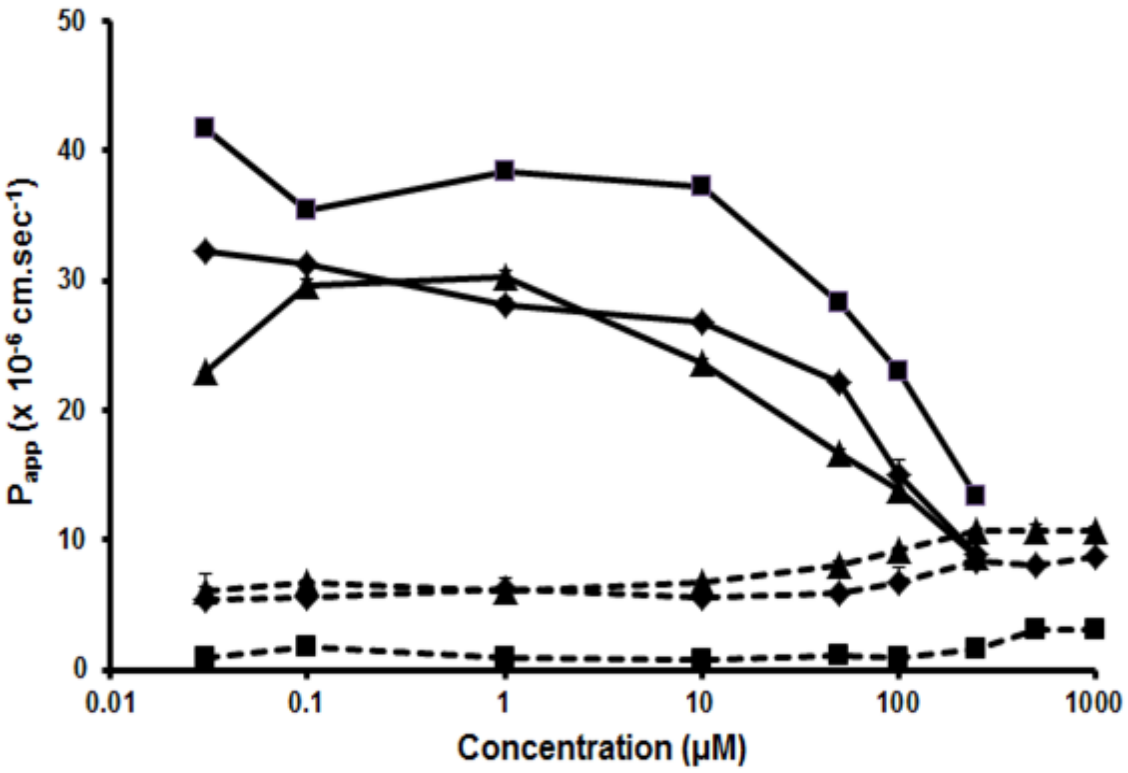

Figure 7-9. The A-to-B (dashed lines) and B-to-A (solid lines) transport of VBL at increasing concentrations increasing concentrations in 21d filter-grown Caco-2 cell variants. Low passage (triangles), high passage (diamonds) and Caco-2-VBL (squares) monolayers are shown as Mean±SD of n=3 filters for each condition.

7.3.5 Permeability and Kinetic Estimates of VBL by Compartmental Modelling

A three-compartment model describing the Transwell experimental system of each cell variant was used to estimate $P_{passive}$ and the active kinetic parameters CLint, Jmax, Km for a single apical membrane efflux component. The structural components describing the experimental system and entered into the model as the known or 'fixed' parameters, together with the initial estimates of the unknown or 'floating' parameters which require estimation from the statistical fitting procedure, are provided in Table 7-4. The volume of the cell monolayer is estimated from whole cell lysate data determined by BCA assay for each Caco-2 cell variant (Figure 3-11), using a conversion factor of 3.65 µL/mg protein (Burnham and Fondacaro, 1989). The estimated pore radius of the monolayers was based on the relationship between LY permeability and pore size (Equation 7-1) determined by Saitoh et al., (Saitoh et al., 2004). Using the LY permeability described in Table 7-2, the pore radius for each Caco-2 cell monolayer ranged from 5.38 to 5.68 Å. Given that the radius of VBL is 10 Å (Modok, 2010), it was assumed that VBL transport through the paracellular tight junction route was negligible. The expression levels of the CYP3A enzyme family in Caco-2 cells are very low under normal culture conditions (Cummins et al., 2001), therefore the metabolism of VBL by the CYP3A family of enzymes (Zhou-Pan et al., 1993) is also assumed to be negligible.

$$Pore\ Radius = 2.94 \cdot 10^{6} \cdot P_{LY} + 4.94$$ Equation 7-1.

Initial simulations focussed on estimating $P_{passive}$ using the experimentally obtained VBL concentrations in the donor (time=0 min) and for the 5 samples in the receiver compartments under verapamil incubation conditions. The fitting procedure was performed simultaneously on A-to-B and B-to-A transport with apical efflux CLint set to zero. The best model fits were found when the model only accounted for a single membrane, *i.e.,* the permeability at the apical and basaloteral membranes of the Caco-2 cell monolayers were assumed to be equal. Poorer fits of the observed data were found when the unionised fractions (fui) in each compartment and binding to filter were incorporated (data not shown). Furthermore, applying a 3-fold higher surface area to the basal membrane (Trotter and Storch, 1991), as undertaken previously when modelling VBL transport in Transwell systems by compartmental modelling (Sugano et al., 2011), did not provide a better fit of the data (data not shown). However, an improved fit was found when accounting for the dilution after sampling when replacing with blank transport buffer in the receiver compartments. The estimates for $P_{Passive}$ (Table 7-5) in all Caco-2 cell variants were at least 3-fold higher than the experimental estimates, which might suggest that the three-compartment model is too simple to

characterise all the components of the experimental system that influence the $P_{Passsive}$ for VBL. An overall poorer fit of the observed data in the B-to-A direction compared to the A-to-B transport (GMFE = 1.05, low passage cells) was found which led to the GMFE's provided in Table 7-5.

Table 7-4.Three-compartment model structural parameters and initial drug parameter estimates.

Parameter	Value	Source	Comments
Fixed Parameters			
Apical Chamber Volume (µL)	400	Experimental	-
Basal Chamber Volume (µL)	1200	Experimental	-
Monolayer Volume (µL)		Experimental Protein Content	Conversion factor 3.65 µL/mg protein (Burnham and Fondacaro, 1989)
Low Passage	1.31		
High Passage	1.27		
Caco-2-VBL	1.07		
Surface Area (cm^2)	1.13	Experimental	Filter area
Unionised Fraction (fui)		Hendersson-Hasselbalch equation	– Dibasic pKa 5.4 & 7.57
Apical (pH 6.5)	0.105		
Cell (pH 7.4)	0.495		
Basal (pH 7.4)	0.495		
Fraction bound to filter (at 30 nM VBL)		Experimental	Estimated from blank filter assay
pH 6.5	0.92		
pH 7.4	0.97		
Initial Estimates – Floating Parameters			
$P_{Passive}$ (x 10^{-6} cm sec^{-1})		Experimental	Estimated in presence of Verapamil or ≥250 µM VBL
Low Passage	10.7		
High Passage	8.25		
Caco-2-VBL	7.25		
CLint (µL/min/cm^2)	10.42	Literature- (Korzekwa and Nagar, 2014)	Three-compartment model estimate
Jmax (pmol/min/cm^2)	41.4	Literature- (Korzekwa and Nagar, 2014)	Three-compartment model estimate
Km (µM)	3.97		

Table 7-5. Model estimates of $P_{Passive}$ after simultaneous fitting of bi-directional VBL data.

			Model Performance		
Cell Variant	**$P_{Passive}$ (x 10^{-6} cm sec^{-1})**	**Confidence Interval (5^{th}-95^{th})**	**GMFE**	**GMFB**	**RMSE**
Low Passage	32.5	30 - 36	1.32	1.12	0.0004
High Passage	29	27 - 32	1.18	1.06	0.0001
Caco-2-VBL	30.4	26 - 35	1.41	1.2	0.0008

Geometric Mean Fold Error (GMFE), Geometric Mean Fold Bias (GMFB), Root Mean Squared Error (RMSE)

The $P_{passive}$ estimates (Table 7-5) were used in subsequent simulations to estimate the kinetic parameters for all cell lines using the data from the bi-directional saturation curves (Figure 7-9). The CLint, Jmax and Km estimates, model performance metrics and P-gp abundances are provided in Table 7-6. Two separate simulations were performed for each cell variant, the first was to estimate a CLint where the Jmax and Km terms described in Equation 2-6 & Equation 2-7 were replaced with CLint and the second estimated Jmax and Km simultaneously. The GMFE ranged from 1.18 to 1.58 with a good prediction of observed VBL concentrations in the basolateral receiver chamber (*i.e.,* A-to-B transport). However, for the apical chamber (B-to-A transport), the model could not capture the observed VBL profiles in lower VBL concentration filters (Figure 7-10) using the globally identified solution, which may owe to the complexity of the dataset, *i.e.,* VBL concentrations spanning 7-orders of magnitude. An overview of the goodness of fit across the span of experiments is shown in Figure 7-11. Overall, the estimates for CLint matched to the ranking of P-gp abundance for each cell variant. However, there were considerable inconsistencies in model estimates for the Jmax and Km between the different Caco-2 cells, highlighted by a 6.5-fold difference in Km, which is a considerable range for this notional biochemical constant. This may be due to the limited saturation observed for A-to-B permeability profiles upon application of increasing concentrations of VBL, providing a challenge to the model to identify a consistent estimate of Km, particularly for high passage and Caco-2-VBL cells. Further simulations were performed using the A-to-B or B-to-A data, independently fitted. When only the A-to-B data was fitted, the model could not estimate the kinetic parameters with any certainty, in many cases the CLint and Jmax reached the lower boundary constraints set within the model. This may indicate that $P_{Passive}$ is sufficient to capture the observed data. In contrast, the CLint estimates were substantial, approaching $1x10^6$ µL/min using only the B-to-A transport data, yet the model still underestimated the observed data, while the Km value was estimated with considerable uncertainty, Km=0.0002 µM (CV ~$1.8x10^5$%).

The efficiency of VBL transport by P-gp was evaluated by correcting the CLint and Jmax from bi-directional inputs, by the P-gp abundance to obtain an estimate of transport per unit mole of protein. It is clear when assessing P-gp corrected CLint that there is a diminished function of P-gp-dependent VBL transport in high passage Caco-2 cells compared to the other variants. The Caco-2-VBL cells also display 1.7-fold higher P-gp corrected CLint compared to low passage cells. The generation of catalytic rate constants (K_{CAT}) from the P-gp corrected Jmax data are questionable given the reliance of Jmax estimates on simultaneous fitting of Km. Therefore, the assertion that a 'functional redundancy' is operating for P-gp-dependent VBL transport in cells containing varying levels of P-gp may not hold true across different laboratories.

Table 7-6. Kinetic parameter estimates from simultaneous fitting by a three-compartment model and their relationship to P-gp abundance.

				Model Performance			Abundance-Activity Relationship		
Cell Variant	**Parameter**	**Estimate**	**Confidence Interval (5^{th}-95^{th})**	**GMFE**	**GMFB**	**RMSE**	**P-gp Abundance (fmol/µg)**	**CLint/P-gp (µL/min/pmol)**	**P-gp K_{CAT} (pmol/min/pmol)**
Low Passage	CLint (µL/min)	**3.05**	2.65 - 3.45	1.36	1.1	2.16	**1.99**	**1.53**	**-**
	Jmax (pmoL/min)	**73.39**	40.91 - 105.87	1.33	1.05	1.81		**2.51***	**36.69**
	Km (µM)	**14.76**	7.27 - 22.25						**-**
High Passage	CLint (µL/min)	**3.43**	2.96-3.9	1.18	1.06	1.73	**4.8**	**0.71**	**-**
	Jmax (pmoL/min)	**380.94**	136.8 - 598.42	1.44	1.23	1.49		**3.97***	**79.36**
	Km (µM)	**95.89**	26.1 – 156.8						**-**
Caco-2-VBL	CLint (µL/min)	**26.3**	24.31 - 28.3	1.58	1.04	1.61	**10.02**	**2.62**	**-**
	Jmax (pmoL/min)	**1989**	1723 - 2255	1.49	1.08	1.78		**36.23***	**195**
	Km (µM)	**54.89**	45.6 – 64.2					-	

*Denotes CLint (µL/min**)** determined from ratio of the estimated Jmax (pmol/min) and Km. K_{CAT} catalytic rate constant for P-gp, ratio of Jmax to P-gp abundance.

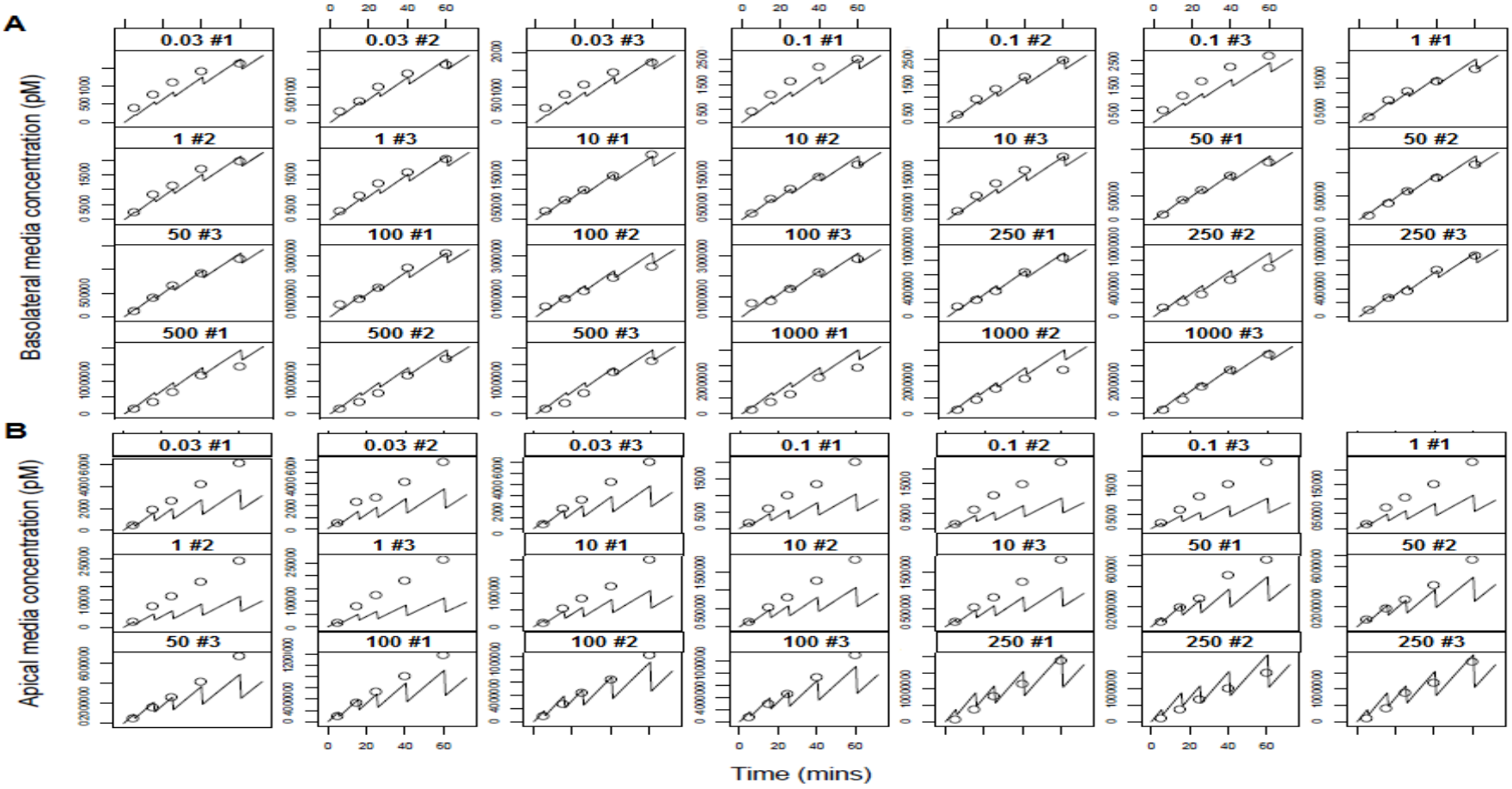

Figure 7-10. Bi-directional fitting of VBL in the receiver chamber of a Transwell Caco-2 cell (low passage) system using a three-compartment model. A, shows the fitting of VBL at all concentrations (0.03–1000 μM, triplicate filters) in the basolateral chamber (A-to-B transport direction). B, shows the fitting of VBL at all concentrations (0.03–250 μM) in the apical chamber (B-to-A transport direction, triplicate filters). The open circles denote experimental VBL concentrations while the lines represented simulated values. The concentrations and filter replicate number are given above each individual plot.

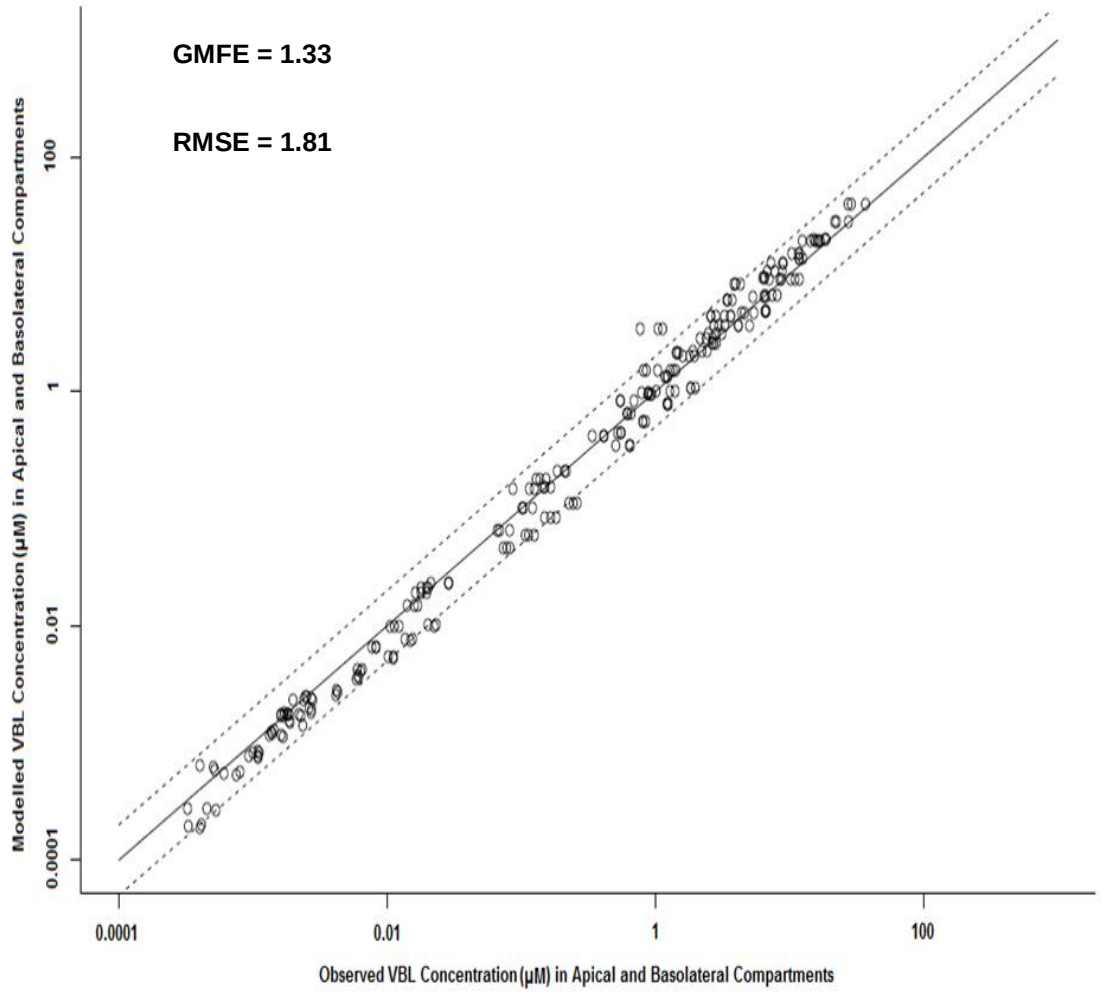

Figure 7-11. Observed and model predicted VBL concentrations following simultaneous fitting of bi-directional transport in low passage Caco-2 cell monolayers. This is an example of a procedure to estimate Jmax and Km. The solid line represents unity and the dashed line represents 2-fold either side of unity.

7.4 Discussion

Scaling factors bridging any mechanistic differences between the *in vitro* and *in vivo* system are routinely employed in IVIVE-PBPK. Recombinant systems engineered to possess high levels of CYP450 enzymes are a fundamental tool for the drug discovery pipeline to identify the enzymes responsible for a compounds metabolic turnover (Chen et al., 2011). The development of the ISEF scaling factor (Proctor et al., 2004), corrects for differences in the activity per unit of enzyme in recombinant systems compared to human liver microsomes. Investigations to establish whether a similar approach was required for transporter-based IVIVE scaling were therefore proposed (Harwood et al., 2013). In this study, it was confirmed by QTAP methods that Caco-2 cells differing by >75 passages and those selected for P-gp by cultivation in media containing VBL, possessed significantly different abundances of P-gp. Differences in P-gp protein abundance between cells appeared to be more closely related to the ER of the P-gp probe VBL, than to MDR1 mRNA levels. Finally, the relationship between P-gp abundance and function was described after estimating the transporter kinetics and $P_{Passive}$ using a compartmental modelling approach. The rank order of CLint estimates between cell variants matched the respective P-gp abundances, however when corrected for the P-gp abundance, a lower VBL-CLint per pmol of P-gp in high passage cells was found. In addition, rather than showing a functional redundancy, a greater CLint per pmol of P-gp was shown for the high P-gp expressing Caco-2-VBL cell line.

Caco-2 cell monolayers of passage numbers ranging from 20 to 116 are used for permeability/transport assays (Thwaites et al., 2002; Miliotis et al., 2011b). Higher passage Caco-2 cells have shown a tendency for higher TEER compared to their lower passage counter-parts (Lu et al., 1996; Briske-Anderson et al., 1997; Yu et al., 1997; Sambuy et al., 2005). However, work presented here shows similarities to the study of Behrens, et al., (Behrens et al., 2004) in which TEER was lower in Caco-2 cells cultivated over 26 passages. It is assumed cell density is the same from both low and high passage Caco-2 cells given the similarity in protein content from cell lysates (Figure 3-11). Given that TEER was shown to be inversely related to the paracellular permeability of the monolayer integrity marker mannitol (Briske-Anderson et al., 1997), the finding that high passage Caco-2 cells exhibited lower TEER's and lower LY transport compared to low passage Caco-2 cells was unexpected. Similarly, the TEER of VBL selected cells resembled that of the high passage normal Caco-2 cells, while LY transport was similar to the low passage cells. The measurement of TEER with chopstick electrodes may be relatively imprecise, while LY integrity

may be considered a more robust measure of monolayer integrity. Yet, there is little data in the literature outlining any monolayer integrity differences for Caco-2 cells undergoing VBL selection pressure in respect to counter-part controls. Nevertheless, the monolayer integrity markers were well within the cut-off limits for this study. The influence of inter-laboratory differences in cell culture technique can have a considerable impact on Caco-2 phenotypic traits (Hayeshi et al., 2008), therefore it is perhaps not unexpected to observe such differences in markers of monolayer integrity between studies.

To examine the expression levels of MDR1/P-gp between the Caco-2 cell variants, their relative mRNA gene expression and absolute abundances were determined. Previous work with Caco-2 cells from other groups, have found that filter-grown Caco-2-VBL cells exhibited a 2.8 and 5.5-fold higher MDR1 mRNA expression compared to wild type non-selected controls (Shirasaka et al., 2006; Siissalo et al., 2007). These increases were higher than found in this study, which show a maximum 2-fold higher expression of MDR1 in Caco-2-VBL cells. However, it was reported in the study of Sissalo et al., (Siissalo et al., 2007), that the extent of increasing expression could be dependent on the baseline MDR1 mRNA levels, which were shown to be considerably more variable in normal compared to Caco-2-VBL cells. Thus, in this study, the normal Caco-2 cells may be expressing relatively high baseline levels of MDR1/P-gp, resulting in a modest increase in MDR1 expression. There is an agreement when comparing the rank order of mRNA gene expression to P-gp protein abundance in the TM fraction for the three cell variants. However, based on a linear relationship of MDR1 mRNA expression to P-gp protein abundances, it was expected that P-gp abundance in low passage cells would be higher. Two and 5-fold higher P-gp protein abundances were found in the TM fraction of Caco-2-VBL cells compared to high and low passage cells, respectively. To date, there are no other studies reporting the impact of VBL-selection pressure on P-gp absolute abundance in Caco-2 cells. In the pioneering work of Anderle et al., (Anderle et al., 1998), cultivation of undifferentiated Caco-2 cells with VBL, elicited a 7.5-fold increase in P-gp expression, as determined by confocal laser scanning microscopy. In differentiated Caco-2 cells grown on filters for 5-days, a 3.9-fold increase in P-gp expression was measured after immunoblot densitometry analysis (Shirasaka et al., 2008). Yet, the findings of Shirasaka et al., 2008 were from Caco-2 cells monolayers undergoing a short term culture regime (5 day cultivation) therefore, the findings presented here may not be entirely comparable to their work. It also interesting that there were reduced levels of P-gp in the PM fraction relative to the TM fraction. This finding was not anticipated as confocal microscopy showed that P-gp was

predominantly localised on the apical membrane in Caco-2-VBL cell monolayers (Laska et al., 2002) and may indicate selective loss of P-gp protein in the final stages of fractionation, as similar losses were not observed for Na/K-ATPase. This is contrary to the recent findings of Kumar et al., (Kumar et al., 2015), who demonstrate that drug transporter protein abundances correlated to Na/K-ATPase abundances in liver tissue and a MDCK-II cells using a commercially available plasma membrane kit. This difference may be due to the dissimilar fractionation methods or different cell lines used in both studies.

MRP2 is also postulated to play a role in VBL transport (Evers et al., 1998; Litman et al., 2000; Taipalensuu et al., 2004), therefore, it was interesting that VBL selection had little effect on MRP2 mRNA expression in Caco-2 cells. This is in agreement with other studies measuring MRP2 mRNA expression in Caco-2-VBL cell monolayers (Shirasaka et al., 2006; Siissalo et al., 2007). Yet, a clear increase in MRP2 expression is observed after immunoblotting Caco-2-VBL cell monolayers grown for up to 11 days (Laska et al., 2002). It would be interesting to perform further analysis of our Caco-2-VBL cells for MRP2 absolute abundances compared to normal controls. Consistent with our work, BCRP was down-regulated at the mRNA level after VBL selection (Siissalo et al., 2007), the mechanism responsible for this and the translation to BCRP protein abundance remains to be elucidated.

The ER's for the lowest concentrations of VBL were assessed in each Caco-2 cell variant to investigate the relationship of mRNA expression and P-gp abundance to function. The observation that the ER of VBL closely correlated with P-gp protein abundance in each cell variant suggests that determination of protein abundances are required in preference to mRNA expression for incorporation into IVIVE-PBPK modelling strategies for P-gp. Miliotis et al., showed in normal Caco-2 cells that there was a good agreement between digoxin ER and P-gp protein abundance (Miliotis et al., 2011b). These authors also commented that a similar relationship was observed for mRNA. However, when mRNA data presented in an associated poster from this group was evaluated, it seems clear that a better correlation between digoxin ER and P-gp protein absolute abundance than mRNA exists (Miliotis et al., 2011a).

According to the FDA's criteria for assessing transporter-mediated DDI risk, an ER of ≥2 within bi-directional transport assays, which reduces as a result of administration of a P-gp inhibitor, indicates the compound is a P-gp substrate (Zhang et al., 2010). Under the FDA's criteria, within our Caco-2 cell systems presented, VBL would be classified as a P-gp substrate. While the

exclusive transport of drug molecules by a single transporter protein is not necessarily commonplace (Lin et al., 2011), the presence of a residual ER at the lowest VBL concentration, after incubating with the P-gp, but not MRP2 inhibitor verapamil (Matsson et al., 2009), under pH gradient conditions, indicates another mechanism may be responsible for VBL efflux, such as MRP2 (Evers et al., 1998). However, in the low and high passage Caco-2 cells, a residual ER ≤1.45 after verapamil incubation indicates that the role of a transporter like MRP2 is limited compared to P-gp and may not warrant further investigation for DDI risk assessment according to the FDA guidelines. However, for Caco-2-VBL cells, the residual ER of 2.45 after verapamil incubation indicates a more prominent role for another transporter in VBL transport. Further studies, including measurement of MRP2 protein abundances in Caco-2-VBL-cells will be needed to clarify this. The role of MRP2 on VBL transport certainly appears to be accentuated in transfected MDCK-II-MRP2 cell lines understood to express relatively low levels of endogenous canine P-gp relative to MRP2, compared to the heterogeneous transporter expressing Caco-2 cell line (Evers et al., 1998; Taipalensuu et al., 2004). Nevertheless, even if MRP2 activity in the presence of normal P-gp expression is relatively low, its activity does require accounting for in a fully mechanistic IVIVE-PBPK modelling strategy. To confirm if MRP2 was responsible for the residual efflux in low passage Caco-2 cells after verapamil incubation, an assay to inhibit MRP2 was performed. Previous efforts failed to dissociate P-gp and MRP2-mediated VBL efflux using the P-gp inhibitor LY335979 and the P-gp, MRP2 and BCRP inhibitor MK571 in Caco-2 cells (Mease et al., 2012). Therefore, a strategy utilising a more specific MRP2 inhibitor was devised. Bromosulfalein is the compound showing the greatest inhibitory potential for MRP2 without affecting P-gp or BCRP (Matsson et al., 2009). In this case, bromosulfalein was not selected for MRP2 inhibition studies due to the red/orange colour it elicits when dissolved in buffer and its interference with LY-based monolayer integrity assessments. Therefore, lansoprazole was selected as the next best MRP2 inhibitor, which is postulated to not influence P-gp or BCRP function (Matsson et al., 2009). Incubation of VBL with both verapamil and lansoprazole increased the residual ER compared to assays in the presence of verapamil alone, which may indicate that MRP2 is not involved in VBL transport or that lansoprazole modulates the activity of MRP2 and other transporters. Evidence has shown that lansoprazole is also a potent Organic Cation Transporter (OCT) inhibitor (Nies et al., 2011), yet, OCT1-3 mRNA expression is low in Caco-2 cells (Hilgendorf et al., 2007; Ahlin et al., 2009), and was not above detection limits in an early QTAP transporter analysis of Caco-2 cell monolayers (Uchida et al., 2007). Differential ionisation of

in pH 6.5 and 7.4 buffers may also play a role in VBL $P_{Passive}$. The greater ionisation of this basic molecule at pH 6.5 might lead to lower a $P_{Passive}$ in the A-to-B versus the B-to-A transport directions, based on the pH partition hypothesis (Neuhoff et al., 2003). However, the mechanistic basis for these observations requires further investigation.

The complete abolition of the ER without a pH gradient (pH7.4-7.4) under verapamil incubation contrasted with the 1.3-fold residual ER observed under pH 6.5-7.4 assay conditions and may indicate the influence of ionisation on VBL $P_{Passive}$ (Neuhoff et al., 2003), reducing the role of transporter efflux to negligible levels in the presence of verapamil. The impact of ionisation on permeability could be accounted for in future studies by incorporating a Nerst-Planck framework into parameter estimations, as it is postulated that both the ionised and unionised molecular species permeate the lipid bilayer (Ghosh et al., 2014).

To investigate the impact of transporters on drug disposition within PBPK models, the activity of each transporter isoform is modelled based on Michealis-Menten model kinetic parameter estimates Km, Jmax or CLint (Bolger et al., 2009; Darwich et al., 2010; Neuhoff et al., 2013). There have been a host of studies in which apical membrane-based efflux kinetic parameter estimates for VBL in Caco-2 cell monolayers have been performed (Hunter et al., 1993; Cavet et al., 1996; Tang et al., 2002b; Tang et al., 2002a; Shirasaka et al., 2008; Tachibana et al., 2010; Korzekwa and Nagar, 2014). However, the study of Shirasaka et al., 2008 was the basis of the VBL concentrations and pH conditions used within this study due to the striking saturation of A-to-B VBL transport at concentrations ranging from 10-1000 µM VBL at pH 6.5. For the kinetic studies preceding Shirasaka et al., the maximum concentration of VBL used was 150 µM which is likely to be due to the solubility limits at VBL concentrations greater than 150-250 µM at pH 7.4, as observed in this study. However, there are some potentially important methodological differences between Shirasaka et al., and the study presented here. A short term Caco-2 cell cultivation period (5 days) with specialised differentiation medium containing butyric acid was used prior to transport assay initiation in Shirasaka et al.,. This protocol provided improved P-gp activity in Caco-2 monolayers compared to a 21d growth protocol (Yamashita et al., 2002), which may due to the transcriptional activation effects of sodium butyrate (Cummins et al., 2001). In contrast, a more commonly used 21 day cultivation period was used in the present study. In addition, our study used a stirring system, whereas Shirasaka et al., did not stir during the transport assay. A large aqueous boundary layer (ABL) exists on the apical side of the cell monolayer and adjacent to the basal

surface of the filter which can exert an additional diffusion barrier to the cell membrane (Karlsson and Artursson, 1991; Adson et al., 1995). Depending on the physico-chemical properties of the drug, this layer can have a considerable impact on drug permeability estimates, which could result in measuring the aqueous permeability rather than that associated to the monolayer. By stirring or shaking the monolayer throughout the transport assay, the height of this layer can be dramatically reduced (Karlsson and Artursson, 1991; Adson et al., 1995). In turn, the aqueous diffusion coefficient of a molecule is related to its molecular weight (Avdeef et al., 2004). As VBL-sulfate has a large molecular weight (909 g/mol) relative to other drugs categorised as 'small molecules' (*i.e.,* excluding biological drugs), it is postulated here that the ABL will have an impact on VBL permeability estimates. Evidence for this is based on comparing studies determining VBL permeability in Caco-2 cell monolayers which either employ rotational stirring (Lentz et al., 2000; Campbell et al., 2003), shaking (Garberg et al., 1999; Horie et al., 2003; Celius et al., 2004) or that do not stir (Achira et al., 1999; Tang et al., 2002b; Balimane et al., 2004; Shirasaka et al., 2008). In the present study, it is notable that the A-to-B Papp at VBL concentration ≤10 µM for both low and high passage Caco-2 cells typically exceeds 5 x 10^{-6} cm sec^{-1}, similar to the studies employing rotational stirring. In contrast, studies using shaking or an absence of stirring typically report VBL A-to-B Papp values of approximately 1 x 10^{-6} cm sec^{-1}. The presence of a marked ABL in the *in vitro* systems studied by Shirasaka et al., may confound the kinetic parameter estimates from subsequent studies utilising their permeability data. In addition to the cell monolayer impedance to VBL permeation, the impedance resulting from ABL diffusion will also be a factor in their kinetic estimates (Tachibana et al., 2010; Sugano et al., 2011; Korzekwa and Nagar, 2014). This is not an issue if the ABL *in vivo* is similar to that in the unstirred *in vitro* system. However, the GI tract ABL thickness is 30-100 µM (Avdeef et al., 2004) and Caco-2 cell monolayer systems may range from 500-1200 µM thickness (Karlsson and Artursson, 1991; Adson et al., 1995). Therefore, $P_{Passive}$ and active kinetic estimates for VBL from these studies may be a composite of the ABL and monolayer barriers. What is additionally required for the study presented here is an assessment of stirring on ABL thickness, which requires undertaking the assay at multiple stirring speeds including assays without stirring to determine if there is a marked ABL effect on VBL transport.

A compartmental modelling approach is advocated to estimate kinetic parameters for transporters within *in vitro* monolayer systems (Zamek-Gliszczynski et al., 2013). This approach attempts to describe the structure of the *in vitro* system and together with ordinary differential equations and drug concentration data at multiple time points over the duration of the transport assay, the model

statistically fits the kinetic parameters based on the experimentally determined drug concentrations in each compartment. This has advantages over the conventional approach to determining kinetic parameters as the time-dependent concentration of the drug is estimated within each compartment rather than utilising the nominal drug concentration in the donor compartment. For efflux transporters, in which it is postulated that intracellular or intramembrane binding of drug is required for transport activity to be conferred (Aller et al., 2009), Km estimates based on the relevant concentration are thought to be important to reduce any bias introduced by neglecting the structure and temporal aspects of experimental system/assay (Korjamo et al., 2007; Shirasaka et al., 2008; Tachibana et al., 2010). However, obtaining the free intracellular concentrations can be challenging experimentally. In the interests of brevity, further details as to the utility of compartmental modelling of transporter kinetics can be found in these references (Harwood et al., 2013; Zamek-Gliszczynski et al., 2013; Nagar et al., 2014).

A relatively simple three-compartment model is employed in this study to estimate $P_{Passive}$, CLint, Km and Jmax. Initial simulations sought to estimate the $P_{Passive}$ within the model from verapamil incubation assays. The 3-4-fold higher $P_{Passive}$ estimates from simulations compared to experimental data may indicate the influence of residual active transport processes operating and/or the presence of additional barriers in the experimental set-up which are not accounted for in this model. Compartments representing additional barriers could be introduced as implemented in a quinidine five-compartmental model (Heikkinen et al., 2010). A three-compartment model was also described as being insufficient to capture experimentally observed lag times, attributed to partitioning of drugs into the membranes, for numerous compounds (Korzekwa et al., 2012). However, there was no discernible lag in drug flux in this study (data not shown), therefore the higher $P_{Passive}$ might be due to the presence of an ABL in this study which is not represented within the model.

A redundancy in active efflux transport associated with increasing P-gp expression was previously shown for VBL (Tachibana et al., 2010; Korzekwa and Nagar, 2014). However, it is possibly erroneous to assume that efflux activity is entirely attributable to P-gp due to evidence of a minor role of MRP2 on VBL transport. The assumption in this study however, is that P-gp activity is the dominant apical membrane efflux process. Thus, to identify if abundance-activity scaling factors might require development for transporter IVIVE-PBPK, an assessment of the linear relationship between P-gp abundance and activity, *i.e.,* CLint/pmol P-gp and Jmax/pmol P-gp (K_{CAT}), was

performed. The CLint estimates broadly reflected the rank order of P-gp abundances between cell variants, however a higher CLint/pmol P-gp in Caco-2-VBL cells indicate these data do not concur with estimates based on the experimental data presented by Shirasaka et al., (Tachibana et al., 2010; Korzekwa et al., 2012). The potential up-regulation in expression of another transporter such as MRP2 in Caco-2-VBL cells may contribute to the efflux activity and explain this observation. No increase in MRP2 mRNA expression was observed in Caco-2-VBL, however this may not be a reliable indicator of changes in protein levels and further studies to determine MRP2 protein abundance are necessary.

The estimation of a consistent Km proved a considerable challenge across the cell variants. The ratio of Jmax to Km (Equation 1-2) gave similar estimates to the simulations fitting of CLint (steady-state) alone (Table 7-6), however, the variability of the Km estimates between cell lines is not expected when using compartmental modelling approaches. Previously, Km estimates for VBL of 3-4 µM across cells with variable P-gp expression was found (Shirasaka et al., 2008; Tachibana et al., 2010; Korzekwa and Nagar, 2014). This variability is likely to have resulted from VBL possessing a high $P_{Passive}$ leading to a limited saturation of active efflux in the A-to-B direction. When fitting the A-to-B data alone, the model fails to identify a reasonable solution for CLint or Jmax (*i.e.,* the model hits lower boundary for estimates). This highlights the impact that the experimental conditions *i.e.,* stirring, might have in drug permeability within *in vitro* monolayer systems. From this data it is difficult to conclude with any certainty if an ISEF scaling factor incorporating abundance and activity for transporters is required for IVIVE-PBPK. Kinetic analysis of the P-gp probe compounds quinidine and verapamil showed a linear relationship between activity and P-gp protein expression (Korzekwa and Nagar, 2014). A linear relationship between abundance and Vmax was also found in plated CHO-OATP1B1 and MDCK-II-BCRP plated cells when using a conventional non-compartmental approach for Vmax estimation (Kumar et al., 2015). Further work to determine transporter abundances across multiple laboratories and also the activity of multiple probe compounds in their in-house transporter expressing *in vitro* systems will be required to identify whether an activity-abundance scalar is needed (Harwood et al., 2013).

In general compartmental models are extremely simplistic compared to the complex cell systems in which transporter assays are undertaken. With regulatory agency guidelines evolving, an appreciation of the practical requirements for performing *in vitro* transporter assays is required to facilitate the widespread employment of compartmental models by experimental scientists

generating data from transporter assays. The advent of 'off the shelf' compartmental models such as those recently developed by solution providers GastroPlus 'MembranePlus' and Simcyp Ltd 'SIVA', offer experimental scientists a ready to use platform to harness their own *in vitro* transporter data without requiring expert skills in model development and statistics. However, there are currently no guidelines on best practices when generating suitable experimental data for estimating kinetic parameters by compartmental models, in order to assess transporter-mediated DDI's by IVIVE-PBPK. The dataset provided in this study provides some perspectives on the limitations of using the compartmental model approaches for complex drugs. Experimental and drug-specific considerations such as; pH, ionisation, stirring, metabolism, intracellular and non-specific binding, intracellular sequestration/trapping, filter impedance, paracellular permeability and transporter specificity which may all be relevant for the complex molecules being generated in the drug discovery pipeline should be considered when modelling experimental transporter assay data. Therefore, guidelines on the design of transport assays to generate suitable data for *in vitro* system modelling are required together with selection of the appropriate model.

Future work should focus on determining MRP2 expression in Caco-2-VBL cells and undertaking multiple concentration assays with verapamil to estimate a CLint for MRP2. Performing assays with multiple stirring rates should enable the ABL volume or height to be determined which can be incorporated into a compartmental model to provide estimates with a dramatically reduced aqueous barrier. For basic compounds which are candidates for lysosomal sequestration, performing an assay in the presence and absence of a lysosomal sequestration inhibitor would enable the impact of trapping in this compartment on $P_{Passive}$ and other kinetic estimates to be assessed (Heikkinen et al., 2010). It would also be interesting to ascertain if VBL does indeed undergo active uptake at either membrane. Ideally, all the processes which act on a drug should be incorporated into an IVIVE-PBPK approach.

7.5 Conclusion

It is anticipated that academic and industrial research groups adopt the proteomic and kinetic modelling approaches described here to distinguish the relationships between protein abundances and function in a host of *in vitro* recombinant, immortalised cells, primary cultures and tissue extracts and an array of compounds to enable the generation of suitable IVIVE scaling factors. There is a considerable way to go within the transporter protein field to fully understand functional-abundance relationships, and only by a concerted effort across groups will this be achieved. However, in the near future the potential for standardising QTAP and *in vitro* transporter kinetic modelling approaches should be described for translation across groups.

Chapter 8 - Lost in Centrifugation! Accounting for Transporter Losses in Quantitative Targeted Absolute Proteomics

Declaration

This chapter constitutes a published article.

*M.D. Harwood, et al., (**2014**). DMD. 42, 1766-1772.*

I wrote this manuscript with editing undertaken by the co-authors. I retained editorial control for this article.

For a full background description of the theoretical aspects of this work, refer to the article above.

8.1 Introduction

As has been described in considerable detail in Chapter 3, a reduction in the complexity of the cell or tissue by obtaining a membrane fraction is advocated for measuring the abundance of transporter proteins. However, there are a number of stages required to obtain the PM fraction, utilising multiple centrifugation steps, in which various pelleted or supernatant fractions are discarded or retained. The findings presented in Chapter 3 suggested that the yield of the PM fraction constituted only 1-2% of the TP yield representing the starting whole cell lysate in Caco-2 cell monolayers. Therefore, a 50-100-fold enrichment of membrane components including the abundance of transporters is expected in the PM fraction compared to the starting whole cell lysate. However, it was noted that when an AP activity assay was performed to gauge the enrichment of the PM fraction compared to the starting whole cell lysate, only a modest 5-7-fold enrichment was observed, with no difference between the TM and PM fractions. This indicated that there was a large disparity between the marker activity data from the AP assay and the protein content data generated by the BCA assay. It was postulated that these losses of target proteins were occurring within preparatory steps. This has been demonstrated previously when preparing microsomal proteins for the study of metabolic scaling factors used within IVIVE (Barter et al., 2008), and is also alluded to in a review of the challenges associated with membrane proteomics (Orsburn et al., 2011). However, estimates of procedural losses of transporter proteins in membrane fractionation have not been reported. These losses hinder the implementation of reported abundance values into biologically meaningful applications such as PBPK models. Such models require parameters defining the functional transporter compliment of PM's in living tissues. Currently this is only approximated by transporter abundances in processed membranes without considering the confounding effect of the variability in recovery inherent to a method or operator-specific handling for membrane fractionation (Harwood et al., 2014).

This study postulates that by measuring suitable membrane protein markers or target transporter protein abundances in the original, intermediate and end-point membrane fractions, protein loss during fractionation can be calculated. A theoretical framework is developed to account for protein losses during centrifugation, which is applied to generate recovery factors (RF's) after quantifying absolute protein abundances in Caco-2 starting and membrane protein fractions.

8.2 Theoretical Background

8.2.1 Protein Losses in Centrifugation: The Utility of Recovery Factors

When employing procedures involving several stages to obtain a membrane fraction, it is inevitable that protein losses from the target organelle fraction will occur, leading to an under estimation in protein abundances. A study within our group, showed that when attempting to establish the metabolic scaling factor, microsomal protein per gram of liver (MPPGL), using differential centrifugation procedures after tissue homogenisation, a 47% loss of microsomal protein fraction (MSP) was demonstrated (Barter et al., 2008). These losses will hamper the extrapolation of metabolic clearance from subcellular fractions to intact tissue (Wilson et al., 2003). In a consensus study in which collated MPPGL data from the literature was presented, MPPGL values were corrected for losses incurred during preparation in all 10 studies (Barter et al., 2007). Generating RF's is achieved by calculating the fractional loss of MSP by measuring the P450 content in the initial liver homogenate and microsomal fraction (Equation 8-1). The resulting RF (1 minus the fractional loss of MSP) can be utilized to calculate a corrected MPPGL (Equation 8-2) (Barter et al., 2008).

$$\text{Fractional loss of MSP} = 1 - \left(\frac{\text{P450}_{\text{microsomal}}(\text{nmols})}{\text{P450}_{\text{homogenate}}(\text{nmols})}\right) \qquad \text{Equation 8-1}$$

$$\text{MPPGL } (\text{mg g}^{-1}) = \left(\frac{\text{Yield of MSP } (\text{mg g}^{-1})}{(1 - \text{fractional loss of MSP})}\right) \qquad \text{Equation 8-2}$$

From a physiological perspective, obtaining protein abundances within an entire organ is a valuable parameter for estimating the impact of that protein's function on drug disposition. An approach to calculating whole organ abundance has been proposed using CYP3A and CYP2E1 abundances to determine the CYP content within intact livers (Lipscomb et al., 2003). The calculation combines concurrent quantification of CYP3A and CYP2E1 in whole liver homogenate and MSP fraction with the scaling factors MPPGL and liver weight to obtain whole organ abundance. Obtaining data on enzyme abundances in both initial homogenate and MSP fractions with accompanying protein content data allows the evaluation of the potential CYP3A and CYP2E1 loss and the generation of sample specific RF's (Harwood et al., 2014).

8.2.2 Accounting for Protein losses in QTAP Abundance Analysis

At present, there are no ADME proteomic studies reporting the completeness of membrane extraction, *i.e.,* that negligible loss of target transporter proteins from the starting material through to the final enriched membrane fraction occur. Concerns have been raised that surrogate peptides used to quantify protein absolute abundances by an AQUA technique, may not reflect the abundance of the entire protein. To verify this, a study to quantify Sodium Taurocholate Cotransporting Polypeptide (NTCP) in human livers by AQUA (Qiu et al., 2013), was compared to a Stable Isotope Labelling by Amino Acids in Mammals (SILAM) method, in which entire proteins are isotope labelled by ingestion of labelled amino acids from dietary sources (Kruger et al., 2008). A dual protocol was run, where either the internal standard SILAM protein was added prior to membrane purification, or the SIL peptide was added after tryptic digestion of the liver samples, as is standard procedure. Losses of NTCP during the procedure were assessed by comparing endpoint abundances with both methods and comparable abundances of NTCP were quantified between the SIL and SILAM approaches, *i.e.,* comparable signal intensities at the mass spectrometry detection system. The SILAM assay provides a QC for the complete workflow of the SIL peptide assay, yet, an assessment of the membrane recovery and target protein loss was not undertaken. Similar signal intensities measured in the standard and native peptide are not an indicator of the potential for protein losses during fractionation or otherwise. A loss of protein during the fractionation procedure would lead to lower signal intensities of the selected transitions at the detector system of the mass spectrometer and lower protein abundance quantifications in the sample for both standard and the native protein (Harwood et al., 2014).

An alternative and less direct method to estimate loss during fractionation is to attempt quantification of target proteins in discarded, cytosolic and non-plasma membrane enriched fractions. This approach has been applied to the quantification of OATP1B1, OATP1B3 and OATP2B1 (Ji et al., 2012). However, abundances were not quantified in the starting lysate fraction, thus a full proteomic balance sheet for the target protein could not be evaluated. The sensitivity of the assay applied to discarded fractions must also be questionable since a substantial proportion of target protein might be lost to a discarded fraction, or substantially diluted by cytosolic and other proteins that it was rendered undetectable by the assay, a ‘muffling effect’ (Harwood et al., 2014).

Ideally, an approach that estimates target protein loss between whole tissue and the purified membrane fraction is required for PBPK models. This will enable the scaling of abundances in

subcellular fractions to accurately reflect whole cell or organs abundances. The estimate is constucted from the protein content, determined by a BCA assay or similar, and peptide abundance determined by LC-MS/MS, in both whole cell lysate and purified membrane fractions. Near complete release of peptides during digest would require confirmation via another QC procedure to ensure peptide abundance remained an accurate surrogate measure for each proteins abundance, analogous to enzyme mass balance sheets (Huber et al., 2003; Harwood et al., 2014).

To our knowledge two studies, Ohtsuki et al., (Ohtsuki et al., 2013) and Kunze et al., (Kunze et al., 2014) provide data sets that enable the calculation of membrane RF's. Ohtsuki et al., reported transporter protein abundances for both whole cell lysate and the plasma membrane fractions of a blood brain barrier cell model (Figure 8-1). Differential enrichment of the proteins was achieved ranging from 1.3 for 4F2hc to 11 for P-glycoprotein, as can be viewed in Figure 8-1. The yield of PM protein from the total starting fraction was not provided in the report by Ohtsuki et al., 2013., however as already alluded to in this chapter and Chapter 3, if the PM yield is similar to that of Caco-2 cell monolayers, human hepatocytes and Human Embryonic Kidney (HEK)-293 Cells (Kunze et al., 2014), *i.e.,* 1-2%, then the expected enrichment in transporter protein abundance in the starting TP *versus* the plasma membrane fraction would be 50-100-fold (Equation 8-3). If the plasma membrane yield in the blood brain barrier cell model used in Ohtsuki et al., 2013 were similar to our Caco-2 yield, the fold enrichments in protein abundances ranging from 1.3 to 11 from the whole cell fraction to the plasma membrane are much lower than expected from the Caco-2 protein yield data. However, it should be noted that the protein yields in each enriched fraction will be dependent on the biological system under study as well as the procedures used. As mentioned on several occasions in this thesis, the unexpectedly lower Na/K-ATPase abundance in the TM compared to PM fraction of human livers (Ohtsuki et al., 2012), may also suggest that losses are occurring at the final membrane fractionation stage (Harwood et al., 2014).

$$\text{Expected Enrichment (PMF)} = \frac{\text{Total Protein Content (TP)}}{\text{Protein Content in CMF or PMF}} \qquad \text{Equation 8-3}$$

where CMF is the crude membrane fraction and PMF is the plasma membrane fraction.

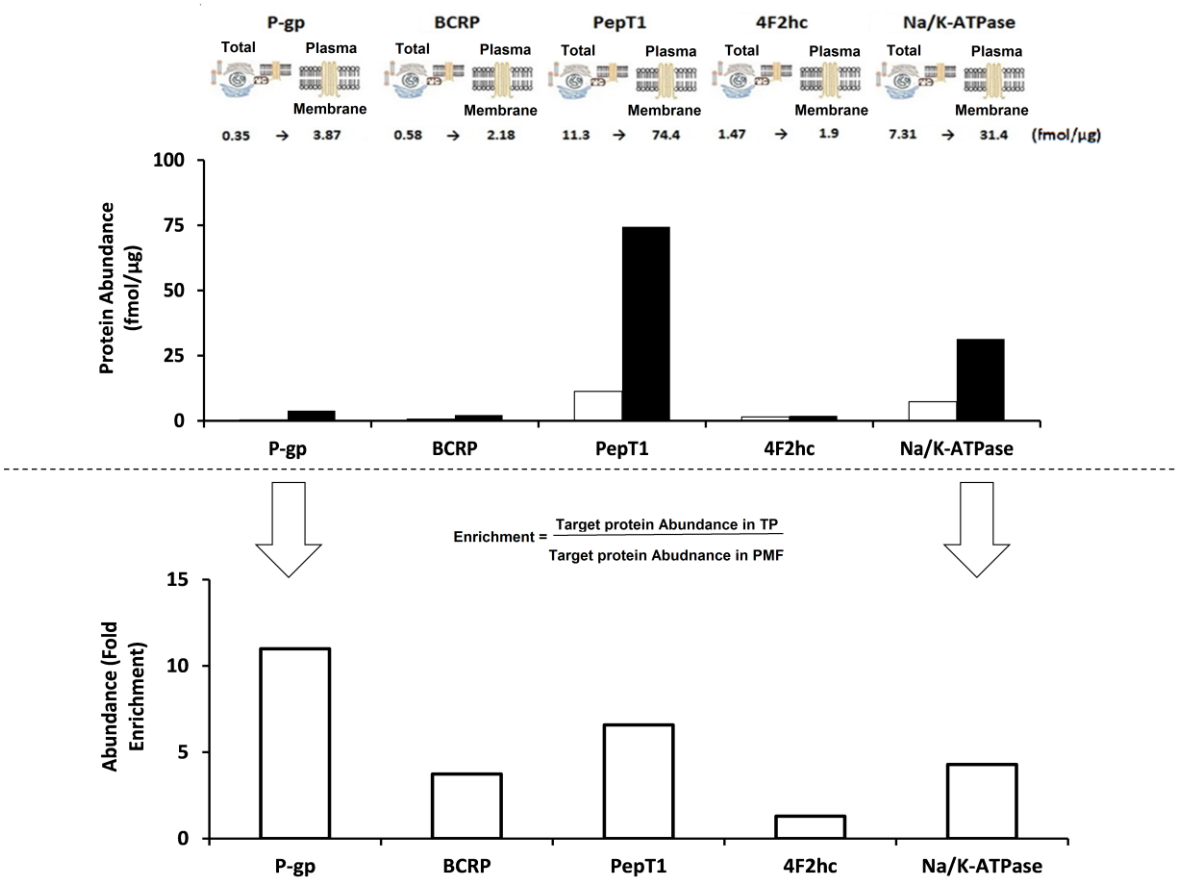

Figure 8-1. A - The fold enrichment 'actual enrichment' in selected peptide abundances measured in the whole cell and PM fraction of matched samples of the blood brain barrier cell model (hCMEC/D3) is provided from data reported in (Ohtsuki et al., 2013). The text above the bars refers to abundance in fmol/µg of protein, with the abundances in the whole cell fraction given as the first number and white bars, and the abundances after the arrow and black bars as the abundance in the PM fraction. B. The whole cell & PM fraction abundance ratio 'the actual enrichment' has been calculated from Equation 8-4 in this chapter and is provided in the histogram.

8.2.3 Correcting for Protein Losses in Centrifugation

Accurate determination of the functional abundance of transporter protein(s) in the whole organs of individuals is essential for predicting temporal drug profiles in whole body PBPK models in a fully mechanistic manner. Whole organ transporter abundances have not yet been reported in the literature, therefore scaling factors such as the plasma membrane protein per gram of liver (PMPPGL) and liver weight are required to scale the abundances reported in the membrane fraction to the whole organ (Figure 8-2). It should also be considered that PMPPGL may in itself require application of a RF to correct for losses in centrifugation in a similar manner to that reported for MPPGL (Harwood et al., 2014).

A value for the expected enrichment of the membrane fraction (Equation 8-3), is required prior to assessing the final transporter abundances. This is obtained by performing a protein assay to

calculate the yield of protein in the starting TP fraction, which could be a whole cell lysate, or tissue homogenate and the crude/total or PM fraction, in which transporter abundance determinations have routinely been performed (Figure 8-2) (Harwood et al., 2014).

The actual enrichment of the target protein is calculated from the abundance(s) of target protein(s) quantified in the TP fraction and the membrane fraction in QTAP assays (Equation 8-4):

$$\text{Actual Enrichment (PMF)} = \frac{\text{Target Protein Abundance in CMF or PMF}}{\text{Target Protein Abundance in TP}} \quad \text{Equation 8-4}$$

To correct for losses of protein throughout centrifugation, the fraction recovered (FR) is determined as the ratio of the actual and expected enrichments for a transporter isoform (Equation 8-5) and together with Equation 8-6 can be used to generate an RF which is used to correct the abundances generated in the membrane fraction (Equation 8-7). The corrected protein abundance is scaled to the whole organ abundance using the requisite scaling factors for the evaluated organ.

$$\text{Fraction Recovered (FR)} = \frac{\text{Actual Enrichment}}{\text{Expected Enrichment}} \quad \text{Equation 8-5}$$

$$\text{Recovery Correction Factor (RCF)} = \frac{1}{\text{FR}} \quad \text{Equation 8-6}$$

$$\text{Corrected Abundance of Target Protein in PMF} = \text{PMA} \cdot \text{RCF} \quad \text{Equation 8-7}$$

where PMA is the measured abundance of target protein in the plasma membrane sample (Harwood et al., 2014).

Having described the theoretical aspects of generating RF's to account for transporter losses in membrane preparations, a pilot study to assess the feasibility of this framework for generating RCF's was performed Caco-2 cells.

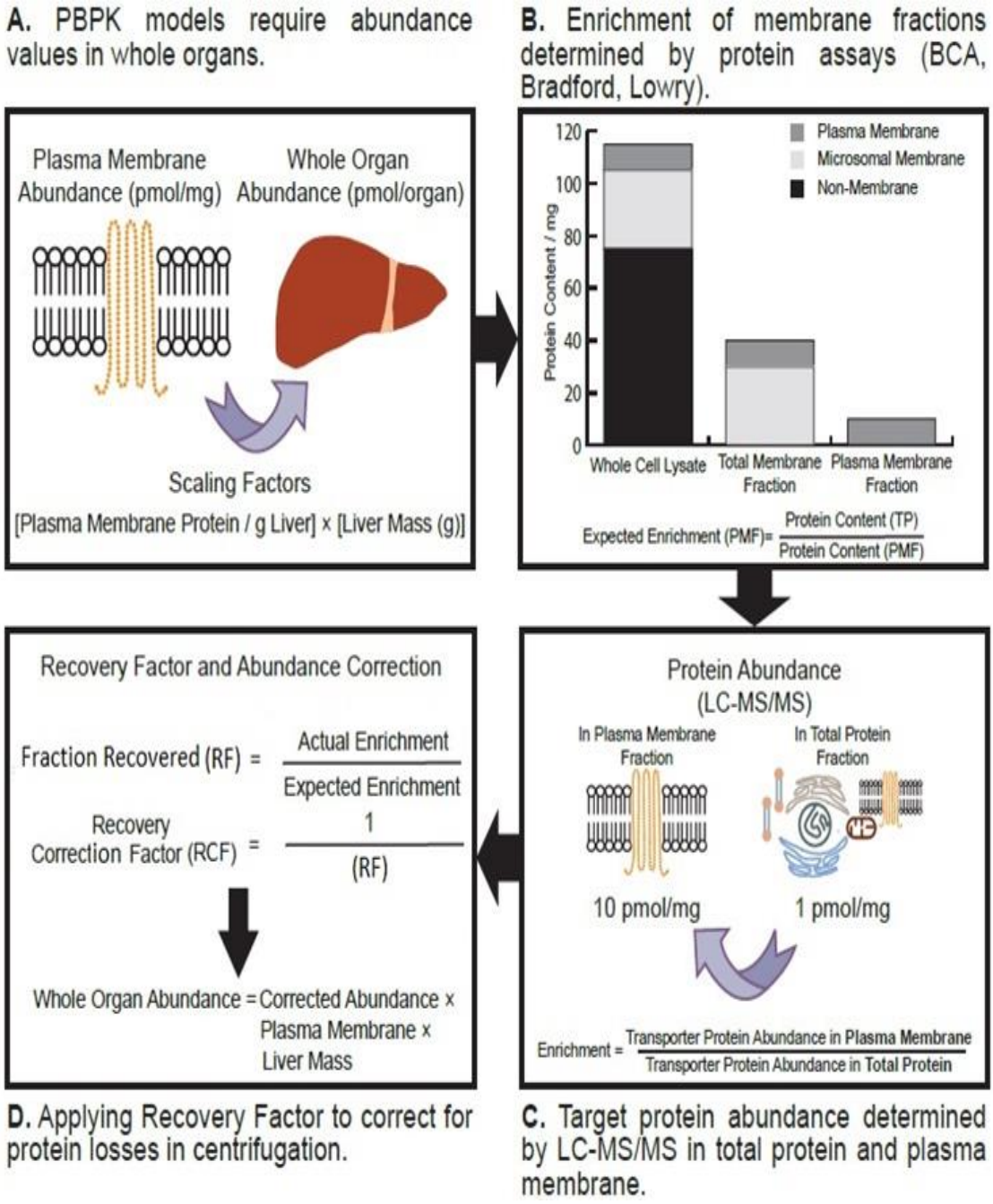

Figure 8-2. A schematic describing the generation of recovery factors (RF's) to correct transporter abundances in membrane fractions for protein losses encountered during centrifugation. Whole organ protein abundances require generating from membrane fractions using the appropriate physiological scaling factors, *i.e.,* plasma membrane protein per gram of liver (PMPPGL) (A). By measuring protein content in the starting Total Protein (TP) and the endpoint membrane fraction, *i.e.,* the plasma membrane fraction (PMF), the expected enrichment of the target protein can be obtained (B). Quantifying the target protein abundances in the starting TP and endpoint membrane fractions provides the actual target protein enrichment (C). If the expected and actual enrichments are matched, the recovery factor is by definition one. If there is a disparity between the expected and actual enrichment, a recovery factor can be generated and be applied to the endpoint membrane abundance and is scaled to obtain whole organ abundances (D).

8.3 Methods

Low passage Caco-2 cells (n=4) were seeded and cultivated for 10, 16 and 29d on 44 cm^2 Transwell filters and membrane fractions were harvested as described in detail in Section 2.2.2.2. The TP constituting and representing the whole cell lysate/starting fraction and the TM and PM fractions was sampled, and a BCA assay was performed to measure protein content of each fraction. The various protein samples were digested as described in Section 2.2.7.1 and the abundances of the AQUA peptides for Villin and Na/K-ATPase were determined. Using a combination of protein content and absolute protein abundances, RF's were obtained for the above described framework to correct for protein losses during membrane fractionation.

8.4 Results

8.4.1 The Expected & Actual Enrichment in Abundance

The expected protein enrichment of the sub-cellular fraction from differential centrifugation is obtained by measuring the protein content in the starting TP whole cell lysate and subsequent TM and PM fractions (Equation 8-3). As shown in Figure 8-3, the TM and PM fractions represent 4 and 1% of the starting TP fraction. From this data, it is expected that there is an approximate 100-fold enrichment in the PM fraction from the TP fraction. Therefore, the abundances of the PM-associated proteins, Na/K-ATPase and Villin should also show 100-fold enrichment when quantified after LC-MS/MS analysis.

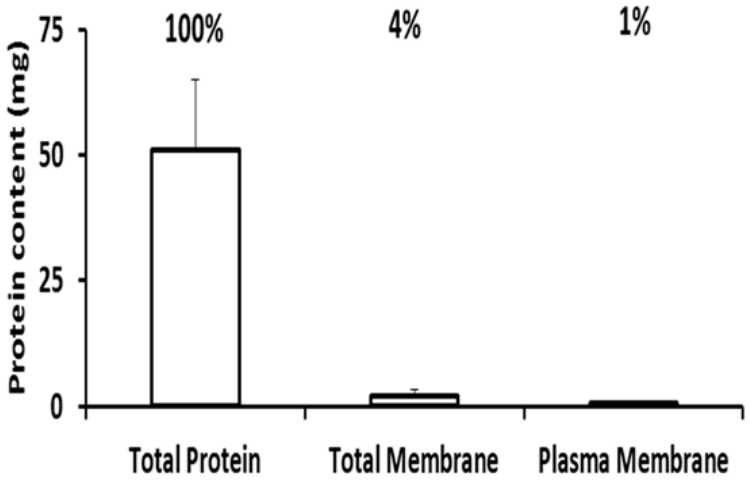

Figure 8-3. The protein content and the yield of protein as a percentage of the TP lysate in Caco-2 cell monolayers. The data was obtained after a BCA assay. The values above the bars represent the percentage yield of protein with regard to the TP. The values are given as Mean±SD, Caco-2 cell extractions (n=4).

To determine the actual enrichment in abundance, an AQUA-QTAP strategy was applied to the TP, TM and PM fractions. The abundances of Na/K-ATPase and Villin are provided in Figure 8-4**.** There is a step-wise increase in Na/K-ATPase and Villin abundances from TP to PM as expected. However, Na/K-ATPase and Villin abundances (Equation 8-3) do not reach the expected 100-fold enrichment in the PM fraction (Figure 8-3), indicating that losses of target protein occur during the fractionation procedure. It is also noteworthy that the fold enrichments are different for the two membrane marker proteins, which may indicate a preferential enrichment or greater procedural losses of the basal and apical membranes.

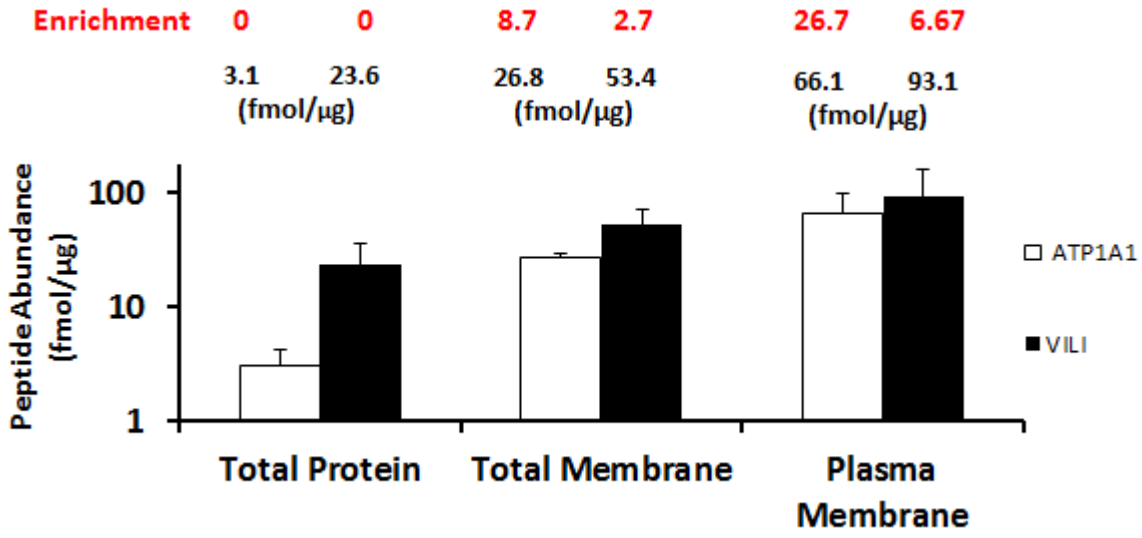

Figure 8-4. The abundances of Na/K-ATPase (white) and Villin (black) in Caco-2 cell monolayer TP lysate and membrane fractions. The mean abundance values (fmol/µg protein) are given in black text above. The fold enrichment in abundances relative to the TP fraction are provided in red text, values above bars for each peptide derived using Equation 8-4. The values are given as Mean±SD, for n=4 Caco-2 cell extractions.

8.4.2 Generating & Applying Recovery Correction Factors to Correct for Protein Losses

To correct for losses of protein during centrifugation, the FR is determined for a transporter isoform (Equation 8-5). Equation 8-6 generates a Recovery Correction Factor (RCF, Table 8-1) to correct the abundances measured in the TM or PM (Equation 8-7 & Figure 8-5).

When applying the RCF's to obtain a corrected abundance in the PM fraction (Equation 8-7) for each individual sample, there is a 4.9-fold and 28.6-fold increase in the Na/K-ATPase and villin abundances, respectively, compared to abundances without correction (Figure 8-5). A pilot study in different Caco-2 samples to that performed with the AQUA peptides was also undertaken using the validated QconCAT (6 transporter proteins) approach. However, this could only be run with digested peptides stored frozen for 6 months. In these samples, low abundances for all proteins were found in the TP sample, negating the generation of recovery factors, with the exception of Na/K-ATPase which gave a similar RCF of 5 to the AQUA approach (RCF 5.55, Table 8-1). In the event that lower abundance proteins are below the limit of quantification in the TP fraction, it is suggested to use a RCF for the membrane in which the transporter is expressed, based on RCF's generated from higher abundance proteins, such as Na/K-ATPase for the basal membrane and villin and HPT1 for the apical membrane.

Table 8-1.Recovery correction factors (RCF's) generated for Na/K-ATPase and villin to correct for protein loss in membrane fractionation.

	Na/K-ATPase	Villin
Sample	RCF	RCF
Caco-2 – 10d (#1)	5.16	26.65
Caco-2 – 10d (#2)	3.24	9.41
Caco-2 – 16d	8.45	40.55
Caco-2 – 29d	5.34	64.24
Mean	**5.55**	**35.21**
SD	**2.16**	**23.17**

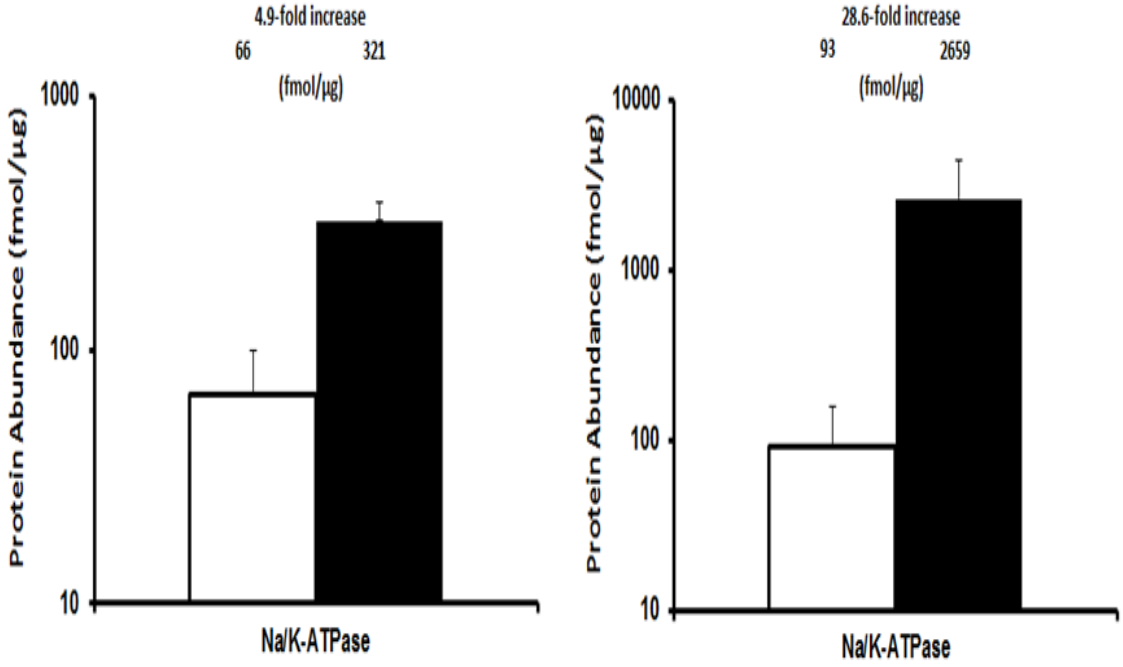

Figure 8-5. The corrected abundances for Na/K-ATPase (A) and villin (B) from Caco-2 cell monolayer total protein (whole cell lysate) and PM fractions. The non-corrected abundances (white) and the corrected abundances (black) were generated after applying the corresponding RCF (Table 8-1). The fold enrichment in abundance is provided after RCF application (Equation 8-7) with the abundance values shown above the bars. The values are given as Mean±SD, for n=4 Caco-2 cell extractions.

8.5 Discussion

Characterising protein or peptide losses throughout QTAP workflows is vital if transporter protein abundances are to be incorporated into PBPK models without distortions from peptide-dependent biases inherent to the QTAP assays. Here, an approach to correct for targeted protein losses after centrifugation to obtain membrane fractions is postulated, by combining data generated from assays to measure protein content and QTAP methods to obtain absolute protein abundance. This proof of concept study demonstrates that RCF's can be generated by quantifying the high abundance basal and apical membrane marker proteins, Na/K-ATPase and villin, respectively, alongside a routine BCA protein assay. The RCF's are utilised to correct for losses of targeted proteins in endpoint membrane fractions to establish an absolute abundance corrected for protein losses.

In its present form, this study can only be taken as a proof of concept due the AQUA technique employed having not been validated for precision, accuracy, linearity and an external calibration curve with QC samples. The QconCAT method was also employed for this pilot study, however only Na/K-ATPase, HPT1, P-gp and BCRP abundances were above the limit of quantification. Furthermore, for BCRP a lack of enrichment in abundance from the TP to PM fraction was observed (Equation 8-5), which suggests a possible matrix effect, potentially affecting digestion efficiency for this peptide. There are no other data describing the absolute quantification of Na/K-ATPase and villin in Caco-2 cells to directly compare the corrected abundances generated here. However, early QconCAT work with chicken muscle showed that the high abundance protein GAPDH was expressed in the soluble fraction at approximately 450 fmol/µg (Rivers et al., 2007). In a relative proteomic analysis of Caco-2 cells, villin was expressed at 1.4-fold lower levels than GAPDH (Wisniewski et al., 2012), thus, the corrected villin abundances presented here may be an overestimation. Nevertheless, working with TP matrix requires further validation work, with a suggested starting point being to run the same tissue samples through the QTAP workflow to identify if RCF's can be generated with precision. Once this is established, it will enable a reasonable assessment of the performance of this model.

The preliminary data obtained suggests that the higher RCF for the apical membrane indicates a greater loss of protein compared to the basal membrane. It is possible that this is due to the different densities of each membrane. When separating a crude membrane fraction into apical brush border and basal membranes from Caco-2 cells via sucrose gradient differential

centrifugation, the fraction found at the 35-45% boundary biochemically reflected the brush border (apical) membrane, whereas the basal membrane resolved at the 30-35% sucrose interface (Ellis et al., 1992). This indicates that the apical membrane possesses a higher density compared to the basal membrane. If a 45% sucrose layer was required for obtaining a purified apical membrane, then it is possible that components of this membrane with higher densities permeate through our 38% sucrose layer. In some instances, the sucrose component of the centrifugation tube did display turbidity which may reflect apical membrane components. Occasionally, a small pellet formed at the base of the centrifuge tube indicating complete permeation of a fraction of the material through the sucrose compartment. However, the AP activity of the pellet was found to be low (data not shown), suggesting this did not originate from PM, and may reflect organelles with higher density, *i.e.,* nuclear or mitochondrial components that were not completely removed in previous steps. Identification of differential losses of protein from membrane regions is an important step to characterising losses in the QTAP workflow. These steps will enable rational improvements to existing protocols to reduce loss of target membranes/proteins in order to move toward obtaining 'absolute' abundances from a physiological perspective.

In addition to assessing protein losses, characterising contaminating fractions from other organelles, *i.e.,* mitochondria should also be undertaken, as the presence of these will dilute abundances within the target fraction. This could be achieved by the simple cost effective approach enzyme activity marker assays. Additionally, proteomic analysis, whether global or targeted, could offer an insight into the constituents of the membrane fraction and potentially allow for a correction factor based on impurities of organelle marker proteins. However, we are some way from the application of robust loss or impurity factors in QTAP assays, therefore it has been suggested that a reasonable approach at present for utilising absolute transporter protein abundances in IVIVE-PBPK is to generate IVIVE scaling factors, such as the REF, rather than absolute protein abundances for organs (Stieger et al., 2014).

As was highlighted in the QConCAT assay, the limitation to this strategy is the ability to quantify low abundance peptides in the TP sample. In this instance, a transporter from the same membrane (apical or basal) and protein subfamily that can be quantified could be used as the basis for a recovery factor. Utilising the abundance in the TP sample may not be applicable for incorporation into IVIVE-PBPK models, as there are no assurances that the selected peptide is derived from a fully formed protein resident in the PM as opposed to protein fragments in the process of

translation. A study has shown that P-gp is located predominantly in the PM of intestine and Caco-2 cells (Ahlin et al., 2009). However, there is evidence for intracellular MRP1 and MRP2 localisation (Sekine et al., 2008; Ahlin et al., 2009), and, as a result, the utility of this approach may be compromised, especially if the transporter resides in a soluble compartment such as the cytosol, which is likely to be discarded in the first centrifugation step after tissue homogenisation or cell lysing. Furthermore, as demonstrated in Section 4.3.2.2, assessing peptide losses downstream of subcellular fractionation stages requires consideration and incorporation into QTAP workflows, *i.e.,* membrane solubilisation, peptide digestion efficiency, loss of peptides during preparation, chromatographic stability and transition through the mass spectrometer (Harwood et al., 2014).

Upon incorporation of transporter protein abundances into an IVIVE-PBPK workflow, any underestimation of transporter abundance could lead to inaccuracies in: 1) the generation of scaling factors that are utilized to scale between the *in vitro* and *in vivo* systems and, 2) scaling the transporter activity within the *in vivo* system to predict transporter isoform clearance in the whole organ. Thus, any differences in procedural losses of target proteins between the *in vitro* and *in vivo* system, *i.e.,* a matrix-specific effect, could lead to a bias in the generation of expression-based scaling factors utilised in an IVIVE approach (Harwood et al., 2013; Vildhede et al., 2014). Furthermore, a transporter isoform's Jmax is typically related to its protein abundance (Li et al., 2010a). Therefore, an underestimation in whole organ transporter abundances will impact on the prediction of drug disposition and the magnitude of DDI exhibited in that individual.

A recent study has incorporated absolute transporter protein abundance data into an IVIVE strategy. The study by Vildhede et al., 2014, quantified the absolute transporter abundances of hepatic uptake transporters OATP1B1, OATP1B3, OATP2B1, NTCP and the canalicular efflux transporter P-gp in human livers, isolated hepatocytes and HEK293 single transfected cells (Vildhede et al., 2014). A scaling strategy incorporating the abundances of the uptake transporters was developed and a REF approach was employed to account for the differences in transporter expression between the *in vitro* and *in vivo* systems. An *in vitro* V_{max} was used to assign a fractional contribution of each isoform to the overall uptake clearance, while the variability in the abundance of the transporters in 12 livers enabled an estimate of the expected variability in the magnitude of DDI between individuals. Two key assumptions within this strategy are; 1) that activity (V_{max} or J_{max}) is proportional to expression, which may not be the case particularly for over-expressing systems (Korzekwa and Nagar, 2014). and, 2) the recovery of each transporter isoform throughout the

procedure is uniform and not biased by the matrix in which it resides, and that digestion is complete in both systems (Prasad and Unadkat, 2014). Any differences in the magnitude of transporter protein loss should be accounted for, which could affect the scaling factors employed to predict transporter-mediated clearance and DDI, hindering the accuracy of the IVIVE strategy. Indeed, incorporation of the abundance and activity into a PBPK model should enable the success of this strategy to be ascertained in regard to recovery of pharmacokinetic profiles in human populations.

Dr Bhagwat Prasad (Acting Assistant Professor, The University of Washington) who is actively engaged in transporter abundance quantification by QTAP strategies, with a view to translating this data into PBPK models, believes that with the current data available we are not in a position to utilise the available data for abundance scaling to the whole organ (Personal communication, November 2014). This is supported by recent findings that a commercially available kit intended for isolating a PM fraction, was contaminated with other subcellular fractions, particularly the golgi and mitochondria (Kumar et al., 2015). The candidate is in agreement with Dr Prasad in that obtaining absolute protein abundances for whole organs is not currently achievable, based on confounding factors, many of which have been discussed in this thesis, such as;

- the difficulty in obtaining a pure PM fraction, *i.e.,* contamination by non-targeted organelles
- not accounting for protein losses in membrane fractionation and digestion phases
- a lack of membrane scaling factors to enable whole organ abundance determination
- selection of the peptide as a surrogate for whole protein quantification
- challenges in deducing the completeness of proteolytic digestion

Assuming the potential confounding factors are the same in the *in vitro* and *in vivo* systems, or if they are not, that these are accounted for, then obtaining a REF IVIVE scaling factor is permissible. Obtaining the variability within a set of samples is also possible if the assay precision is within defined limits. At present, this approach does not mirror the fully mechanistic approach developed for CYP450 enzymes. For these enzymes, not only are abundance-function scalars, ISEF's, available for scaling from recombinant expression systems (Chen et al., 2011), but whole organ metabolic clearance is calculated via CYP450 isoform abundance within the whole organ. The aspiration within transporter IVIVE-PBPK is to parallel the success observed for CYP450-mediated drug disposition and DDI prediction using the fully mechanistic IVIVE-PBPK approach, in order to improve our prediction for transporters by obtaining whole organ abundances that approximate to *in vivo* expression.

8.6 Conclusion

Fractionation strategies to harvest a PM typically give a low final yield relative to that in the starting sample. The PM samples are also contaminated with other organelle components and are subject to losses of protein. Therefore, identifying the level of targeted protein loss is critical if we are to obtain a physiologically meaningful 'absolute abundance', *i.e.,* the protein abundance in a whole organ. This framework provides a starting point to assess losses in membrane purification. Other groups working in this field are encouraged to attempt the assessment of protein losses using this strategy with membrane extraction kits or their own in-house differential centrifugation methods. This will define procedural differences in losses between laboratories and facilitate development of improved extraction techniques that minimise protein losses and contamination. Alternative techniques such as extracting PM proteins via affinity chromatography after labelling might be another means to extract the integral membrane proteins of interest with higher specificity (Orsburn et al., 2011). Ultimately, the goal is to obtain accurate transporter protein levels in high quality purified PM fractions, or purified apical and basal membranes. Losses are inevitable during cell fractionation procedures and correcting for these losses is a key requirement if we are to achieve reliable whole organ absolute abundances.

Chapter 9 - Final Conclusion & Future Work

Given the increasing emphasis placed on the pharmaceutical industry to elucidate the role of transporters on ADME-T by drug regulatory agencies, it has never been more crucial to successfully predict transporter-mediated drug disposition and DDI. As advocated by regulatory agencies and routinely employed in the pharmaceutical industry, IVIVE-PBPK strategies offer the opportunity to predict the fate of drugs computationally. By harnessing the transporter activity data acquired from established cell models expressing relevant human transporter proteins, in combination with the appropriate algorithms and scaling factors, predictions of the impact of transporters on drug disposition and DDIs, can be made in virtual human populations. However, successfully predicting the impact of transporter function on drug disposition is particularly challenging when employing transporter-mediated IVIVE-PBPK. The Simcyp consortium recognised that this was an area requiring further work, as the scaling factors used for transporter-mediated predictions were not nearly as sophisticated as those for drug metabolism-based IVIVE-PBPK. Therefore, projects, including that described within this thesis, were initiated to focus on developing more mechanistic scaling factors for transporter-mediated IVIVE-PBPK.

In collaboration with the Manchester Pharmacy School and Manchester Interdisciplinary Biosciences Centre, this PhD project sought to quantify transporter protein abundances in a Caco-2 cell model and human intestinal enterocytes, using targeted proteomic strategies. In addition, the relationship between BCRP and P-gp transporter gene expression, abundance and function were assessed in Caco-2 cell monolayers cultivated for varying times, passage age and selection pressures. Transporter scaling factors developed from cell model and human intestinal immunoblotting have been utilised in intestinal IVIVE-PBPK strategies, however these have been based on only a single intestinal sample. Furthermore, *in vitro* systems over-expressing transporters are used for elucidating transporter function. Thus, studies assessing the relationship between increases in protein abundance and function may shed some light on the requirement for scaling factors to account for non-linear activity-abundance relationships, akin to those developed for drug metabolising enzymes. Transporter abundances that accurately reflect plasma membrane expression in the various intestinal regions are also required for a fully mechanistic IVIVE-PBPK approach. Little data was available for Caco-2 cells or human intestinal abundances from QTAP strategies prior to starting this project.

Numerous methods are available to isolate membrane fractions to quantify transporter abundances. However, within the transporter QTAP field, developing and validating the membrane isolation technique has not been reported. The purity or quality of the membrane in which transporter abundances are studied could be critical to obtaining abundances that accurately reflect those in the plasma membrane. Therefore, the initial studies in this thesis concentrated on the development of a differential centrifugation procedure to extract plasma membranes from cell models and characterisation of membrane purity using marker enzyme activity assays. Although these assays are relatively simple, they offer the opportunity to assess enrichment of target organelles without requiring state of the art equipment and time-consuming assay development. The studies showed that the postulated plasma membrane fraction was not enriched compared to the preceding total membrane fraction using alkaline phosphatase activity as a plasma membrane marker. Furthermore, a contamination of endoplasmic reticular components in the plasma membrane fraction was also exhibited. If similar contaminations are translated across studies, it is undoubted that transporter protein 'absolute' abundances relevant to function, *i.e.,* plasma membrane localised transporters, are being globally under-predicted. Moreover, it was also shown that a discrepancy existed between the protein yield (BCA assay) at each stage of the membrane fractionation procedure and alkaline phosphatase activity enrichment. This led to concerns over procedural losses of the plasma membrane and hence, that transporter proteins were also lost during centrifugation steps. To correct for such losses, a theoretical framework was provided which relies on determining both protein content and transporter abundances in starting and endpoint fractions. The limitation to this strategy is the ability to measure the proteins in the un-refined starting whole cell/tissue homogenate. Yet, if losses or contamination of target proteins and samples are neglected, this poses a considerable problem for scientists seeking to implement transporter abundances into organs of PBPK models, as these abundances may not approximate to the *in vivo* milieu. However, in order to establish if transporter abundances were indeed enriched in the plasma membrane *versus* the preceding, un-refined fractions, the development of QTAP assays was required.

To quantify absolute protein abundances, using QTAP approaches, unique peptide standards are generated that contain a differing mass to the analyte under study and are also susceptible to cleavage by trypsin. Typically, the addition of mass to the standard peptide(s) is via isotope labelling. Therefore, a QconCAT strategy was employed to generate a construct containing a string of selected peptides that is isotopically labelled and expressed in a host vector. The QconCAT

construct, once extracted from the vector, can serve as an almost limitless source of greater than 40 isotope labelled standards. A construct containing peptide standards for transporter protein quantification was developed. However, considerable delays in its successful expression were encountered. This, together with challenges in achieving a reliable digestion procedure to obtain the selected peptides in the biological matrix, posed significant difficulties to the project's progression. While development of the digestion procedures continued within the project, a contingency was sought to establish if transporter abundances could be determined in Caco-2 and human intestinal membrane samples using established techniques. Samples were analysed by Bertin Pharma in France who use techniques acquired from Prof. Terasaki's laboratory at the University of Tohoku. Simultaneously, a significant advance in the development of the digestion procedures was made within this project that enabled the development and validation of a QTAP workflow for 'in-house' quantification of six transporters in human intestinal samples. In the small number of samples within the validation set, considerably higher abundances were noted for BCRP and P-gp in these samples compared to abundances generated in jejunal samples reported by the University of Greifswald using QTAP techniques. It would be interesting to establish if these differences were due to the inherent inter-individual variability in abundances between human samples or if these originate from technical differences employed within the QTAP workflow between the groups. Within this study an appraisal of the enterocyte harvesting method was performed in jejunal samples. Little difference in P-gp and BCRP abundance were found when eluting enterocytes by chelation, or crushing the mucosal tissue by homogenisation, suggesting this aspect of the protocol may not be responsible for the observed differences. The intestinal abundances generated from this project, although from a small sample set, provide a considerable addition to our knowledge base on intestinal transporter abundances given the relative paucity of data currently reported.

Utilising the services of Bertin Pharma led to the project standing in an enviable, if not slightly fortuitous position, of possessing transporter abundance data from two different laboratories on a selection of the same samples. This permitted a cross-laboratory comparison, in which a diverse set of procedures was employed between each laboratory in order to determine the abundances of three key proteins and REF scaling factors. Overall, there was a reasonable similarity in abundances for Na/K-ATPase and BCRP between laboratories. However, for P-gp systematically higher abundances were determined by the University of Manchester. It is postulated that Bertin Pharma's P-gp peptide standard was prone to missed-cleavage by trypsin, potentially leading to

the lower abundance quantifications. Due to Bertin Pharma's systematically lower P-gp expression levels, the jejunal-Caco-2 REF was not different between laboratories. However, for BCRP, the REF was different, which may due to a bias in BCRP abundance quantification in Caco-2 cell samples between laboratories. This indicates that caution should be exercised when interpreting data reported as an 'absolute' abundance from a biological context and for the generation of scaling factors from one laboratory to another. Laboratories undertaking QTAP strategies should continuously refine their workflows in order to quantify tissue/cell abundances without distortions arising from the procedures employed. This affirms the challenges for scientists seeking to implement absolute transporter abundances with accuracy into PBPK models. The potential for adopting standardised procedures for 'best practices' in QTAP workflow design across laboratories should be encouraged, to avoid the problems observed when translating permeability/transporter data for cell models across laboratories. Further studies investigating all the stages comprising protein abundance quantification should facilitate a consensus approach to ADME QTAP studies.

Similar transporter abundances in the postulated 'total' and 'plasma membrane' fractions from Caco-2 cell samples were consistently shown, confirming the lack of enrichment in the plasma membrane fraction by alkaline phosphatase activity assays. Until evidence is provided that a procedure can harvest a 'plasma membrane' fraction that is relatively uncontaminated with other organelle components, there is a strong case for only reporting abundance data from total membranes.

The current study suggests that for both BCRP and P-gp, protein abundance data is a better proxy for gauging transporter function than mRNA gene expression, when measuring efflux ratio in Caco-2 cell monolayer bi-directional transport assays. Expression-based scaling factors should be specifically generated within each laboratory intending to employ a transporter-based IVIVE approach. These findings therefore suggest that, expression-based scaling factors are generated by employing QTAP assays, in preference to assays determining relative gene expression. Furthermore, as the transport assays were performed at sub-saturating probe concentrations, these data may only be relevant to steady state predictions.

In previous studies, discrepancies between protein expression and function for the P-gp probe VBL were noted. A reduction in drug transport relative to protein expression was found as protein expression increased, a 'functional redundancy'. If such a phenomenon is in operation, IVIVE scaling factors solely incorporating the expression differences between the *in vitro* and *in vivo*

system may not possess the capacity for accurate scaling predictions in over-expressing systems. By generating Caco-2 cells with differing P-gp abundances, the relationship between VBL transport kinetics, determined using a simultaneous-fitting-compartmental-modelling approach and increasing P-gp abundance could be assessed. Although, VBL intrinsic clearances reasonably approximated to P-gp abundance, the inability to obtain consistent Km estimates between cells expressing varying P-gp levels may have resulted from a reduction of the apical boundary layer volume upon stirring the assay, leading to higher absorptive Papp at sub-saturating VBL concentrations. Approximately 5-fold lower Papp's at sub-saturating P-gp concentrations were observed by another group, in which there was no reports of stirring, therefore, it was postulated that the experimental design may be the source of the observed lack of saturation. This is an important finding, which emphasises that transport assay design requires careful consideration, so that kinetic estimates that are intrinsic to the transporter protein and lipid bilayers, rather than other intrinsic factors. There has been moderate progression on identifying if abundance-function scaling factors are required, thus, further studies in this area across multiple groups using multiple probe compounds for each transporter isoform in a variety biologically relevant systems is advocated. The overlapping substrate and inhibitor transporter specificity also adds to the complexity in defining these relationships, particularly for heterogeneous transporter expressing systems.

A summary of the key findings in this project are given below;

1. Obtaining a purified plasma membrane is challenging as contamination from other organelle fractions is likely. While, the abundances of transporter proteins in total and plasma membrane fractions are not different, this could be caused by loss of target proteins in centrifugation steps. These losses could be accounted for by quantifiying protein content and marker protein abundances in starting lysates and end point fractions.
2. A QTAP workflow using a QconCAT approach was developed to quantify 6 transporters in human intestine and Caco-2 cells of varying ages, passage numbers and phenotypes
3. A bias in abundance quantification for transporter proteins between 2 laboratories was observed for P-gp. In addition, a between-laboratory difference in IVIVE scaling factor (REF) generation for BCRP was observed.
4. Functional studies in Caco-2 cells using E-3-S and vinblastine as probes for BCRP and P-gp, respectively, show that protein abundance is more closely correlated to transporter activity than mRNA expression.

5. Challenges were faced in establishing abundance-function relationshsips using transporter kinetics, as robust Michaelis constants for vinblastine in Caco-2 cells after compartmental modelling of *in vitro* transport assay data was not achieved across cells expressing variable levels of P-gp. This may be due to the experimental design of the transport assay.

Overall, this project faced many practical challenges, but raised many important questions regarding the limitations of the procedures for quantifying transporter protein abundances, which requires appreciation by scientists seeking to use abundance data for IVIVE-PBPK. The project has facilitated the development of transporter quantification assays which will be used in a host of concurrent and future projects, including transporter quantification in human brain microvessels, kidney and liver. At present, the implementation of transporter abundances into PBPK organs should be approached with caution. Yet, it should be possible to generate robust REF scaling factors to bridge abundance differences between *in vitro* and *in vivo* systems. This is provided that the validated QTAP, or even label free MS approaches, quantifying the abundances in both the *in vivo* and *in vitro* samples use the same workflows.

Work is currently underway to quantify the abundance of transporters in a further 35 intestinal membrane fractions for which mRNA gene expression data is available, in addition to the patients' drug history. This will enhance our knowledge as to the relationship between gene expression, protein abundance, inter-individual variability, disease and environmental factors for building improved virtual patient populations. Further work across multiple laboratories investigating abundance-function relationships should identify whether IVIVE scaling factors incorporating activity are required. Attempts to account for losses of target proteins during membrane fractionation and peptide digestion, in order to obtain more accurate abundance estimates, will greatly aid in the confidence of utilising abundance data for PBPK models.

Finally, the undertaking of a Pan European Collaboration to quantify enzyme and transporter abundances in matched liver tissues across multiple research groups, should provide invaluable information on the existence of procedural biases in operation between laboratories quantifying the abundance of proteins with PK relevance. In time, this may foster a consensus between groups as to the best practices and standardised workflow for LC-MS/MS-based abundance quantifications.

Appendices

Appendix 1

Appendix Table A-1. Donor demographics of intestinal samples, including recent drug history, in which alkaline phosphatase activity was determined.

Intestinal Region	Gender	Age	Ethnicity	Smoking Status	Disease/Complication/Operative Procedure
Proximal Jejunum	Female	56	Caucasian	Unknown	Reversal of double barrelled ileostomy. Resection of Ileum
Jejunum	Female	65	Caucasian	Unknown	Resection of jejunal fistula
Distal Jejunum	Female	67	Caucasian	Unknown	Small bowel fistula
Distal Jejunum	Female	70	Caucasian	Non-smoker	Enterocutaneous fistula followed by laparascopic nephrectomy
Distal Ileum	Male	52	Caucasian	Unknown	Diverticular Disease
Distal Colon	Female	70	Caucasian	Unknown	Adenocarcinoma
Distal Colon	Female	48	Caucasian	Non-smoker	Diverticular Disease

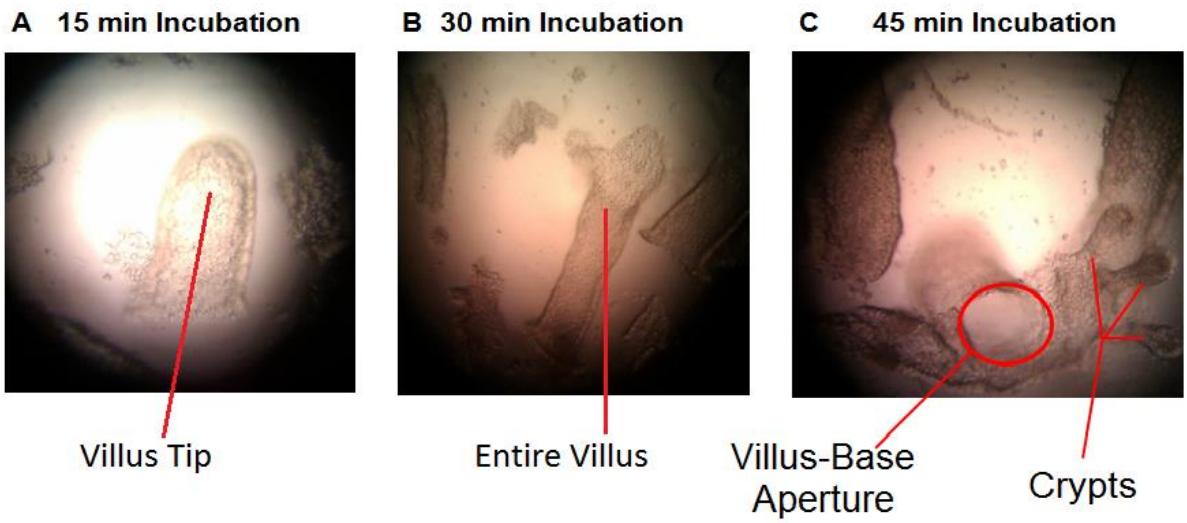

Appendix Figure A-1. Images of eluted material sampled onto slides from a human jejunum sample after 5 mM EDTA incubation over 45 min at (x 200 magnification, inverted microscope). A shows at 15 min there is shedding of villus tips. B shows at 30 min the presence of entire villus structures shed from the mucosa and C shows the presence of crypts attached to the base of a villus structure. Please note, the images are not of the highest quality as they were taken with a mobile phone-digital camera down the objective lens. There was no permanent digital camera affixed to this microscope.

Appendix 2

A

Protein View: VILI_HUMAN

Villin-1 OS=Homo sapiens GN=VIL1 PE=1 SV=4

Database:	UniProt
Score:	135
Nominal mass (M$_r$):	93093
Calculated pI:	5.99
Taxonomy:	Homo sapiens

Sequence similarity is available as an NCBI BLAST search of VILI_HUMAN against nr.

Search parameters

MS data file:	C:\X_Data\MassSpecData\20130813_RostamiAmin_RussellMathew\20130809_MR1_CACO_SLC.mgf
Enzyme:	Trypsin: cuts C-term side of KR unless next residue is P.
Fixed modifications:	Carbamidomethyl (C)
Variable modifications:	Oxidation (M)

Protein sequence coverage: 14%

Matched peptides shown in ***bold red***.

```
   1 MTKLSAQVKG SLNITTPGLQ IWRIEAMQMV PVPSSTFGSF FDGDCYIILA
  51 IHKTASSLSY DIHYWIGQDS SLDEQGAAAI YTTQMDDFLK GRAVQHREVQ
 101 GNESEAFRGY FKQGLVIRKG GVASGMKHVE TNSYDVQRLL HVKGKRNVVA
 151 GEVEMSWKSF NRGDVFLLDL GKLIIQWNGP ESTRMERLRG MTLAKEIRDQ
 201 ERGGRTYVGV VDGENELASP KLMEVMNHVL GKRRELRAAV PDTVVEPALK
 251 AALKLYHVSD SEGNLVVREV ATRPLTQDLL SHEDCYILDQ GGLKIYVWKG
 301 KKANEQEKKG AMSHALNFIK AKQYPPSTQV EVQNDGAESA VFQQLFQKWT
 351 ASNRTSGLGK THTVGSVAKV EQVKFDATSM HVKPQVAAQQ KMVDDGSGEV
 401 QVWRIENLEL VPVDSKWLGH FYGGDCYLLL YTYLIGEKQH YLLYVWQGSQ
 451 ASQDEITASA YQAVILDQKY NGEPVQIRVP MGKEPPHLMS IFKGRMVVYQ
 501 GGTSRTNNLE TGPSTRLFQV QGTGANNTKA FEVPARANFL NSNDVFVLKT
 551 QSCCYLWCGK GCSGDEREMA KMVADTISRT EKQVVVEGQE PANFWMALGG
 601 KAPYANTKRL QEENLVITPR LFECSNKTGR FLATEIPDFN QDDLEEDDVF
 651 LLDVWDQVFF WIGKHANEEE KKAAATTAQE YLKTHPSGRD PETPIIVVKQ
 701 GHEPPTFTGW FLAWDPFKWS NTKSYEDLKA ELGNSRDWSQ ITAEVTSPKV
 751 DVFNANSNLS SGPLPIFPLE QLVNKPVEEL PEGVDPSRKE EHLSIEDFTQ
 801 AFGMTPAAFS ALPRWKQQNL KKEKGLF
```

High ranking proteotypic peptide sequence for Villin AQUA SIL generation

B

Sodium/potassium-transporting ATPase subunit alpha-1 OS=Homo sapiens GN=ATP1A1 PE=1 SV=1

Database:	UniProt
Score:	524
Nominal mass (M$_r$):	114135
Calculated pI:	5.33
Taxonomy:	Homo sapiens

Sequence similarity is available as an NCBI BLAST search of AT1A1_HUMAN against nr.

Search parameters

MS data file:	C:\X_Data\MassSpecData\20130813_RostamiAmin_RussellMathew\20130809_MR5_CACO_PM.mgf
Enzyme:	Trypsin: cuts C-term side of KR unless next residue is P.
Fixed modifications:	Carbamidomethyl (C)
Variable modifications:	Oxidation (M)

Protein sequence coverage: 23%

Matched peptides shown in ***bold red***.

```
   1 MGKGVGRDKY EPAAVSEQGD KKGKKGKKDR DMDELKKEVS MDDHKLSLDE
  51 LHRKYGTDLS RGLTSARAAE ILARDGPNAL TPPPTTPEWI KFCRQLFGGF
 101 SMLLWIGAIL CFLAYSIQAA TEEEPQNDNL YLGVVLSAVV IITGCFSYYQ
 151 EAKSSKIMES FKNMVPQQAL VIRNGEKMSI NAEEVVVGDL VEVKGGDRIP
 201 ADLRIISANG CKVDNSSLTG ESEPQTRSPD FTNENPLETR NIAFFSTNCV
 251 EGTARGIVVY TGDRTVMGRI ATLASGLEGG QTPIAAEIEH FIHIITGVAV
 301 FLGVSFFILS LILEYTWLEA VIFLIGIIVA NVPEGLLATV TVCLTLTAKR
 351 MARKNCLVKN LEAVETLGST STICSDKTGT LTQNRMTVAH MWFDNQIHEA
 401 DTTENQSGVS FDKTSATWLA LSRIAGLCNR AVFQANQENL PILKRAVAGD
 451 ASESALLKCI ELCCGSVKEM RERYAKIVEI PFNSTNKYQL SIHKNPNTSE
 501 PQHLLVMKGA PERILDRCSS ILLHGKEQPL DEELKDAFQN AYLELGGLGE
 551 RVLGFCHLFL PDEQFPEGFQ FDTDDVNFPI DNLCFVGLIS MIDPPRAAVP
 601 DAVGKCRSAG IKVIMVTGDH PITAKAIAKG VGIISEGNET VEDIAARLNI
 651 PVSQVNPRDA KACVVHGSDL KDMTSEQLDD ILKYHTEIVF ARTSPQQKLI
 701 IVEGCQRQGA IVAVTGDGVN DSPALKKADI GVAMGIAGSD VSKQAADMIL
 751 LDDNFASIVT GVEEGRLIFD NLKKSIAYTL TSNIPEITPF LIFIIANIPL
 801 PLGTVTILCI DLGTDMVPAI SLAYEQAESD IMKRQPRNPK TDKLVNERLI
 851 SMAYGQIGMI QALGGFFTYF VILAENGFLP IHLLGLRVDW DDRWINDVED
 901 SYGQQWTYEQ RKIVEFTCHT AFFVSIVVVQ WADLVICKTR RNSVFQQGMK
 951 NKILIFGLFE ETALAAFLSY CPGMGVALRM YPLKPTWWFC AFPYSLLIFV
1001 YDEVRKLIIR RRPGGWVEKE TYY
```

High ranking proteotypic peptide selected for Na/K-ATPase AQUA SIL generation

Appendix Figure B-1. Caco-2 PM digest submitted for fragmentation by an Orbitrap mass spectrometer and data-dependent acquisition (DDA). Regions in red represent peptide sequences identified after a Mascot search for A. Human Villin and B. Human Na/K-ATPase, with selected peptides within the black boxes.

A B

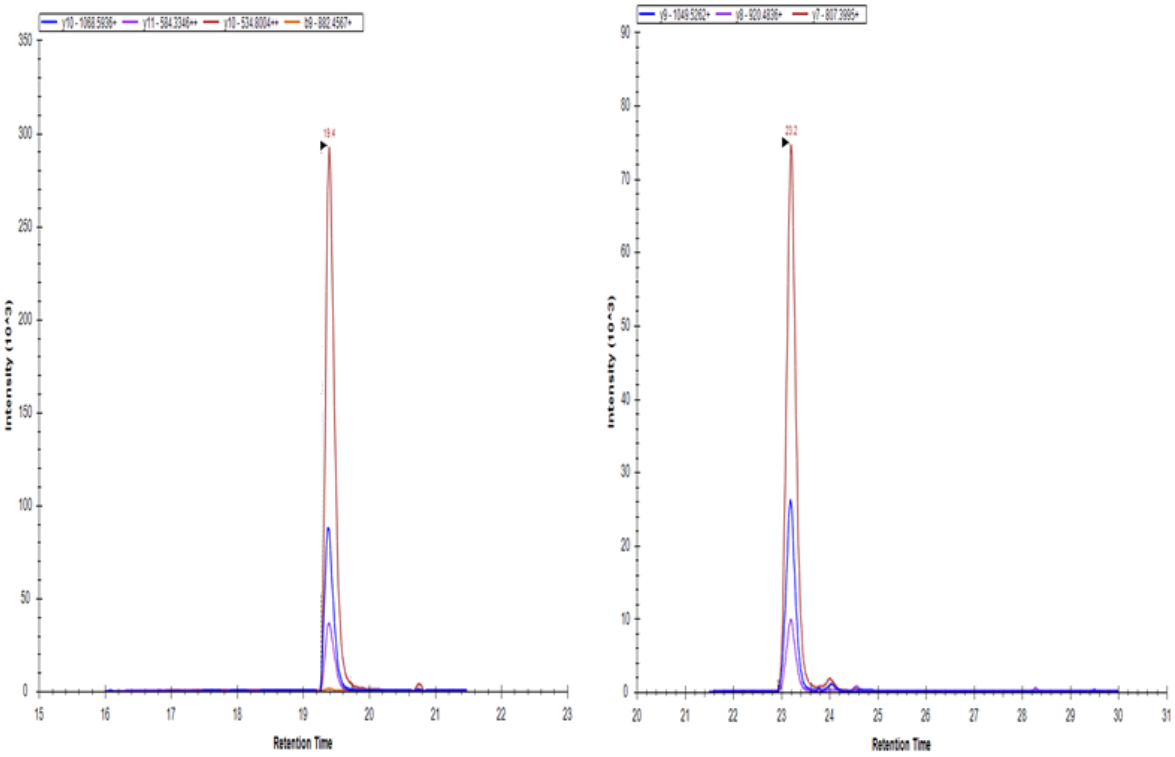

Appendix Figure B-2. Selected transition of the native peptides of a 21d-Grown Caco-2 cell plasma membrane DOC-digest for Villin (A) and Na/K-ATPase (B).

Appendix 3

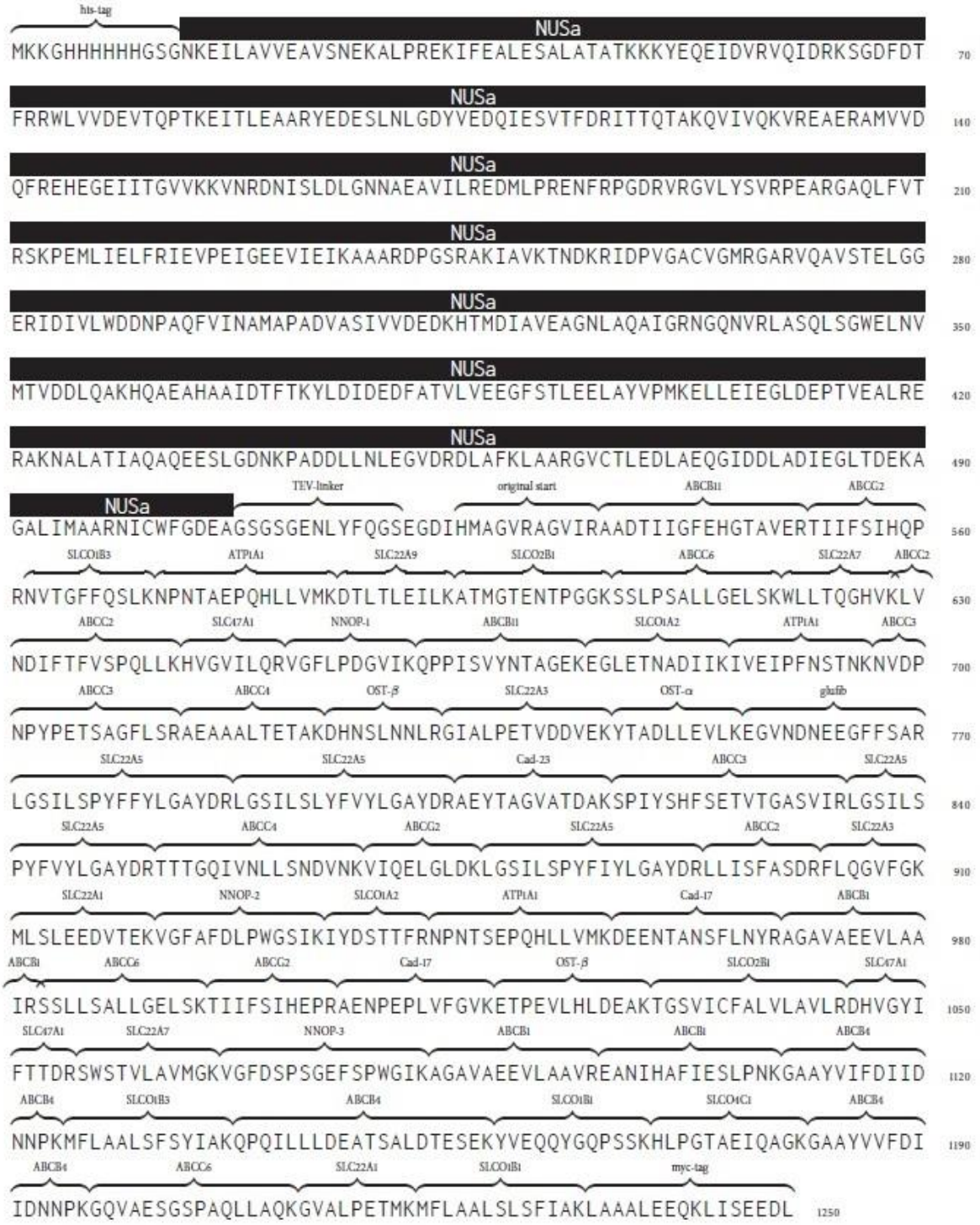

Appendix Figure C-1. The TransCAT construct sequence annotating the target transporter and supporting peptides to permit successful expression in the host E.Coli vector (published as supporting information in (Russell et al., 2013).

Appendix 4

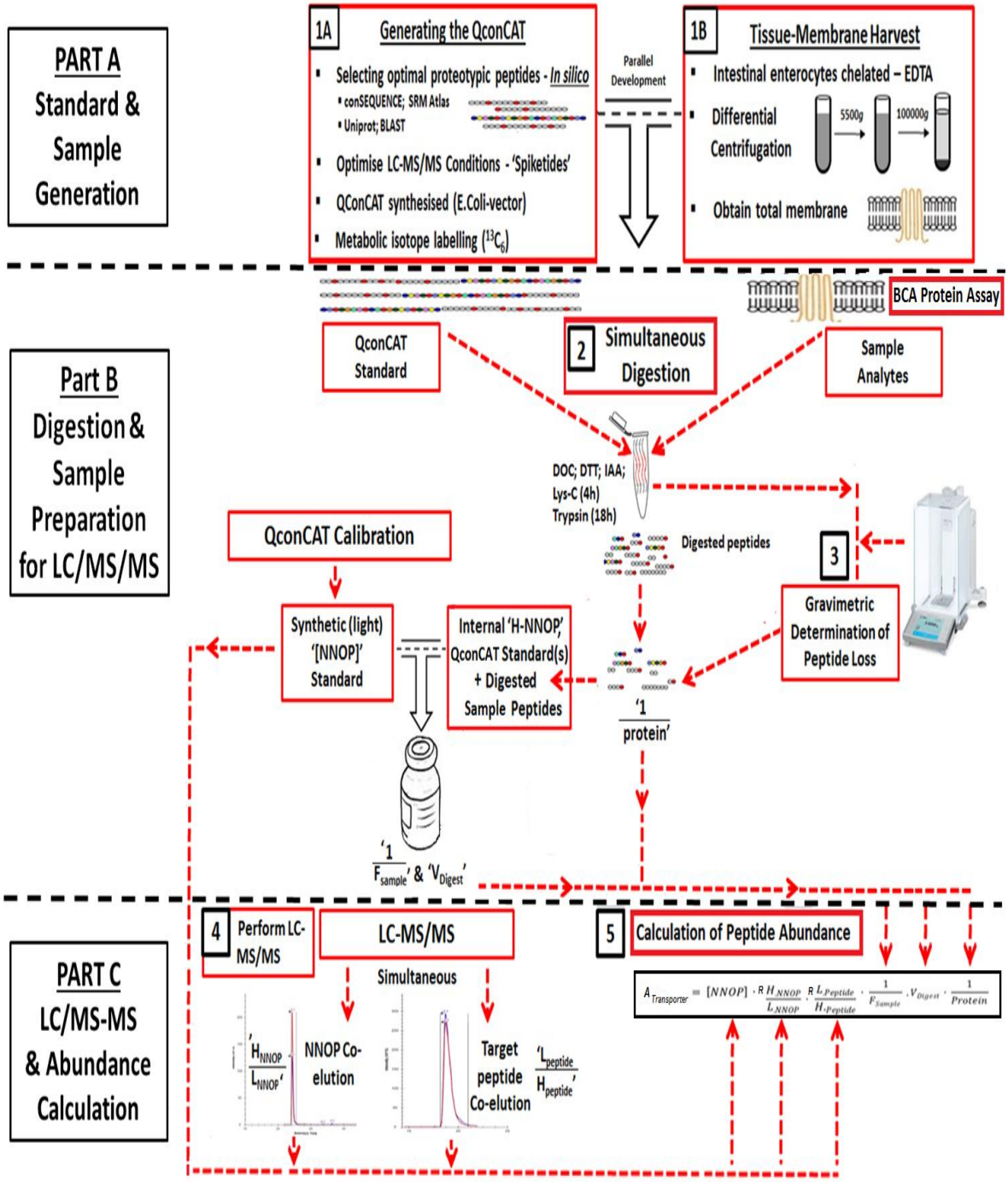

Appendix Figure D-1. A schematic of the workflow to measure human intestinal transporter protein absolute abundance using a QconCAT method. Part A describes the parallel development of the QconCAT (1A) and the human intestinal enterocyte chelation protocol (1B). Part B describes sample digestion and preparation for LC-MS/MS, where IAA is iodoacetamide. The simultaneous digestion of the extracted QconCAT peptide containing the isotope labelled standards and the total membrane fraction (post BCA protein assay), typically 50 µg, from the chelated intestinal enterocytes is performed (2). During the digestion procedure, prior to loading the digested sample into a vial for LC-MS/MS, peptide losses are determined gravimetrically. The digested peptides containing the sample and isotope labelled peptide standards are combined with a synthetic unlabelled calibrator NNOP of known concentration and are submitted for LC-MS/MS analysis. Part C describes obtaining co-elution profiles (labelled and unlabelled) for both the NNOP and target peptide(s) simultaneously and this information is incorporated into Equation 2-1. Any term in this figure enclosed with apostrophes directly feeds into the calculation of transporter protein abundance ($A_{transporter}$).

Gravimetric derivation of peptide mass in tube prior to LC sampling

The following sections (Part A and B) describe calculating the protein content (*i.e.*, the peptide digest) prior to LC sampling, termed from now on as 'Protein Content'. The protein content relates the abundance in fmol of the target peptide in the digest to an abundance per µg in the 'Protein' matrix under study (fmol/µg).

In order to derive peptide mass by gravimetric means, there are a series of instances in which sample tubes and their contents mass (µg) are measured. Accordingly, volumes (µL) of tube contents are required for calculations which are also defined. The following sections are incorporated into subsequent calculations (Parts A and B).

Definition of measured masses

A_{TM} = Mass of tube plus mass of digested sample – prior to removal of sodium deoxycholate

A_{SP} = Mass of tube plus mass of remaining precipitate (dried overnight)

A_{MVC} = Mass of tube entered for vacuum centrifugation (VC)

A_{SVC} = Mass of tube plus mass of sample entered for VC

A_{TSPVC} = Mass of tube plus mass of sample post-VC

Definition of volumes

V_D = Volume of protein plus QconCAT in-solution prior to denaturation stage

V_{QC} = Volume of QconCAT prior to denaturation stage

V_P = Volume of peptide digest in LC tube

V_{NNOP} = Volume of NNOP (*i.e.*, Glu-Fib) in LC tube

Part A

The total amount of peptide generated after evaporation by VC (A_{VC}) requires deriving in order to express the target peptide abundance as a concentration per mass of protein, where the mass of protein in this instance is defined as A_{LC}, or more precisely, the amount of peptide in the LC tube. Part A deals with derivation of A_{VC}.

$$A_{DD} = A_{TM} - A_{SP}$$ Equation S1

where A_{DD} is the mass of the solution digest prior to sodium deoxycholate removal.

$$A_D = A_{SVC} - A_{MVC}$$ Equation S2

where A_D is the mass of the digested sample prior to VC.

$$F_{AP} = \frac{A_D}{A_{DD}}$$ Equation S3

where F_{AP} is the fractional mass of peptide in solution prior to VC

$$A_{VCQ} = F_{AP} \cdot P_N$$ Equation S4

where P_N is the nominal mass of protein entering the in-solution digestion procedure (typically 50 µg) and A_{VCQ} is the mass of the peptide material prior to VC.

$$F_{QconCAT} = \frac{V_D}{(V_D - V_{QC})}$$ Equation S5

where $F_{QconCAT}$ is the factor required to correct for dilution of the protein quantity entering the denaturation stage by addition of the QconCAT.

$$A_{VC} = \frac{A_{VCQ}}{F_{QconCAT}}$$ Equation S6

Part B

Part B describes the amount of peptide entering the LC tube ('Protein Content') which is the term used for correcting peptide abundance (fmol) to an abundance per unit of protein (fmol/µg).

$$V_{LC} = V_P + V_{NNOP}$$ Equation S7

where V_{LC} is the volume of sample in the LC tube.

$$A_{SPVC} = A_{TSPVC} - A_{MVC}$$ Equation S8

where A_{SPVC} is the mass of the sample after VC without accounting for mass fraction correction.

$$F_{sample} = \frac{V_{LC}}{V_P}$$ Equation S9

where F_{sample} is the factor required to correct for dilution of peptide digest in the LC tube when NNOP is added.

$$A_{CS} = \frac{A_{VC}}{A_{SPVC}} \quad \text{Equation S10}$$

where A_{CS} is the mass concentration of the peptides (µg/ µg) in the starting material for entering into the LC tube.

$$A_{CSC} = \frac{A_{CS}}{F_{sample}} \quad \text{Equation S11}$$

where A_{CSC} is the mass concentration of the digest analysed by LC-MS/MS after correction for NNOP dilution.

$$A_{SLC} = \rho \cdot V_{LC} \quad \text{Equation S12}$$

where ρ is the density (mass : volume ratio) of the peptide mix after VC and A_{SLC} is the mass of the solution (peptides + NNOP) in the LC tube.

$$'Protein' = A_{SLC} \cdot A_{CSC} \quad \text{Equation S13}$$

Ultimately, the 'Protein Content' term defines the amount of protein in the entire LC vial. Accordingly, the concentration of peptide (fmol) as determined from the ratio of light : heavy target peptides is defined for the entire LC tube.

Protocol deviation for AQUA (University of Manchester)

For the AQUA procedure, Equations S1-4 are incorporated into the workflow and equations S5-6 are omitted as QconCAT correction is not required prior to the denaturation stage. Therefore, A_{VCQ} derived in Equation S4 is to be used in Equation S10 rather than the numerator A_{VC}. The density was not measured for the AQUA quantification. In these cases it was assumed that density was equivalent to 1 mg/mL and therefore did not require correction. It should be noted that the mean density from other Caco-2 quantifications performed for the QconCAT strategy was 0.97 mg/mL.

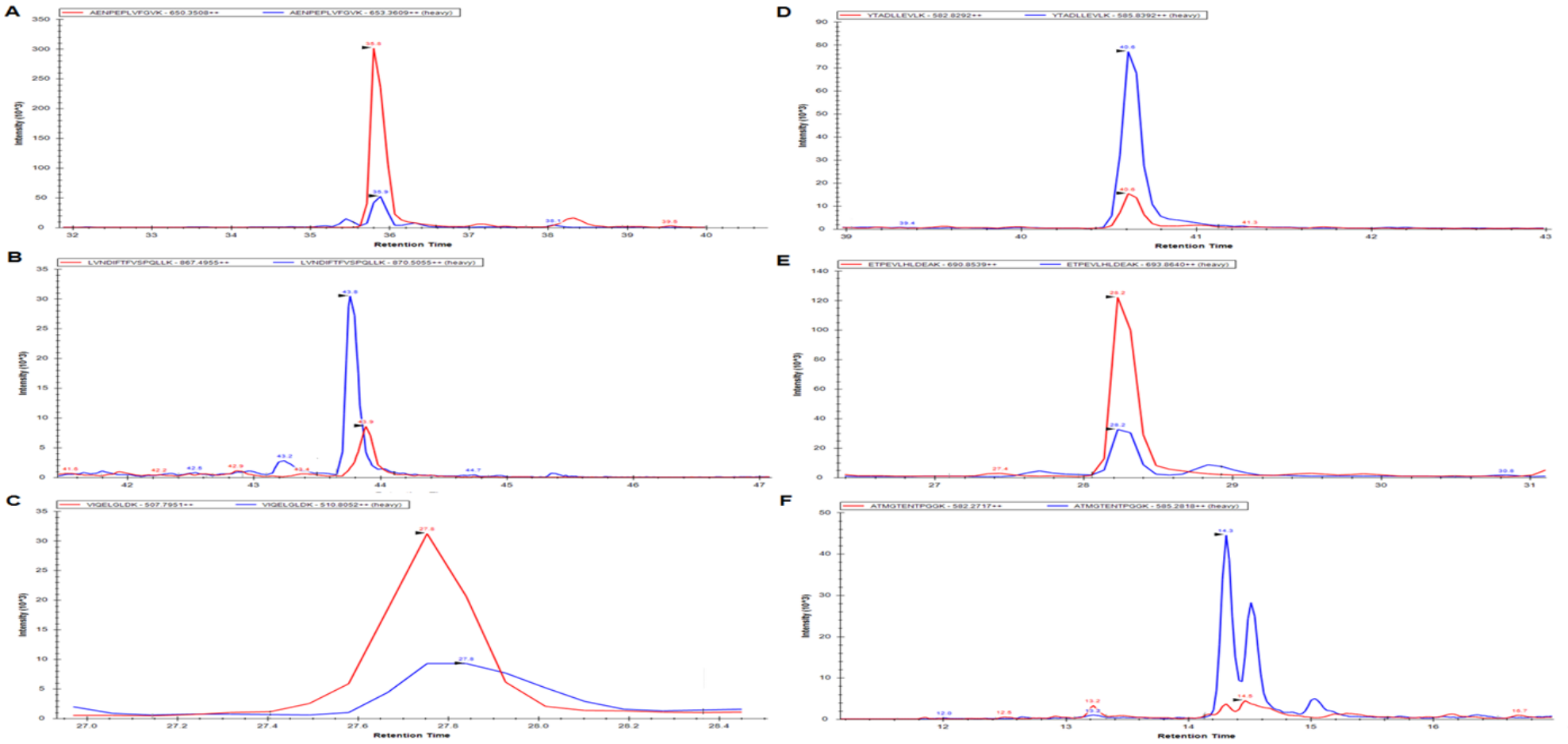

Appendix Figure D-2. Co-elution profiles for HPT1 (A), MRP2 (B), BCRP (C), OST-α (D), OST-β (E), and OATP2B1 (F). The red lines are the cumulative profiles for the selected native peptide transitions and the blue lines are the cumulative profiles for the selected standard peptide transitions.

Appendix Table D-1. Individual transporter protein abundance data from human intestinal tissues quantified by the QconCAT (also see Figure 4-12).

Sample	Human Intestinal Protein Abundance (fmol/µg)							
	Na/K-ATPase	HPT1	P-gp	MRP2	BCRP	OST-α	OST-β	OATP2B1
Jejunum 1	41.93	10.57	3.07	0.37	2.28	BLQ	1.98	0.29
Jejunum 2	34.58	7.17	0.98	0.85	1.92	BLQ	1.93	BLQ
Jejunum 3	29.57	4.48	1.62	0.55	3.49	0.47	3.18	BLQ
Ileum 1	24.47	6.93	0.2	BLQ	1.6	0.28	1.55	BLQ

Appendix 5

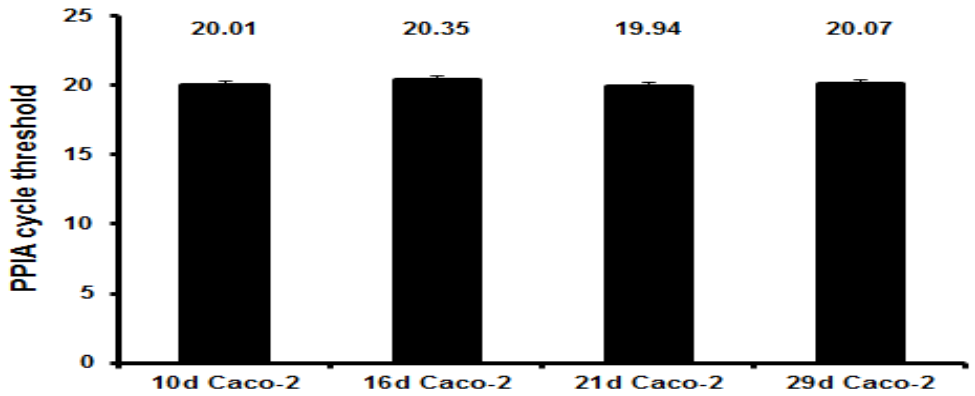

Appendix Figure E-1. The stability of the housekeeper gene PPIA in Caco-2 cell monolayers cultured from 10 to 29 days on filters. The values above the bars are the mean for n=3 extractions on separate days, the PCR analysis is run on two different days. Values are given as Mean±SD.

Appendix Table E-1. Individual PPIA normalised mRNA gene expression of P-gp, MRP2 and BCRP in low passage Caco-2 cells.

Caco-2 Low Passage (growth age)	PPIA Normalised Gene Expression		
	P-gp	**MRP2**	**BCRP**
10d	0.014, 0.015, 0.016 (n=3)	0.006, 0.005, 0.006 (n=3)	0.021, 0.020, 0.027 (n=3)
16d	0.034, 0.048, 0.036 (n=3)	0.007, 0.008, 0.005 (n=3)	0.028, 0.042, 0.031 (n=3)
21d	0.072, 0.037, 0.034 (n=3)	0.017, 0.015, 0.01 (n=3)	0.035, 0.053, 0.047 (n=3)
29d	0.061, 0.048, 0.028 (n=3)	0.012, 0.01, 0.012 (n=3)	0.048, 0.021, 0.03 (n=3)

Appendix Table E-2. Individual PPIA normalised mRNA gene expression of OATP2B1, OST-α and OST-β in low passage Caco-2 cells.

Caco-2 Low Passage (growth age)	PPIA Normalised Gene Expression		
	OATP2B1	**OST-A**	**OST-B**
10d	0.135, 0.151, 0.015 (n=3)	0.021, 0.019, 0.016 (n=3)	0.04, 0.044, 0.057 (n=3)
29d	0.323, 0.205, 0.301 (n=3)	0.063, 0.029, 0.04 (n=3)	0.057, 0.063, 0.073 (n=3)

Appendix Table E-3. Individual Na/K-ATPase abundances in 10 to 29d cultured Caco-2 cells (p25-35) quantified at Bertin Pharma. Each data point is n=3 pooled filters constituting 1 experiment. The boxed values represent samples which were also quantified by the UoM.

	Na/K-ATPase Abundance (fmol/µg)					
	Caco-2 (10d)		**Caco-2 (21d)**		**Caco-2 (29d)**	
	Total Membrane	Plasma Membrane	Total Membrane	Plasma Membrane	Total Membrane	Plasma Membrane
	55.7	56.8	52.8	80.9	66.4	72.9
	38.1	45.6	56.7	60.8	55.2	83.0
	29.4	48.9	50.7	63.7	46.4	63.7
			51.6		49.3	
			56.7		74.8	
			65.9		52.4	
Mean	41.04	50.46	55.73	68.47	57.44	73.18
SD	13.41	5.77	5.57	10.90	10.95	9.69

Appendix Table E-4. Individual Na/K-ATPase abundances in 10 to 29d cultured Caco-2 cells (p25-35) quantified at the University of Manchester. Each data point is n=3 pooled filters constituting 1 experiment.

	Na/K-ATPase Abundance (fmol/µg)					
	Caco-2 (10d)		Caco-2 (21d)		Caco-2 (29d)	
	Total Membrane	Plasma Membrane	Total Membrane	Plasma Membrane	Total Membrane	Plasma Membrane
	N.S	N.S	84.56	N.S	79.39	N.S
	N.S	11.85	48.35	N.S	55.70	N.S
	N.S	N.S	58.91	N.S	60.33	24.85
Mean	N.S	11.85	63.94	N.S	65.14	24.85
SD	N.S	N.S	18.62	N.S	12.56	N.S

Matched samples analysed in both Bertin pharma and The University of Manchester relating to Figure 5-7 Figure 5-8 are highlighted by colour coded boxes.

Appendix Table E-5. Individual P-gp abundances in 10 to 29d cultured Caco-2 cells (p25-35) quantified at Bertin Pharma. Each data point is n=3 pooled filters constituting 1 experiment.

	P-gp Abundance (fmol/µg)					
	Caco-2 (10d)		Caco-2 (21d)		Caco-2 (29d)	
	Total Membrane	Plasma Membrane	Total Membrane	Plasma Membrane	Total Membrane	Plasma Membrane
	3.59	3.34	0.72	0.82	2.60	2.53
	2.53	2.87	2.08	1.59	1.53	1.61
	3.36	5.04	2.89	2.23	1.26	1.20
			1.89		1.64	
			2.27		2.29	
			2.07		1.98	
Mean	3.16	3.75	1.99	1.54	1.79	1.78
SD	0.56	1.14	0.71	0.71	0.71	0.68

Appendix Table E-6. Individual P-gp abundances in 10 to 29d cultured Caco-2 cells (p25-35) quantified at the University of Manchester. Each data point is n=3 pooled filters constituting 1 experiment.

	P-gp Abundance (fmol/µg)					
	Caco-2 (10d)		Caco-2 (21d)		Caco-2 (29d)	
	Total Membrane	Plasma Membrane	Total Membrane	Plasma Membrane	Total Membrane	Plasma Membrane
	N.S	N.S	5.25	N.S	8.35	N.S
	N.S	2.97	4.53	N.S	6.84	N.S
	N.S	N.S	4.35	N.S	5.77	1.64
Mean	N.S	2.97	4.71	N.S	6.99	1.64
SD	N.S	N.S	0.48	N.S	1.30	N.S

Matched samples analysed in both Bertin pharma and The University of Manchester relating to Figure 5-9 and Figure 5-10 are highlighted by colour coded boxes.

Appendix Table E-7. Individual BCRP abundances in 10 to 29d cultured Caco-2 cells (p25-35) quantified at Bertin Pharma. Each data point is n=3 pooled filters constituting 1 experiment.

	BCRP Abundance (fmol/µg)					
	Caco-2 (10d)		Caco-2 (21d)		Caco-2 (29d)	
	Total Membrane	Plasma Membrane	Total Membrane	Plasma Membrane	Total Membrane	Plasma Membrane
	3.32	3.38	0.83	0.51	1.09	1.90
	2.92	3.70	2.12	1.36	1.36	1.36
	2.96	4.58	1.46	1.29	0.72	0.58
			1.70		1.34	
			1.94		1.64	
			1.94		1.51	
Mean	3.06	3.89	1.67	1.05	1.28	1.28
SD	0.22	0.62	0.47	0.47	0.33	0.67

Appendix Table E-8. Individual BCRP abundances in 10 to 29d cultured Caco-2 cells (p 25-35) quantified at the University of Manchester. Each data point is n=3 pooled filters constituting 1 experiment.

	BCRP Abundance (fmol/µg)					
	Caco-2 (10d)		Caco-2 (21d)		Caco-2 (29d)	
	Total Membrane	Plasma Membrane	Total Membrane	Plasma Membrane	Total Membrane	Plasma Membrane
	N.S	N.S	1.19	N.S	1.13	N.S
	N.S	2.17	1.17	N.S	0.72	N.S
	N.S	N.S	1.13	N.S	0.76	2.80
Mean	N.S	2.17	1.16	N.S	0.87	2.80
SD	N.S	N.S	0.03	N.S	0.23	N.S

Matched samples analysed in both Bertin pharma and the University of Manchester relating to Figure 5-11 & Figure 5-12 are highlighted by colour coded boxes

Appendix Table E-9. Batch differences for Na/K-ATPase, P-gp, and BCRP protein abundances in Caco-2 cell 21 and 29d harvested TM fractions sent to Bertin Pharma.

	Na/K-ATPase (fmol/µg)				P-gp (fmol/µg)				BCRP (fmol/µg)			
	Caco-2 (21d)		Caco-2 (29d)		Caco-2 (21d)		Caco-2 (29d)		Caco-2 (21d)		Caco-2 (29d)	
	Batch 1	Batch 2	Batch 1	Batch 2	Batch 1	Batch 2	Batch 1	Batch 2	Batch 1	Batch 2	Batch 1	Batch 2
	52.8	51.6	66.4	49.3	0.72	1.89	2.60	1.64	0.83	1.70	1.09	1.34
	56.7	56.7	55.2	74.8	2.08	2.27	1.53	2.29	2.12	1.94	1.36	1.64
	50.7	65.9	46.4	52.4	2.89	2.07	1.26	1.98	1.46	1.94	0.72	1.51
Mean	53.40	58.06	56.03	58.85	1.90	2.08	1.79	1.97	1.47	1.86	1.06	1.50
SD	3.01	7.24	10.02	13.91	1.10	0.19	0.71	0.32	0.64	0.14	0.33	0.15

There are no differences between the quantifications in batch 1 and batch 2 for any protein. Note, that these are not matched samples and the TM were generated at least 7 months apart.

Appendix Table E-10. Individual MRP2, OATP2B1, OST-α and OST-β abundances in 10 to 29d cultured Caco-2 cells (p25-35) quantified at the University of Manchester. Each data point is n=3 pooled filters constituting 1 experiment.

	MRP2 Abundance (fmol/µg)					
	Caco-2 (10d)		Caco-2 (21d)		Caco-2 (29d)	
	Total Membrane	Plasma Membrane	Total Membrane	Plasma Membrane	Total Membrane	Plasma Membrane
	N.S	N.S	0.27	N.S	BLQ	N.S
	N.S	0.67	BLQ	N.S	BLQ	N.S
	N.S	N.S	0.24	N.S	BLQ	Issue
Mean	N.S	0.67	0.26	N.S	BLQ	N.S
SD	N.S	N.S	0.02	N.S	BLQ	N.S

	OATP2B1 Abundance (fmol/µg)					
	Caco-2 (10d)		Caco-2 (21d)		Caco-2 (29d)	
	Total Membrane	Plasma Membrane	Total Membrane	Plasma Membrane	Total Membrane	Plasma Membrane
	N.S	N.S	Issue	N.S	1.55	N.S
	N.S	1.06	BLQ	N.S	BLQ	N.S
	N.S	N.S	0.43	N.S	0.21	1.50
Mean	N.S	1.06	0.43	N.S	0.88	1.50
SD	N.S	N.S	N.S	N.S	0.95	N.S

	OST-α Abundance (fmol/µg)					
	Caco-2 (10d)		Caco-2 (21d)		Caco-2 (29d)	
	Total Membrane	Plasma Membrane	Total Membrane	Plasma Membrane	Total Membrane	Plasma Membrane
	N.S	N.S	0.85	N.S	0.59	N.S
	N.S	BLQ	0.76	N.S	0.44	N.S
	N.S	N.S	0.62	N.S	0.40	0.74
Mean	N.S	BLQ	0.74	N.S	0.48	0.74
SD	N.S	N.S	0.12	N.S	0.10	N.S

	OST-β Abundance (fmol/µg)					
	Caco-2 (10d)		Caco-2 (21d)		Caco-2 (29d)	
	Total Membrane	Plasma Membrane	Total Membrane	Plasma Membrane	Total Membrane	Plasma Membrane
	N.S	N.S	2.44	N.S	2.26	N.S
	N.S	2.17	1.60	N.S	1.10	N.S
	N.S	N.S	1.10	N.S	1.13	3.44
Mean	N.S	2.17	1.71	N.S	1.50	3.44
SD	N.S	N.S	0.68	N.S	0.66	N.S

Appendix Table E-11. E-3-S and Ko143 permeability for individual Caco-2 monolayers at pH6.5/7.4.

E-3-S P_{app} (x 10^{-6} cm s^{-1}) Caco-2 (10d)		E-3-S + Ko143 P_{app} (x 10^{-6} cm s^{-1}) Caco-2 (10d)		E-3-S P_{app} (x 10^{-6} cm s^{-1}) Caco-2 (29d)		E-3-S + Ko143 P_{app} (x 10^{-6} cm s^{-1}) Caco-2 (29d)	
A-to-B	**B-to-A**	**A-to-B**	**B-to-A**	**A-to-B**	**B-to-A**	**A-to-B**	**B-to-A**
2.34	17.9	3.27	4.39	1.49	20.12	2.23	1.97
2.6	14.83	3.7	3.83	1.26	17.94	2.00	1.81
2.61	12.69	2.85	3.18	1.34	16.41	1.95	1.85
2.38	12.92	2.82	3.38	1.39	15.71	2.13	1.49
3.03	22.83	3.59	5.21	1.52	14.02	2.27	1.58
2.87	19.76	3.03	5.12	1.42	13.66	2.02	1.5
2.54	19.88	3.32	5.41	4.26	13.48		
				4.44	11.85		
				4.41	12.99		
				3.81	12.02		
				3.21	10.25		
				3.76	10.28		

Appendix Table E-12. E-3-S and Ko143 permeability for individual Caco-2 monolayers at pH7.4/7.4.

E-3-S P_{app} (x 10^{-6} cm s^{-1}) Caco-2 (10d)		E-3-S + Ko143 P_{app} (x 10^{-6} cm s^{-1}) Caco-2 (10d)		E-3-S P_{app} (x 10^{-6} cm s^{-1}) Caco-2 (29d)		E-3-S + Ko143 P_{app} (x 10^{-6} cm s^{-1}) Caco-2 (29d)	
A-to-B	**B-to-A**	**A-to-B**	**B-to-A**	**A-to-B**	**B-to-A**	**A-to-B**	**B-to-A**
3.68	21.14			5.06	13.5	3.24	1.64
3.01	19.7			3.68	13.72	3.58	1.49
3.1	20			3.55	12.24	3.00	1.69
2.34	16.58			5.12	11.98		2.4
2.23	15.66			4.11	11.63		2.9
2.01	16.98			4.33	14.09		3.04
2.18	18.73				14.34	3.43	1.87
1.93	17.91			3.63	13.33	3.67	1.83
1.97	16.93			4.19	13.23	3.75	1.89
2.74	34.05	4.74	6.96	4.58	15.43		
2.85	23.64	4.44	5.95	3.09	14.65		
2.69	22.66	4.54	5.76		15.94		
2.36	34.64	4.75	6.78				
2.19	24.49	4.29	5.95				
2.2	25.67	4.36	6.29				

Appendix Table E-13. E-3-S and Ko143 permeability for individual Caco-2 monolayers at pH6.5/6.5.

E-3-S P_{app} (x 10^{-6} cm s^{-1}) Caco-2 (10d)		E-3-S + Ko143 P_{app} (x 10^{-6} cm s^{-1}) Caco-2 (10d)		E-3-S P_{app} (x 10^{-6} cm s^{-1}) Caco-2 (29d)		E-3-S + Ko143 P_{app} (x 10^{-6} cm s^{-1}) Caco-2 (29d)	
A-to-B	B-to-A	A-to-B	B-to-A	A-to-B	B-to-A	A-to-B	B-to-A
3.06	23.25	No Data	No Data	1.61	15.22	2.31	1.96
2.66	19.49	Assay not run	Assay not	1.86	12.03	1.72	1.87
3.34	20.98		run	2.32	14.00	2.32	2.03
2.4	20.85			1.90	23.65	4.03	2.06
2.27	15.98			2.22	18.42	4.07	2.49
2.16	16.43			2.09	16.86	2.61	2.61
2.38	21.73			4.89	16.43	4.24	2.00
2.25	17.99			4.80	14.38	4.44	1.78
2.09	16.05			4.22	14.29		1.76
				3.35	18.35		
				3.71	15.46		
				3.51	17.27		

Appendix 6

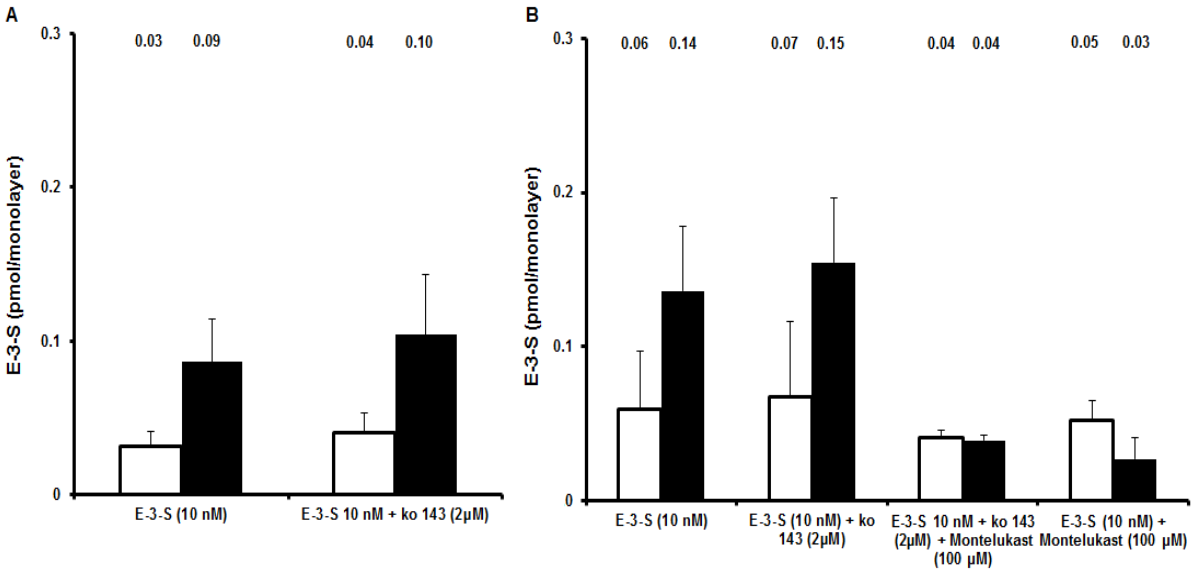

Appendix Figure F-1. E-3-S monolayer content in 10 and 29d Caco-2 cells after incubation with Ko143 and montelukast at pH 6.5/7.4. A denotes the 10d and B the 29d monolayers. The A-to-B and B-to-A Papp are represented by white & black bars, respectively. The text above the bars is the mean Papp under each condition. The values are Mean±SD of a minimum of n=7 filters of N=3 experiments for conditions without montelukast and n=3 filters, N=1 experiments with montelukast.

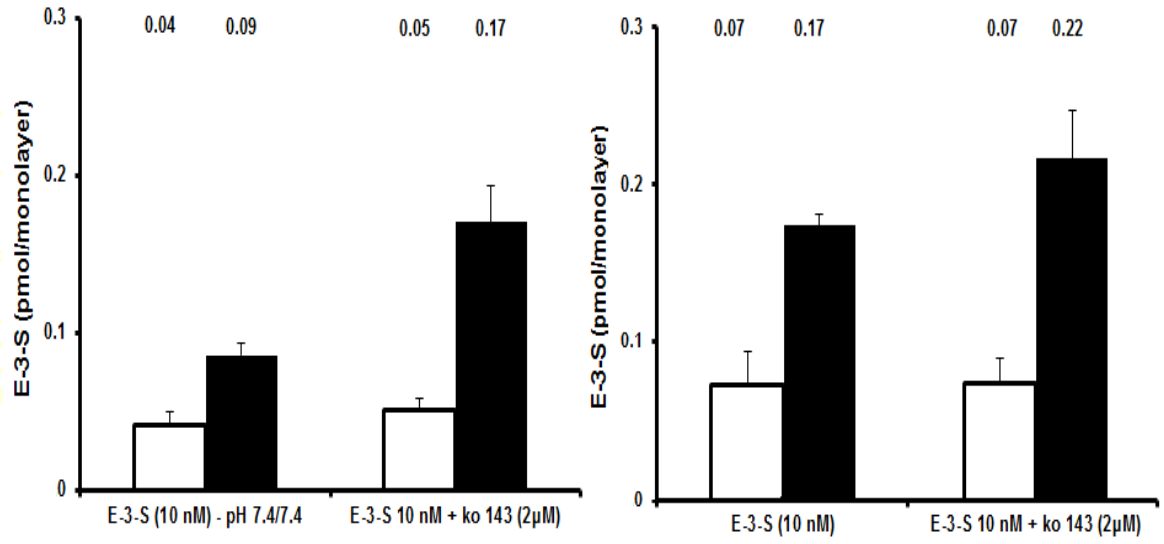

Appendix Figure F-2. E-3-S monolayer content in 10 and 29d Caco-2 cells after incubation with Ko143 at pH 7.4/7.4. A denotes the 10d and B the 29d monolayers. The A-to-B and B-to-A Papp are represented by white black bars, respectively. The text above the bars is the mean Papp under each condition. The values are Mean±SD of a minimum of n=6 filters of N=2 experiments.

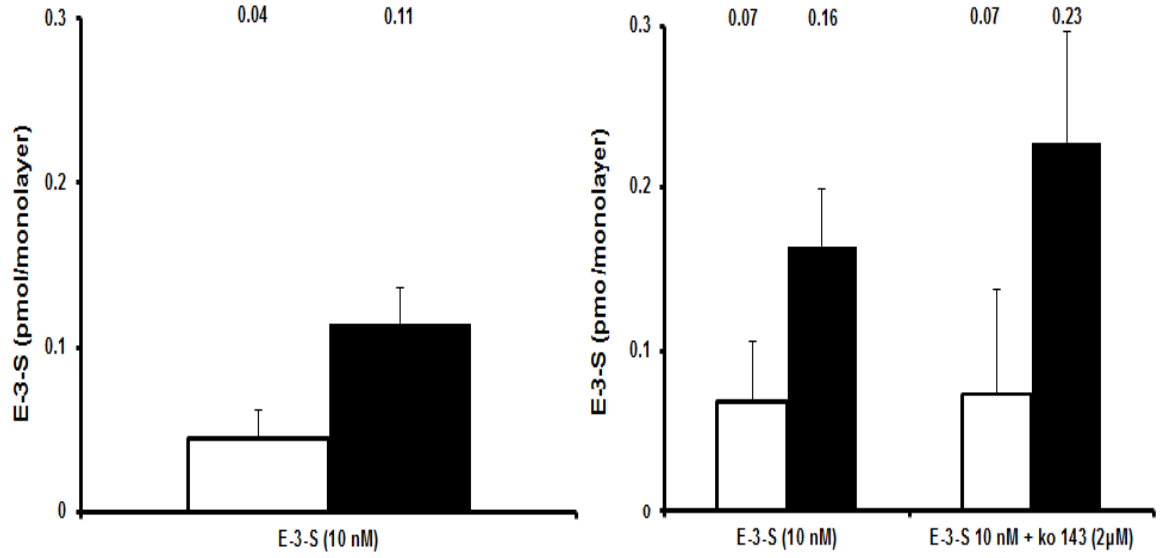

Appendix Figure F-3. E-3-S monolayer content in 10 and 29d Caco-2 cells at pH 6.5/6.5. A denotes the 10d and B the 29d monolayers. The A-to-B and B-to-A Papp are represented by white black bars, respectively. The text above the bars is the mean Papp under each condition. The values are Mean±SD of n=9 filters of N=3 experiments.

Due to time constraints, E-3-S incubation with Ko143 in 10d monolayers was not performed.

Appendix 7

Appendix Table G-1. Individual PPIA normalised mRNA gene expression of P-gp, MRP2 and BCRP in Caco-2 cell variants.

Caco-2 Variants (21d-grown)	PPIA Normalised Gene Expression		
	P-gp	**MRP2**	**BCRP**
Low passage	0.072, 0.037, 0.034 (n=3)	0.017, 0.015, 0.01 (n=3)	0.035, 0.053, 0.047 (n=3)
High Passage	0.048, 0.082, 0.055 (n=3)	0.009, 0.009, 0.01 (n=3)	0.008, 0.010, 0.008 (n=3)
VBL-Selected	0.095, 0.131, 0.069 (n=3)	0.01, 0.012, 0.01 (n=3)	0.004, 0.004, 0.003 (n=3)

Appendix Table G-2. Individual Na/K-ATPase abundances in 21 day cultured Caco-2 cells variants quantified at Bertin Pharma. Each data point is n=3 pooled filters constituting 1 experiment.

	Na/K-ATPase Abundance (fmol/µg)					
	Caco-2 (21d)		**Caco-2 (21d) High Passage**		**Caco-2 - VBL (21d)**	
	Total Membrane	Plasma Membrane	Total Membrane	Plasma Membrane	Total Membrane	Plasma Membrane
	52.8	80.9	55.1	68.4	49.6	52.8
	56.7	60.8	51.8	90.4	37.7	32.2
	50.7	63.7	50.8	56.6	39.9	53.5
	51.6					
	56.7					
	65.9					
Mean	55.73	68.47	52.59	71.80	42.39	46.17
SD	5.57	10.90	2.26	17.19	6.35	12.10

Appendix Table G-3. Individual P-gp abundances in 21 day cultured Caco-2 cells variants quantified at Bertin Pharma. Each data point is n=3 pooled filters constituting 1 experiment.

	P-gp Abundance (fmol/µg)					
	Caco-2 (21d)		Caco-2 (21d) High Passage		Caco-2 - VBL (21d)	
	Total Membrane	Plasma Membrane	Total Membrane	Plasma Membrane	Total Membrane	Plasma Membrane
	0.72	0.82	5.26	5.57	10.55	7.78
	2.08	1.59	4.30	7.84	9.05	6.66
	2.89	2.23	4.83	4.93	10.45	7.19
	1.89					
	2.27					
	2.07					
Mean	1.99	1.54	4.80	6.11	10.02	7.21
SD	0.71	0.71	0.48	1.53	0.84	0.56

Appendix Table G-4. Individual Caco-2 monolayer variant permeability's of vinblastine (0.03 µM) with and without verapamil.

Permeability of Vinblastine with and without verapamil in Caco-2 cell variants (x 10^{-6} cm s^{-1})											
Low Passage Caco-2				High Passage Caco-2				VBL-Selected Caco-2			
A-to-B Control	B-to-A Control	A-to-B Verapamil	B-to-A Verapamil	A-to-B Control	B-to-A Control	A-to-B Verapamil	B-to-A Verapamil	A-to-B Control	B-to-A Control	A-to-B Verapamil	B-to-A Verapamil
7.36	19.78	9.85	12.60	5.49	36.14	8.10	11.35	2.52	24.63	4.26	10.4
6.77	20.14	9.15	12.24	5.23	30.08	8.11	12.10	2.27	24.02	3.82	9.78
7.02	20.58	9.76	13.12	5.77	30.49	8.65	12.69	1.82	26.28	4.09	9.66

Appendix Table G-5. Kinetic bi-directional permeability data (in triplicate filters) in Caco-2 variants for vinblastine.

Low Passage

A-to-B

Concentration (µM)	0.03	0.1	1	10	50	100	250	500	1000
Papp (x 10^{-6} cm.sec^{-1})	6.10	6.81	6.10	6.80	8.03	9.26	10.74	10.73	10.66
SD	0.05	0.42	0.42	0.45	0.26	1.11	1.28	0.63	1.73

B-to-A

Concentration (µM)	0.03	0.1	1	10	50	100	250	500	1000
Papp (x 10^{-6} cm.sec^{-1})	22.99	29.61	30.30	23.59	16.69	13.94	8.80	No Data	No Data
SD	0.87	2.07	2.49	0.76	0.49	1.18	0.90	No Data	No Data

High Passage

A-to-B

Concentration (µM)	0.03	0.1	1	10	50	100	250	500	1000
Papp (x 10^{-6} cm.sec^{-1})	5.50	5.56	6.21	5.53	5.86	6.82	8.41	8.01	8.69
SD	0.27	0.11	0.11	0.10	0.32	0.21	0.18	0.55	0.40

B-to-A

Concentration (µM)	0.03	0.1	1	10	50	100	250	500	1000
Papp (x 10^{-6} cm.sec^{-1})	32.24	31.18	28.20	26.74	22.13	15.10	8.86	No Data	No Data
SD	3.39	1.97	0.66	1.19	0.15	0.25	0.37	No Data	No Data

Caco-2-VBL

A-to-B

Concentration (µM)	0.03	0.1	1	10	50	100	250	500	1000
Papp (x 10^{-6} cm.sec^{-1})	0.89	1.76	0.97	0.81	1.13	0.97	1.63	3.03	3.02
SD	0.06	0.08	0.06	0.10	0.07	0.06	0.25	0.22	0.34

B-to-A

Concentration (µM)	0.03	0.1	1	10	50	100	250	500	1000
Papp (x 10^{-6} cm.sec^{-1})	41.73	35.48	38.37	37.23	28.27	22.99	13.36	No Data	No Data
SD	2.17	2.39	1.20	1.47	1.55	1.82	0.32	No Data	No Data

Bibliography

Abuasal BS, Bolger MB, Walker DK and Kaddoumi A (2012) In silico modeling for the non-linear absorption kinetics of UK-343,664: a P-gp and CYP3A4 substrate. *Mol Pharm* **9:**492-504.

Achira M, Suzuki H, Ito K and Sugiyama Y (1999) Comparative studies to determine the selective inhibitors for P-glycoprotein and cytochrome P4503A4. *AAPS PharmSci* **1:**E18.

Achler C, Filmer D, Merte C and Drenckhahn D (1989) Role of microtubules in polarized delivery of apical membrane proteins to the brush border of the intestinal epithelium. *J Cell Biol* **109:**179-189.

Achour B and Barber J (2013) The activities of Achromobacter lysyl endopeptidase and Lysobacter lysyl endoproteinase as digestive enzymes for quantitative proteomics. *Rapid Commun Mass Spectrom* **27:**1669-1672.

Achour B, Russell MR, Barber J and Rostami-Hodjegan A (2014) Simultaneous quantification of the abundance of several cytochrome P450 and uridine 5'-diphospho-glucuronosyltransferase enzymes in human liver microsomes using multiplexed targeted proteomics. *Drug Metab Dispos* **42:**500-510.

Adson A, Burton PS, Raub TJ, Barsuhn CL, Audus KL and Ho NF (1995) Passive diffusion of weak organic electrolytes across Caco-2 cell monolayers: uncoupling the contributions of hydrodynamic, transcellular, and paracellular barriers. *J Pharm Sci* **84:**1197-1204.

Agarwal S, Arya V and Zhang L (2013) Review of P-gp inhibition data in recently approved new drug applications: utility of the proposed [I(1)]/IC(50) and [I(2)]/IC(50) criteria in the P-gp decision tree. *J Clin Pharmacol* **53:**228-233.

Agoram B, Woltosz WS and Bolger MB (2001) Predicting the impact of physiological and biochemical processes on oral drug bioavailability. *Adv Drug Deliv Rev* **50** (suppl 1) : S41-67.

Ahlin G, Hilgendorf C, Karlsson J, Szigyarto CA, Uhlen M and Artursson P (2009) Endogenous gene and protein expression of drug-transporting proteins in cell lines routinely used in drug discovery programs. *Drug Metab Dispos* **37:**2275-2283.

Aller SG, Yu J, Ward A, Weng Y, Chittaboina S, Zhuo R, Harrell PM, Trinh YT, Zhang Q, Urbatsch IL and Chang G (2009) Structure of P-glycoprotein reveals a molecular basis for poly-specific drug binding. *Science* **323:**1718-1722.

Anderle P, Niederer E, Rubas W, Hilgendorf C, Spahn-Langguth H, Wunderli-Allenspach H, Merkle HP and Langguth P (1998) P-Glycoprotein (P-gp) mediated efflux in Caco-2 cell monolayers: the influence of culturing conditions and drug exposure on P-gp expression levels. *J Pharm Sci* **87:**757-762.

Artursson P (1990) Epithelial transport of drugs in cell culture. I: A model for studying the passive diffusion of drugs over intestinal absorptive (Caco-2) cells. *J Pharm Sci* **79:**476-482.

Artursson P and Karlsson J (1991) Correlation between oral drug absorption in humans and apparent drug permeability coefficients in human intestinal epithelial (Caco-2) cells. *Biochem Biophys Res Commun* **175:**880-885.

Avdeef A, Nielsen PE and Tsinman O (2004) PAMPA--a drug absorption in vitro model 11. Matching the in vivo unstirred water layer thickness by individual-well stirring in microtitre plates. *Eur J Pharm Sci* **22:**365-374.

Badee J, Achour B, Rostami-Hodjegan A, Galetin A (2015) Meta-analysis of expression of hepatic organic anion transporting polypeptide (OATP) transporters in cellular systems relative to human tissues. *Drug Metab Dispos* **42:** 500-510.

Badhan R, Penny J, Galetin A and Houston JB (2009) Methodology for development of a physiological model incorporating CYP3A and P-glycoprotein for the prediction of intestinal drug absorption. *J Pharm Sci* **98**: 2180-97.

Balakrishnan A, Hussainzada N, Gonzalez P, Bermejo M, Swaan PW and Polli JE (2007) Bias in estimation of transporter kinetic parameters from overexpression systems: Interplay of transporter expression level and substrate affinity. *J Pharmacol Exp Ther* **320:**133-144.

Balimane PV, Patel K, Marino A and Chong S (2004) Utility of 96 well Caco-2 cell system for increased throughput of P-gp screening in drug discovery. *Eur J Pharm Biopharm* **58:**99-105.

Ballatori N, Christian WV, Lee JY, Dawson PA, Soroka CJ, Boyer JL, Madejczyk MS and Li N (2005) OSTalpha-OSTbeta: a major basolateral bile acid and steroid transporter in human intestinal, renal, and biliary epithelia. *Hepatology* **42:**1270-1279.

Balogh LM, Kimoto E, Chupka J, Zhang H and Lai Y (2013) Membrane Protein Quantification by Peptide-Based Mass Spectrometry Approaches: Studies on the Organic Anion-Transporting Polypeptide Family. *J Proteomics Bioinform* **6:**229-236.

Bannon C, Davies PJ, Collett A and Warhurst G (2009) Potentiation of flagellin responses in gut epithelial cells by interferon-gamma is associated with STAT-independent regulation of MyD88 expression. *Biochem J* **423:**119-128.

Barter ZE, Bayliss MK, Beaune PH, Boobis AR, Carlile DJ, Edwards RJ, Houston JB, Lake BG, Lipscomb JC, Pelkonen OR, Tucker GT and Rostami-Hodjegan A (2007) Scaling factors for the extrapolation of in vivo metabolic drug clearance from in vitro data: reaching a consensus on values of human microsomal protein and hepatocellularity per gram of liver. *Curr Drug Metab* **8:**33-45.

Barter ZE, Chowdry JE, Harlow JR, Snawder JE, Lipscomb JC and Rostami-Hodjegan A (2008) Covariation of human microsomal protein per gram of liver with age: absence of influence of operator and sample storage may justify interlaboratory data pooling. *Drug Metab Dispos* **36:**2405-2409.

Behrens I, Kamm W, Dantzig AH and Kissel T (2004) Variation of peptide transporter (PepT1 and HPT1) expression in Caco-2 cells as a function of cell origin. *J Pharm Sci* **93:**1743-1754.

Benet LZ (2009) The drug transporter-metabolism alliance: uncovering and defining the interplay. *Mol Pharm* **6:**1631-1643.

Berggren S, Gall C, Wollnitz N, Ekelund M, Karlbom U, Hoogstraate J, Schrenk D and Lennernas H (2007) Gene and protein expression of P-glycoprotein, MRP1, MRP2, and CYP3A4 in the small and large human intestine. *Mol Pharm* **4:**252-257.

Beynon RJ, Doherty MK, Pratt JM and Gaskell SJ (2005) Multiplexed absolute quantification in proteomics using artificial QCAT proteins of concatenated signature peptides. *Nat Methods* **2:**587-589.

Blakemore SJ, Aledo JC, James J, Campbell FC, Lucocq JM and Hundal HS (1995) The GLUT5 hexose transporter is also localized to the basolateral membrane of the human jejunum. *Biochem J* **309 (Pt 1) :**7-12.

Blitzer BL and Donovan CB (1984) A new method for the rapid isolation of basolateral plasma membrane vesicles from rat liver. Characterization, validation, and bile acid transport studies. *J Biol Chem* **259:**9295-9301.

Bolger MB, Lukacova V and Woltosz WS (2009) Simulations of the nonlinear dose dependence for substrates of influx and efflux transporters in the human intestine. *AAPS J* **11:**353-363.

Bosgra S, van de Steeg E, Vlaming ML, Verhoeckx KC, Huisman MT, Verwei M and Wortelboer HM (2014) Predicting carrier-mediated hepatic disposition of rosuvastatin in man by scaling from individual transfected cell-lines in vitro using absolute transporter protein quantification and PBPK modeling. *Eur J Pharm Sci* **65C:**156-166.

Bow DA, Perry JL, Miller DS, Pritchard JB and Brouwer KL (2008) Localization of P-gp (Abcb1) and Mrp2 (Abcc2) in freshly isolated rat hepatocytes. *Drug Metab Dispos* **36:**198-202.

Bowley KA, Morton MJ, Hunter M and Sandle GI (2003) Non-genomic regulation of intermediate conductance potassium channels by aldosterone in human colonic crypt cells. *Gut* **52:**854-860.

Bree F, Urien S, Nguyen P, Tillement JP, Steiner A, Vallat-Molliet C, Testa B, Visy J and Simonyi M (1993) Human serum albumin conformational changes as induced by tenoxicam and modified by simultaneous diazepam binding. *J Pharm Pharmacol* **45:**1050-1053.

Breedveld P, Pluim D, Cipriani G, Dahlhaus F, van Eijndhoven MA, de Wolf CJ, Kuil A, Beijnen JH, Scheffer GL, Jansen G, Borst P and Schellens JH (2007) The effect of low pH on breast cancer resistance protein (ABCG2) -mediated transport of methotrexate, 7-hydroxymethotrexate, methotrexate diglutamate, folic acid, mitoxantrone, topotecan, and resveratrol in in vitro drug transport models. *Mol Pharmacol* **71:**240-249.

Briske-Anderson MJ, Finley JW and Newman SM (1997) The influence of culture time and passage number on the morphological and physiological development of Caco-2 cells. *Proc Soc Exp Biol Med* **214:**248-257.

Bruyere A, Decleves X, Bouzom F, Ball K, Marques C, Treton X, Pocard M, Valleur P, Bouhnik Y, Panis Y, Scherrmann JM and Mouly S (2010) Effect of Variations in the Amounts of P-Glycoprotein (ABCB1) , BCRP (ABCG2) and CYP3A4 along the Human Small Intestine on PBPK Models for Predicting Intestinal First Pass. *Mol Pharm* **7:**1596-1607.

Burnham DB and Fondacaro JD (1989) Secretagogue-induced protein phosphorylation and chloride transport in Caco-2 cells. *Am J Physiol* **256:**G808-816.

Campbell L, Abulrob AN, Kandalaft LE, Plummer S, Hollins AJ, Gibbs A and Gumbleton M (2003) Constitutive expression of p-glycoprotein in normal lung alveolar epithelium and functionality in primary alveolar epithelial cultures. *J Pharmacol Exp Ther* **304:**441-452.

Cavet ME, West M and Simmons NL (1996) Transport and epithelial secretion of the cardiac glycoside, digoxin, by human intestinal epithelial (Caco-2) cells. *Br J Pharmacol* **118:**1389-1396.

CDER (February 2012) Guidance for Industry. Drug Interaction Studies - Study Design, Data Analysis, Implications for Dosing, and Labeling Recommendations., Food and Drug Admininstration, US Department of Health and Human Services.

Celius T, Garberg P and Lundgren B (2004) Stable suppression of MDR1 gene expression and function by RNAi in Caco-2 cells. *Biochem Biophys Res Commun* **324:**365-371.

Chen Y, Liu L, Nguyen K and Fretland AJ (2011) Utility of intersystem extrapolation factors in early reaction phenotyping and the quantitative extrapolation of human liver microsomal intrinsic clearance using recombinant cytochromes P450. *Drug Metab Dispos* **39:**373-382.

Chiva C, Ortega M and Sabido E (2014) Influence of the digestion technique, protease, and missed cleavage peptides in protein quantitation. *J Proteome Res* **13:**3979-3986.

CHMP (2012) *Guidance on the Investigation of Drug Interactions*. European Medicines Agency. *http://www.ema.europa.eu/docs/en_ GB/document_ library/Scientific_ guideline/2012/07/WC500129606.pdf*.

Choi JH, Murray JW and Wolkoff AW (2011) PDZK1 binding and serine phosphorylation regulate subcellular trafficking of organic anion transport protein 1a1. *Am J Physiol Gastrointest Liver Physiol* **300:**G384-393.

Clark ML, Lanz HC and Senior JR (1969) Enzymatic distinction of rat intestinal cell brush border and endoplasmic reticular membranes. *Biochim Biophys Acta* **183:**233-235.

Collett A, Tanianis-Hughes J, Hallifax D and Warhurst G (2004) Predicting P-glycoprotein effects on oral absorption: correlation of transport in Caco-2 with drug pharmacokinetics in wild type and mdr1a(-/-) mice in vivo. *Pharm Res* **21**: 819-26.

Cummins CL, Mangravite LM and Benet LZ (2001) Characterizing the expression of CYP3A4 and efflux transporters (P-gp, MRP1, and MRP2) in CYP3A4-transfected Caco-2 cells after induction with sodium butyrate and the phorbol ester 12-O-tetradecanoylphorbol-13-acetate. *Pharm Res* **18:**1102-1109.

Dahlgren D, Roos C, Sjogren E and Lennernas H (2014) Direct In Vivo Human Intestinal Permeability (P) Determined with Different Clinical Perfusion and Intubation Methods. *J Pharm Sci*.

Dantzig AH, Hoskins JA, Tabas LB, Bright S, Shepard RL, Jenkins IL, Duckworth DC, Sportsman JR, Mackensen D, Rosteck PR, Jr. and et al. (1994) Association of intestinal peptide transport with a protein related to the cadherin superfamily. *Science* **264:**430-433.

Darwich AS, Neuhoff S, Jamei M and Rostami-Hodjegan A (2010) Interplay of metabolism and transport in determining oral drug absorption and gut wall metabolism: a simulation assessment using the "Advanced Dissolution, Absorption, Metabolism (ADAM) " model. *Curr Drug Metab* **11:**716-729.

Deo AK, Prasad B, Balogh L, Lai Y and Unadkat JD (2012) Interindividual variability in hepatic expression of the multidrug resistance-associated protein 2 (MRP2/ABCC2) : quantification by liquid chromatography/tandem mass spectrometry. *Drug Metab Dispos* **40:**852-855.

Di L, Whitney-Pickett C, Umland JP, Zhang H, Zhang X, Gebhard DF, Lai Y, Federico JJ, 3rd, Davidson RE, Smith R, Reyner EL, Lee C, Feng B, Rotter C, Varma MV, Kempshall S, Fenner K, El-Kattan AF, Liston TE and Troutman MD (2011) Development of a new permeability assay using low-efflux MDCKII cells. *J Pharm Sci* **100:**4974-4985.

Drozdzik M, Groer C, Penski J, Lapczuk J, Ostrowski M, Lai Y, Prasad B, Unadkat JD, Siegmund W and Oswald S (2014) Protein Abundance of Clinically Relevant Multidrug Transporters along the Entire Length of the Human Intestine. *Mol Pharm* **11:**3547-3555.

Ellis JA, Jackman MR and Luzio JP (1992) The post-synthetic sorting of endogenous membrane proteins examined by the simultaneous purification of apical and basolateral plasma membrane fractions from Caco-2 cells. *Biochem J* **283 (Pt 2) :**553-560.

Evers R, Kool M, van Deemter L, Janssen H, Calafat J, Oomen LC, Paulusma CC, Oude Elferink RP, Baas F, Schinkel AH and Borst P (1998) Drug export activity of the human canalicular multispecific organic anion transporter in polarized kidney MDCK cells expressing cMOAT (MRP2) cDNA. *J Clin Invest* **101:**1310-1319.

Eyers CE, Lawless C, Wedge DC, Lau KW, Gaskell SJ and Hubbard SJ (2011) CONSeQuence: prediction of reference peptides for absolute quantitative proteomics using consensus machine learning approaches. *Mol Cell Proteomics* **10:**M110 003384.

Fallingborg J, Christensen LA, Ingeman-Nielsen M, Jacobsen BA, Abildgaard K and Rasmussen HH (1989) pH-profile and regional transit times of the normal gut measured by a radiotelemetry device. *Aliment Pharmacol Ther* **3:**605-613.

FDA (2013) Draft Guidance for Industry. Bioanalytical Method Validation. http://www.fda.gov/downloads/Drugs/GuidanceComplianceRegulatoryInformation/Guidances/UCM368107.pdf.

Fleischer S and Kervina M (1974) Subcellular Fractionation of Rat Liver. *Methods in Enzymology* **31:**6-41.

Galetin A and Houston JB (2006) Intestinal and hepatic metabolic activity of five cytochrome P450 enzymes: impact on prediction of first-pass metabolism. *J Pharmacol Exp Ther* **318:**1220-1229.

Garberg P, Eriksson P, Schipper N and Sjostrom B (1999) Automated absorption assessment using Caco-2 cells cultured on both sides of polycarbonate membranes. *Pharm Res* **16:**441-445.

Geilen CC, Wieder T, Haase A, Reutter W, Morre DM and Morre DJ (1994) Uptake, subcellular distribution and metabolism of the phospholipid analogue hexadecylphosphocholine in MDCK cells. *Biochim Biophys Acta* **1211:**14-22.

Gerber SA, Rush J, Stemman O, Kirschner MW and Gygi SP (2003) Absolute quantification of proteins and phosphoproteins from cell lysates by tandem MS. *Proc Natl Acad Sci U S A* **100:**6940-6945.

Gertz M, Cartwright CM, Hobbs MJ, Kenworthy KE, Rowland M, Houston JB and Galetin A (2013) Cyclosporine inhibition of hepatic and intestinal CYP3A4, uptake and efflux transporters: application of PBPK modeling in the assessment of drug-drug interaction potential. *Pharm Res* **30**:761-80.

Ghosh A, Scott DO and Maurer TS (2014) Towards a unified model of passive drug permeation I: origins of the unstirred water layer with applications to ionic permeation. *Eur J Pharm Sci* **52:**109-124.

Glaeser H, Bailey DG, Dresser GK, Gregor JC, Schwarz UI, McGrath JS, Jolicoeur E, Lee W, Leake BF, Tirona RG and Kim RB (2007) Intestinal drug transporter expression and the impact of grapefruit juice in humans. *Clin Pharmacol Ther* **81:**362-370.

Gram LK, Rist GM, Lennernas H and Steffansen B (2009) Impact of carriers in oral absorption: Permeation across Caco-2 cells for the organic anions estrone-3-sulfate and glipizide. *Eur J Pharm Sci* **37:**378-386.

Grandvuinet AS and Steffansen B (2011) Interactions between organic anions on multiple transporters in Caco-2 cells. *J Pharm Sci* **100:**3817-3830.

Greiner B, Eichelbaum M, Fritz P, Kreichgauer HP, von Richter O, Zundler J and Kroemer HK (1999) The role of intestinal P-glycoprotein in the interaction of digoxin and rifampin. *J Clin Invest* **104:**147-153.

Groer C, Bruck S, Lai Y, Paulick A, Busemann A, Heidecke CD, Siegmund W and Oswald S (2013) LC-MS/MS-based quantification of clinically relevant intestinal uptake and efflux transporter proteins. *J Pharm Biomed Anal* **85:**253-261.

Gronert K, Gewirtz A, Madara JL and Serhan CN (1998) Identification of a human enterocyte lipoxin A4 receptor that is regulated by interleukin (IL) -13 and interferon gamma and inhibits tumor necrosis factor alpha-induced IL-8 release. *J Exp Med* **187:**1285-1294.

Harwood MD, Neuhoff S, Carlson GL, Warhurst G and Rostami-Hodjegan A (2013) Absolute abundance and function of intestinal drug transporters: a prerequisite for fully mechanistic in vitro-in vivo extrapolation of oral drug absorption. *Biopharm Drug Dispos* **34:**2-28.

Harwood MD, Russell MR, Neuhoff S, Warhurst G and Rostami-Hodjegan A (2014) Lost in centrifugation: accounting for transporter protein losses in quantitative targeted absolute proteomics. *Drug Metab Dispos* **42:**1766-1772.

Harwood MD, Achour B, Russell MR, Carlson GL, Warhurst G and Rostami-Hodjegan A (2015) Application of an LC-MS/MS Method for the Simultaneous Quantification of Human Intestinal Transporter Proteins Absolute Abundance using a QconCAT Technique. *J Pharm Biomed Anal* **110:**27-33.

Hayeshi R, Hilgendorf C, Artursson P, Augustijns P, Brodin B, Dehertogh P, Fisher K, Fossati L, Hovenkamp E, Korjamo T, Masungi C, Maubon N, Mols R, Mullertz A, Monkkonen J, O'Driscoll C, Oppers-Tiemissen HM, Ragnarsson EG, Rooseboom M and Ungell AL (2008) Comparison of drug transporter gene expression and functionality in Caco-2 cells from 10 different laboratories. *Eur J Pharm Sci* **35:**383-396.

Heikkinen AT, Korjamo T, Lepikko V and Monkkonen J (2010) Effects of experimental setup on the apparent concentration dependency of active efflux transport in in vitro cell permeation experiments. *Mol Pharm* **7:**605-617.

Heikkinen AT, Friedlein A, Matondo M, Hatley OJ, Petsalo A, Juvonen R, Galetin A, Rostami-Hodjegan A, Aebersold R, Lamerz J, Dunkley T, Cutler P and Parrott N (2014) Quantitative ADME Proteomics - CYP and UGT Enzymes in the Beagle Dog Liver and Intestine. *Pharm Res* **32:**74-90.

Hidalgo IJ, Raub TJ and Borchardt RT (1989) Characterization of the human colon carcinoma cell line (Caco-2) as a model system for intestinal epithelial permeability. *Gastroenterology* **96:**736-749.

Hilgendorf C, Ahlin G, Seithel A, Artursson P, Ungell AL and Karlsson J (2007) Expression of thirty-six drug transporter genes in human intestine, liver, kidney, and organotypic cell lines. *Drug Metab Dispos* **35:**1333-1340.

Hirouchi M, Kusuhara H, Onuki R, Ogilvie BW, Parkinson A and Sugiyama Y (2009) Construction of triple-transfected cells [organic anion-transporting polypeptide (OATP) 1B1/multidrug resistance-associated protein (MRP) 2/MRP3 and OATP1B1/MRP2/MRP4] for analysis of the sinusoidal function of MRP3 and MRP4. *Drug Metab Dispos* **37:**2103-2111.

Horie K, Tang F and Borchardt RT (2003) Isolation and characterization of Caco-2 subclones expressing high levels of multidrug resistance protein efflux transporter. *Pharm Res* **20:**161-168.

Horio M, Chin KV, Currier SJ, Goldenberg S, Williams C, Pastan I, Gottesman MM and Handler J (1989) Transepithelial transport of drugs by the multidrug transporter in cultured Madin-Darby canine kidney cell epithelia. *J Biol Chem* **264:**14880-14884.

Hosoya KI, Kim KJ and Lee VH (1996) Age-dependent expression of P-glycoprotein gp170 in Caco-2 cell monolayers. *Pharm Res* **13:**885-890.

Hubatsch I, Ragnarsson EG and Artursson P (2007) Determination of drug permeability and prediction of drug absorption in Caco-2 monolayers. *Nat Protoc* **2:**2111-2119.

Huber LA, Pfaller K and Vietor I (2003) Organelle proteomics: implications for subcellular fractionation in proteomics. *Circ Res* **92:**962-968.

Hunter J, Jepson MA, Tsuruo T, Simmons NL and Hirst BH (1993) Functional expression of P-glycoprotein in apical membranes of human intestinal Caco-2 cells. Kinetics of vinblastine secretion and interaction with modulators. *J Biol Chem* **268:**14991-14997.

Igunnu A, Osalaye DS, Olorunsogo OO, Malomo SO and Olorunniji FJ (2011) Distinct metal ion requirements for the phosphomonoesterase and phosphodiesterase activities of calf intestinal alkaline phosphatase. *Open Biochem J* **5:**67-72.

Imai Y, Asada S, Tsukahara S, Ishikawa E, Tsuruo T and Sugimoto Y (2003) Breast cancer resistance protein exports sulfated estrogens but not free estrogens. *Mol Pharmacol* **64:**610-618.

Inui K, Yamamoto M and Saito H (1992) Transepithelial transport of oral cephalosporins by monolayers of intestinal epithelial cell line Caco-2: specific transport systems in apical and basolateral membranes. *J Pharmacol Exp Ther* **261:**195-201.

Jamei M, Turner D, Yang J, Neuhoff S, Polak S, Rostami-Hodjegan A and Tucker G (2009) Population-based mechanistic prediction of oral drug absorption. *AAPS J* **11:**225-237.

Jemnitz K, Heredi-Szabo K, Janossy J, Ioja E, Vereczkey L and Krajcsi P (2010) ABCC2/Abcc2: a multispecific transporter with dominant excretory functions. *Drug Metab Rev* **42:**402-436.

Ji C, Tschantz WR, Pfeifer ND, Ullah M and Sadagopan N (2012) Development of a multiplex UPLC-MRM MS method for quantification of human membrane transport proteins OATP1B1, OATP1B3 and OATP2B1 in in vitro systems and tissues. *Anal Chim Acta* **717:**67-76.

Jones H and Rowland-Yeo K (2013) Basic concepts in physiologically based pharmacokinetic modeling in drug discovery and development. *CPT Pharmacometrics Syst Pharmacol* **2:**e63.

Jones HM, Parrott N, Ohlenbusch G and Lave T (2006) Predicting Pharmacokinetic food effects using biorelevant solubility media and physiologically based modelling. *Clin Pharmacokinet* **45**:1213-1226.

Jones HM, Barton HA, Lai Y, Bi YA, Kimoto E, Kempshall S, Tate SC, El-Kattan A, Houston JB, Galetin A and Fenner KS (2012) Mechanistic pharmacokinetic modeling for the prediction of transporter-mediated disposition in humans from sandwich culture human hepatocyte data. *Drug Metab Dispos* **40:**1007-1017.

Jonsson AP (2001) Mass spectrometry for protein and peptide characterisation. *Cell Mol Life Sci* **58:**868-884.

Juliano RL and Stamp D (1978) Pharmacokinetics of liposome-encapsulated anti-tumor drugs. Studies with vinblastine, actinomycin D, cytosine arabinoside, and daunomycin. *Biochem Pharmacol* **27:**21-27.

Kalvass JC and Pollack GM (2007) Kinetic considerations for the quantitative assessment of efflux activity and inhibition: implications for understanding and predicting the effects of efflux inhibition. *Pharm Res* **24:**265-276.

Kamiie J, Ohtsuki S, Iwase R, Ohmine K, Katsukura Y, Yanai K, Sekine Y, Uchida Y, Ito S and Terasaki T (2008) Quantitative atlas of membrane transporter proteins: development and application of a highly sensitive simultaneous LC/MS/MS method combined with novel in-silico peptide selection criteria. *Pharm Res* **25:**1469-1483.

Kamiyama E, Sugiyama D, Nakai D, Miura S and Okazaki O (2009) Culture period-dependent change of function and expression of ATP-binding cassette transporters in Caco-2 cells. *Drug Metab Dispos* **37:**1956-1962.

Kararli TT (1995) Comparison of the gastrointestinal anatomy, physiology, and biochemistry of humans and commonly used laboratory animals. *Biopharm Drug Dispos* **16:**351-380.

Karlgren M, Vildhede A, Norinder U, Wisniewski JR, Kimoto E, Lai Y, Haglund U and Artursson P (2012) Classification of inhibitors of hepatic organic anion transporting polypeptides (OATPs) : influence of protein expression on drug-drug interactions. *J Med Chem* **55:**4740-4763.

Karlsson J and Artursson P (1991) A method for the determination of cellular permeability coefficients and aqueous boundary layer thickness in monolayers of intestinal epithelial (Caco-2) cells grown in permeable filter chambers. *Int J Pharm* **71:**55-64.

Kell DB and Oliver SG (2014) How drugs get into cells: tested and testable predictions to help discriminate between transporter-mediated uptake and lipoidal bilayer diffusion. *Front Pharmacol* **5:**231.

Khan AA, Chow EC, Porte RJ, Pang KS and Groothuis GM (2009) Expression and regulation of the bile acid transporter, OSTalpha-OSTbeta in rat and human intestine and liver. *Biopharm Drug Dispos* **30:**241-258.

Kobayashi D, Nozawa T, Imai K, Nezu J, Tsuji A and Tamai I (2003) Involvement of human organic anion transporting polypeptide OATP-B (SLC21A9) in pH-dependent transport across intestinal apical membrane. *J Pharmacol Exp Ther* **306:**703-708.

Korjamo T, Kemilainen H, Heikkinen AT and Monkkonen J (2007) Decrease in intracellular concentration causes the shift in Km value of efflux pump substrates. *Drug Metab Dispos* **35:**1574-1579.

Korzekwa K, Nagar S, Tucker J, Weiskircher EA, Bhoopathy S and Hidalgo IJ (2012) Models to predict unbound intracellular drug concentrations in the presence of transporters. *Drug Metab Dispos* **40:**865-876.

Korzekwa K and Nagar S (2014) Compartmental models for apical efflux by P-glycoprotein: part 2--a theoretical study on transporter kinetic parameters. *Pharm Res* **31:**335-346.

Kroetz DL, Pauli-Magnus C, Hodges LM, Huang CC, Kawamoto M, Johns SJ, Stryke D, Ferrin TE, DeYoung J, Taylor T, Carlson EJ, Herskowitz I, Giacomini KM and Clark AG (2003) Sequence diversity and haplotype structure in the human ABCB1 (MDR1, multidrug resistance transporter) gene. *Pharmacogenetics* **13:**481-494.

Kruger M, Moser M, Ussar S, Thievessen I, Luber CA, Forner F, Schmidt S, Zanivan S, Fassler R and Mann M (2008) SILAC mouse for quantitative proteomics uncovers kindlin-3 as an essential factor for red blood cell function. *Cell* **134:**353-364.

Kumar V, Prasad B, Patilea G, Gupta A, Salphati L, Evers R, Hop CE and Unadkat JD (2015) Quantitative transporter proteomics by liquid chromatography with tandem mass spectrometry: addressing methodologic issues of plasma membrane isolation and expression-activity relationship. *Drug Metab Dispos* **43:**284-288.

Kunze A, Huwyler J, Camenisch G and Poller B (2014) Prediction of organic anion-transporting polypeptide 1B1- and 1B3-mediated hepatic uptake of statins based on transporter protein expression and activity data. *Drug Metab Dispos* **42:**1514-1521.

Lai Y, Bakken AH and Unadkat JD (2002) Simultaneous expression of hCNT1-CFP and hENT1-YFP in Madin-Darby canine kidney cells. Localization and vectorial transport studies. *J Biol Chem* **277:**37711-37717.

Landrier JF, Eloranta JJ, Vavricka SR and Kullak-Ublick GA (2006) The nuclear receptor for bile acids, FXR, transactivates human organic solute transporter-alpha and -beta genes. *Am J Physiol Gastrointest Liver Physiol* **290:**G476-485.

Laska DA, Houchins JO, Pratt SE, Horn J, Xia X, Hanssen BR, Williams DC, Dantzig AH and Lindstrom T (2002) Characterization and application of a vinblastine-selected CACO-2 cell line for evaluation of p-glycoprotein. *In Vitro Cell Dev Biol Anim* **38:**401-410.

Lawless C and Hubbard SJ (2012) Prediction of missed proteolytic cleavages for the selection of surrogate peptides for quantitative proteomics. *OMICS* **16:**449-456.

Lennernas H, Nilsson D, Aquilonius SM, Ahrenstedt O, Knutson L and Paalzow LK (1993) The effect of L-leucine on the absorption of levodopa, studied by regional jejunal perfusion in man. *Br J Clin Pharmacol* **35:**243-250.

Lennernas H (2007) Intestinal permeability and its relevance for absorption and elimination. *Xenobiotica* **37:**1015-1051.

Lentz KA, Polli JW, Wring SA, Humphreys JE and Polli JE (2000) Influence of passive permeability on apparent P-glycoprotein kinetics. *Pharm Res* **17:**1456-1460.

Li N, Nemirovskiy OV, Zhang Y, Yuan H, Mo J, Ji C, Zhang B, Brayman TG, Lepsy C, Heath TG and Lai Y (2008) Absolute quantification of multidrug resistance-associated protein 2

(MRP2/ABCC2) using liquid chromatography tandem mass spectrometry. *Anal Biochem* **380:**211-222.

Li N, Zhang Y, Hua F and Lai Y (2009a) Absolute difference of hepatobiliary transporter multidrug resistance-associated protein (MRP2/Mrp2) in liver tissues and isolated hepatocytes from rat, dog, monkey, and human. *Drug Metab Dispos* **37:**66-73.

Li N, Palandra J, Nemirovskiy OV and Lai Y (2009b) LC-MS/MS mediated absolute quantification and comparison of bile salt export pump and breast cancer resistance protein in livers and hepatocytes across species. *Anal Chem* **81:**2251-2259.

Li N, Bi YA, Duignan DB and Lai Y (2009c) Quantitative expression profile of hepatobiliary transporters in sandwich cultured rat and human hepatocytes. *Mol Pharm* **6:**1180-1189.

Li N, Singh P, Mandrell KM and Lai Y (2010a) Improved extrapolation of hepatobiliary clearance from in vitro sandwich cultured rat hepatocytes through absolute quantification of hepatobiliary transporters. *Mol Pharm* **7:**630-641.

Li Q and Shu Y (2014) Role of solute carriers in response to anticancer drugs. *Molecular and Cellular Therapies* **2:**15.

Li X, Lin C and O'Connor PB (2010b) Glutamine deamidation: differentiation of glutamic acid and gamma-glutamic acid in peptides by electron capture dissociation. *Anal Chem* **82:**3606-3615.

Lin X, Skolnik S, Chen X and Wang J (2011) Attenuation of intestinal absorption by major efflux transporters: quantitative tools and strategies using a Caco-2 model. *Drug Metab Dispos* **39:**265-274.

Lipscomb JC, Teuschler LK, Swartout JC, Striley CA and Snawder JE (2003) Variance of Microsomal Protein and Cytochrome P450 2E1 and 3A Forms in Adult Human Liver. *Toxicol Mech Methods* **13:**45-51.

Litman T, Brangi M, Hudson E, Fetsch P, Abati A, Ross DD, Miyake K, Resau JH and Bates SE (2000) The multidrug-resistant phenotype associated with overexpression of the new ABC half-transporter, MXR (ABCG2) . *J Cell Sci* **113 (Pt 11) :**2011-2021.

Lu K, Yap HY and Loo TL (1983) Clinical pharmacokinetics of vinblastine by continuous intravenous infusion. *Cancer Res* **43:**1405-1408.

Lu S, Gough AW, Bobrowski WF and Stewart BH (1996) Transport properties are not altered across Caco-2 cells with heightened TEER despite underlying physiological and ultrastructural changes. *J Pharm Sci* **85:**270-273.

Lucas ML, Cooper BT, Lei FH, Johnson IT, Holmes GK, Blair JA and Cooke WT (1978) Acid microclimate in coeliac and Crohn's disease: a model for folate malabsorption. *Gut* **19:**735-742.

Lucke H, Berner W, Menge H and Murer H (1978) Sugar transport by brush border membrane vesicles isolated from human small intestine. *Pflugers Arch* **373:**243-248.

MacLean B, Tomazela DM, Shulman N, Chambers M, Finney GL, Frewen B, Kern R, Tabb DL, Liebler DC and MacCoss MJ (2010a) Skyline: an open source document editor for creating and analyzing targeted proteomics experiments. *Bioinformatics* **26:**966-968.

Maclean B, Tomazela DM, Abbatiello SE, Zhang S, Whiteaker JR, Paulovich AG, Carr SA and Maccoss MJ (2010b) Effect of collision energy optimization on the measurement of

peptides by selected reaction monitoring (SRM) mass spectrometry. *Anal Chem* **82:**10116-10124.

Maeno K, Nakajima A, Conseil G, Rothnie A, Deeley RG and Cole SP (2009) Molecular basis for reduced estrone sulfate transport and altered modulator sensitivity of transmembrane helix (TM) 6 and TM17 mutants of multidrug resistance protein 1 (ABCC1) . *Drug Metab Dispos* **37:**1411-1420.

Mateus A, Matsson P and Artursson P (2013) Rapid measurement of intracellular unbound drug concentrations. *Mol Pharm* **10:**2467-2478.

Matsson P, Pedersen JM, Norinder U, Bergstrom CA and Artursson P (2009) Identification of novel specific and general inhibitors of the three major human ATP-binding cassette transporters P-gp, BCRP and MRP2 among registered drugs. *Pharm Res* **26:**1816-1831.

Mease K, Sane R, Podila L and Taub ME (2012) Differential selectivity of efflux transporter inhibitors in Caco-2 and MDCK-MDR1 monolayers: a strategy to assess the interaction of a new chemical entity with P-gp, BCRP, and MRP2. *J Pharm Sci* **101:**1888-1897.

Meier M, Blatter XL, Seelig A and Seelig J (2006) Interaction of verapamil with lipid membranes and P-glycoprotein: connecting thermodynamics and membrane structure with functional activity. *Biophys J* **91:**2943-2955.

Meier Y, Eloranta JJ, Darimont J, Ismair MG, Hiller C, Fried M, Kullak-Ublick and Vavricka SR (2007) Regional distribution of solute carrier mRNA expression along the human intestinal tract. *Drug Metab and Dispos* **35**: 590-594.

Menochet K, Kenworthy KE, Houston JB and Galetin A (2012a) Simultaneous assessment of uptake and metabolism in rat hepatocytes: a comprehensive mechanistic model. *J Pharmacol Exp Ther* **341:**2-15.

Menochet K, Kenworthy KE, Houston JB and Galetin A (2012b) Use of mechanistic modeling to assess interindividual variability and interspecies differences in active uptake in human and rat hepatocytes. *Drug Metab Dispos* **40:**1744-1756.

Miliotis T, Hilgendorf C, Karlsson J, Andersson TB and Abrahamsson P (2011a) Development of an LC-MRM method for quantification of P-glycoprotein *http://www.chem-agilent.com/pdf/WP08_ 177.pdf* **(Poster)** .

Miliotis T, Ali L, Palm JE, Lundqvist AJ, Ahnoff M, Andersson TB and Hilgendorf C (2011b) Development of a highly sensitive method using liquid chromatography-multiple reaction monitoring to quantify membrane P-glycoprotein in biological matrices and relationship to transport function. *Drug Metab Dispos* **39:**2440-2449.

Mirza SP, Halligan BD, Greene AS and Olivier M (2007) Improved method for the analysis of membrane proteins by mass spectrometry. *Physiol Genomics* **30:**89-94.

Modok S (2010) Three Dimensional Models of Chemotherapeutic Agent Transport in Tumours, in: *2nd Department of Medicine, Albert Szent Gyorgyi Clinical Centre*, ,University of Szeged.

Mukonzo JK, Waako P, Ogwal-Okeng J, Gustafsson LL and Aklillu E (2010) Genetic variations in ABCB1 and CYP3A5 as well as sex influence quinine disposition among Ugandans. *Ther Drug Monit* **32:**346-352.

Nagar S, Tucker J, Weiskircher EA, Bhoopathy S, Hidalgo IJ and Korzekwa K (2014) Compartmental models for apical efflux by P-glycoprotein--part 1: evaluation of model complexity. *Pharm Res* **31:**347-359.

Neuhoff S, Ungell AL, Zamora I and Artursson P (2003) pH-dependent bidirectional transport of weakly basic drugs across Caco-2 monolayers: implications for drug-drug interactions. *Pharm Res* **20:**1141-1148.

Neuhoff S, Ungell AL, Zamora I and Artursson P (2005) pH-Dependent passive and active transport of acidic drugs across Caco-2 cell monolayers. *Eur J Pharm Sci* **25:**211-220.

Neuhoff S, Artursson P, Zamora I and Ungell AL (2006) Impact of extracellular protein binding on passive and active drug transport across Caco-2 cells. *Pharm Res* **23:**350-359.

Neuhoff S, Yeo KR, Barter Z, Jamei M, Turner DB and Rostami-Hodjegan A (2013) Application of permeability-limited physiologically-based pharmacokinetic models: part I-digoxin pharmacokinetics incorporating P-glycoprotein-mediated efflux. *J Pharm Sci* **102:**3145-3160.

Neville DM, Jr. (1960) The isolation of a cell membrane fraction from rat liver. *J Biophys Biochem Cytol* **8:**413-422.

Nies AT, Hofmann U, Resch C, Schaeffeler E, Rius M and Schwab M (2011) Proton pump inhibitors inhibit metformin uptake by organic cation transporters (OCTs) . *PLoS One* **6:**e22163.

Nies AT, Niemi M, Burk O, Winter S, Zanger UM, Stieger B, Schwab M and Schaeffeler E (2013) Genetics is a major determinant of expression of the human hepatic uptake transporter OATP1B1, but not of OATP1B3 and OATP2B1. *Genome Med* **5:**1.

Niessen J, Jedlitschky G, Grube M, Kawakami H, Kamiie J, Ohtsuki S, Schwertz H, Bien S, Starke K, Ritter C, Strobel U, Greinacher A, Terasaki T and Kroemer HK (2010) Expression of ABC-type transport proteins in human platelets. *Pharmacogenet Genomics* **20:**396-400.

Nishimura M and Naito S (2005) Tissue-specific mRNA expression profiles of human ATP-binding cassette and solute carrier transporter superfamilies. *Drug Metab and Pharmacokinet* **20**:452-477.

Oehlke J, Ehrlich A, Krause E, Pritz S, Wiesner B and Beyermann M (2011) Growth factor- and adhesion protein-like components of fetal calf serum can significantly enhance the intracellular delivery of Peptide nucleic acids. *Nucleic Acid Ther* **21:**285-291.

Ohtsuki S, Uchida Y, Kubo Y and Terasaki T (2011) Quantitative targeted absolute proteomics-based ADME research as a new path to drug discovery and development: methodology, advantages, strategy, and prospects. *J Pharm Sci* **100:**3547-3559.

Ohtsuki S, Schaefer O, Kawakami H, Inoue T, Liehner S, Saito A, Ishiguro N, Kishimoto W, Ludwig-Schwellinger E, Ebner T and Terasaki T (2012) Simultaneous Absolute Protein Quantification of Transporters, Cytochromes P450, and UDP-Glucuronosyltransferases as a Novel Approach for the Characterization of Individual Human Liver: Comparison with mRNA Levels and Activities. *Drug Metab Dispos* **40:**83-92.

Ohtsuki S, Ikeda C, Uchida Y, Sakamoto Y, Miller F, Glacial F, Decleves X, Scherrmann JM, Couraud PO, Kubo Y, Tachikawa M and Terasaki T (2013) Quantitative targeted absolute proteomic analysis of transporters, receptors and junction proteins for validation of human

cerebral microvascular endothelial cell line hCMEC/D3 as a human blood-brain barrier model. *Mol Pharm* **10:**289-296.

Olorunniji FJ, Iggunnu A, Adebayo JO, Arise RO and Malomo SO (2007) Cofactor interactions in the activation of tissue non-specific alkaline phosphatase: Synergistic effects of Zn2+ and Mg2+ ions. *Biokemistri* **19:**43-48.

Orsburn BC, Stockwin LH and Newton DL (2011) Challenges in plasma membrane phosphoproteomics. *Expert Rev Proteomics* **8:**483-494.

Oswald S, Groer C, Drozdzik M and Siegmund W (2013) Mass Spectrometry-Based Targeted Proteomics as a Tool to Elucidate the Expression and Function of Intestinal Drug Transporters. *AAPS J* **15:**1128-1140.

Owellen RJ, Hartke CA and Hains FO (1977) Pharmacokinetics and metabolism of vinblastine in humans. *Cancer Res* **37:**2597-2602.

Ozawa S, Soyama A, Saeki M, Fukushima-Uesaka H, Itoda M, Koyano S, Sai K, Ohno Y, Saito Y and Sawada J (2004) Ethnic differences in genetic polymorphisms of CYP2D6, CYP2C19, CYP3As and MDR1/ABCB1. *Drug Metab Pharmacokinet* **19:**83-95.

Panorchan P, Thompson MS, Davis KJ, Tseng Y, Konstantopoulos K and Wirtz D (2006) Single-molecule analysis of cadherin-mediated cell-cell adhesion. *J Cell Sci* **119:**66-74.

Poirier A, Portmann R, Cascais AC, Bader U, Walter I, Ullah M and Funk C (2014) The need for human breast cancer resistance protein substrate and inhibition evaluation in drug discovery and development: why, when, and how? *Drug Metab Dispos* **42:**1466-1477.

Prasad B, Lai Y, Lin Y and Unadkat JD (2013) Interindividual variability in the hepatic expression of the human breast cancer resistance protein (BCRP/ABCG2) : effect of age, sex, and genotype. *J Pharm Sci* **102:**787-793.

Prasad B and Unadkat JD (2014) Optimized Approaches for Quantification of Drug Transporters in Tissues and Cells by MRM Proteomics. *AAPS J* **16:**634-648.

Prasad B, Evers R, Gupta A, Hop CE, Salphati L, Shukla S, Ambudkar SV and Unadkat JD (2014) Interindividual variability in hepatic organic anion-transporting polypeptides and P-glycoprotein (ABCB1) protein expression: quantification by liquid chromatography tandem mass spectroscopy and influence of genotype, age, and sex. *Drug Metab Dispos* **42:**78-88.

Proctor NJ, Tucker GT and Rostami-Hodjegan A (2004) Predicting drug clearance from recombinantly expressed CYPs: intersystem extrapolation factors. *Xenobiotica* **34:**151-178.

Proctor WR, Bourdet DL and Thakker DR (2008) Mechanisms underlying saturable intestinal absorption of metformin. *Drug Metab Dispos* **36:**1650-1658.

Prost O, Ottignon Y, Remy-Martin A, Vuitton D, Miguet JP and Adessi GL (1984) Steroid sulfatase activities in normal and cirrhotic livers and plasma levels of estrone sulfate, estrone and estradiol-17 beta in men. *Steroids* **43:**189-199.

Prueksaritanont T, Chu X, Gibson C, Cui D, Yee KL, Ballard J, Cabalu T and Hochman J (2013) Drug-drug interaction studies: regulatory guidance and an industry perspective. *AAPS J* **15:**629-645.

Qiu X, Bi YA, Balogh LM and Lai Y (2013) Absolute measurement of species differences in sodium taurocholate cotransporting polypeptide (NTCP/Ntcp) and its modulation in cultured hepatocytes. *J Pharm Sci* **102:**3252-3263.

Qiu X, Zhang H and Lai Y (2014) Quantitative targeted proteomics for membrane transporter proteins: method and application. *AAPS J* **16:**714-726.

Reinoso RF, Telfer BA, Brennan BS and Rowland M (2001) Uptake of teicoplanin by isolated rat hepatocytes: comparison with in vivo hepatic distribution. *Drug Metab Dispos* **29:**453-459.

Rivers J, Simpson DM, Robertson DH, Gaskell SJ and Beynon RJ (2007) Absolute multiplexed quantitative analysis of protein expression during muscle development using QconCAT. *Mol Cell Proteomics* **6:**1416-1427.

Rodgers T and Rowland M (2007) Mechanistic approaches to volume of distribution predictions: understanding the processes. *Pharm Res* **24:**918-933.

Rolsted K, Rapin N and Steffansen B (2011) Simulating kinetic parameters in transporter mediated permeability across Caco-2 cells. A case study of estrone-3-sulfate. *Eur J Pharm Sci* **44:**218-226.

Romsicki Y and Sharom FJ (1999) The membrane lipid environment modulates drug interactions with the P-glycoprotein multidrug transporter. *Biochemistry* **38:**6887-6896.

Rostami-Hodjegan and Tucker GT (2007) Simulation and prediction of in vivo drug metabolism in human populations from in vitro data. *Nat Rev Drug Discov* **6**: 140-148

Rostami-Hodjegan A, Tamai I and Pang KS (2012) Physiologically based pharmacokinetic (PBPK) modeling: It is here to stay! *Biopharm Drug Dispos* **33:**47-50.

Rowland A, Elliot DJ, Knights KM, Mackenzie PI and Miners JO (2008) The "albumin effect" and in vitro-in vivo extrapolation: sequestration of long-chain unsaturated fatty acids enhances phenytoin hydroxylation by human liver microsomal and recombinant cytochrome P450 2C9. *Drug Metab Dispos* **36:**870-877.

Russell MR, Achour B, McKenzie EA, Lopez R, Harwood MD, Rostami-Hodjegan A and Barber J (2013) Alternative fusion protein strategies to express recalcitrant QconCAT proteins for quantitative proteomics of human drug metabolizing enzymes and transporters. *J Proteome Res* **12:**5934-5942.

Saitoh R, Sugano K, Takata N, Tachibana T, Higashida A, Nabuchi Y and Aso Y (2004) Correction of permeability with pore radius of tight junctions in Caco-2 monolayers improves the prediction of the dose fraction of hydrophilic drugs absorbed by humans. *Pharm Res* **21:**749-755.

Sakamoto A, Matsumaru T, Ishiguro N, Schaefer O, Ohtsuki S, Inoue T, Kawakami H and Terasaki T (2011) Reliability and robustness of simultaneous absolute quantification of drug transporters, cytochrome P450 enzymes, and Udp-glucuronosyltransferases in human liver tissue by multiplexed MRM/selected reaction monitoring mode tandem mass spectrometry with nano-liquid chromatography. *J Pharm Sci* **100:**4037-4043.

Sambuy Y, De Angelis I, Ranaldi G, Scarino ML, Stammati A and Zucco F (2005) The Caco-2 cell line as a model of the intestinal barrier: influence of cell and culture-related factors on Caco-2 cell functional characteristics. *Cell Biol Toxicol* **21:**1-26.

Sandle GI, McNicholas CM and Lomax RB (1994) Potassium channels in colonic crypts. *Lancet* **343:**23-25.

Schaefer O, Ohtsuki S, Kawakami H, Inoue T, Liehner S, Saito A, Sakamoto A, Ishiguro N, Matsumaru T, Terasaki T and Ebner T (2012) Absolute Quantification and Differential

Expression of Drug Transporters, Cytochrome P450 Enzymes, and UDP-Glucuronosyltransferases in Cultured Primary Human Hepatocytes. *Drug Metab Dispos* **40:**93-103.

Segawa M, Ogura J, Seki S, Itagaki S, Takahashi N, Kobayashi M, Hirano T, Yamaguchi H and Iseki K (2013) Rapid stimulating effect of the antiarrhythmic agent amiodarone on absorption of organic anion compounds. *Drug Metab Pharmacokinet* **28:**178-186.

Seithel A, Karlsson J, Hilgendorf C, Bjorquist A and Ungell AL (2006) Variability in mRNA expression of ABC- and SLC-transporters in human intestinal cells: comparison between human segments and Caco-2 cells. *Eur J Pharm Sci* **28:**291-299.

Sekine S, Ito K and Horie T (2008) Canalicular Mrp2 localization is reversibly regulated by the intracellular redox status. *Am J Physiol Gastrointest Liver Physiol* **295:**G1035-1041.

Seward DJ, Koh AS, Boyer JL and Ballatori N (2003) Functional complementation between a novel mammalian polygenic transport complex and an evolutionarily ancient organic solute transporter, OSTalpha-OSTbeta. *J Biol Chem* **278:**27473-27482.

Shawahna R, Uchida Y, Decleves X, Ohtsuki S, Yousif S, Dauchy S, Jacob A, Chassoux F, Daumas-Duport C, Couraud PO, Terasaki T and Scherrmann JM (2011) Transcriptomic and quantitative proteomic analysis of transporters and drug metabolizing enzymes in freshly isolated human brain microvessels. *Mol Pharm* **8:**1332-1341.

Shirasaka Y, Kawasaki M, Sakane T, Omatsu H, Moriya Y, Nakamura T, Sakaeda T, Okumura K, Langguth P and Yamashita S (2006) Induction of human P-glycoprotein in Caco-2 cells: development of a highly sensitive assay system for P-glycoprotein-mediated drug transport. *Drug Metab Pharmacokinet* **21:**414-423.

Shirasaka Y, Sakane T and Yamashita S (2008) Effect of P-glycoprotein expression levels on the concentration-dependent permeability of drugs to the cell membrane. *J Pharm Sci* **97:**553-565.

Shirasaka Y, Konishi R, Funami N, Kadowaki Y, Nagai Y, Sakaeda T and Yamashita S (2009) Expression levels of human P-glycoprotein in in vitro cell lines: correlation between mRNA and protein levels for P-glycoprotein expressed in cells. *Biopharm Drug Dispos* **30:**149-152.

Shirasaka Y, Mori T, Shichiri M, Nakanishi T and Tamai I (2012) Functional pleiotropy of organic anion transporting polypeptide OATP2B1 due to multiple binding sites. *Drug Metab Pharmacokinet* **27:**360-364.

Shirazi-Beechey SP, Davies AG, Tebbutt K, Dyer J, Ellis A, Taylor CJ, Fairclough P and Beechey RB (1990) Preparation and properties of brush-border membrane vesicles from human small intestine. *Gastroenterology* **98:**676-685.

Siegmund W, Altmannsberger S, Paneitz A, Hecker U, Zschiesche M, Franke G, Meng W, Warzok R, Schroeder E, Sperker B, Terhaag B, Cascorbi I and Kroemer HK (2002) Effect of levothyroxine administration on intestinal P-glycoprotein expression: consequences for drug disposition. *Clin Pharmacol Ther* **72:**256-264.

Siissalo S, Laitinen L, Koljonen M, Vellonen KS, Kortejarvi H, Urtti A, Hirvonen J and Kaukonen AM (2007) Effect of cell differentiation and passage number on the expression of efflux proteins in wild type and vinblastine-induced Caco-2 cell lines. *Eur J Pharm Biopharm* **67:**548-554.

Simpson DM and Beynon RJ (2012) QconCATs: design and expression of concatenated protein standards for multiplexed protein quantification. *Anal Bioanal Chem* **404:**977-989.

Sjogren E, Abrahamsson B, Augustijns P, Becker D, Bolger MB, Brewster M, Brouwers J, Flanagan T, Harwood M, Heinen C, Holm R, Juretschke HP, Kubbinga M, Lindahl A, Lukacova V, Munster U, Neuhoff S, Nguyen MA, Peer A, Reppas C, Rostami Hodjegan A, Tannergren C, Weitschies W, Wilson C, Zane P, Lennernas H and Langguth P (2014) In vivo methods for drug absorption - comparative physiologies, model selection, correlations with in vitro methods (IVIVC) , and applications for formulation/API/excipient characterization including food effects. *Eur J Pharm Sci* **57:**99-151.

Smith BJ (2012) An industrial perspective on contemporary applications of PBPK models in drug discovery and development. *Biopharm Drug Dispos* **33:**53-54.

Soars MG, Grime K, Sproston JL, Webborn PJ and Riley RJ (2007) Use of hepatocytes to assess the contribution of hepatic uptake to clearance in vivo. *Drug Metab Dispos* **35:**859-865.

Stephens RH, O'Neill CA, Warhurst A, Carlson GL, Rowland M and Warhurst G (2001) Kinetic profiling of P-glycoprotein-mediated drug efflux in rat and human intestinal epithelia. *J Pharmacol Exp Ther* **296:**584-591.

Stewart WW (1978) Functional connections between cells as revealed by dye-coupling with a highly fluorescent naphthalimide tracer. *Cell* **14:**741-759.

Stieger B, Unadkat JD, Prasad B, Langer O and Gali H (2014) Role of (Drug) Transporters in Imaging in Health and Disease. *Drug Metab Dispos* **42:**2007-2015.

Su Y, Hu P, Lee SH and Sinko PJ (2007) Using novobiocin as a specific inhibitor of breast cancer resistant protein to assess the role of transporter in the absorption and disposition of topotecan. *J Pharm Pharm Sci* **10:**519-536.

Sugano K, Shirasaka Y and Yamashita S (2011) Estimation of Michaelis-Menten constant of efflux transporter considering asymmetric permeability. *Int J Pharm* **418:**161-167.

Sun AQ, Balasubramaniyan N, Xu K, Liu CJ, Ponamgi VM, Liu H and Suchy FJ (2007) Protein-protein interactions and membrane localization of the human organic solute transporter. *Am J Physiol Gastrointest Liver Physiol* **292:**G1586-1593.

Sun D, Lennernas H, Welage LS, Barnett JL, Landowski CP, Foster D, Fleisher D, Lee KD and Amidon GL (2002) Comparison of human duodenum and Caco-2 gene expression profiles for 12,000 gene sequences tags and correlation with permeability of 26 drugs. *Pharm Res* **19:**1400-1416.

Sun H, Zhang L, Chow EC, Lin G, Zuo Z and Pang KS (2008) A catenary model to study transport and conjugation of baicalein, a bioactive flavonoid, in the Caco-2 cell monolayer: demonstration of substrate inhibition. *J Pharmacol Exp Ther* **326:**117-126.

Sun H and Pang KS (2010) Physiological modeling to understand the impact of enzymes and transporters on drug and metabolite data and bioavailability estimates. *Pharm Res* **27**: 1237-54.

Sun N and Avdeef A (2011) Biorelevant pK(a) (37 degrees C) predicted from the 2D structure of the molecule and its pK(a) at 25 degrees C. *J Pharm Biomed Anal* **56:**173-182.

Suzuki M, Suzuki H, Sugimoto Y and Sugiyama Y (2003) ABCG2 transports sulfated conjugates of steroids and xenobiotics. *J Biol Chem* **278:**22644-22649.

Tachibana T, Kitamura S, Kato M, Mitsui T, Shirasaka Y, Yamashita S and Sugiyama Y (2010) Model analysis of the concentration-dependent permeability of P-gp substrates. *Pharm Res* **27:**442-446.

Taipalensuu J, Tavelin S, Lazorova L, Svensson AC and Artursson P (2004) Exploring the quantitative relationship between the level of MDR1 transcript, protein and function using digoxin as a marker of MDR1-dependent drug efflux activity. *Eur J Pharm Sci* **21:**69-75.

Tam D, Tirona RG and Pang RS. (2003) Segmental intestinal transporters and metabolic enzymes on intestinal drug absorption. *Drug Metab Dispos* **31**: 373-83.

Tamai I, Nezu J, Uchino H, Sai Y, Oku A, Shiman M and Tsuji A (2000) Molecular identification and characterization of novel members of the human organic anion transporter (OATP) family. *Biochem Biophys Res Comm* **273**, 251-260.

Tang F, Horie K and Borchardt RT (2002a) Are MDCK cells transfected with the human MRP2 gene a good model of the human intestinal mucosa? *Pharm Res* **19:**773-779.

Tang F, Horie K and Borchardt RT (2002b) Are MDCK cells transfected with the human MDR1 gene a good model of the human intestinal mucosa? *Pharm Res* **19:**765-772.

Tchaparian E, Tang L., Xu G HT and L J (2008) Cell Based Experimental Models for the Prediction of Human Intestinal Absorption. *Conference proceeding. 15th North American Regional International Society for the Study of Xenobiotics Meeting*.

Terasaki T, Hakata Y, Tachikawa M, Uchida Y and Ohtsuki S (2014) Absolute Expression levels of Organic Anion Transporting Polypeptide 1B1 in Human Liver. *Poster at the 19th North American ISSX Meeting and 29th JSSX Annual Meeting*.

Thwaites DT, Hirst BH and Simmons NL (1993) Direct assessment of dipeptide/H+ symport in intact human intestinal (Caco-2) epithelium: a novel method utilising continuous intracellular pH measurement. *Biochem Biophys Res Commun* **194:**432-438.

Thwaites DT, Kennedy DJ, Raldua D, Anderson CM, Mendoza ME, Bladen CL and Simmons NL (2002) H/dipeptide absorption across the human intestinal epithelium is controlled indirectly via a functional Na/H exchanger. *Gastroenterology* **122:**1322-1333.

Trotter PJ and Storch J (1991) Fatty acid uptake and metabolism in a human intestinal cell line (Caco-2) : comparison of apical and basolateral incubation. *J Lipid Res* **32:**293-304.

Troutman MD and Thakker DR (2003a) Novel experimental parameters to quantify the modulation of absorptive and secretory transport of compounds by P-glycoprotein in cell culture models of intestinal epithelium. *Pharm Res* **20:**1210-1224.

Troutman MD and Thakker DR (2003b) Efflux ratio cannot assess P-glycoprotein-mediated attenuation of absorptive transport: asymmetric effect of P-glycoprotein on absorptive and secretory transport across Caco-2 cell monolayers. *Pharm Res* **20:**1200-1209.

Tucker TG, Milne AM, Fournel-Gigleux S, Fenner KS and Coughtrie MW (2012) Absolute immunoquantification of the expression of ABC transporters P-glycoprotein, breast cancer resistance protein and multidrug resistance-associated protein 2 in human liver and duodenum. *Biochem Pharmacol* **83:**279-285.

Uchida Y, Kamiie J, Iwase R, Ohmine K, Ohtsuki S and Terasaki T (2007) Protein Expression Profile of 29 Human Transporters in Caco-2 Cells Depending on Culture Periods. *Poster at: 8th ISSX International meeting, Sendai, Japan, 2007*.

Uchida Y, Ohtsuki S, Katsukura Y, Ikeda C, Suzuki T, Kamiie J and Terasaki T (2011) Quantitative targeted absolute proteomics of human blood-brain barrier transporters and receptors. *J Neurochem* **117:**333-345.

Uchida Y, Tachikawa M, Obuchi W, Hoshi Y, Tomioka Y, Ohtsuki S and Terasaki T (2013) A study protocol for quantitative targeted absolute proteomics (QTAP) by LC-MS/MS: application for inter-strain differences in protein expression levels of transporters, receptors, claudin-5, and marker proteins at the blood-brain barrier in ddY, FVB, and C57BL/6J mice. *Fluids Barriers CNS* **10:**21.

Uchida Y, Ohtsuki S and Terasaki T (2014) Pharmacoproteomics-based reconstruction of in vivo P-glycoprotein function at blood-brain barrier and brain distribution of substrate verapamil in pentylenetetrazole-kindled epilepsy, spontaneous epilepsy, and phenytoin treatment models. *Drug Metab Dispos* **42:**1719-1726.

Urquhart BL, Ware JA, Tirona RG, Ho RH, Leake BF, Schwarz UI, Zaher H, Palandra J, Gregor JC, Dresser GK and Kim RB (2008) Breast cancer resistance protein (ABCG2) and drug disposition: intestinal expression, polymorphisms and sulfasalazine as an in vivo probe. *Pharmacogenet Genomics* **18:**439-448.

van de Steeg E, Greupink R, Schreurs M, Nooijen IH, Verhoeckx KC, Hanemaaijer R, Ripken D, Monshouwer M, Vlaming ML, DeGroot J, Verwei M, Russel FG, Huisman MT and Wortelboer HM (2013) Drug-drug interactions between rosuvastatin and oral antidiabetic drugs occurring at the level of OATP1B1. *Drug Metab Dispos* **41:**592-601.

van den Broek I, Smit NP, Romijn FP, van der Laarse A, Deelder AM, van der Burgt YE and Cobbaert CM (2013) Evaluation of interspecimen trypsin digestion efficiency prior to multiple reaction monitoring-based absolute protein quantification with native protein calibrators. *J Proteome Res* **12:**5760-5774.

Varma MV, Ambler CM, Ullah M, Rotter CJ, Sun H, Litchfield J, Fenner KS and El-Kattan AF (2010) Targeting intestinal transporters for optimizing oral drug absorption. *Curr Drug Metab* **11:**730-742.

Varma MV, Rotter CJ, Chupka J, Whalen KM, Duignan DB, Feng B, Litchfield J, Goosen TC and El-Kattan AF (2011) pH-sensitive interaction of HMG-CoA reductase inhibitors (statins) with organic anion transporting polypeptide 2B1. *Mol Pharm* **8:**1303-1313.

Varma MV, Lai Y, Feng B, Litchfield J, Goosen TC and Bergman A (2012) Physiologically based modeling of pravastatin transporter-mediated hepatobiliary disposition and drug-drug interactions. *Pharm Res* **29:**2860-2873.

Varma MV, Lai Y, Kimoto E, Goosen TC, El-Kattan AF and Kumar V (2013) Mechanistic modeling to predict the transporter- and enzyme-mediated drug-drug interactions of repaglinide. *Pharm Res* **30:**1188-1199.

Varum FJ, Merchant HA and Basit AW (2010) Oral modified-release formulations in motion: the relationship between gastrointestinal transit and drug absorption. *Int J Pharm* **395:**26-36.

Verhoeckx KCM, Ripken D, van de Steeg E, Vlaming MLH, Verwei M, Bosgra S, DeGroot J and Wortelboer HM (2011) Quantitative Determination of Transporter Protein Expression Using UPLC-MS-MS in: *Biomedical Transporters Conference*, Grindelwald, Switzerland.

Vildhede A, Karlgren M, Svedberg EK, Wisniewski JR, Lai Y, Noren A and Artursson P (2014) Hepatic Uptake of Atorvastatin: Influence of Variability in Transporter Expression on Uptake Clearance and Drug-drug Interactions. *Drug Metab Dispos* **42:**1210-1218.

Vogel C and Marcotte EM (2012) Insights into the regulation of protein abundance from proteomic and transcriptomic analyses. *Nat Rev Genet* **13:**227-232.

von Richter O, Burk O, Fromm MF, Thon KP, Eichelbaum M and Kivisto KT (2004) Cytochrome P450 3A4 and P-glycoprotein expression in human small intestinal enterocytes and hepatocytes: a comparative analysis in paired tissue specimens. *Clin Pharmacol Ther* **75:**172-183.

Wang Q, Strab R, Kardos P, Ferguson C, Li J, Owen A and Hidalgo IJ (2008) Application and limitation of inhibitors in drug-transporter interactions studies. *Int J Pharm* **356:**12-18.

Ward PE, Sheridan MA, Hammon KJ and Erdos EG (1980) Angiotensin I converting enzyme (kininase II) of the brush border of human and swine intestine. *Biochem Pharmacol* **29:**1525-1529.

Weingartl HM and Derbyshire JB (1993) Binding of porcine transmissible gastroenteritis virus by enterocytes from newborn and weaned piglets. *Vet Microbiol* **35:**23-32.

Weiser MM (1973) Intestinal epithelial cell surface membrane glycoprotein synthesis. I. An indicator of cellular differentiation. *J Biol Chem* **248:**2536-2541.

Weller S, Blum MR, Doucette M, Burnette T, Cederberg DM, de Miranda P and Smiley ML (1993) Pharmacokinetics of the acyclovir pro-drug valaciclovir after escalating single- and multiple-dose administration to normal volunteers. *Clin Pharmacol Ther* **54:**595-605.

Wetterich U, Spahn-Langguth H, Mutschler E, Terhaag B, Rosch W and Langguth P (1996) Evidence for intestinal secretion as an additional clearance pathway of talinolol enantiomers: concentration- and dose-dependent absorption in vitro and in vivo. *Pharm Res* **13:**514-522.

Wilson JW and Webb KE, Jr. (1990) Simultaneous isolation and characterization of brush border and basolateral membrane vesicles from bovine small intestine. *J Anim Sci* **68:**583-590.

Wilson ZE, Rostami-Hodjegan A, Burn JL, Tooley A, Boyle J, Ellis SW and Tucker GT (2003) Inter-individual variability in levels of human microsomal protein and hepatocellularity per gram of liver. *Br J Clin Pharmacol* **56:**433-440.

Winiwarter S, Bonham NM, Ax F, Hallberg A, Lennernas H and Karlen A (1998) Correlation of human jejunal permeability (in vivo) of drugs with experimentally and theoretically derived parameters. A multivariate data analysis approach. *J Med Chem* **41:**4939-4949.

Wisniewski JR, Ostasiewicz P, Dus K, Zielinska DF, Gnad F and Mann M (2012) Extensive quantitative remodeling of the proteome between normal colon tissue and adenocarcinoma. *Mol Syst Biol* **8:**611.

Wisniewski JR, Hein MY, Cox J and Mann M (2014) A "proteomic ruler" for protein copy number and concentration estimation without spike-in standards. *Mol Cell Proteomics* **13:**3497-3506.

Xia CQ, Liu N, Yang D, Miwa G and Gan LS (2005) Expression, localization, and functional characteristics of breast cancer resistance protein in Caco-2 cells. *Drug Metab Dispos* **33:**637-643.

Xu S, Sun AQ and Suchy FJ (2014) A novel RARalpha/CAR-mediated mechanism for regulation of human organic solute transporter-beta gene expression. *Am J Physiol Gastrointest Liver Physiol* **306:**G154-162.

Yamashita S, Konishi K, Yamazaki Y, Taki Y, Sakane T, Sezaki H and Furuyama Y (2002) New and better protocols for a short-term Caco-2 cell culture system. *J Pharm Sci* **91:**669-679.

Yang J, Jamei M, Yeo KR, Tucker GT and Rostami-Hodjegan A (2007) Prediction of intestinal first-pass drug metabolism. *Curr Drug Metab* **8:**676-684.

Yu H, Cook TJ and Sinko PJ (1997) Evidence for diminished functional expression of intestinal transporters in Caco-2 cell monolayers at high passages. *Pharm Res* **14:**757-762.

Yu LX and Amidon GL (1999) A compartmental absorption and transit model for estimating oral drug absorption. *Int J Pharm* **186**:119-125.

Zamek-Gliszczynski MJ, Lee CA, Poirier A, Bentz J, Chu X, Ellens H, Ishikawa T, Jamei M, Kalvass JC, Nagar S, Pang KS, Korzekwa K, Swaan PW, Taub ME, Zhao P and Galetin A (2013) ITC recommendations for transporter kinetic parameter estimation and translational modeling of transport-mediated PK and DDIs in humans. *Clin Pharmacol Ther* **94:**64-79.

Zhang L, Reynolds KS, Zhao P and Huang SM (2010) Drug interactions evaluation: an integrated part of risk assessment of therapeutics. *Toxicol Appl Pharmacol* **243:**134-145.

Zhang QY, Dunbar D, Ostrowska A, Zeisloft S, Yang J and Kaminsky LS (1999) Characterization of human small intestinal cytochromes P-450. *Drug Metab Dispos* **27:**804-809.

Zhang W, Li J, Allen SM, Weiskircher EA, Huang Y, George RA, Fong RG, Owen A and Hidalgo IJ (2009) Silencing the breast cancer resistance protein expression and function in caco-2 cells using lentiviral vector-based short hairpin RNA. *Drug Metab Dispos* **37:**737-744.

Zhang Y, Schuetz JD, Elmquist WF and Miller DW (2004) Plasma membrane localization of multidrug resistance-associated protein homologs in brain capillary endothelial cells. *J Pharmacol Exp Ther* **311:**449-455.

Zhang Y, Li N, Brown PW, Ozer JS and Lai Y (2011) Liquid chromatography/tandem mass spectrometry based targeted proteomics quantification of P-glycoprotein in various biological samples. *Rapid Commun Mass Spectrom* **25:**1715-1724.

Zhao P, Rowland M and Huang SM (2012) Best practice in the use of physiologically based pharmacokinetic modeling and simulation to address clinical pharmacology regulatory questions. *Clin Pharmacol Ther* **92:**17-20.

Zhou-Pan XR, Seree E, Zhou XJ, Placidi M, Maurel P, Barra Y and Rahmani R (1993) Involvement of human liver cytochrome P450 3A in vinblastine metabolism: drug interactions. *Cancer Res* **53:**5121-5126.

Zhou XJ, Placidi M and Rahmani R (1994) Uptake and metabolism of vinca alkaloids by freshly isolated human hepatocytes in suspension. *Anticancer Res* **14:**1017-1022.